Load Transfer Mechanism of Fully Grouted Cable Bolts

Jianhang Chen

A thesis in fulfilment of the requirements for the degree of

Doctor of Philosophy

UNSW AUSTRALIA

School of Mining Engineering

Faculty of Engineering

November 2016

PLEASE TYPE

THE UNIVERSITY OF NEW SOUTH WALES
Thesis/Dissertation Sheet

Surname or Family name: Chen

First name: Jianhang | Other name/s:

Abbreviation for degree as given in the University calendar: PhD

School: Minining Engineering | Faculty: Engineering

Title: Load transfer mechanism of fully grouted cable bolts

Abstract 350 words maximum: (PLEASE TYPE)

Fully grouted cable bolts have been used in the mining industry for more than fifty years. However, failure of cable bolting systems still occurs in mine sites, as a result of insufficient load transfer between the rock mass and the cable bolt.

Numerous research studies have been conducted to understand the load transfer mechanism of cable bolts in the laboratory. However, there are many shortcomings in previous methods. This thesis aims to propose a new approach to study the load transfer mechanism of cable bolts.

As part of this research, a modified Laboratory Short Encapsulation Pull Test (LSEPT) facility was developed. It was mainly composed of two parts, namely the embedment section and the anchor section. The influence of termination methods, borehole roughness and pre-confinement on the performance of cable bolts was investigated. The results show that the pre-confinement has a significant effect on the performance of cable bolts.

The load transfer behaviour of two types of cable bolts, the Superstrand cable and the MW9 cable, was studied. The influence of different parameters including the cable surface geometry, borehole size and confining medium strength was evaluated. The results show that bond failure of Superstrand cable bolting systems always occurred at the cable/grout interface. However, for the MW9 cable installed in a standard borehole, bond failure occurred at the grout/rock interface in the weak confining medium.

An analytical model was used to study the load transfer behaviour of cable bolts. Experimental results were adopted to validate this model. It was found that the cable/grout interface undergoes different stages in a pull-out test and the non-uniform shear stress distribution is more apparent in long embedment length.

The shear performance of the Stratabinder grout in the constant normal stress and constant normal stiffness conditions was also studied. The results reveal that the low normal stiffness has little impact on the performance of the grout.

FLAC2D software package was used to simulate the axial behaviour of cable bolts. The calibration process of samples and the pull-out performance of cable bolts were validated with experimental results. It was found that the modified surface geometry has an obvious influence on inducing more confining pressure in pull-out tests.

Declaration relating to disposition of project thesis/dissertation

		19/05/16
…………………………………………………………	………………………………………………	………………………………………
Signature	Witness Signature	Date

FOR OFFICE USE ONLY | Date of completion of requirements for Award:

THIS SHEET IS TO BE GLUED TO THE INSIDE FRONT COVER OF THE THESIS

ORIGINALITY STATEMENT

'I hereby declare that this submission is my own work and to the best of my knowledge it contains no materials previously published or written by another person, or substantial proportions of material which have been accepted for the award of any other degree or diploma at UNSW or any other educational institution, except where due acknowledgement is made in the thesis. Any contribution made to the research by others, with whom I have worked at UNSW or elsewhere, is explicitly acknowledged in the thesis. I also declare that the intellectual content of this thesis is the product of my own work, except to the extent that assistance from others in the project's design and conception or in style, presentation and linguistic expression is acknowledged.'

Signed ……………………………………………….............

Date 19/05/16 ……………………………………………….............

COPYRIGHT STATEMENT

Signed ……………………………………………..........................

Date 19/05/16 ……………………………………………..........................

AUTHENTICITY STATEMENT

‘I certify that the Library deposit digital copy is a direct equivalent of the final officially approved version of my thesis. No emendation of content has occurred and if there are any minor variations in formatting, they are the result of the conversion to digital format.’

Signed ……………………………………………..........................

Date 19/05/16 ……………………………………………..........................

ABSTRACT

Fully grouted cable bolts have been used in the mining industry for more than fifty years. However, failure of cable bolting systems still occurs in mine sites, as a result of insufficient load transfer between the rock mass and the cable bolt.

Numerous research studies have been conducted to understand the load transfer mechanism of cable bolts in the laboratory. However, there are many shortcomings in previous methods. This thesis aims to propose a new approach to study the load transfer mechanism of cable bolts.

As part of this research, a modified Laboratory Short Encapsulation Pull Test (LSEPT) facility was developed. It was mainly composed of two parts, namely the embedment section and the anchor section. The influence of termination methods, borehole roughness and pre-confinement on the performance of cable bolts was investigated. The results show that the pre-confinement has a significant effect on the performance of cable bolts.

The load transfer behaviour of two types of cable bolts, the Superstrand cable and the MW9 cable, was studied. The influence of different parameters including the cable surface geometry, borehole size and confining medium strength was evaluated. The results show that bond failure of Superstrand cable bolting systems always occurred at the cable/grout interface. However, for the MW9 cable installed in a standard borehole, bond failure occurred at the grout/rock interface in the weak confining medium.

An analytical model was used to study the load transfer behaviour of cable bolts. Experimental results were adopted to validate this model. It was found that the cable/grout interface undergoes different stages in a pull-out test and the non-uniform shear stress distribution is more apparent in long embedment length.

The shear performance of the Stratabinder grout in the constant normal stress and constant normal stiffness conditions was also studied. The results reveal that the low normal stiffness has little impact on the performance of the grout.

FLAC2D software package was used to simulate the axial behaviour of cable bolts. The calibration process of samples and the pull-out performance of cable bolts were validated with experimental results. It was found that the modified surface geometry has an obvious influence on inducing more confining pressure in pull-out tests.

ACKNOWLEDGEMENTS

I would like to express my sincere gratitude and appreciation to my supervisors, Associate Professors Paul Hagan and Serkan Saydam for their invaluable supervision, support, guidance, and encouragement through the course of this project. They have provided constructive advice during my study, which I respect and admire. This thesis could not have been accomplished without their help.

This research project was supported by the Australian Coal Association Research Program (project number C22010). The assistance provided by the following organisations is also acknowledged: Jennmar Australia (in particular Peter Craig), Megabolt Australia (in particular Ron Mckenzie) and Orica Group.

Also, I want to thank Dr. Hossein Masoumi for his valuable recommendations on the analytical modelling. Appreciation is also given to Dr. Joung Oh, thanking him for spending time in discussing and providing guidance on my numerical simulation work. The field practices and experiences offered by Professors Bruce Hebblewhite and Fidelis Suorineni are also appreciated.

I give great thanks to the technical staff in the School of Mining Engineering, especially Kanchana Gamage, for the laboratory assistance. All tests in this thesis were conducted under his tremendous support. I also want to thank Mark Whelan for programming the data logging system.

Particular thanks are given to my family for encouraging me all these years. I appreciate the financial support provided by the China Scholarship Council.

Contents

List of Figures

List of Tables

CHAPTER ONE

INTRODUCTION

1.1 Background

A cable bolt, as shown in Figure 1 - 1, is a flexible tendon consisting of a number of wound wires that are often fully grouted in boreholes to provide ground reinforcement and support in civil and mining applications for rock slopes on the surface and in underground excavations (Hutchinson and Diederichs, 1996). Cable bolts were introduced into the mining industry in the 1960s, and since the early 1970s they have been used in both hard rock and coal mining operations (Thorne and Muller, 1964). Over the time, cable bolts have become increasingly favoured in highly stressed ground conditions due to their much higher load bearing capacity compared with rockbolts.

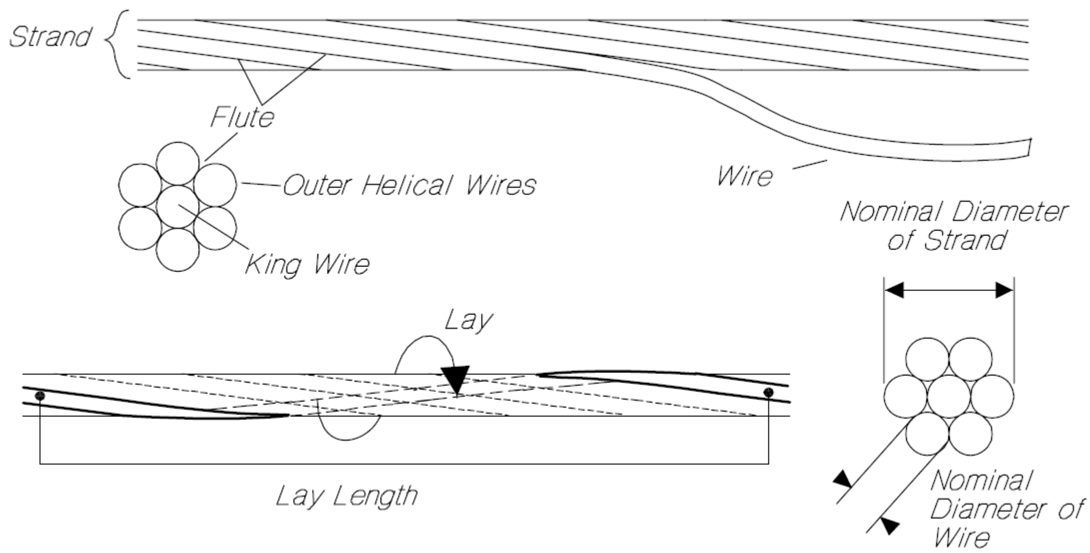

Figure 1 - 1 Geometrical properties of a seven-wire cable bolt (Hutchinson and Diederichs, 1996)

Originally, cable bolts were only intended as a temporary means of rock reinforcement.

One reason is that many of the earlier cables were made from discarded steel ropes, having very poor load transfer properties. They lacked ribs, such as ones found on rockbolts. Over subsequent years, a number of modifications were made to basic plain cables, such as buttoned cables (Schmuck, 1979), double plain strands (Matthews *et al.*, 1983), epoxy-coated cables (Dorsten *et al.*, 1984), fiberglass cables (Mah, 1994), birdcage cables (Hutchins *et al.*, 1990), bulbed cables (Garford, 1990), and nutcage cable bolts (Hyett *et al.*, 1993). These changes to the cable surface geometry were undertaken in an effort to improve the anchorage capacity, which resulted in the more widespread use of cable bolts for permanent ground reinforcement.

Although cable bolts have been used in the industry for more than fifty years, failure of the cable bolting system still occurs. Different failure modes of the cable bolting system have been previously reported. It is most common to encounter the bond failure along the cable/grout or grout/rock interface, especially the former, as shown in Figure 1 - 2. Bond failure along the cable/grout interface usually occurs in strong rock applications while bond failure along the grout/rock interface can occur in weak rocks when modified cable bolts are used in rock reinforcement applications (Hutchinson and Diederichs, 1996).

The load transfer is induced by differential movement within a rock mass such as bed separation or movement along joints. More importantly, the cementitious or resin grout column provides the mechanism for transferring force between the cable bolt and surrounding rock mass.

To evaluate the load transfer performance of cable bolts, pull-out tests are used. The load versus displacement relationship of the cable bolting system, especially the peak load, is used to indicate the load transfer efficiency.

Figure 1 - 2 Bond failure along the cable/grout interface (Blanco Martín, 2012)

Hartman and Hebblewhite (2003) stated that there are generally three sets of factors which have an impact on the load transfer of cable bolts: the reinforcing element, the rock mass and the loading conditions. Specifically, the parameters include: the cable bolt diameter, cable surface geometry, embedment length, borehole size, grout quality, confinement, termination methods, loading rate, tension, and rock strength.

A great deal of research has been conducted to study the influence of those parameters on load transfer behaviour of cable bolts, such as by Fuller and Cox (1975), Stheeman (1982), Farah and Aref (1986b), Nguyen *et al.* (1986), Hassani and Rajaie (1990), Rajaie (1990), Goris (1991a), Reichert (1991), Hyett *et al.* (1992a), Renwick (1992), Hyett and Bawden (1994), Pakalnis *et al.* (1994), Hyett *et al.* (1995a), Thompson and Windsor (1995), Moosavi *et al.* (1996), Moosavi (1997), Satola (1999), Clifford *et al.* (2001), Ito *et al.* (2001), Satola (2001), Aoki *et al.* (2002), Bigby (2004), Bigby and Reynolds (2005), Chen and Mitri (2005), Zhang *et al.* (2008), Mosse-Robinson and Sharrock (2010), Meikle *et al.* (2012), Blanco Martín *et al.* (2013), Faulkner *et al.* (2013), Thompson and Villaescusa (2013) and others. These research results have had a paramount impact on improving the understanding of the load transfer mechanism of fully grouted cable bolts. Nevertheless, there are still limitations involved in these previous methods which are discussed in Chapter two.

1.2 Research objectives

This research aims to use a new approach to study the load transfer mechanism of cable bolts, especially in weak rock conditions. To achieve this, a new test rig was developed for axial testing of various cable bolts including plain and modified. This test approach is able to overcome the shortcomings occurring in previous methods.

Furthermore, the load transfer mechanism of fully grouted cable bolts was studied. Specifically, bearing capacity and failure modes of plain and modified cable bolts installed in weak artificial confining medium were evaluated. The effects of different parameters such as the confining medium strength, the cable surface geometry, the borehole size and the embedment length on the axial performance of cable bolts were analysed.

Also, an analytical model was used to study the maximum load bearing capacity of cable bolts with varying embedment length. The non-uniform shear stress distribution along the cable/grout interface when peak load reached was acquired. Also, the shear stress propagation in the pull-out process was studied.

Additionally, the shear performance of a modified Portland cement grout under two different boundary conditions, namely constant normal stress and constant normal stiffness, was achieved. The influence of boundary condition on the shear failure envelope, cohesion and friction angle of the material was analysed.

Lastly, the pull-out behaviour of cable bolts was simulated with the numerical code FLAC2D. The elastic and post-failure behaviour of the cable bolting system was simulated. The confining pressure when peak load occurred was acquired.

1.3 Thesis outline

Chapter One aims to provide the general introduction and research objectives. The structure of the thesis is also presented.

Chapter Two provides a literature review on load transfer behaviour of cable bolts. The historic development of cable bolts, grouting materials, cable bolt installation methods, failure modes of cable bolting systems and load transfer mechanisms are included. Furthermore, the previous test approaches and their shortcomings are explained. The influence of different parameters on the performance of cable bolts is listed. Lastly, previous analytical modelling work on axial performance of cable bolts is presented.

Chapter Three examines the mechanical properties of the cementitious grout used in this project. The results of Uniaxial Compressive Strength (UCS) and Brazilian tests were provided. Important parameters including the UCS, Young's Modulus, Poisson's Ratio and tensile strength are acquired.

Chapter Four provides the direct shear test results of a modified Portland cement grout in the constant normal stress and constant normal stiffness conditions. The influence of boundary condition on the shear performance of the grout material is discussed.

Chapter Five presents the modified Laboratory Short Encapsulation Pull Test approach. The influence of confining medium size on the bond capacity of cable bolts is studied. The design process of the anchor tube is given. Furthermore, the anti-rotation devices including the locking key and nuts are explained. Preliminary tests are conducted to evaluate the influence of borehole roughness, pre-confinement and termination methods on performance of cable bolts.

Chapter Six studies the influence of different parameters on the load transfer behaviour of cable bolts. Bearing capacity and failure modes of plain and modified cable bolts in weak confining medium are compared and analysed. Additionally, the influence of borehole size and confining medium strength on the performance of cable bolts is investigated.

Chapter Seven uses an analytical model to study the maximum load bearing capacity of cable bolts with different embedment length. The shear stress distribution and propagation along the cable/grout interface are analysed.

Chapter Eight explains using the numerical code FLAC2D to simulate the pull-out behaviour of cable bolts. The calibration process for the strong and weak samples is illustrated. The important parameters including the UCS, Young's Modulus and Poisson's Ratio are compared and validated with experimental results. Then, the elastic and post-peak behaviour of cable bolts is simulated.

Chapter Nine provides the conclusions and recommendations for future research.

1.4 Publications associated with this thesis

The papers published in association with this thesis are listed below:

[1] **Chen, J.**, Hagan, P. C. and Saydam, S., 2016. Load transfer behaviour of fully grouted cable bolts reinforced in weak rocks under tensile loading conditions, *Geotechnical Testing Journal*, 39(2): 252-263.

[2] **Chen, J.**, Hagan, P. C. and Saydam, S., 2016. Parametric study on the axial performance of a fully grouted cable bolt with a new pull-out test, *International Journal of Mining Science and Technology*, 26(1): 53-58.

[3] **Chen, J.**, Saydam, S. and Hagan, P. C., 2015. An analytical model of the load transfer behavior of fully grouted cable bolts, *Construction and Building Materials*, 101 (2015):1006-1015.

[4] **Chen, J.**, Hagan, P. C. and Saydam, S., 2015. Axial performance of a fully grouted modified cable bolt tested with a new laboratory short encapsulation pull test, *International Conference on Ground Control in Mining*, Morgantown, USA, pp. 1-8.

[5] Hagan, P. C., **Chen, J.** and Saydam, S., 2015. A comparison of the anchorage performance of cable bolts based on a newly developed testing methodology,

13th International Congress on Rock Mechanics, Montreal, Canada, pp. 313-323.

[6] Ur-Rahman, I., Hagan, P. C. and **Chen, J.**, 2015. The influence of concrete sample testing dimensions on assessing cable bolt load carrying capacity, *Coal Operators' Conference*, Wollongong, Australia, pp. 138-146.

[7] Hagan, P. C. and **Chen, J.**, 2015. *Optimising the selection of fully grouted cable bolts in varying geotechnical environments* (Internal report), pp. 1-94 (Australian Coal Association Research Program: Sydney).

[8] **Chen, J.**, Hagan, P. C. and Saydam, S., 2014. Mechanical properties of cementitious grout serving in fully grouted cable bolting systems, *Third Australasian Ground Control in Mining Conference*, Sydney, Australia, pp. 269-275.

[9] **Chen, J.**, Hagan, P. C., Saydam, S. and Zhang, S., 2014. Consideration of the factors impacting on the design of the laboratory short encapsulation test for cable bolts, *8th Asian Rock Mechanics Symposium*, Sapporo, Japan, pp. 1379-1388.

[10] **Chen, J.**, Saydam, S. and Hagan, P. C., 2014. The load transfer mechanics of fully grouted cable bolts: A theoretical analysis, *ISRM European Regional Symposium*, Vigo, Spain, pp. 1045-1050.

[11] Hagan, P. C., **Chen, J.** and Saydam, S., 2014. The load transfer mechanism of fully grouted cable bolts under laboratory tests, *Coal Operators' Conference*, Wollongong, Australia, pp. 137-146.

CHAPTER TWO

LOAD TRANSFER BEHAVIOUR OF FULLY GROUTED CABLE BOLTS

2.1 Introduction

The stability of underground openings including chambers, drifts and stopes is of paramount importance in mining activities because instability issues can result in life-threatening injuries and property loss. After excavations are made underground, movement of the surrounding rock mass occurs until a stable equilibrium status is reached. Most mining openings need to be supported to maintain their integrity.

Various rock support and rock reinforcement methods are used to maintain the stability of a rock mass. Generally, support methods can be classified as temporary or permanent. As indicated by Brady and Brown (1985), temporary support represents the approaches adopted to ensure a secure working environment during mining while permanent support is used where stable openings are required for an extended period of time such as rail tunnels and underground power stations.

Although the terms support and reinforcement are usually used interchangeably, there are differences amongst them. According to Windsor and Thompson (1993), support indicates techniques and devices that are used at the face of an excavation, while reinforcement refers to all approaches or elements applied within rock masses. The rock reinforcement systems can be further classified as Continuously Mechanically Coupled (CMC) system, Continuously Frictionally Coupled (CFC) system, and Discretely

Mechanically or Frictionally Coupled (DMFC) system (Windsor, 1997). Later research showed that these group methods are also appropriate for the current reinforcing systems (Thompson *et al.*, 2012). Based on this classification, fully grouted cable bolts belong to the CMC class.

This chapter provides a review of the load transfer performance of fully grouted cable bolts. First, the historic development of cable bolts is given. Then, the cable bolt installation methods and its field applications are given. The failure modes and load transfer mechanism of fully grouted cable bolting system are then explained. Furthermore, laboratory axial and shear tests on cable bolts are reviewed. The theoretical background on rock tendons subjected to tensile load is summarised chronologically. Finally, the main research tasks of this thesis are presented.

2.2 Development of cable bolts

The first use of cable bolts in the mining industry was reported in the Free State Geduld Mines Ltd. in South Africa in the 1960s when Thorne and Muller (1964) used steel wires to maintain the stability of underground chambers. In the early 1970s, mine sites in Broken Hill, New South Wales, Australia started to use cable bolts to secure the integrity of rock masses. Later, this cable bolting technique was applied in reinforcing strata in a salt mine in Canada (Muir and Hedley, 1973). During the 1970s, there was a widespread application of cable bolts in the mining industry (Clifford, 1974; Gramoli, 1975; Palmer *et al.*, 1976; Davis, 1977; Hunt and Askew, 1977; Schmuck, 1979).

In earlier years, cable bolts were often used as temporary reinforcement elements. One reason for this was that initial cable bolts were sourced from discarded steel ropes. However they were subsequently found to have poor load transfer properties because of their smooth surface profile. Often these were plain cables constructed by winding seven steel wires to form a 15.2 mm diameter tendon. As they were relatively inexpensive, easy to install, and could be used in boreholes with lengths measured in tens of metres, cables were adopted for use in several underground mining systems such as overhand cut and fill.

Gradually, in an effort to improve the mechanical interlock and friction between the cable bolt and grout column, steel discs or buttons were inserted within the standard strand. These were termed buttoned or swaged strand (Schmuck, 1979). The swaged cable increased the effective resistance to axial loads although it required a larger diameter borehole to accommodate the increased of the cable diameter. Another approach was to insert two strands in one borehole together with spacers to provide some separation between cables. These are referred as double-plain strand cables (Matthews *et al.*, 1983). A common issue with these types of cable bolts was corrosion of the steel strands, which led to the development of epoxy-coated strands (Dorsten *et al.*, 1984). This extended the service life but it was difficult to install with a faceplate near the outside of the borehole.

A rapid development in cable bolt design began in the 1990s. The birdcaged strand was fabricated by unwinding the cable at regular intervals forming a suite of nodes and antinodes along the cable (Hutchins *et al.*, 1990). Although this enhanced the carrying capacity, it also increased the difficulty of inserting the cable into a hole. Windsor (1990) proposed the ferruled cable bolt by fixing metal ferrules along the strand, but this also brought in additional costs. The bulbed strand is another popular cable produced by compressing the cable axially to create a number of bulbs along the strand (Garford, 1990). The advantage of this design is that the bulb diameter and spacing can be varied to suite particular rock mass conditions. Ferruled cable bolts were developed and reported to be superior to standard cables due to the enlarged cross-section (Renwick, 1992). Another variant is the nutcaged strand produced by installing a hexagonal nut on the central or king wire of a standard cable and spinning peripheral six wires round the king wire. The big advantage of this design was that it doubled the capacity compared to plain cable bolts making it suited for support in highly fractured ground (Hyett *et al.*, 1993). A typical example of nutcaged cable bolts is the Megabolt strand which is commonly used in the Australian mining industry. As an alternative to the traditional steel cable, Mah (1994) proposed a cuttable strand made up of fiberglass. A graphical illustration of cable bolts mentioned above is shown in Figure 2 - 1 (Hutchinson and Diederichs, 1996).

Tadolini *et al.* (2012) suggested the indented strand with indentations along each steel wire, as shown in Figure 2 - 2. This cable bolt has an enhanced mechanical interlock between cables and surrounding grout column, resulting in an 89% increase in the bearing capacity compared with the conventional cable.

These products were generically termed modified cable bolts. The modified cable surface geometry improved the load transfer efficiency contributing to more widespread use of cable bolts for permanent reinforcement.

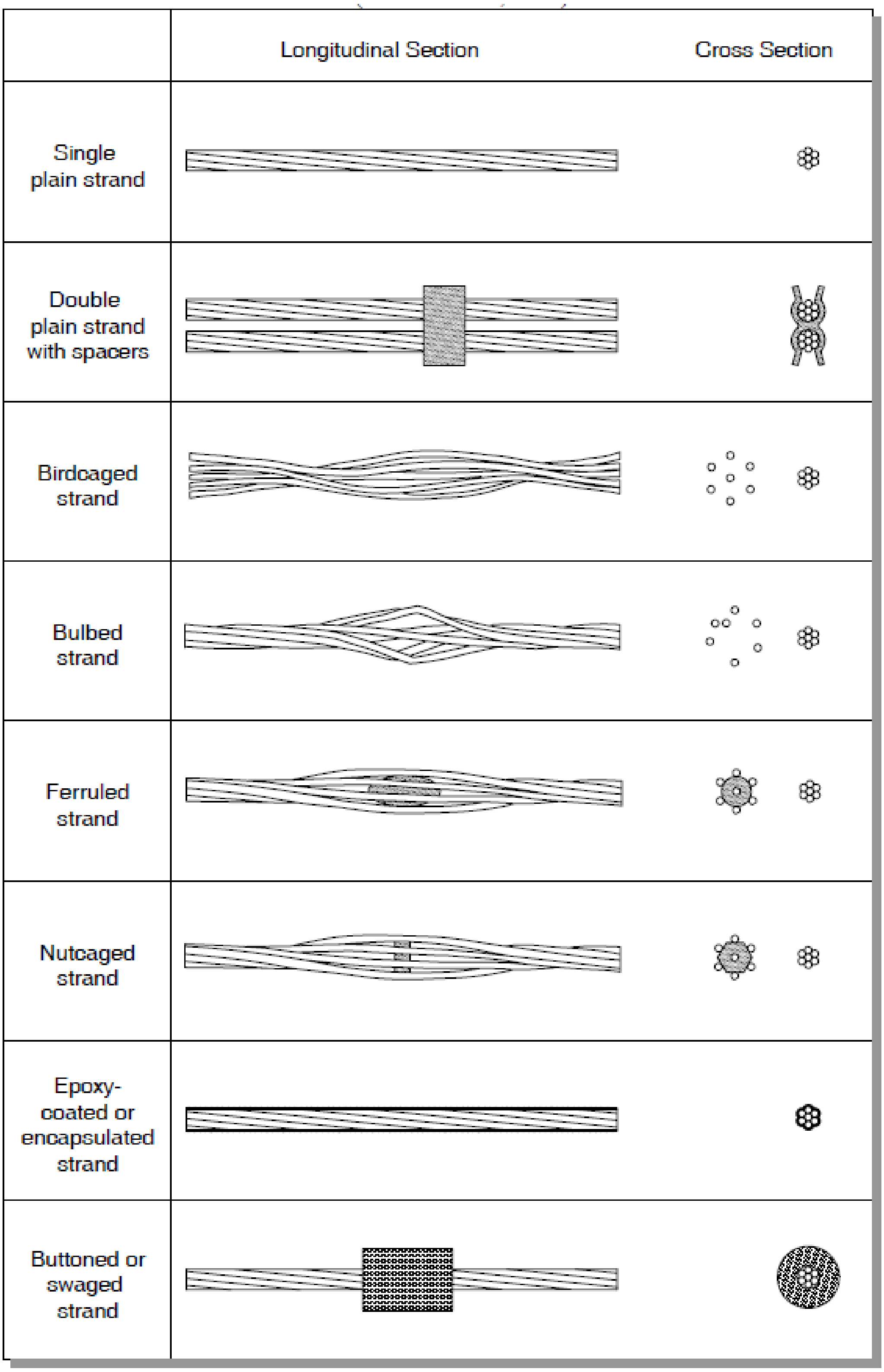

Figure 2 - 1 Cable bolt toolbox (Hutchinson and Diederichs, 1996)

Figure 2 - 2 Steel wires with indentations along the strand (Tadolini *et al.*, 2012)

2.3 Grout materials

For fully grouted cable bolts, there are generally two different types of grouts in use. One is cementitious grout and the other is resin-based grout.

2.3.1 Cementitious grout

Cementitious grout is the primary bonding material in cable bolting practices. It is generally made from appropriate materials such as limestone and clay, heated together and pulverized to form a powder (Hutchinson and Diederichs, 1996). This thesis mainly focused on cement-based grout.

Although various cement types exist in the market, most are based on Portland cement or its variants. The fundamental minerals are quite similar but with distinct differences in the proportions used in the mix. The properties of cementitious grout play a significant role in determining the performance of cable bolts and are usually controlled by varying the water-to-cement (w/c) ratio, which is defined as the ratio between the mass of water (m_w) and the mass of cement powder (m_c), as depicted in Equation (2 - 1):

$$w/c = m_w / m_c \qquad (2 - 1)$$

Hyett *et al.* (1992a) conducted comprehensive research in evaluating the influence of w/c ratio on the mechanical properties of Portland cement grout. The w/c ratio varied between 0.30 and 0.70. The influence of w/c ratio on the UCS is shown in Figure 2 - 3. The results showed that the grout UCS decreased with the w/c ratio. Nevertheless, a w/c ratio of 0.3 was not recommended, being too thick to be pumped. Furthermore, the scatter of strength results made a w/c ratio of 0.3 undesirable for field applications.

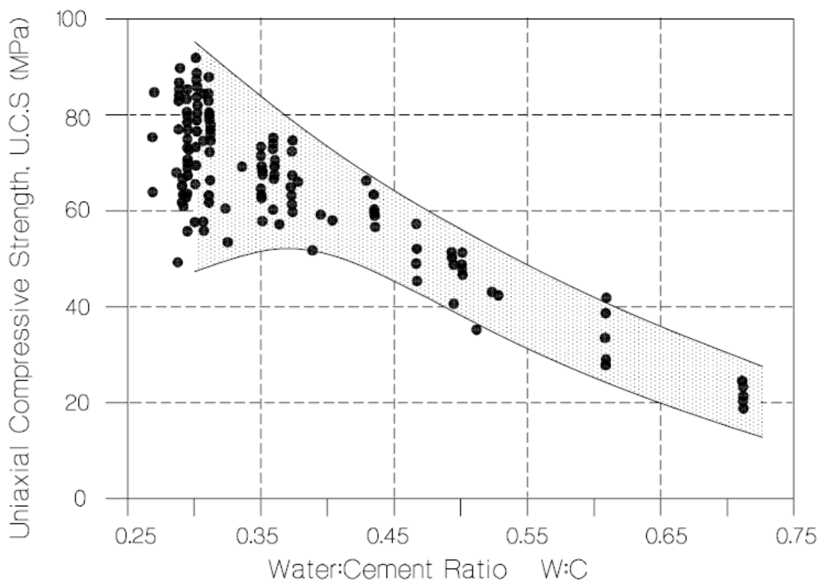

Figure 2 - 3 Effect of w/c ratio on UCS of Portland cement grout (Hyett *et al.*, 1992a)

The influence of w/c ratio on the Young's Modulus of Portland cement grout is shown in Figure 2 - 4. As can be seen, increasing the w/c ratio had a similar effect on the grout's Young's Modulus. And, it was recommended to use a w/c ratio ranging between 0.35 and 0.40 (Hyett *et al.*, 1992a).

In cable bolting practices, admixtures may be added to the grout mixture to improve the grout pumpability. The grout admixtures are normally organic or inorganic chemical substances in small amounts that physically alter the properties and behaviour of the cement paste (Hutchinson and Diederichs, 1996). Currently, there are a vast number of admixture types, such as plasticizers, retarders, accelerators, water retention admixtures and strength enhancing agents. Additionally, aggregates such as sands, gravels, crushed stones and slags may also be added to the grout mixture to increase the grout strength.

Moosavi and Bawden (2003) designed a direct shear box (Figure 2 - 5) and conducted shear tests on Portland cement grout. The results showed that increasing the normal pressure had an apparent impact on improving the shear strength of cement-based grout. However, their research was only limited to the Constant Normal Load (CNL) condition.

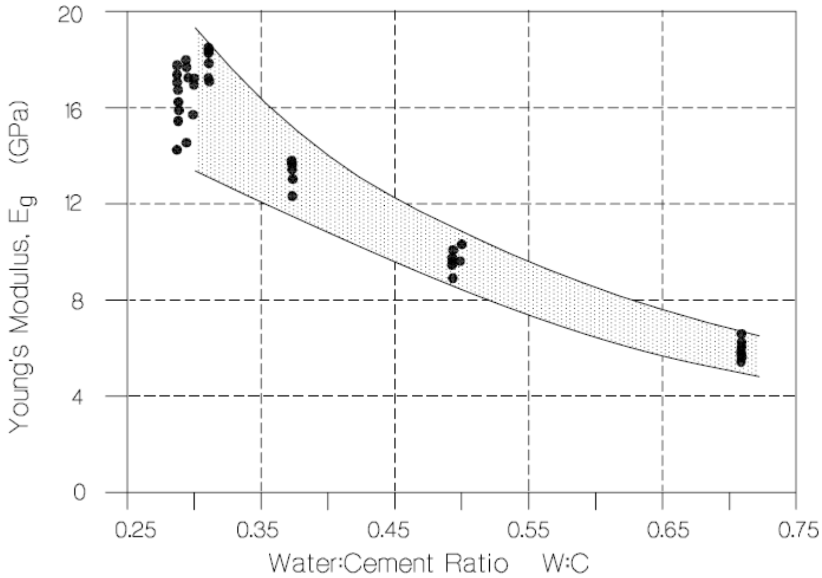

Figure 2 - 4 Effect of w/c ratio on Young's Modulus of Portland cement grout (Hyett *et al.*, 1992a)

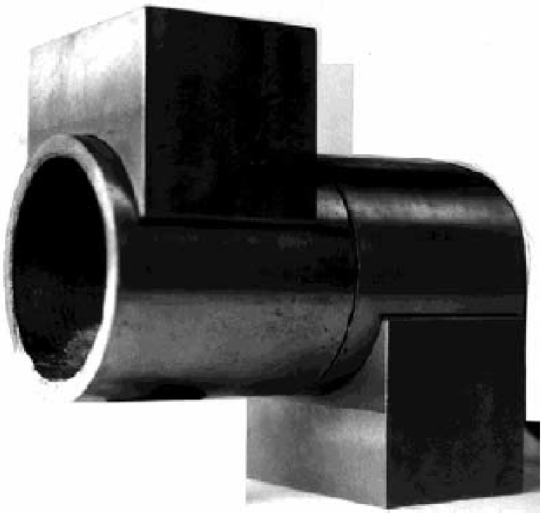

Figure 2 - 5 Direct shear box for cement-based samples (Moosavi and Bawden, 2003)

2.3.2 Resin-based grout

According to Tadolini (1994), resin-based grout was first used in cable bolting in the United States of America in 1992. Field practices showed that the resin-based grout was quite effective in weak rock masses and heavily loaded conditions (Campoli *et al.*, 1999). However, the resin-based grout has limited use in cable bolting practices, mainly due to the difficulty in spinning and installing cable bolts in boreholes filled with resin cartridges. Furthermore, using resin-based grout with cable bolts also increases the cost.

2.4 Installation methods

In practice, installation of cable bolts also has a significant impact on the *in-situ* mechanical behaviour (Hustrulid and Bullock, 2001). There are generally two different approaches to install cable bolts. One is the breather tube method and the other is the grout tube method.

- Breather tube method: This method is also named as “Bottom-up grouting”. Specifically, after the cable bolt is inserted into the borehole, a breather tube is pushed in the borehole until it is close to the borehole toe, as shown in Figure 2 - 6. Then, a plug is used to seal the borehole collar. The cementitious grout is pumped into the borehole via the grout pipe and the grout flows upwards from the bottom up to the top of the borehole. Meanwhile, the air is forced out from the borehole. It should be mentioned that this approach is mainly applicable to upholes and the w/c ratio usually ranges between 0.375 to 0.450.

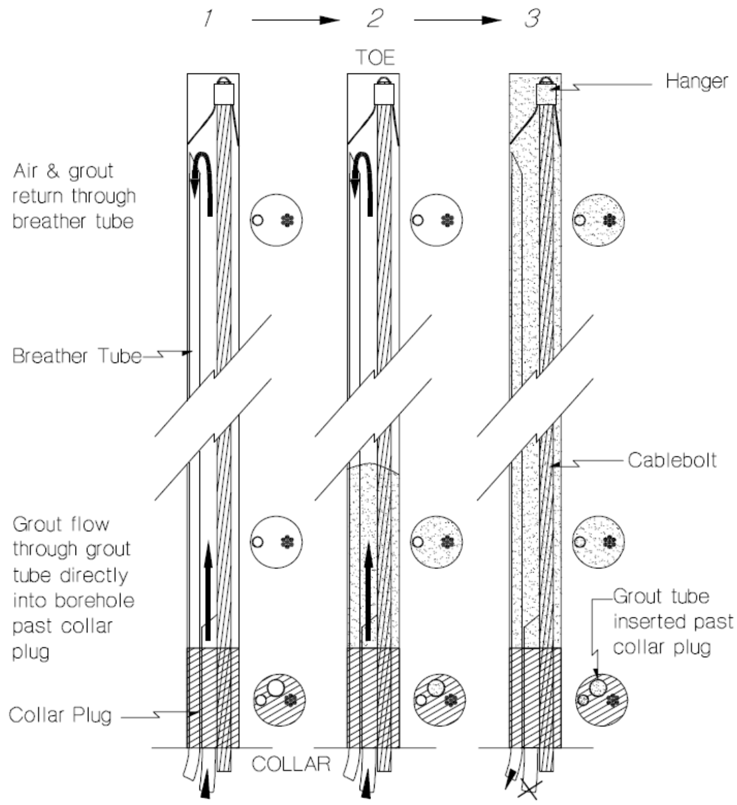

Figure 2 - 6 Breather tube method for cable bolt installation (Hutchinson and Diederichs, 1996)

- Grout tube method: It is also known as “Top-down grouting”. During installation, both the cable bolt and the grout tube are pushed to the back of the borehole and then the grout is pumped into the borehole, propagating from the top of the borehole to the borehole collar, as depicted in Figure 2 - 7. Although this approach can be used for boreholes with any orientation, the grout mixed should be thick, having a w/c ratio ranging from 0.300 to 0.375.

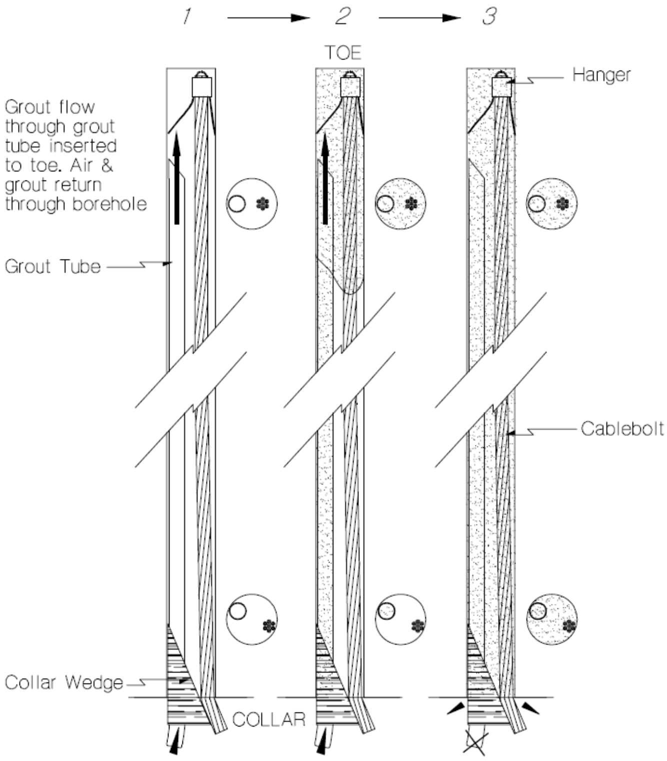

Figure 2 - 7 Grout tube method for cable bolt installation (Hutchinson and Diederichs, 1996)

2.5 Field applications

Fully grouted cable bolts are commonly installed in most excavations to reinforce the surrounding rock masses. The practical applications of cable bolts in the field are briefly described.

2.5.1 Cut-and-fill applications

In cut-and-fill mining activities, cable bolts are often used to reinforce the backs of stopes. For example, as shown in Figure 2 - 8, a number of fully grouted cable bolts are installed to maintain the stability of the crown of the cut-and-fill stope. The spacing between cable bolts is around 2 m. However, this interval can be varied dependent upon the properties of the surrounding rock mass. Generally, cable bolts are fixed normal to the excavation surface. However, in circumstances where shear movement of rock mass along discontinuities should be restricted, cable bolts would be installed obliquely to those discontinuities. Additionally, cable bolts installed in the cut-and-fill stopes can be used to reinforce the hanging wall, as shown in Figure 2 - 9.

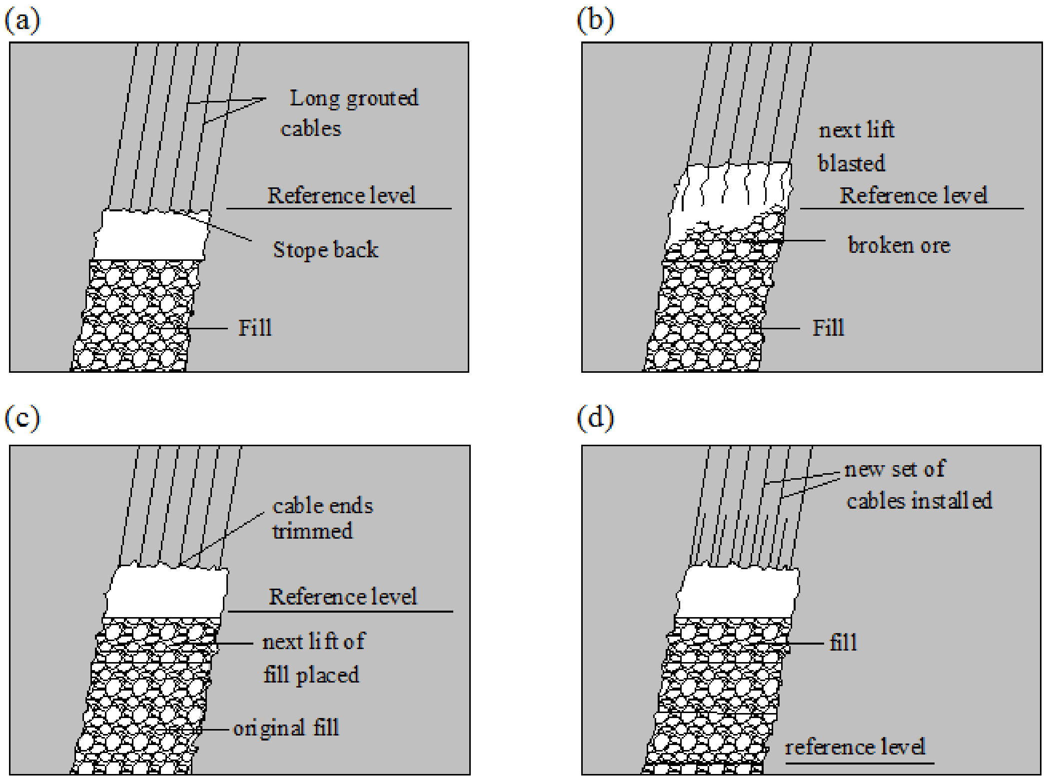

Figure 2 - 8 Cable bolts are installed in cut-and-fill mining activities, after Brady and Brown (1985)

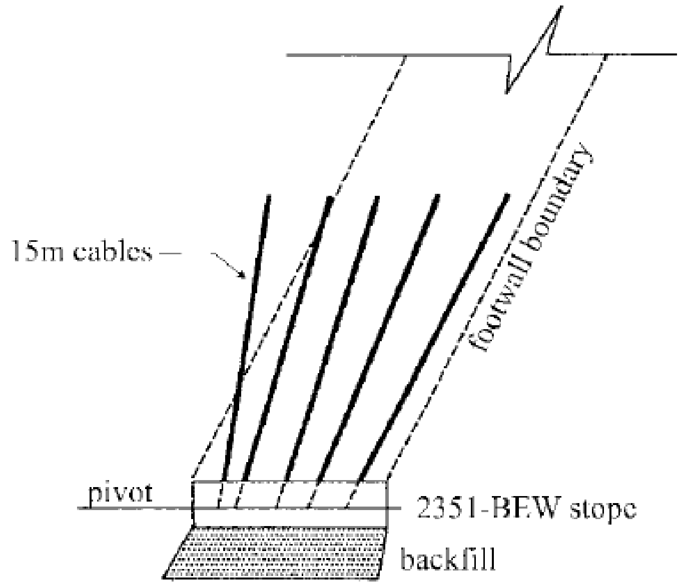

Figure 2 - 9 Reinforcement of the hangingwall with cable bolts (Bourchier *et al.*, 1992)

2.5.2 Open stope applications

In open stopes, cable bolts can be installed to reinforce both the backs and hanging walls, as depicted in Figures 2 - 10 and 11 respectively. Successful applications of cable bolts in open stopes have been previously reported (Matthews *et al.*, 1983; Donovan *et al.*, 1984; Lappalainen and Antikainen, 1987; Thompson *et al.*, 1987; Davidege *et al.*, 1988). Compared with cut-and-fill stopes, more surface areas are exposed in open stopes and slight reinforcement failures are tolerated. As for practical applications, it is recommended that the cable stiffness should be increased if the surrounding rock mass has low stresses. On the other hand, in extremely stressed rock mass, the cable bolt stiffness should be reduced to enable the rock mass to deform gradually (Khan, 1994).

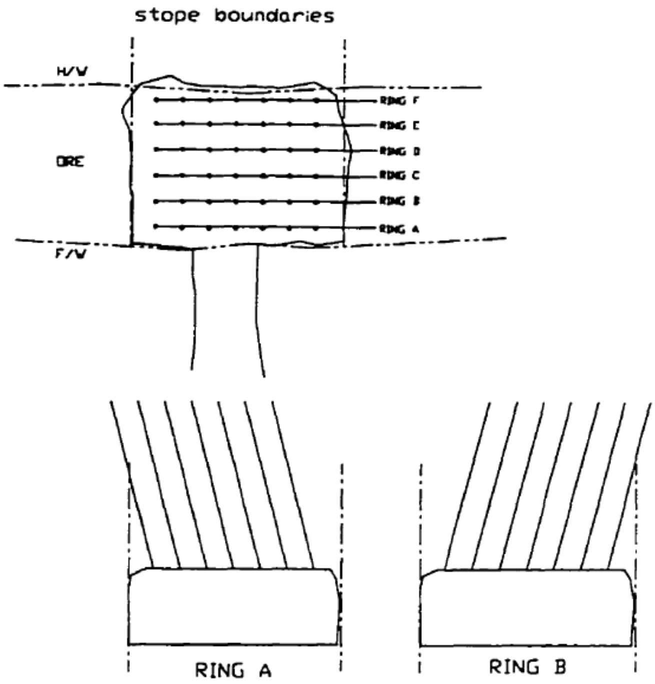

Figure 2 - 10 Interlaced back reinforcement (Anwyll, 1996)

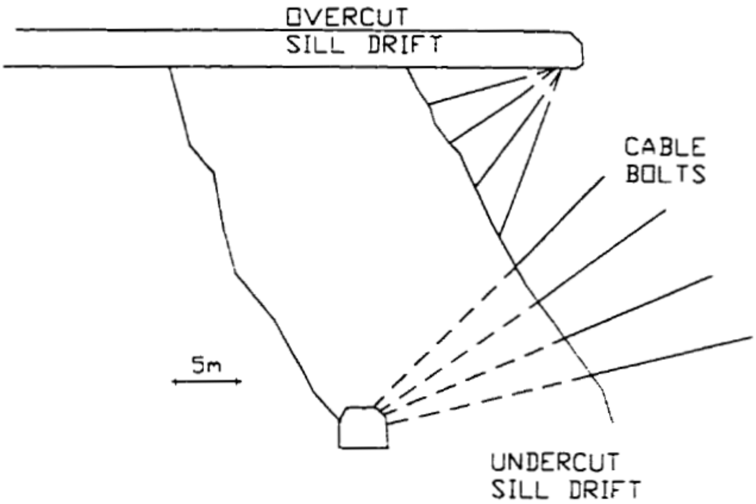

Figure 2 - 11 Attempt of using cable bolts to reinforce the hanging wall (Davis, 1977)

2.5.3 Drifts and intersections applications

It is also common to use cable bolts to provide reinforcement for underground drifts and intersections, as shown in Figure 2 - 12.

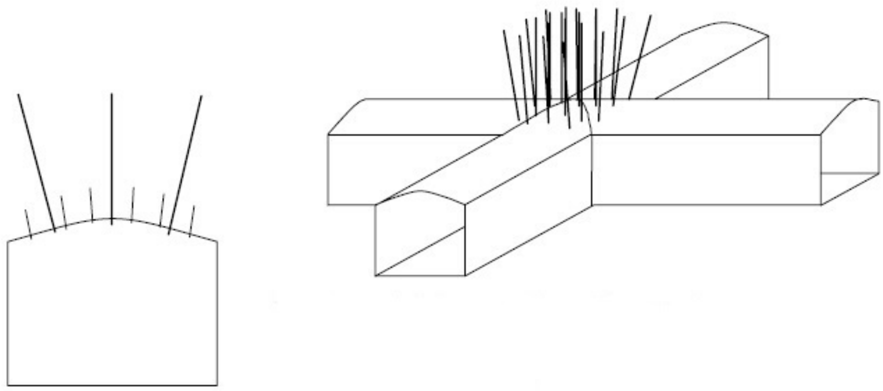

Figure 2 - 12 Reinforcement of the drift and intersection points with cable bolts (Hutchinson and Diederichs, 1996)

2.5.4 Pillar support

As a consequence of underground high stress environment, pillars may fail. To decrease the amount of pillar deformation, fully grouted cable bolts can be installed to provide reinforcement to pillars (Brady and Brown, 1985).

2.5.5 Drawpoint applications

Drawpoints play a significant role in some of the underground mining systems. The rock mass quality around drawpoints may be poor and the drawpoint can be subjected to high stresses. Consequently, failure of the excavation brow can lead to full loss of control of the stope draw operation. In earlier times, plain cable bolts were always used to reinforce drawpoints. But this type of cable bolts often failed in mining process. Thus, as recommended by Stillborg (1986), modified cable bolts were selected and installed in drawpoints in different directions (Figure 2 - 13).

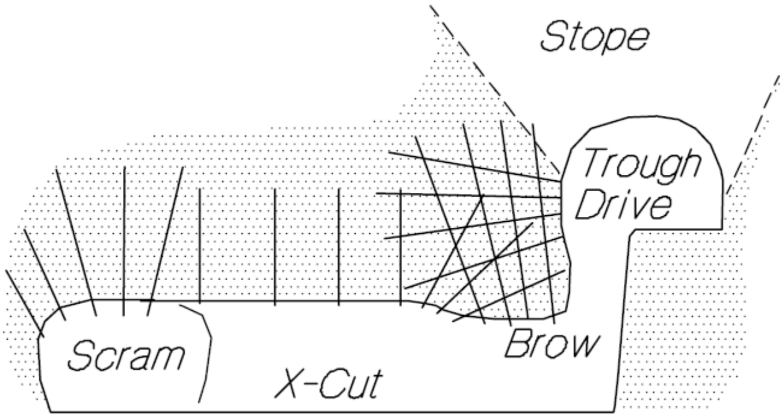

Figure 2 - 13 Drawpoint reinforcement with cable bolts (Stillborg, 1986)

2.5.6 Rockburst control applications

Cable bolts are also used for rockburst control. For example, as shown in Figure 2 - 14, the rock block could be ejected along the longitudinal direction of the cable bolts, reducing the consequence of after-effects of a rockburst accident.

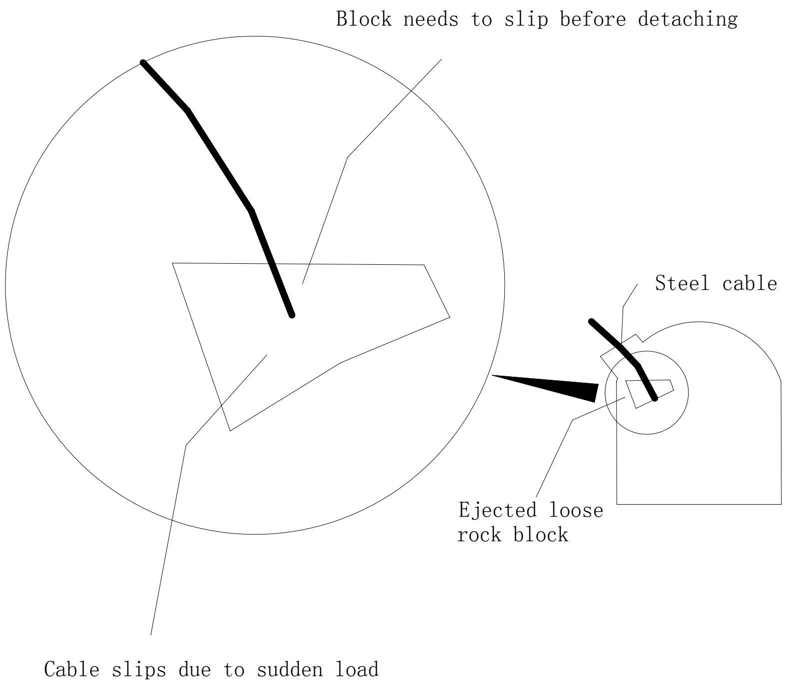

Figure 2 - 14 Slippage of a rock block along the cable bolt after rockburst, after Khan (1994)

2.6 Failure modes of cable bolts

For a fully grouted cable bolting system, there are basically four different mechanical components: the rock mass, the cable bolt element, the internal fixture and the external fixture, as shown in Figure 2 - 15.

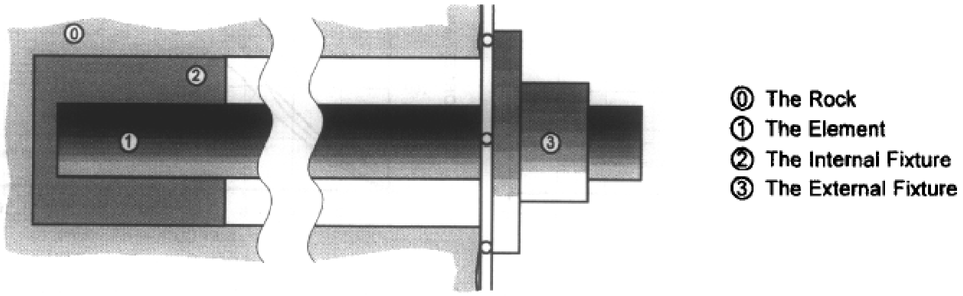

Figure 2 - 15 The major components involved in a bolt reinforcement system (Windsor and Thompson, 1993)

Failure of a cable bolting system can occur in any of those components. Moreover, according to Jeremic and Delaire (1983), generally five possible failure modes are likely to occur: the cable bolt itself (A); cable/grout interface (B); grouting material (C); grout/rock interface (D); and rock mass surrounding the borehole (E), as depicted in Figure 2 - 16.

Failure or rupture of the cable bolt is rarely observed, as a result of a shearing load along the grouted surface of the strand that is larger than the cable's maximum tensile capacity. Potvin *et al.* (1989) stated that it is more likely that a cable bolt will fail at the cable/grout or grout/rock interface, especially the former, determined by the interface shear strengths.

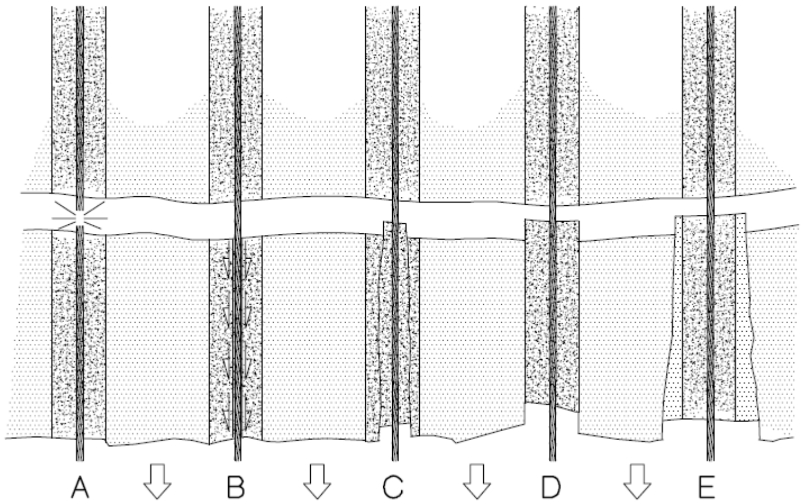

Figure 2 - 16 Possible failure modes of the cable bolting system (Jeremic and Delaire, 1983)

2.7 Load transfer mechanism

The performance of cable bolt reinforcement systems is largely dependent on the ability of load transfer. The load transfer was initially defined by Fabjanczyk and Tarrant (1992) as the mechanism by which force is generated and sustained in a supporting tendon as a consequence of strata deformation. Later, Windsor and Thompson (1993) modified this concept and indicated that it was comprised three fundamental mechanisms: (I) rock movement, which induces the transfer of load from unstable rock mass to the reinforcing tendon, (II) transfer of load from unstable rock mass to interior stable rock mass by means of the reinforcing tendon, and (III) transfer of load from the reinforcing tendon to the interior stable rock mass, as shown in Figure 2 - 17.

Based on the load transfer concept, the grout annulus which is either a cementitious or resin grout, provides the mechanism for transferring force between the rock mass and the cable bolt by means of shearing forces within the grout. Specifically, the shear stresses at the cable/grout and grout/rock mass interfaces are responsible for the load transfer mechanism. However, due to the smaller contact area, the shear stresses at the cable/grout interface are generally larger than the grout/rock interface. Therefore, assuming the rock mass and grouts have similar levels of strength and the anchorage length is insufficient, failure is more likely to occur at the cable/grout interface. However, when the rock mass strength is relatively weak and modified cable bolts, such as birdcage cables, are used, failure is more likely to occur at the grout/rock interface.

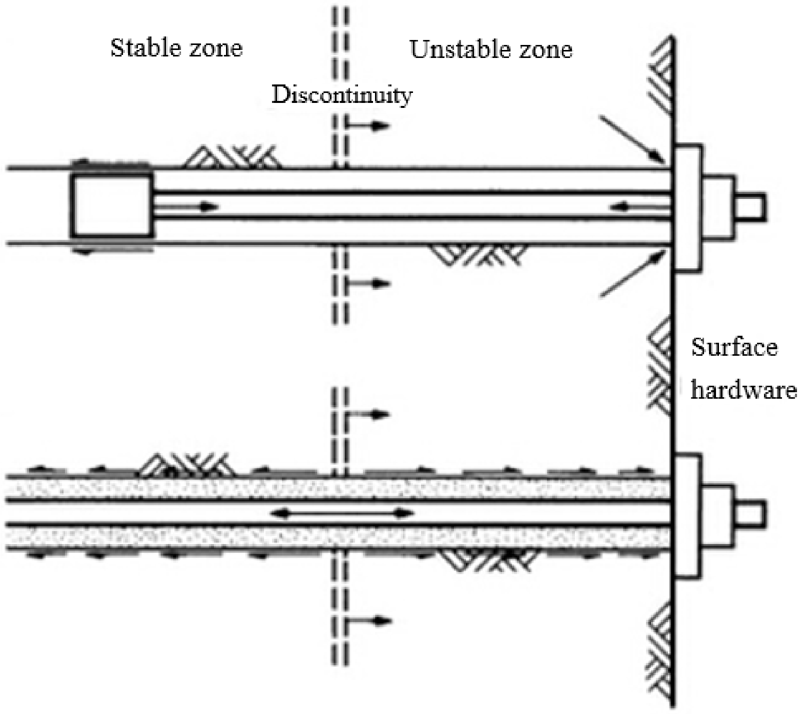

Figure 2 - 17 Load transfer concept of rock reinforcement systems (Windsor and Thompson, 1993)

To evaluate the load transfer efficiency, both peak shear stress capacity and system stiffness must be determined. The peak shear stress capacity is the average shear stress over a given encapsulation length at the maximum applied force (Fabjanczyk and Tarrant, 1992). And the system stiffness is the rate of shear stress produced. Although values for peak shear stress capacity and system stiffness can be analytically determined, most researchers prefer to rely on the load versus displacement relationship to analyse and compare the load transfer characteristics of cable bolts obtained from laboratory and field tests. Additionally, Thomas (2012) proposed the Load Transfer Index (LTI) to evaluate the load transfer efficiency for cable bolts, as depicted in Equation (2 - 2). This formula indicates a larger LTI will be acquired if the peak load is large and the displacement at peak load is small. Furthermore, load transfer efficiency improves with LTI.

$$\text{LTI} = \frac{\text{Peak load}}{\text{Displacement at peak load}} \tag{2 - 2}$$

2.8 Axial tests on cable bolts

2.8.1 Test approaches

Although fully grouted cable bolts are used in mining, there is no common standard for testing cable bolts' performance in the laboratory. Thus, researchers use various approaches to test cable bolts and the results can vary.

The simplest test method is the Single Embedment Pull Test (SEPT), also known as the "gun-barrel" test. Specifically, a cable bolt with a specific length is embedded in a confining medium, usually a metal tube (Figure 2 - 18). Then, the barrel and wedge system is used to grip the cable bolt at one end and a hydraulic cylinder pulls or extrudes the cable bolt out from the confining medium.

This test method has been widely used because of ease of handling (Farah and Aref, 1986b; Hassani and Rajaie, 1990; Mirabile *et al.*, 2010; Holden and Hagan, 2014). However, because of the special helical geometry, the cable bolt is likely to rotate during testing, which is not a true reflection of a cable bolting scenario in the field. As indicated by Bawden *et al.* (1992), rotation behaviour cannot occur along the full encapsulation length, restricted by the surrounding confining medium (Figure 2 - 19).

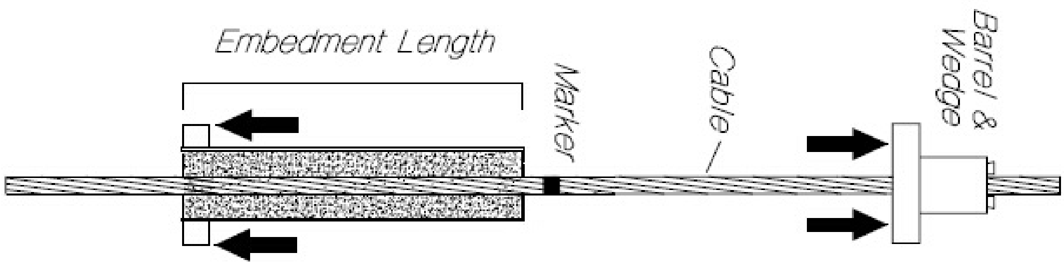

Figure 2 - 18 SEPT for cable bolts (Hutchinson and Diederichs, 1996)

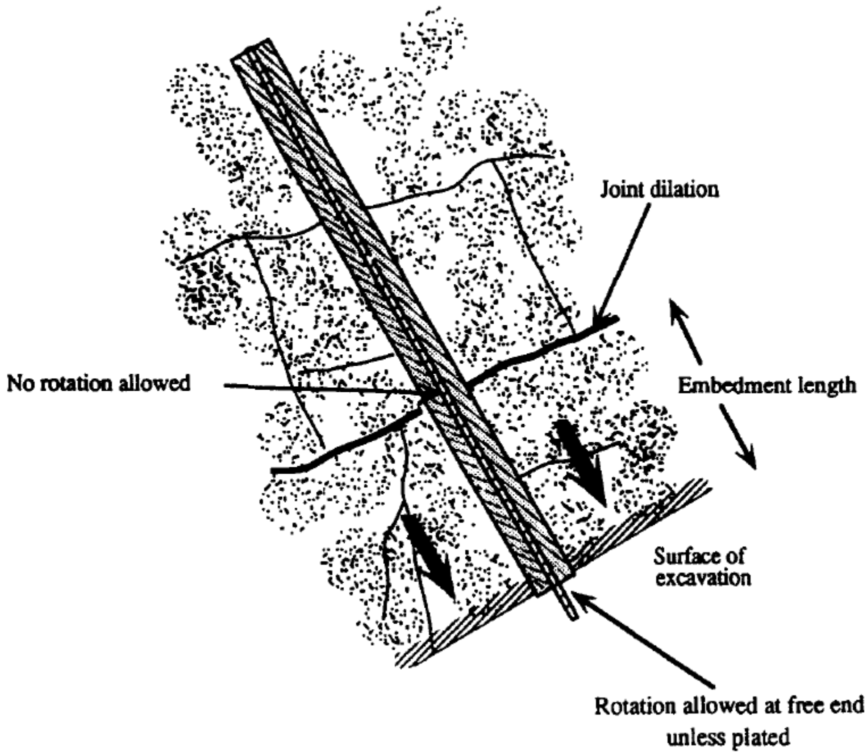

Figure 2 - 19 Scenario of a cable bolting system in the field (Bawden *et al.*, 1992)

Rotation of cable bolts is detrimental to performance in the SEPT because the peak load bearing capacity is much smaller than the cable bolt's non-rotating performance, as shown in Figure 2 - 20.

The pioneering work in non-rotating tests of cable bolts was conducted by Fuller and Cox (1975), in which a "Split-Pipe" Pull Test (SPPT) set up was proposed. The apparatus is basically composed of two parts, namely the upper section (or anchor length) and the lower section (or embedment length), as shown in Figure 2 - 21. Tubes made up of mild steel or other materials are used to simulate the rock mass, confining the grouted cable bolts in the upper and lower sections individually. The embedment length is the most important part and usually has a range from 250 mm to 450 mm. A washer is installed in the middle of the two sections, representing the rock joint. A Linear Variable Differential Transformer (LVDT) is attached to measure the axial displacement and a load cell is used to monitor the pulling load.

This equipment is effective in preventing cable bolts from rotating. Thus, the SPPT has been used many times by later researchers (Cox and Fuller, 1977; Nguyen *et al.*, 1986; Goris and Conway, 1987; Goris, 1991b; Mah, 1994; Thompson and Villaescusa, 2013). It should be mentioned that most of the SPPTs were conducted under the Constant Normal Stiffness (CNS) environment because the stiffness of the confining pipe was invariable in the whole test process. Macsporran (1993) performed a number of SPPTs under the CNL condition by using a modified Hoek cell to confine the grouted cable bolt in the embedment length, as shown in Figure 2 - 22.

Although the SPPT had long been accepted, Reichert (1991), mentioned that an extra confinement force may occur in the embedment length because of the gripping equipment at the unloaded end, which resulted in larger pulling load. To overcome this issue, a modified SPPT rig was developed by Reichert (1991), depicted in Figure 2 - 23. Compared with the conventional SPPT, the pulling head was fixed at the joint position and no extra confinement force was applied within the whole embedment section. Later, the modified SPPT approach was adopted by many researchers such as Hyett *et al.* (1992b), Hyett *et al.* (1993), Hyett and Bawden (1994) and Hyett *et al.* (1995a).

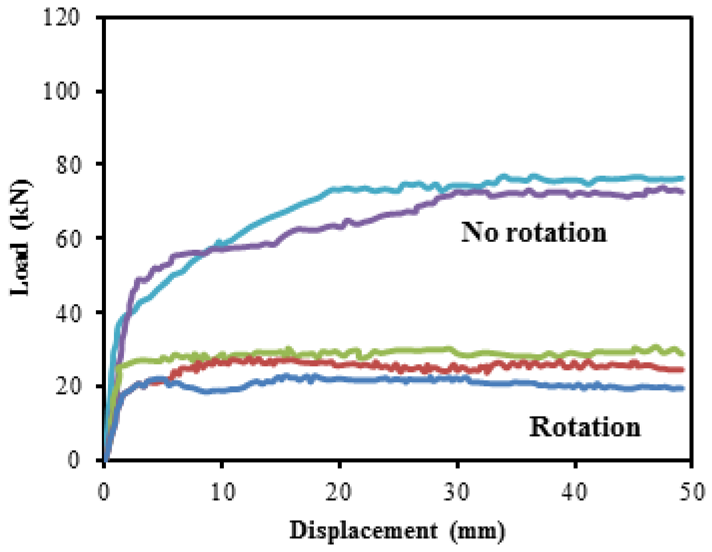

Figure 2 - 20 Comparison between rotating and non-rotating results, after Bawden *et al.* (1992)

Another test method that is able to prevent cable bolts from rotating is the Double Embedment Pull Test (DEPT), which was initially developed by Hutchins *et al.* (1990). As shown in Figure 2 - 24, a cable bolt was installed two individual steel tubes with the same length, and a gap between the two pipes simulates the rock joint. This test approach has the advantage of evaluating the load transfer capacity of cable bolts on either side of the discontinuity. As a result, this method was widely adopted in cable bolt testing (Renwick, 1992; Satola, 2001; Satola and Hakala, 2001; Satola and Aromaa, 2003; Satola and Aromaa, 2004; Satola, 2007). And the British Standards Institution adopted this approach to test the performance of birdcaged cable bolts (BS7861-2, 2009).

An issue common to both the SPPT and DEPT is the measured axial performance of the cable bolts is much stiffer than the real behaviour. This is due to steel tubes being used to simulate the rock mass, confining the grouted cable bolt and the stress - strain relationship of the steel material is largely different from the rock material. Furthermore, the tubes used are always threaded internally. Consequently, the failure mode of shear slippage along the cable/grout interface is artificially induced. Furthermore, this design prevents studying failure along the grout/rock interface.

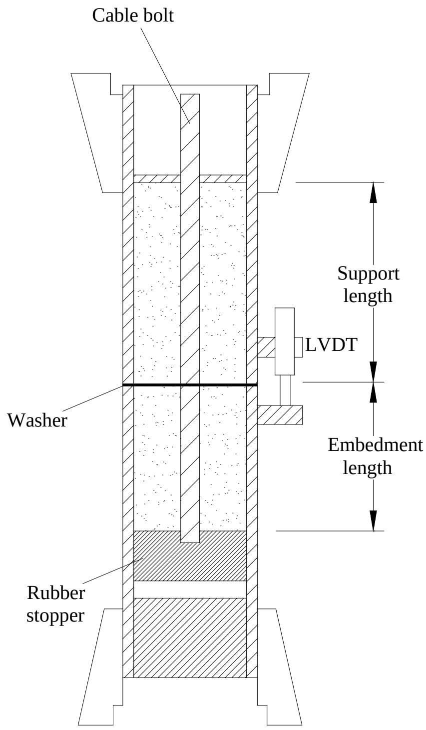

Figure 2 - 21 SPPT apparatus for testing cable bolts, after Fuller and Cox (1975)

To overcome this issue, Clifford *et al.* (2001) proposed the LSEPT, as shown in Figure 2 - 25. Specifically, a 142 mm diameter cylindrical sandstone confining medium is used to represent the rock material, confining the cable bolt with a length of 320 mm. Surrounding the sandstone core, a bi-axial cell is used to confine the cable bolt, grout and sandstone confining medium with a pressure of 10 MPa. The LSEPT has since been adopted as the preferred testing method for cable bolts (Altounyan and Clifford, 2001;

Kent and Bigby, 2001; Bigby, 2004; Bigby and Reynolds, 2005; Reynolds, 2006; Blanco Martín, 2012; Thomas, 2012). Furthermore, the LSEPT was later incorporated in the British Standard to especially test flexible bolts (BS7861-2, 2009).

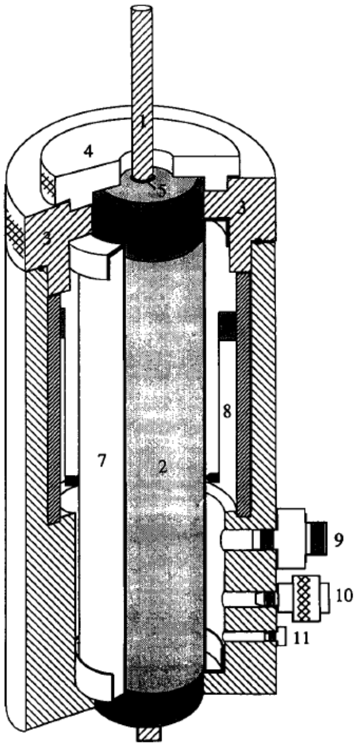

Figure 2 - 22 Sketch of the modified Hoek cell: 1) cable bolt; 2) cement annulus; 3) pressure vessel endcap; 4) endcap; 5) PVC pipe for debonding; 6) pipe for overcoming end-effects; 7) bladder; 8) strain gauge arms; 9) feedthrough; 10) high pressure fitting; 11) pressure transducer (Macsporran, 1993)

Nevertheless, there are still some problems involved in the current LSEPT. For example, as indicated by Khan (1994), the dimension of the bearing plate has an effect on the axial performance of the cable bolts. However, the standard LSEPT does not consider this bearing plate impact. Then, at times, the designed anchorage system is not able to provide reliable bond strength within the anchor length and in some cases, failure was found to occur in the anchor section (Reynolds, 2006). A constant confining pressure provided by the bi-axial cell is not a true reflection of the field stress which varies within the whole service life of cable bolts (Thomas, 2012). Moreover, plain strands tested in the LSEPT were likely to unscrew from the sandstone core, which is not a typical representative of the underground situation (Corbett, 2013). Additionally, it is difficult to ensure uniform properties of sandstone cores extracted from the field, and this workability can contribute to significant differences in pull-out performance of the cable bolts (Brown *et al.*, 2013).

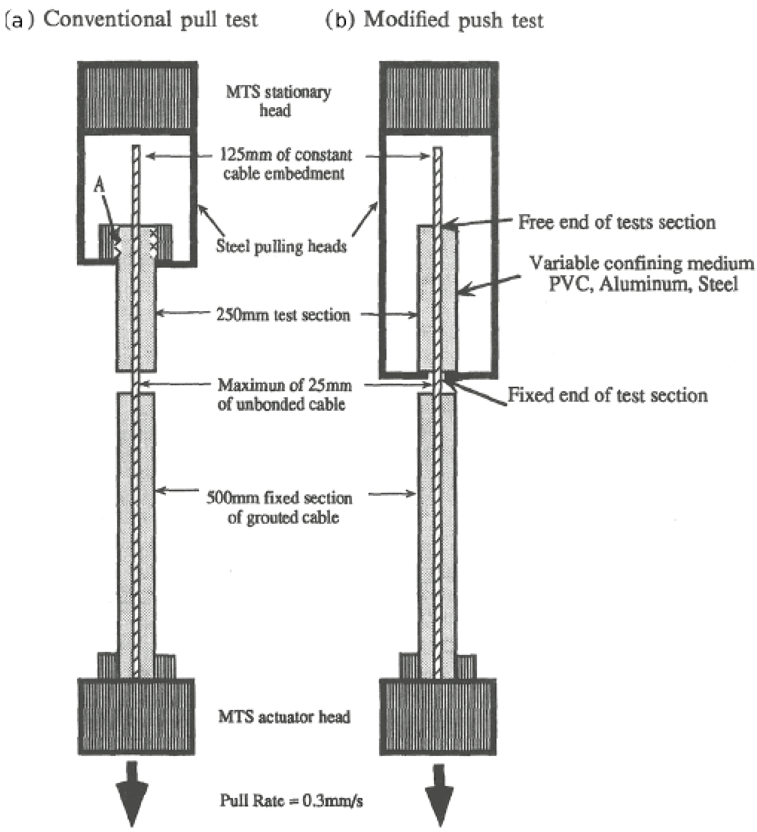

Figure 2 - 23 A comparison between the traditional SPPT and modified SPPT (Reichert, 1991)

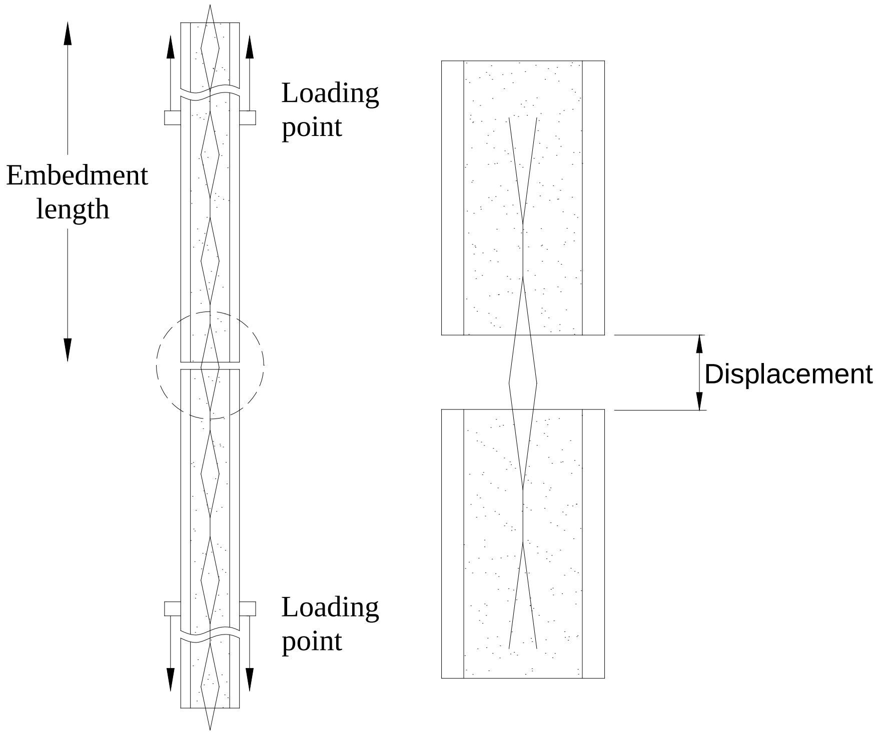

Figure 2 - 24 DEPT for cable bolts, after Hutchins *et al.* (1990)

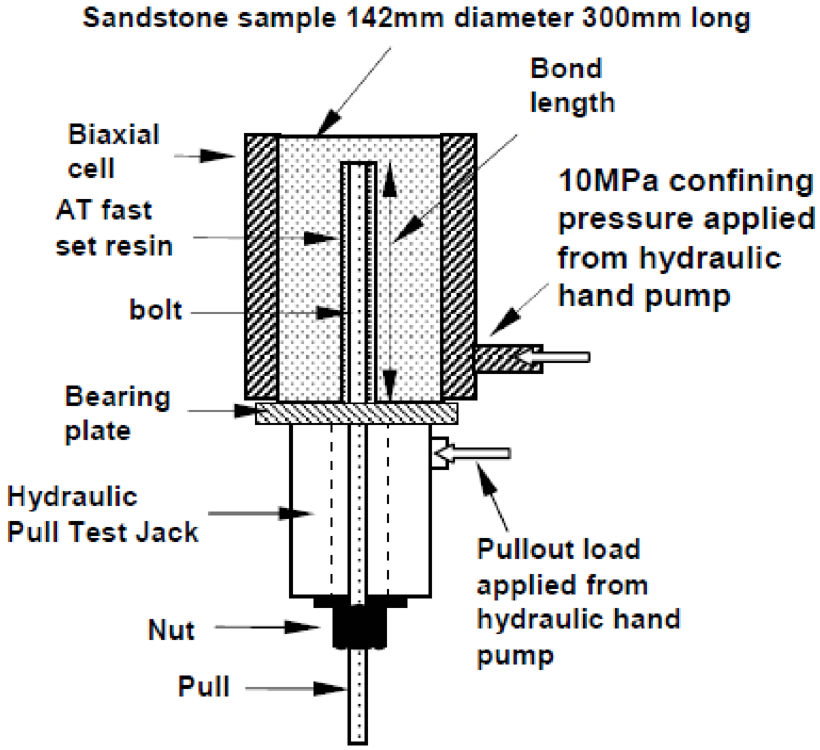

Figure 2 - 25 LSEPT for rock tendons (Clifford *et al.*, 2001)

2.8.2 Performance of cable bolts

Much research has been performed on the axial performance of fully grouted cable bolts in the laboratory. The effect of various parameters on the load transfer behaviour of cable bolts is listed.

2.8.2.1 Rock stiffness

Reichert (1991) evaluated the effect of rock stiffness on traditional seven wire cable bolts. Cable bolts were grouted with a constant embedment length of 250 mm in three types of tubes, namely steel, aluminium and PVC, respectively, simulating strong, medium and weak rock mass. Additionally, one test was performed in a heatshrink sleeve which could provide little confinement to the grouted cable bolt for comparison. Three series of experiments were conducted with the w/c ratio ranging from 0.3 to 0.5. A typical test result is shown in Figure 2 - 26. The graph shows that the bearing capacity of cable bolts pulled from steel pipes was more than double that for PVC pipes, indicating that the rock stiffness has a significant effect on determining the performance of plain cable bolts. A similar conclusion was also confirmed later by Hassani *et al.* (1992).

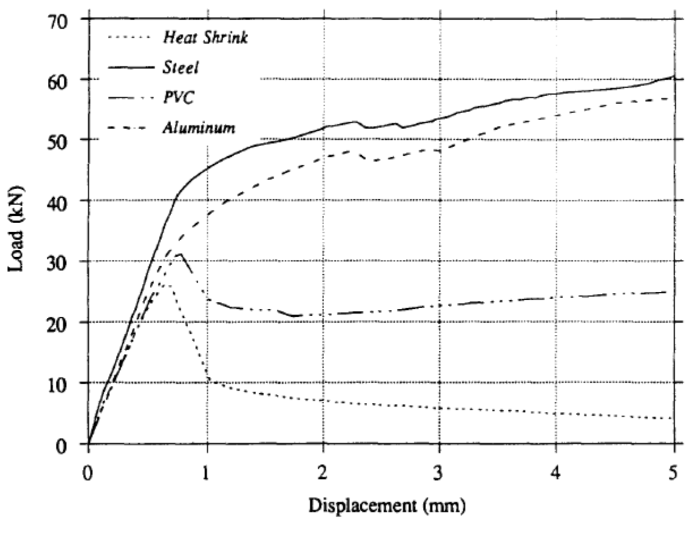

Figure 2 - 26 Load transfer performance of plain cable bolts under different confinement conditions (Reichert, 1991)

Reichert *et al.* (1992) conducted further research by conducting pull-out tests on same plain strands from granite, limestone and shale in the field and comparing the laboratory and field test results together. The confining medium stiffness was calculated. To calculate the pipe stiffness, the thick wall cylinder theory or Equation (2 - 3) was used:

$$K_r = \frac{2E}{(1+v)}\left(\frac{d_o^2 - d_i^2}{d_i\left[(1-2v)d_i^2 + d_o^2\right]}\right) \tag{2 - 3}$$

Where, K_r = the radial stiffness, N/m; E and v = the Young's Modulus and the Poisson's Ratio of the confining pipe respectively, Pa; d_o and d_i = the outside and inside diameter of the pipe, m. As for the cable bolt hole stiffness, Equation (2 - 4) was adopted:

$$K_c = \frac{d_d}{d_c}K_d \tag{2 - 4}$$

Where, K_c = the cable bolt hole stiffness, N/m; K_d = the dilatometer hole stiffness and was measured by using a high pressure dilatometer, N/m; d_d = the dilatometer hole diameter, m; and d_c = the cable bolt hole diameter, m.

With these experiments, the relationship between the maximum load bearing capacity of plain strands and confining medium stiffness was acquired. A typical example is depicted in Figure 2 - 27, which showed a good correlation between laboratory and field test results.

Hyett *et al.* (1992b) analysed both laboratory and field test results, determining that the pull-out load versus displacement curves of cable bolts can be divided into four different stages, as shown in Figure 2 - 28.

Stage 1: A linear relationship existed between the load and displacement, determined by the cable bolt, grout material and cable/grout interface property. Three different components, namely cohesion, mechanical interlock and friction, contributed to the bond resistance along the cable/grout interface.

Stage 2: Slippage along the cable/grout interface probably occurred when one of the following two conditions were satisfied: (1) radial splitting of the grout column; and (2) shear failure along the cable/grout interface. Either of those two different conditions would result in a reduction in the confinement of the surrounding medium.

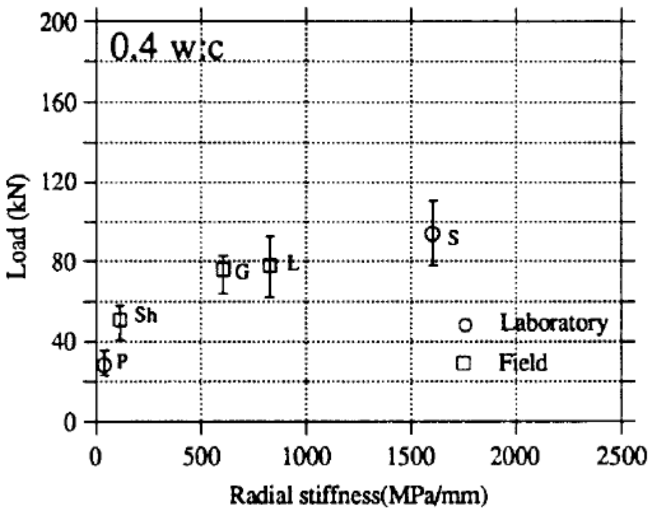

Figure 2 - 27 Comparison between laboratory and field test results. P = PVC; S = Steel; Sh = Shale; G = Granite; L = limestone (Reichert *et al.*, 1992)

Stage 3: The pull-out load acquired within this stage was mainly determined by two parts, namely the frictional resistance along the cable/grout interface and the residual strength of the grout column. Furthermore, two different failure mechanisms might occur. Specifically, if the confinement pressure was low, the surrounding rock mass would be split into wedges and the failure mechanism was radial movement of those wedges. However, once the confinement pressure was large, the failure would be the shear slippage of the cable tendon along the interface surface of the grout column.

Stage 4: The ultimate load bearing capacity of cable bolts was normally acquired when the pull-out displacement reached 40 or even 50 mm. In this stage, the geometric mismatch between cable bolts and grout column is maximal. After the peak load, the bearing capacity might decrease quickly, as a result of two causes: (1) a negative dilation angle of the cable/grout interface; and (2) ongoing cracking of the grout column. However, the tests and analysis mentioned above are only based on standard plain strands. The effect of radial stiffness on modified cable bolts was not studied in that period.

Hyett and Bawden (1994) focused on the impact of rock mass stiffness on modified cable bolts. Three types of metal tubes, namely Sch. 40 - aluminium, Sch. 80 - steel and Sch. 80 - aluminium, were tested. A number of tests were conducted on 25 mm Garford bulb cable bolts. Typical pulling results obtained from aluminium pipes are shown in Figure 2 - 29. The results showed that the load versus displacement performance of cable bolts was quite similar and there was no apparent difference between peak loads. Thus, the rock stiffness had almost no influence on determining the load transfer capacity of bulbed cable bolts. As for the reason, it was explained that the natural confinement pressure created in pulling bulbed cable bolts, was less sensitive to the stiffness of the confining medium, due to the special bulb geometry.

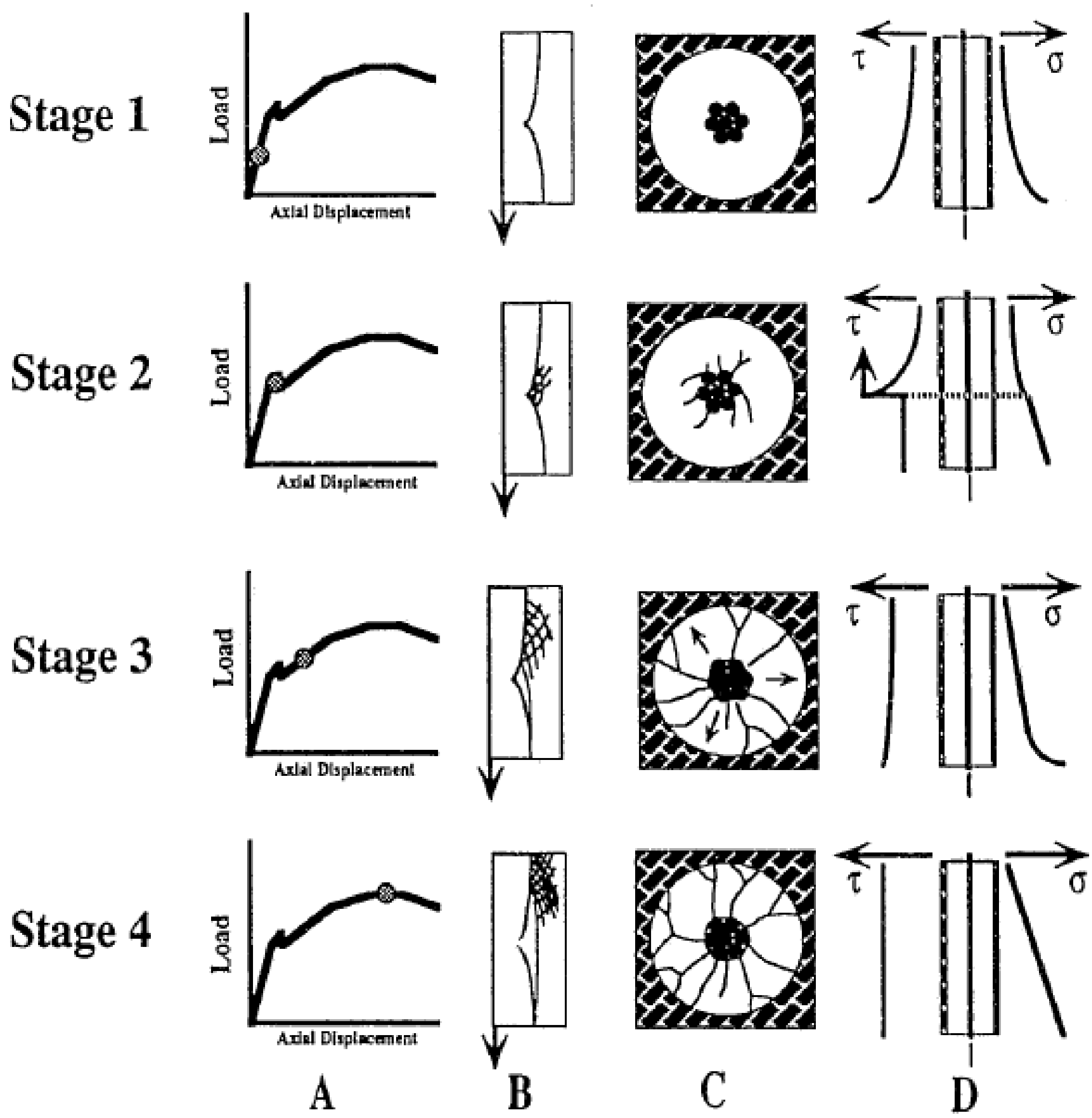

Figure 2 - 28 Four plots for a pull-out test: A) stage location of a load versus displacement curve; B) grout failure process in each stage; C) rock mass failure process; D) distribution of shear stress along the cable/grout interface and axial stress along the cable bolt (Hyett *et al.*, 1992b)

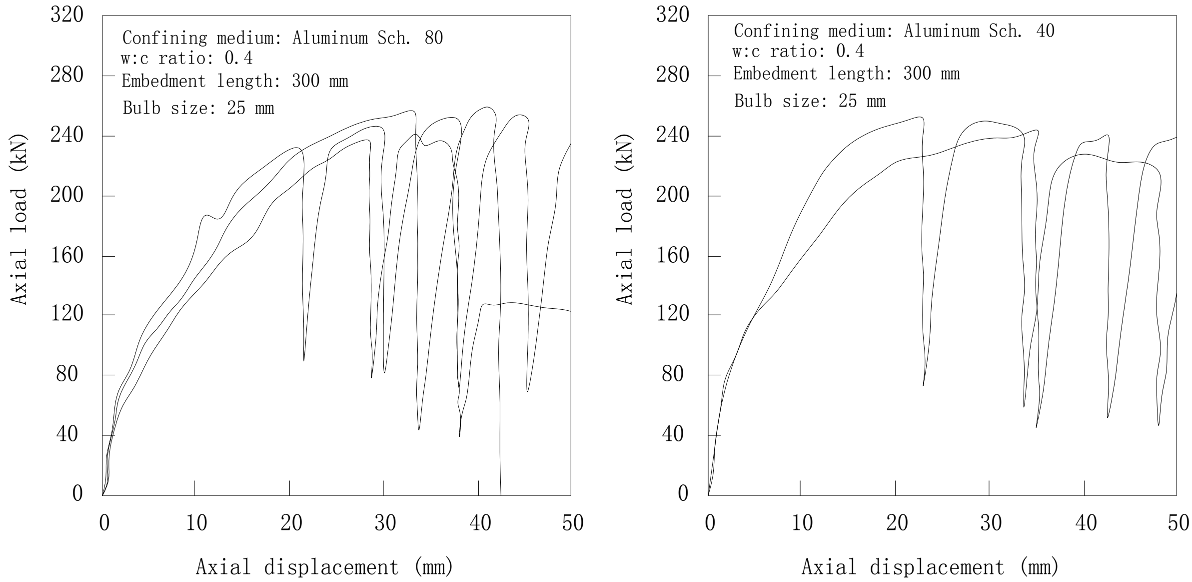

Figure 2 - 29 A comparison between results obtained from Sch. 40 and 80 aluminium pipes, after Hyett and Bawden (1994)

2.8.2.2 Embedment length

Fuller and Cox (1975) conducted a number of pull-out tests on 7 mm steel wires to study the influence of embedment length on the peak capacity of wires. The tested embedment length ranged from 100 mm to 700 mm. It was analysed that there was a linear relationship between peak load and embedment length. However, there is a large scatter of test results, reducing the credibility of this analysis.

A vast number of experiments were performed by Stillborg (1984) to evaluate the influence of embedment length on performance of cable bolts. Cable bolts with a diameter of 38 mm were installed in cylindrical confining medium with the embedment length ranging from 76 mm to 266 mm. The test results showed that there was a proportional relationship between the maximum bearing capacity of the cable bolts and embedment length (Figure 2 - 30). Furthermore, the results showed that chemical adhesion along the cable/grout interface was removed easily after only a short displacement of 0.2 mm, indicating that adhesive strength played only a minor role in determining the peak capacity. Nevertheless, the SEPT was used and cable bolts rotated in the pulling process, resulting in a low pulling capacity.

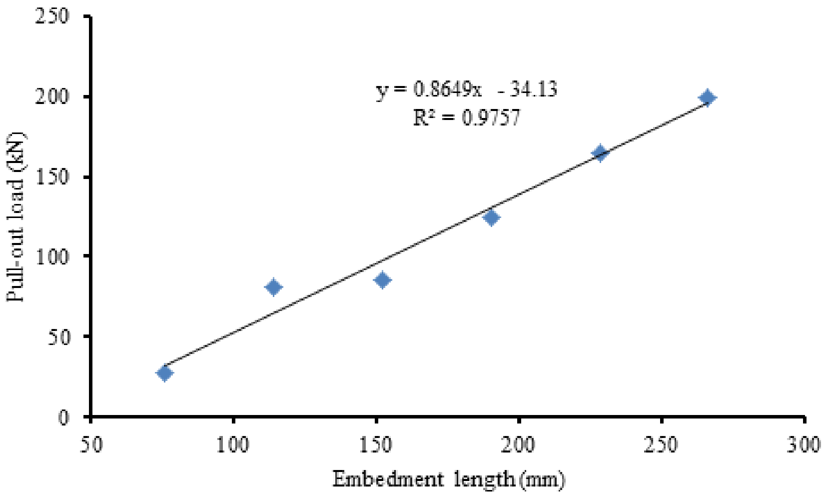

Figure 2 - 30 Peak capacity of cable bolts with different embedment length, after Stillborg (1984)

Since then, the relationship between the peak load and embedment length has been studied by many researchers and most have concluded that there was a linear relationship (Farah and Aref, 1986a; Goris, 1990; Rajaie, 1990; Benmokrane *et al.*, 1992; Hassani *et al.*, 1992; Reynolds, 2006). However, all focused only on plain cable bolts.

Mah *et al.* (1991) performed laboratory pull-out tests, attempting to find the critical embedment length which is defined as the encapsulation length of a pulling specimen required to induce cable bolt failure. Fibreglass Cable Bolts (FCB) were used and the embedment length ranged from 152 mm to 457 mm. The results showed that increasing the embedment length was beneficial to improving the bearing capacity of cable bolts. However, the critical embedment length was not ascertained.

Martin *et al.* (1996) did similar research to find the critical embedment length for standard cable bolts. The results showed that cable bolts ruptured at a pull-out load of 258 kN when the embedment length reached 914 mm. However, the critical embedment length is affected by many factors, such as the grout quality and the property of surrounding rock mass. Thus, the critical embedment length of 914 mm is only applicable to the situation in their research.

Chen and Mitri (2005) especially evaluated the effect of embedment length on bond strength, which is defined as the shear resistance to induce the shear slippage at the cable/grout interface along a unit contact area. Equation (2 - 5) was used to calculate the bond strength of the cable/grout interface:

$$\tau = \frac{P}{c(L-s)} \tag{2 - 5}$$

Where, τ = the interfacial bond strength, Pa; P = the pull-out load, N; c = the perimeter of cable bolts, N; L = the embedment length, N; and s = the shear slippage, m. Test results showed that although there was a linear relationship between the pull-out load and embedment length, the bond strength of the cable/grout interface was not influenced by the embedment length.

Thompson and Villaescusa (2013) conducted tests on plain cable bolts to evaluate the critical embedment length. It was found that within an embedment length of 1500 mm, failure occurred along the cable/grout interface. However, once the embedment length was longer than 2500 mm, the cable tendons ruptured. A non-linear extrapolation approach was used to determine the critical embedment length (Figure 2 - 31).

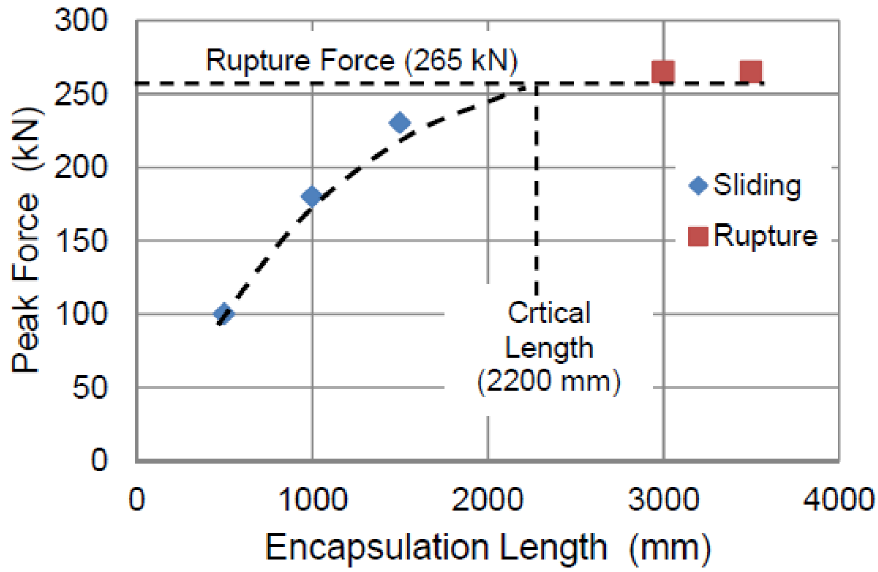

Figure 2 - 31 Predicting of critical embedment length for plain cable bolts (Thompson and Villaescusa, 2013)

2.8.2.3 Cementitious grout property

(1) w/c ratio

Cox and Fuller (1977) studied the effect of w/c ratio on pull-out performance of single wires. Three different w/c ratios were used, having UCS ranging from 18.4 MPa to 38.9 MPa. It was found that the lower the w/c ratio, the higher the grout strength, and as a consequence, the larger the peak load. However this research was only focused on steel wires and no test was attempted to evaluate the w/c ratio impact on cable bolts.

Similar research was later performed by Stheeman (1982) that concentrated on cable bolts. Three different w/c ratios, namely 0.300, 0.375 and 0.450, were used. The results showed that decreasing the w/c ratio was beneficial to improving the peak capacity of cable bolts. This conclusion was later confirmed by many researchers (Farah and Aref, 1986b; Goris, 1990; Mah *et al.*, 1991; Hassani *et al.*, 1992; Mah, 1994; Chen and Mitri, 2005). However, all these tests were conducted under CNS environments.

Macsporran (1993) studied the effect of w/c ratio on performance of plain cable bolts under CNL conditions. The w/c ratio was varied from 0.3 to 0.5 and a comparison between test results is shown in Figure 2 - 32. It can be concluded that a lower w/c ratio and consequently stronger mortar was effective in increasing the bearing capacity of cable bolts.

To investigate the influence of w/c ratio on load transfer performance of modified cable bolts, Hyett *et al.* (1993) tested nutcaged cable bolts with three different w/c ratios, namely 0.3, 0.4 and 0.5. It was found that nutcaged cable bolts could still sustain a large pulling load even when a high w/c ratio was used. Later, Hyett *et al.* (1995a) continued this research by testing w/c ratio effect on 25 mm Garfold bulb cable bolts. The results indicated that the w/c ratio had a little effect on determining the performance of bulbed cable bolts. Based on these two series of tests, it was recommended to use modified cable bolts in the field.

Mosse-Robinson and Sharrock (2010) also studied the influence of w/c ratio on bulbed cable bolts installed in large boreholes ranging from 42 mm to 106 mm. The results showed that increasing the w/c ratio resulted in a marginal decrease of the peak capacity of the bulbed cable bolts.

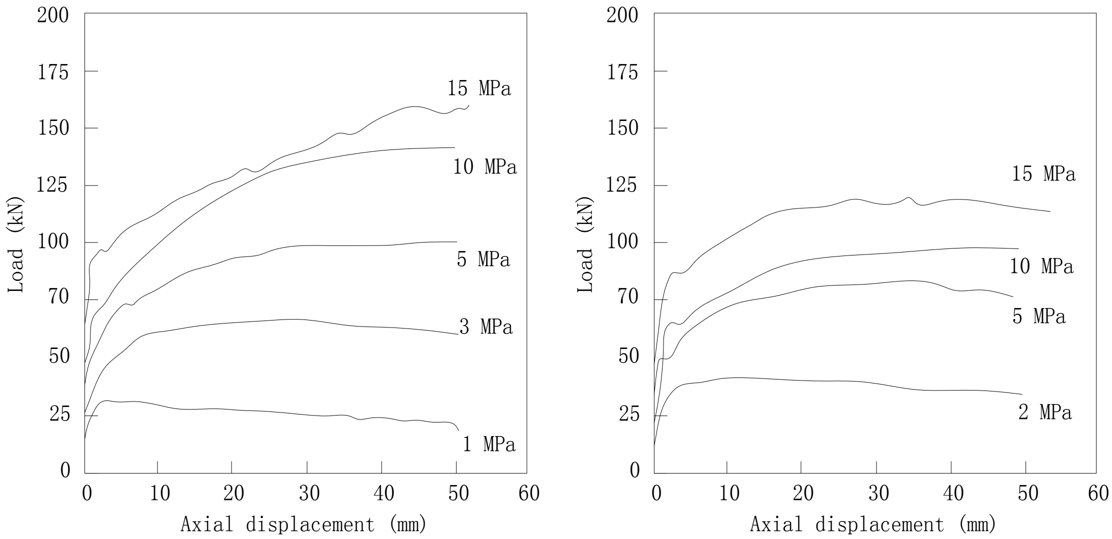

Figure 2 - 32 Performance of cable bolts with different w/c ratios under CNL condition. a) 0.3 w/c ratio (left); b) 0.4 w/c ratio (right), after Macsporran (1993)

(2) Grout additives

Hassani *et al.* (1992) tested high strength cement which was fabricated by adding silica powder into fresh cement on standard cable bolts. It was reported that the silica powder was beneficial to improving the bearing capacity of cable bolts not only in the peak stage but also in the residual range.

Similar research was later performed by Benmokrane *et al.* (1995) to evaluate the influence of grout additives on the performance of cable bolts. Two types of grout, in which one was cement paste with aluminium powder and the other one was cement paste mixed with silica powder and superplasticizer, were made. Test results indicated that the aluminium additive increased the bearing capacity of the cable bolts. On the other hand, silica powder and superplasticizer had minimal influence on the performance of the cable bolts. It was also found that the friction between the cable bolt and grout was the most important part in determining the peak capacity of cable bolting system, compared with mechanical interlock. However, one problem is that the mass of fresh cement was not identical, making the comparison of results difficult.

(3) Grout aggregates

Stheeman (1982) added sands to cement paste, aiming to study the influence of aggregate on load bearing capacity of the cable bolts. The test results showed that the sands reduced the peak capacity of cable bolts. However, the w/c ratio also decreased when adding sands into the grout. Thus, it may be not reasonable to conclude that adding sands by itself has an adverse impact on the performance of cable bolts.

Farah and Aref (1986b) compared the performance of seven wire cable bolts pulled from fresh cement paste and aggregate-cement based grout which was made by mixing cement, sand and coarse aggregates. It was found that the bearing capacity of cable bolts pulled from aggregate-cement based grout decreased slowly after the peak capacity, as shown in Figure 2 - 33. Furthermore, adding aggregates in cement paste was beneficial to improving the maximum load bearing capacity of the cable bolts. However, this research was only limited to standard plain cable bolts.

Hassani and Rajaie (1990) used shotcrete as aggregate and mixed it with cement paste, studying the effect of aggregate-to-cement ratio ranging from 0 to 4 on load transfer behaviour of cable bolts. Typical pull-out load versus displacement results of their study are shown in Figure 2 - 34. The results showed that the shotcrete aggregate had a significant effect on determining the residual performance of cable bolts. Specifically, cable bolts installed in aggregate-cement grout retained high residual load, which was similar to peak load. Moreover, increasing the aggregate-to-cement ratio led to decreasing the bearing capacity of cable bolts. Finally in their study, an optimum aggregate-to-cement ratio of 2 was recommended for field practice.

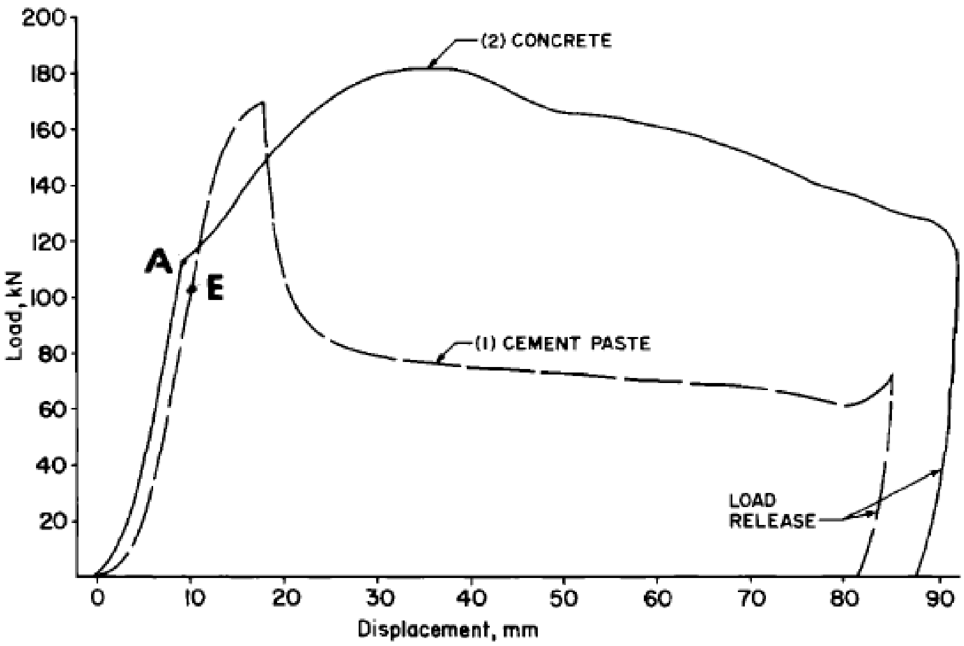

Figure 2 - 33 Load versus displacement curves of plain cable bolts pulled from two different types of grout (Farah and Aref, 1986b)

Benmokrane *et al.* (1992) used two types of grout to bond cable bolts. One was fresh cement paste and the other one was sand-cement based grout. Test results showed that adding an amount of sand increased the initial stiffness and peak capacity of the cable bolting system.

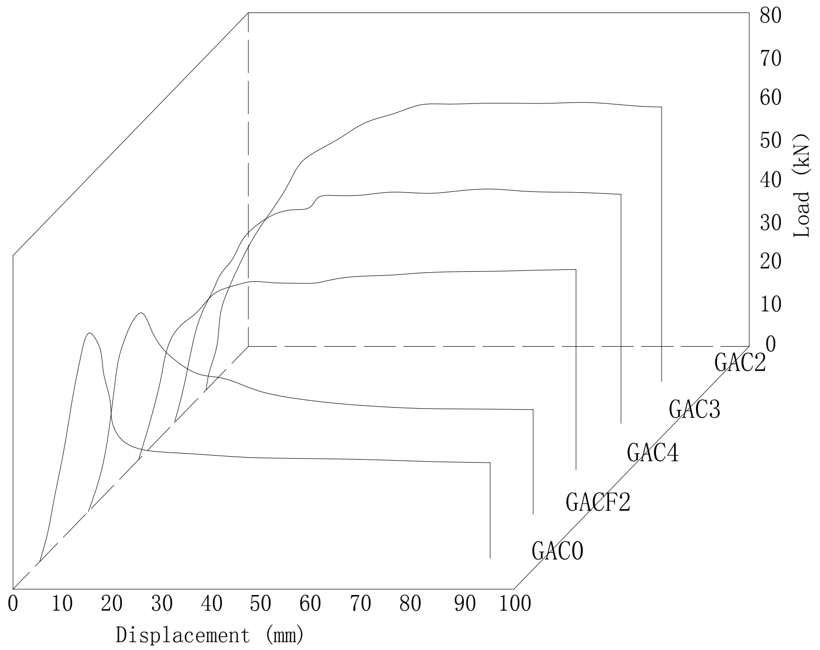

Figure 2 - 34 Pull-out load versus displacement curves of cable bolts. GAC represents grout with agreegate-to-cement ratio of 2, 3, 4; GACF 2 indicates grout with cement and fine aggregate ratio of 2, after Hassani and Rajaie (1990)

(4) Curing time

Mah *et al.* (1991) studied the influence of grout curing time on performance of FCB. Portland cement type III was tested and the curing time was varied from 2 to 10 days. The results showed that increasing the curing time did not apparently improve the bearing capacity of the cable bolts. However, this conclusion is only applicable to a limited curing time up to 10 days.

A different conclusion was derived by Hassani *et al.* (1992). It was found that the curing time has a significant influence on determining the load transfer performance of cable bolts. As shown in Figure 2 - 35, increasing the curing time improved not only the initial stiffness of cable bolting system but also the peak capacity of cable bolts. This conclusion was furthermore confirmed by later researchers (Chen and Mitri, 2005; Bigby *et al.*, 2010; Mosse-Robinson and Sharrock, 2010).

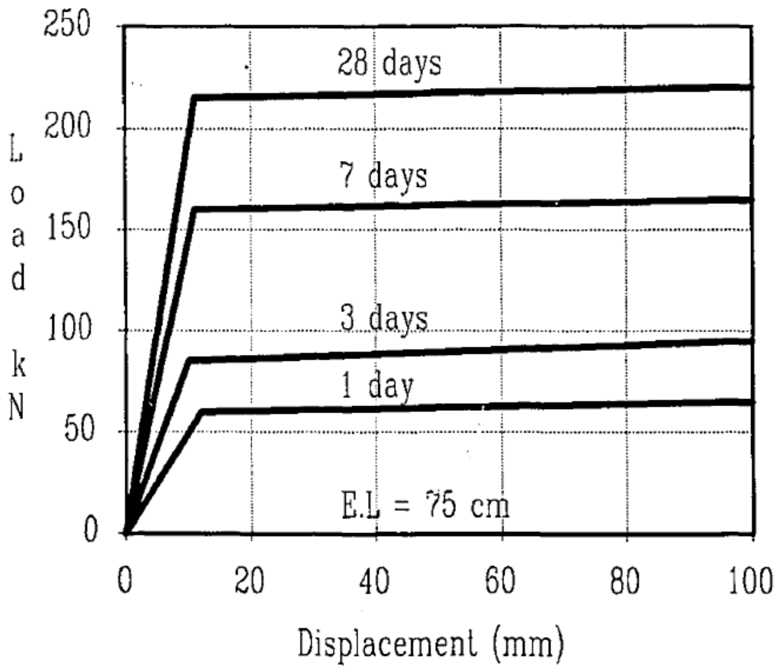

Figure 2 - 35 Curing time effect on performance of plain cable bolts (Hassani *et al.*, 1992)

2.8.2.4 Resin-based grout property

Kent and Bigby (2001) installed two series of Megabolt cable bolts in two different grout anchored systems, in which one was resin and the other was cement grout. After the tests, the performance of the Megabolt strands was compared, showing that the bond strength and initial stiffness of the cement grouted system was better than the resin anchored system.

Meikle *et al.* (2012) found that increasing the curing time from 1 day to 28 days would only improve the peak capacity of cable bolts by a small extent.

Faulkner *et al.* (2013) installed cable bolts in resin anchored systems with different installation methods. In one test, the cable bolt was rotated clockwise when installing and the other test used a counter-clockwise rotation method. The results showed that the counter-clockwise rotation of the cable bolts in resin reduced the bearing capacity of the cable bolting system. It should be noted that the cable bolt strands were twisted in the clockwise direction.

2.8.2.5 Modified geometry

(1) Buttons

Goris and Conway (1987) conducted pull-out tests on buttoned strands and plain cable bolts, finding that adding a button apparently improved the performance of the cable bolts. Furthermore, the button position relative to the joint had an effect on determining the peak capacity of cable bolts. Specifically, the greater the distance between the button and the joint in the embedment section, the greater the bearing capacity of the cable bolts.

Later, more pull-out tests were performed on buttoned cable bolts by Goris (1991a) to find that if the distance between the button and joint was larger than 152.4 mm, the bearing capacity of buttoned cable bolts became stable. Thus, a minimum distance of 111 mm was recommended. However, when installing buttoned cable bolts in field practices, it is rather difficult to determine the distance between the button and known joint.

Martin *et al.* (1996) found that the stiffness of cable bolting systems could also be improved by adding buttons along the cable bolt.

(2) Bulbs

A number of pull-out tests were conducted by Strata Control (1990) to study the influence of bulbs on the bearing capacity of cable bolts. It was found that increasing the bulb frequency along the cable length had a significant effect on improving the maximum load bearing capacity of cable bolts. This finding was later confirmed by other researchers (Hyett and Bawden, 1996; Mosse-Robinson and Sharrock, 2010).

Hyett and Bawden (1994) evaluated the influence of bulb size on load transfer performance of bulbed cable bolts. The bulbs tested were from 25 mm to 40 mm in diameter. The results showed that increasing the bulb size resulted in twisting of the steel wires around the bulb structure, reducing the bearing capacity of the cable bolts. Finally, a standard bulb size of 25 mm was recommended.

Pull-out tests on bulbed cable bolts under CNL conditions were performed by Moosavi *et al.* (1996). The results showed that the occurrence of bulb structure improved the performance of cable bolts to a great extent. Various other researchers used different confining materials to test bulbed cable bolts, and reached the same conclusion (Prasad, 1997; Ito *et al.*, 2001; Satola and Aromaa, 2003; Satola and Aromaa, 2004; Thomas, 2012).

(3) Birdcages

Hutchins *et al.* (1990) evaluated the performance of birdcaged cable bolts, finding that the birdcage geometry improved the bearing capacity of the cable bolts (Figure 2 - 36). Renwick (1992), Clifford *et al.* (2001) and Thomas (2012) had the same result. It was also found that the position of the nodes and antinodes relative to the joint made no apparent difference on the load transfer performance of cable bolts when both of them were embedded in the grout column.

However, Goris (1991a) derived a different conclusion based on his experimental test results. Specifically, a quantity of birdcaged cable bolts were tested and it was found that the position of nodes and anti-nodes had a remarkable effect on deciding the performance of cable bolts. For this reason, it was assumed that antinodes acted like anchors, increasing the bearing capacity of cable bolts. Finally, it was recommended to use grout to fully submerge the antinodes in field practice.

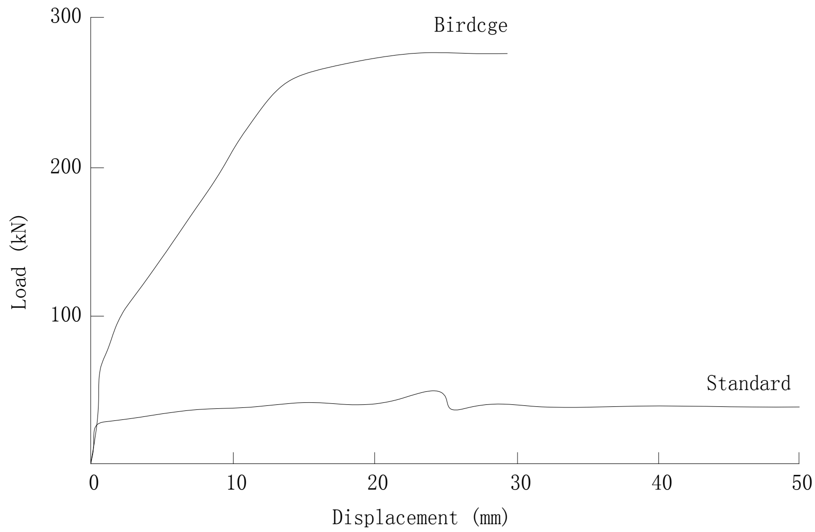

Figure 2 - 36 Comparison between birdcaged and standard cable bolts, after Hutchins *et al.* (1990)

(4) Multi-strands

Goris (1990) conducted pull-out tests on twin plain cable bolts, finding that the bearing capacity of twin plain strands was more than double of single plain cable bolt. Similar research was later performed on bulbed or birdcaged cable bolts by others such as, Strata Control (1990), Goris (1991a), Martin *et al.* (1996), Kent and Bigby (2001) and Thomas (2012), showing that the existences of the second strand could increase the bearing capacity of the cable bolts reach a high value.

(5) Fibreglass material

Mah *et al.* (1991) conducted pull-out tests on cable bolts made up of fibreglass materials. It was reported that the FCB was far more superior to standard plain strands. Further tests showed that the w/c ratio, the encapsulation length and the reinforcement geometry were significant in deciding the performance of FCB (Pakalnis *et al.*, 1994).

(6) Coating materials

Fuller and Cox (1975) studied the influence of rust on performance of steel wires. The results showed that compared with smooth wires, the rusted steel wires had a higher bearing capacity. It was determined that rust improved the mechanical interlock and friction between the wire and surrounding grout, which is beneficial to increasing the bearing capacity. This was further confirmed by Cox and Fuller (1977) with more experiments.

The influence of epoxy coating material on the performance of cable bolts was studied by Dorsten *et al.* (1984), showing that the epoxy coating material is beneficial to improving the performance. This was later confirmed by Goris and Conway (1987), Goris (1991b), Nosé (1993), Satola (2001), Satola and Hakala (2001), Satola and Aromaa (2003) and Satola and Aromaa (2004). Furthermore, Satola (2007) found that galvanized material was also beneficial to increasing the capacity of cable bolts, as shown in Figure 2 - 37.

Stillborg (1984) used a greasy substance as a coating material and painted it along the surface of plain cable bolts. A comparison was performed on pull-out tests on coated cable bolts and plain strands. It was found that the greasy substance reduced the load transfer capacity of the cable bolts. Thus, it was recommended to make the cable bolt surface clean before installation. This conclusion was also confirmed by others, such as Hutchins *et al.* (1990) and Satola (1999). The only difference was that after adding painting materials, modified cable bolts still attained a high load but with a much lower stiffness.

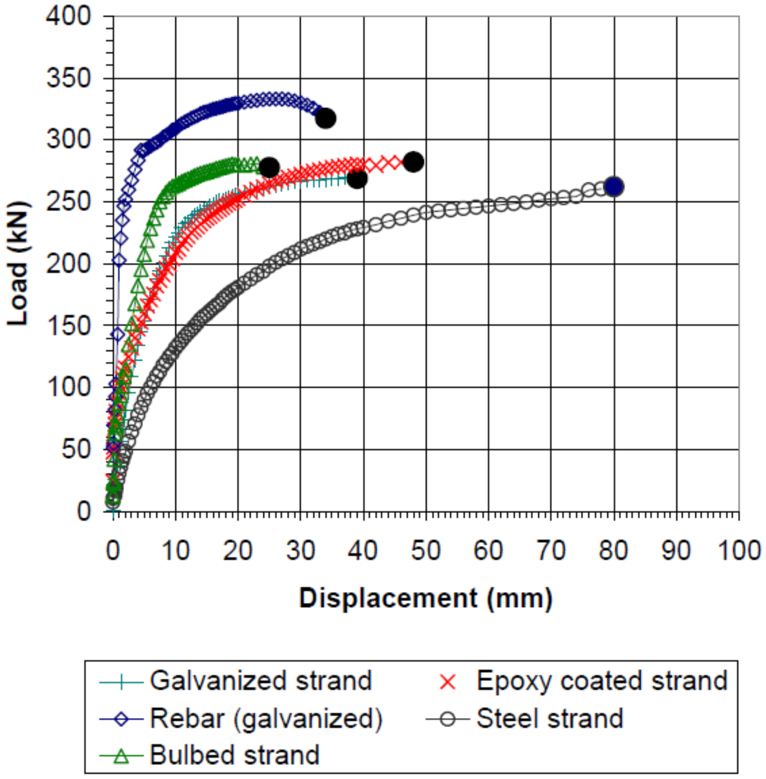

Figure 2 - 37 Comparison on performance of different bolts (Satola, 2007)

Mah *et al.* (1991) tested the performance of uncoated and coated FCB. However, only a few experiments were performed and no definite conclusion was made.

(7) Nutcases and ferrules

Renwick (1992) conducted pull-out tests on the Ultrastrand cable bolts to study the influence of the ferrule on the performance of the cable bolts. The results showed that the ferrule had a remarkable influence on improving the bearing capacity of the cable bolts. Furthermore, the Ultrastrand with a 5 mm ferrule had greater bond strength compared to a 2.5 mm ferrule configuration. However, the ferrule size was only varied in a small range in this research.

Hyett *et al.* (1993) evaluated the pull-out behaviour of nutcaged cable bolts, finding that the nutcaged cable bolt had much better performance than plain cable bolts. Moreover, the optimal nutcase size should be limited to 12.7 mm. The superior performance of nutcaged cable bolts was also confirmed by Moosavi *et al.* (1996) and Moosavi (1997).

A number of axial pull-out tests were performed by Kent and Bigby (2001) to study the influence of ferrules on performance of cable bolts. The results showed that adding a ferrule along the middle grout tube evidently improved the bearing capacity of the cable bolts, which was also agreed by Bigby (2004), Bigby and Reynolds (2005), Reynolds (2006), and Thomas (2012).

(8) Indentations

Fuller and Cox (1975) evaluated the influence of indentation position on performance of steel wires. It was revealed that although the indentation position had little influence on the peak capacity of steel wires, it greatly influenced the residual behaviour.

Tadolini *et al.* (2012) compared the performance of smooth and indented PC strands, finding that the existences of indentations along the wire improved the anchorage capacity of the cable bolts (Figure 2 - 38), which was also determined by Thomas (2012).

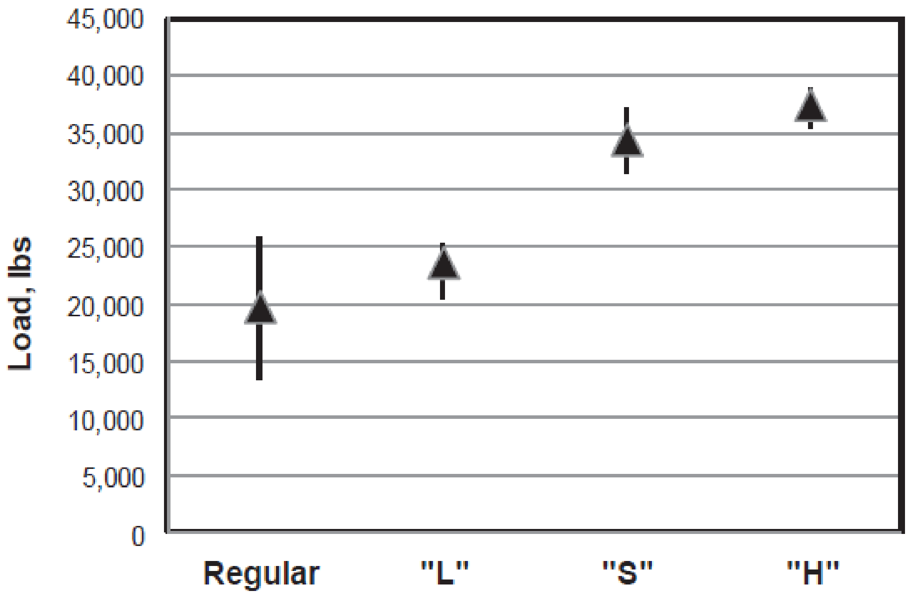

Figure 2 - 38 Comparison among performance of plain strands and indented cable bolts. L, S and H represent different indentation depth (Tadolini *et al.*, 2012)

2.8.2.6 Borehole size

The borehole size effect on the pull-out performance of cable bolts has been studied by a number of researchers. For example, Rajaie (1990) pulled plain cable bolts installed in concrete cylinders with different borehole diameters, finding that the borehole size had no influence on the performance of cable bolts, as shown in Figure 2 - 39. Mah (1994) used steel tubes to represent the rock and pulled FCB from tubes with different diameters, showing that the size of the borehole had minimal influence on the peak capacity of the cable bolts. The same conclusion was later confirmed by many researchers (Hutchinson and Diederichs, 1996; Martin *et al.*, 1996; Chen and Mitri, 2005; Mosse-Robinson and Sharrock, 2010).

Recently, Thomas (2012) used LSEPT to study the borehole size effect on the bond strength of cable bolts, finding that increasing the borehole diameter reduced the bearing capacity of plain cable bolts. On the other hand, for bulbed and nutcaged cable bolts, larger borehole size was beneficial to improving the performance of the cable bolts. But no explanation was given regarding this different influence.

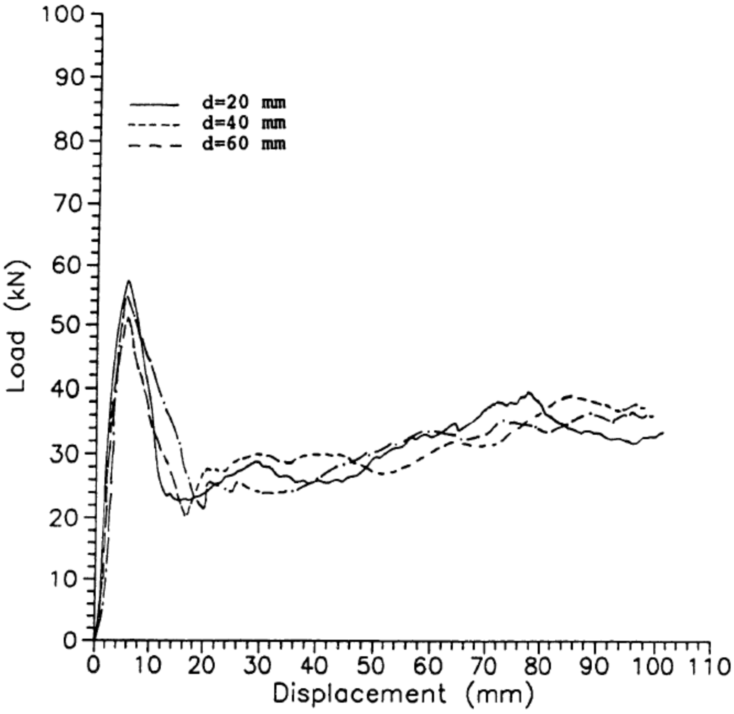

Figure 2 - 39 Effect of borehole size on performance of plain strands (Rajaie, 1990)

2.8.2.7 Rotation

Rotation of cable bolts was monitored by Stillborg (1984) when he pulled plain cable bolts from concrete cylinders. In those tests, many cable bolts unscrewed from the confining material. Furthermore, rotation partly reduced the bearing capacity of the cable bolts (Figure 2 - 40), which has been discussed and confirmed by later research (Bawden *et al.*, 1992; Blanco Martín, 2012; Cao *et al.*, 2012; Cao *et al.*, 2013b).

Moosavi (1997) conducted pull-out tests on bulbed cable bolts, finding that the modified surface geometry was effective in preventing cable bolts from rotating. This phenomenon was also observed by Ito *et al.* (2001).

Zhang *et al.* (2008) compared the performance of plain strands and modified cable bolts, saying that plain strands obviously rotated in axial tests while modified cable bolts only rotated a little bit in axial tests.

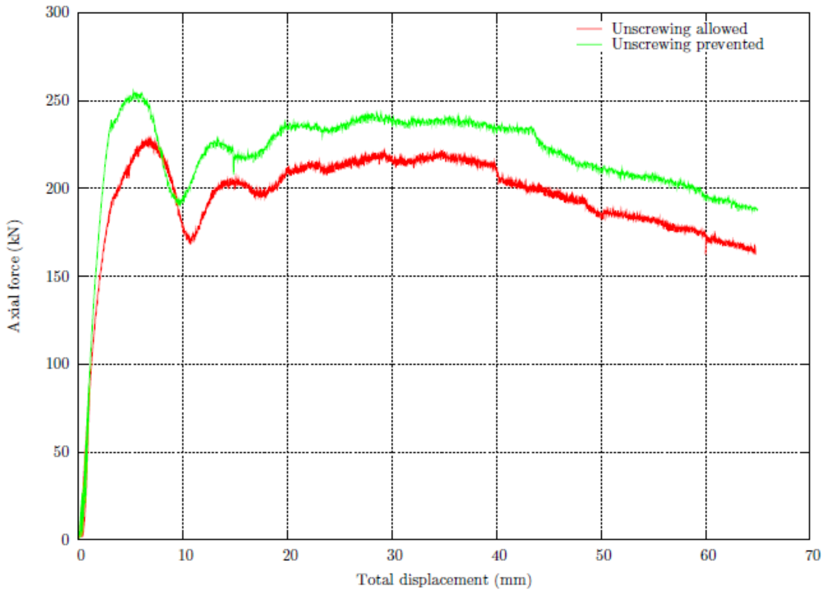

Figure 2 - 40 Influence of rotation on performance of plain cable bolts (Blanco Martín, 2012)

2.8.2.8 Pre-tensioning

Thompson and Windsor (1995) studied the influence of pre-tension on the load transfer of cable bolts. It was found that the pre-tensioning was effective in improving the shear strength of the rock mass. However, it did not make a difference in determining the internal stiffness of cable bolts, which was also confirmed by Mirabile *et al.* (2010).

Kent and Bigby (2001) conducted pull-out tests on pre-tensioned Megabolt cable bolts. The results showed that pre-tension was beneficial to enhancing the performance of cable bolting system especially under a low stiffness environment. However, pre-tension will also undoubtedly increase costs.

2.8.2.9 Stress change

Macsporran (1993) evaluated the influence of confining stress change on the bond strength of cable bolts. A CNL environment was applied on the confining medium and the confining pressure varied from 2 MPa to 15 MPa. The results showed that the performance of cable bolts was critically determined by the confining pressure, as depicted in Figure 2 - 41. However, this conclusion was limited to plain cable bolts.

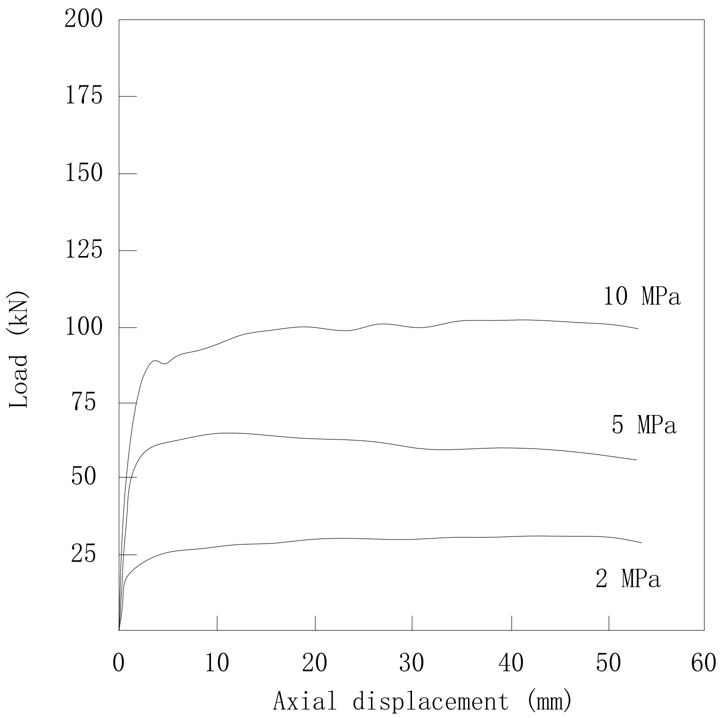

Figure 2 - 41 Performance of plain strands under different confining stress, after Macsporran (1993)

Nosé (1993) used the same approach to test coated cable bolts. He found that modified cable bolts could still retain high load transfer capacity when the confining stress changed, implying that the modified cable bolts were less sensitive to stress change. Later, Prasad (1997) tested bulbed cable bolts and determined the same conclusion.

2.8.2.10 The breather tube

Goris (1990) conducted pulling tests on both single and twin cable bolts to study the influence of the breather tube on the performance of cable bolts. The results showed that the existences of the breather tube did not influence the bond strength of the cable bolt system if the breather tube was filled with grout. This was supported with later research (Reynolds, 2006). Furthermore, the diameter of the breather tube had no influence on the performance of the cable bolts.

2.8.2.11 Loading rate

The influence of loading rate was carefully studied by Farah and Aref (1986b). Three different loading rates were used, simulating rock mass movement from fast to slow. Two types of cement-based materials were used to bond the cable bolt with the confining medium. One was concrete while the other one was cement paste. Testing results showed that cable bolts grouted with concrete had more ductility and larger peak capacity, indicating that using concrete rather than cement paste was more effective under a dynamic loading environment.

However, pull-out tests performed by Hassani *et al.* (1992) showed that for cable bolts installed with shotcrete bonding material, the loading rate had no influence on the axial performance.

2.8.2.12 Confining medium size

Rajaie (1990) studied the influence of cylindrical confining medium size on performance of standard cable bolts. The results showed that if the confining medium diameter was larger than 200 mm, the peak capacity of the cable bolts levelled off, as shown in Figure 2 - 42. However, this result is only applicable to plain cable bolts.

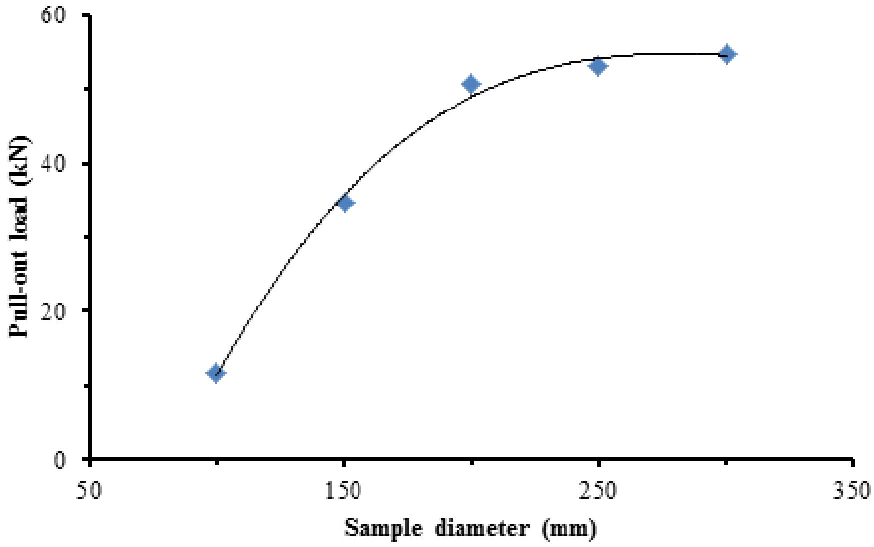

Figure 2 - 42 Size effect of the confining medium on peak capacity of cable bolts, after Rajaie (1990)

Holden and Hagan (2014) used the same approach to study the size effect of test specimens on the load transfer performance of cable bolts with bulbs. The results showed that the bearing capacity of the cable bolts increased with confining medium diameter.

2.8.2.13 Ambient temperature

Goris (1990) found that increasing the curing temperature is beneficial to improving the performance of cable bolts. It was explained that higher temperature increased the hydration of the cement grout, reaching a larger UCS strength sooner.

2.9 Shear tests on cable bolts

It should be mentioned that although the purpose of this thesis is to study the load transfer performance of cable bolts subjected to tensile load, the shear behaviour of cable bolts is also reviewed.

2.9.1 Approaches for shear testing

There are generally two types of setups for shear test on cable bolts, namely the single shear test and the double shear test. Specifically, the single shear test uses only one shear plane, as shown in Figure 2 - 43. The confining medium can be either concrete blocks or metal tubes. The single shear test is easy to perform and many researchers have used this approach to test cable bolts (Dight, 1982; Hutchins *et al.*, 1990; Khan, 1994; Miller and Ward, 1996).

However, there is an issue in the single shear test in that the test block may rotate, as indicated by Mahony and Hagan (2006), requiring additional instruments to prevent blocks from rotation. Furthermore, as indicated by Aziz *et al.* (2014), when metal tubes are used to confine the grouted cable bolt, "guillotine" of cable bolts by surrounding metal tubes always occurs, which is not a true reflection of shear performance between cable bolts and the rock mass.

Craig and Aziz (2010) designed a double shear test for modified cable bolts. Figure 2 - 44 shows that there are two shear planes in this apparatus. The double shear test is effective in preventing the test blocks from rotating (Aziz *et al.*, 2011; Aziz *et al.*, 2014; Aziz *et al.*, 2015b)

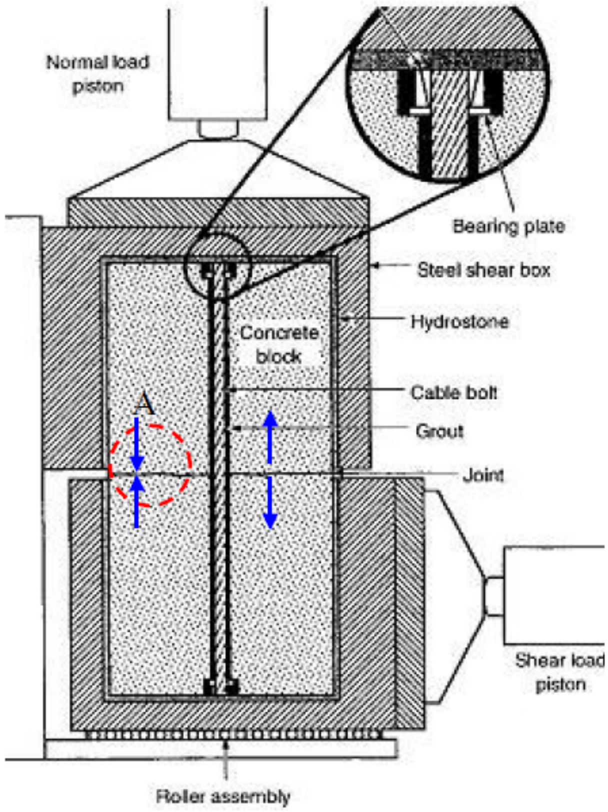

Figure 2 - 43 Single shear test on cable bolts (Goris *et al.*, 1996)

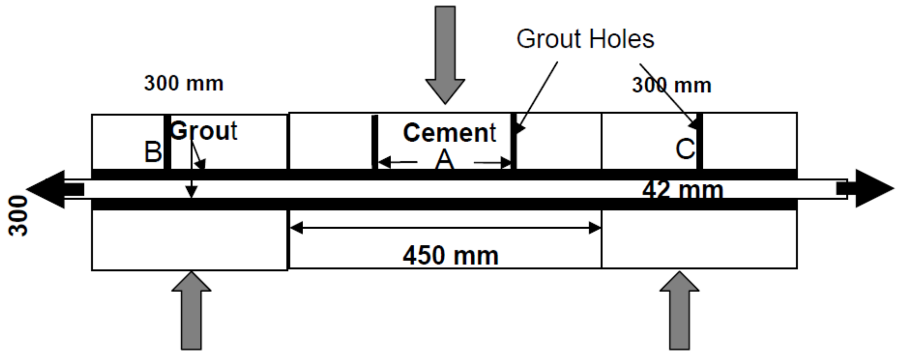

Figure 2 - 44 Double shear test on cable bolts (Craig and Aziz, 2010)

2.9.2 Performance of cable bolts

Dight (1982) studied the influence of embedment length and strand diameter on the performance of cable bolts. It was found that insufficient encapsulation length merely had an impact on the shear behaviour of cable bolt when large displacement occurred. As for the strand diameter, the larger the diameter was, the bigger the shear capacity the strand could provide.

Stillborg (1984) evaluated the influence of the inclination angle of the strands relative to the shear plane on the shear load transfer. The results showed that cable bolts installed with an inclination angle of 45° relative to the joint provided larger shear resistance than those installed of 90°, which was further confirmed by Windsor (1992) and Miller and Ward (1996).

A few shear tests on FCB were performed by Mah (1994), indicating that the FCB had a mean shear strength of 63 kN when the shear load was vertical to the cable bolt axis.

Hutchins *et al.* (1990) executed a number of shear tests on birdcaged cable bolts, finding that the shear capacity of the cable bolts was much lower than the axial rupture load. However, in some tests, the cable bolts were directly cut off by steel tubes.

Khan (1994) used two steel tubes to confine cable bolts and tested the influence of joint spacing on the shear performance of plain cable bolts. The results showed that the shear performance of the cable bolting system was significantly affected by joint spacing. Specifically, larger joint spacing led to a reduction of the shear capacity, as shown in Figure 2 - 45.

Bawden *et al.* (1994) designed a single shear test apparatus, as shown in Figure 2 - 46. This test rig was able to change the shear loading angle from 0 to 90°. Two types of cable bolts, namely plain strand and modified cable bolts, were evaluated. The results showed that with the pull angle increasing, the failure mode changed from bond failure to steel rupture, independent of cable type. Additionally, the peak load of modified cable bolts reduced with the pull angle increasing but this effect was opposite for plain cables.

Goris *et al.* (1996) conducted shear tests on concrete blocks with and without reinforcing cable bolts, showing that the shear resistance of rock joints reinforced by the cable bolt was double to those without cable bolts. Furthermore, the shear capacity of blocks grouted with cable bolts rose quickly at small displacements compared with blocks reinforced by cable bolts without grout materials.

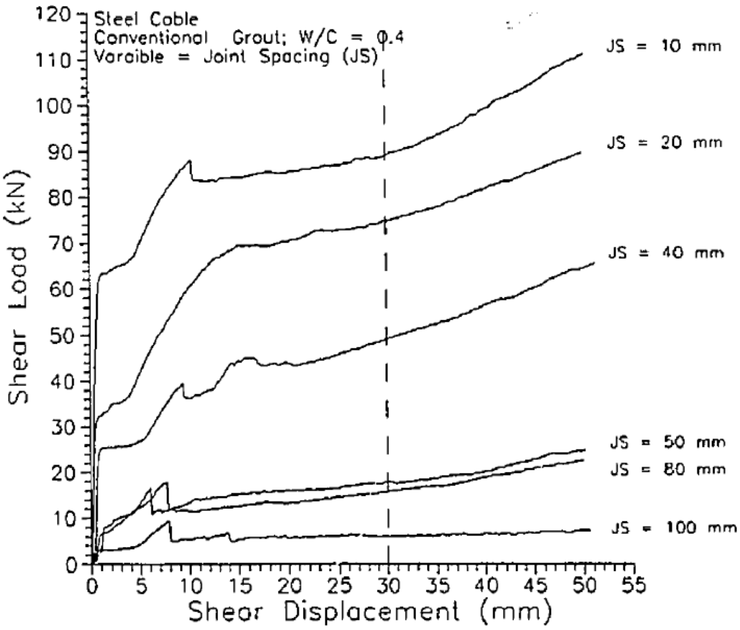

Figure 2 - 45 Joint spacing impact on bearing capacity of cable bolts (Khan, 1994)

Two double shear tests were performed by Craig and Aziz (2010) on plain cable bolts. The study showed that both the shear load and axial load increased with shear displacement. Furthermore, after a displacement of 75 mm, the cable bolt failed by wire rupture, as shown in Figure 2 - 47.

Aziz *et al.* (2015a) evaluated the shear performance of indented cable bolts. The shear load transfer of indented and plain strands was compared, showing that indentations along the steel wires were detrimental to the shear strength of the cable bolts.

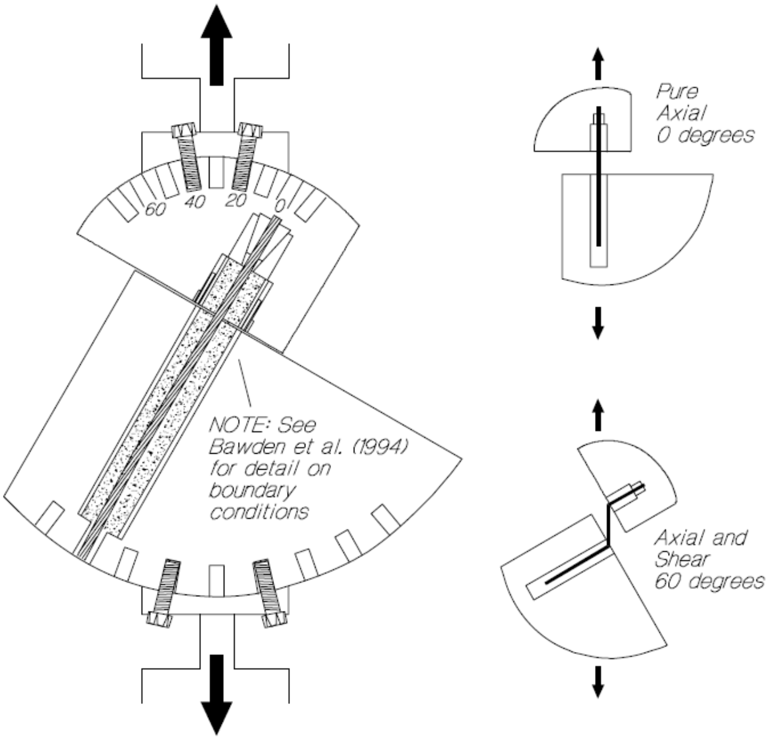

Figure 2 - 46 Single shear test apparatus for cable bolts (Bawden *et al.*, 1994)

Figure 2 - 47 Rupture of steel wires in shear test (Craig and Aziz, 2010)

The shear performance of hollow grouted cable bolts including both plain and indented cable bolts was reported by Aziz *et al.* (2015b), showing that the pre-tension load had an influence on the shear capacity of cable bolts. Moreover, the cable bolt rotation phenomenon was not monitored in the whole test process.

The shear performance of various cable bolts was tested by Rasekh *et al.* (2015). It was found that a large portion of shear load was used to overcome the frictional force between concrete joints, as shown in Figure 2 - 48. Furthermore, increasing the pre-tension load was beneficial to improving the frictional coefficient of joints.

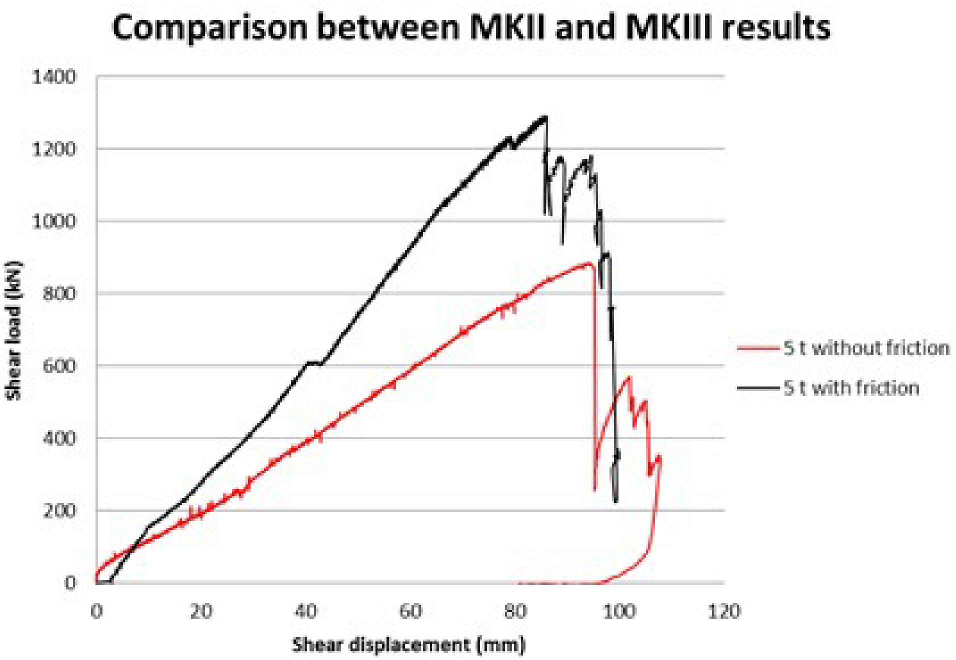

Figure 2 - 48 Comparison test results with and without joint friction (Rasekh, 2017)

2.10 Theoretical background of rock tendons

In theoretical analysis, the cable bolt is always assumed to be a round bar, which is similar to the theoretical analysis for rockbolts. Therefore, in this section, previous analytical modelling on both rockbolts and cable bolts subjected to axial load are reviewed.

The pioneering work on rock tendons should be attributed to Hawkes and Evans (1951), who studied the load transfer mechanism between concrete blocks and steel bars. Equation (2 - 6) is the governing formula.

$$P = \frac{\pi d^2 f}{4A}\left(1 - e^{-\frac{4Al}{d}}\right) \qquad (2 - 6)$$

Where, d = the bar diameter, m; f = the bond stress at the free end, Pa; A = a constant; and l = the distance where the bond stress reduced to zero, m.

Experimental programmes were used to validate this analytical model, showing that a good correlation between experimental and modelling results, as shown in Figure 2 - 49. However, this model assumed that there was a linear relationship between the bond stress and axial stress, which is only valid in the coupling stage.

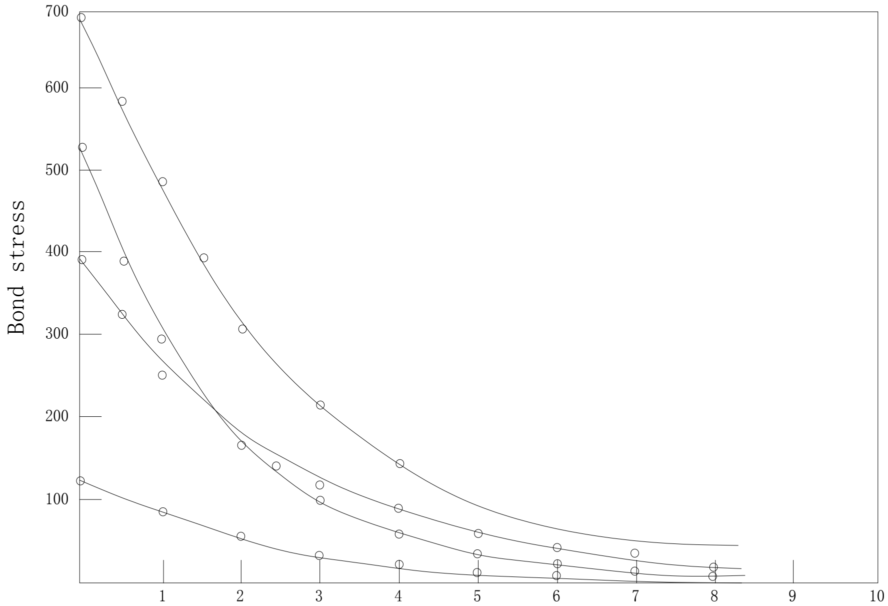

Figure 2 - 49 Bond stress distribution along the embedment length, after Hawkes and Evans (1951)

Farmer (1975) especially studied the shear stress distribution along the rockbolt, proposing that the shear stress corresponded to Equation (2 - 7):

$$\frac{\tau_x}{\sigma_0} = 0.1e^{-\frac{0.2x}{a}} \qquad (2 - 7)$$

Where, τ_x = the shear stress at a distance of x from the loaded end, Pa; σ_0 = the axial stress in the rockbolt at the loaded end, Pa; a = the radius of the rockbolt, m. Although pull-out test results acquired by Dunham (1976) confirmed the credibility of this analytical model, it is also limited to the coupling stage.

Tao and Chen (1983) proposed a formula to estimate the load bearing capacity of rockbolts in the field. It was determined that the rock mass movement equalled Equation (2 - 8):

$$u_r = A_0 \frac{1}{r_t} \tag{2 - 8}$$

Where, u_r = the movement of the rock mass at a radius of r, m; A_0 = the coefficient; r_t = the radius of the tunnel, m. However, this modelling process only considered circular tunnels and whether this model was valid to other type of tunnels was not discussed.

Ballivy and Martin (1983) analysed the shear stress propagation process of a fully grouted rockbolt with a mechanical model. This model considered the elastic, elastic-softening, and elastic-softening-debonding stages. But in the debonding length, the shear stress along the interface was assumed to be zero, neglecting the residual frictional stress along the bolt/grout interface.

John and Dillen (1983) assumed that the pull-out performance of rockbolts was mainly decided by the shear behaviour of the grout annulus. A constitutive model shown in Figure 2 - 50 was proposed to describe the shear behaviour of the grout annulus.

Equation (2 - 9) was proposed to calculate the shear strength of the grout/rock interface:

$$\tau_{peak} = \pi\left(D+2t\right)\tau_I Q_B \tag{2 - 9}$$

Where, τ_{peak} = the shear strength of the grout/rock interface, Pa; D = the bolt diameter, m; t = the grout thickness, m; τ_I = the shear strength of the weaker material between the grout and the rock mass, Pa; and Q_B = bonding quality. However, this model assumed failure occurred along the grout/rock interface and the shear failure along the bolt/grout interface was not considered.

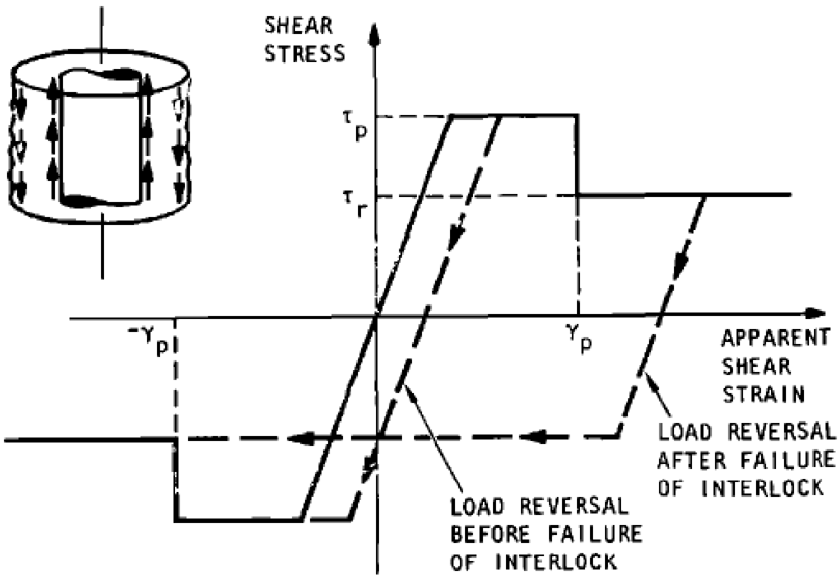

Figure 2 - 50 Shear behaviour of grout annulus in rockbolting system (John and Dillen, 1983)

Aydan *et al.* (1985) performed a comprehensive theoretical study on the performance of fully grouted rockbolts via a tri-linear model. Various parameters, including the strength of the rock mass and grout strength, were studied. However, the analytical results were not validated via experimental tests.

Rajaie (1990) used a tri-linear model to study the shear stress distribution along the full embedment length of cable bolts. To validate this model, the peak capacity of cable bolts acquired from experiments and modelling was compared, as shown in

Figure 2 - 51. Later, this model was used to perform a parametric study on cable bolts (Mitri and Rajaie, 1990). However, this work only focused on plain cable bolts.

A Bond Strength Model (BSM) was proposed by Yazici and Kaiser (1992) to study the load transfer of cable bolts. They assumed that the cable bolt had a rough surface geometry, as shown in Figure 2 - 52.

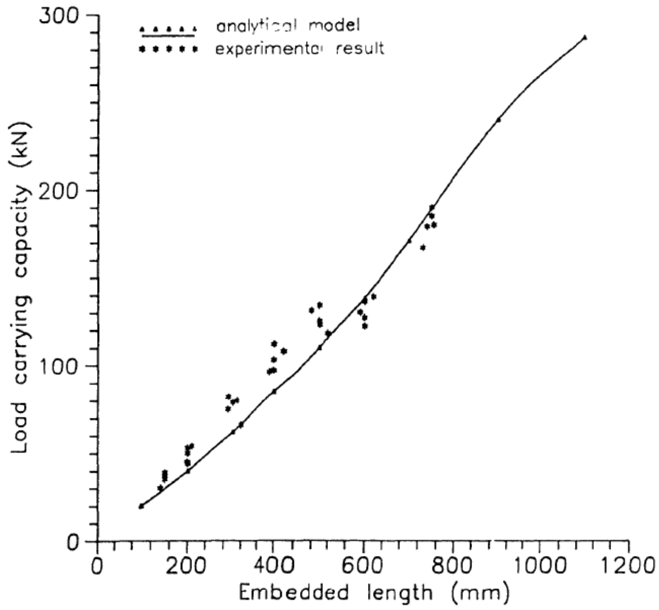

Figure 2 - 51 Comparison between analytical and experimental results (Rajaie, 1990)

The shear stress along the cable/grout interface was calculated by Equation (2 - 10):

$$\tau = \sigma \tan\left(i_0 \left[1 - \left(\frac{\sigma}{\sigma_{\lim}} \right)^{\beta} \right] + \phi \right) \tag{2 - 10}$$

Where, i_0 = the dilation angle, °; σ = the confining pressure on the cable/grout interface, Pa; σ_{lim} = grout compressive strength, Pa; β = the reduction coefficient of dilation angle; and Φ = the friction angle between the cable and grout, °.

The BSM was basically composed of four parts, as shown in Figure 2 - 53. (1) The first quadrant illustrated the shear stress variation along the cable/grout interface with axial displacement. This represented the load versus displacement curves in axial tests of cable bolts. (2) The second quadrant illustrated the relationship between the shear stress on the cable/grout and the interface pressure. (3) The third quadrant calculated the lateral and axial displacement at the cable/grout interface. (4) The fourth quadrant explained the dilation or the lateral displacement of the cable/grout interface.

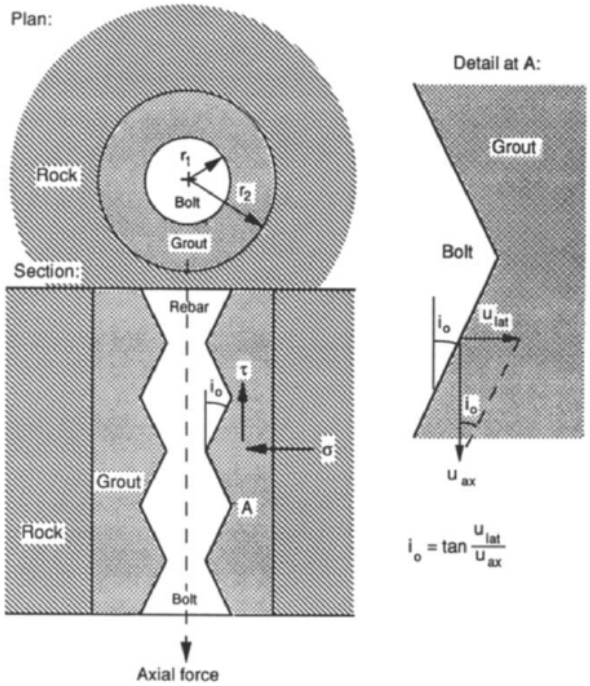

Figure 2 - 52 Zigzag geometry of a rough cable bolt (Yazici and Kaiser, 1992)

The BSM was integrated by bringing in the dilation limit, which represented the maximum lateral displacement of grout along the cable/grout interface and was calculated by Equation (2 - 11):

$$u_{lat} = u_0 \left(1 - \frac{p_1}{\sigma_{Cg}}\right)^{B/\sigma_{Cg}} \quad (2 - 11)$$

Where, u_{lat} = the lateral displacement, m; u_0 = the maximum dilation, m; p_1 = the confining pressure at the cable/grout interface, Pa; σ_{Cg} = the grout compressive strength, Pa; and B = the constant. The credibility of the BSM was successfully validated by the experimental pull-out tests on cable bolts. Later, the BSM was improved by Kaiser *et al.* (1992) and Diederichs *et al.* (1993) to evaluate the influence of stress change and rotation on performance of cable bolts (Figure 2 - 54). However, all this work was only applicable to plain cable bolts.

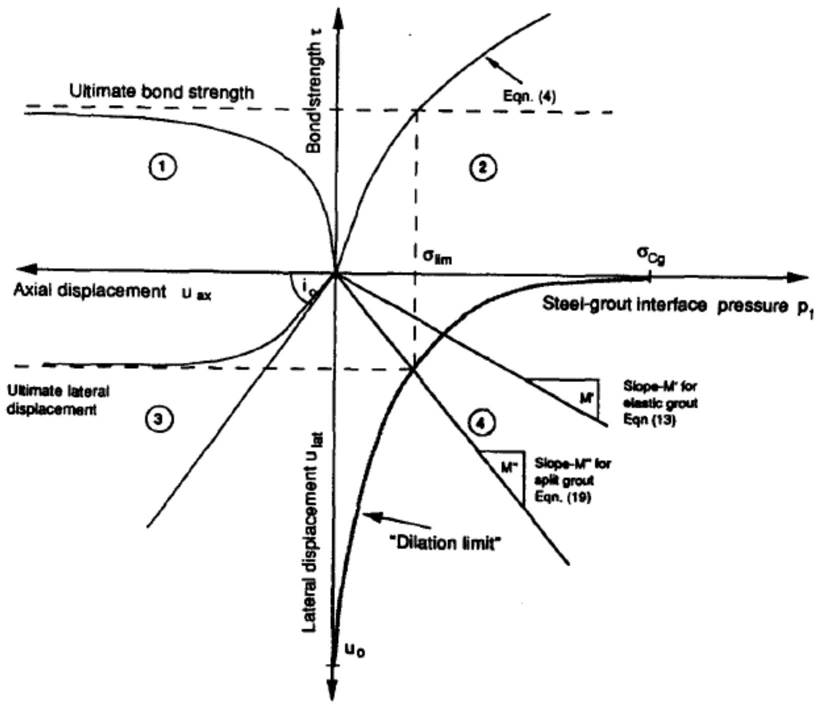

Figure 2 - 53 Schematic diagram regarding the BSM (Yazici and Kaiser, 1992)

Hyett *et al.* (1992b) proposed a conceptual model to study the shear stress distribution along the cable/grout interface. Specifically, around the unloaded end, the shear stress decreased exponentially. However, near the loaded end, the shear stress was uniform, equalling the interfacial residual shear stress. However, no proof was provided to validate this assumption.

Hyett *et al.* (1995b) assumed that the bearing capacity of cable bolts was basically composed of two parts, namely the frictional force and the rotating force. Equation (2 - 12) was proposed to calculate the pull-out load:

$$F_a = A_1 p_1 \tan\phi' + \frac{4\pi^2 C u_a}{l^2\left(u_a + L_f\right)} \tag{2 - 12}$$

Where, F_a = the pull-out load at the loaded end, N; A_1 = the contact area in the frictional part, m^2; Φ' = the grout frictional angle, °; C = the cable bolt torsional stiffness, N/m; l = the cable bolt pitch length, m; u_a = the axial displacement, m; and L_f = the free length of test section and anchor part, m. Although this analytical model was validated via experimental work under both CNL and CNS environments, it was not applicable to the entire pull-out process.

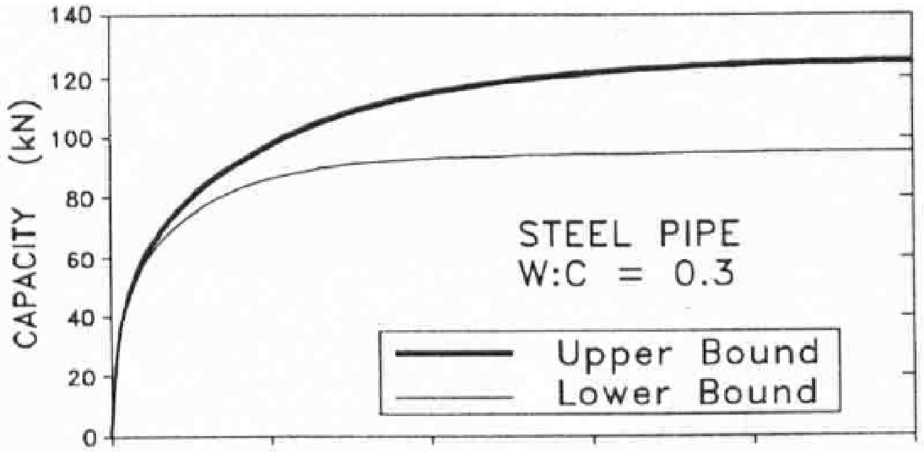

Figure 2 - 54 The modified BSM to predict the performance of cable bolts under non-rotating (upper bound) and rotating (lower bound) conditions (Diederichs *et al.*, 1993)

Benmokrane *et al.* (1995) deduced a constitutive law for the cable/grout interface. This solution considered the elastic, softening and debonding behaviour of the interface, as shown in Figure 2 - 55. For cable bolts having long embedment length, the shear stress distribution along the cable/grout interface was not considered.

Hyett *et al.* (1996) focused on the load distribution along cable bolts with long embedment length. An analytical model was put forward to calculate the load in the cable tendon after the rock mass moved, as shown in Figure 2 - 56. It indicated that when the cable bolt had a long embedment length, an apparent load variation occurred. Later, this model was extended to conduct parametric study on cable bolts by Moosavi *et al.* (2002). Nevertheless, the model was only limited to the coupling period.

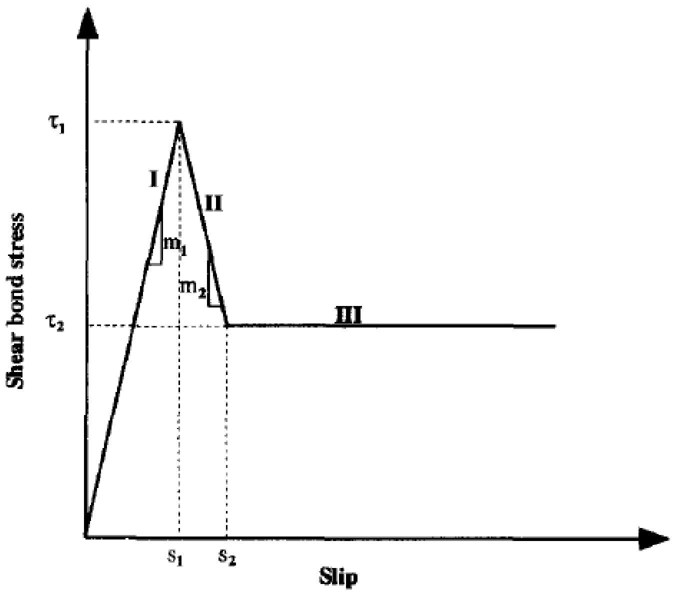

Figure 2 - 55 A tri-linear model for the cable/grout interface (Benmokrane *et al.*, 1995)

Li and Stillborg (1999) proposed an analytical model for rockbolts and the shear stress distribution in this model was shown in Figure 2 - 57. The shear stresses for sections from the left to the right are calculated with Equations (2 - 13) to (2 - 16):

$$\tau_b(\mathrm{x}) = 0 \tag{2 - 13}$$

$$\tau_b(\mathrm{x}) = s_r \tag{2 - 14}$$

$$\tau_b(\mathrm{x}) = \omega s_p + \frac{x - x_1}{\Delta}(1-\omega)s_p \tag{2 - 15}$$

$$\tau_b(\mathrm{x}) = s_p e^{-2\alpha\left(\frac{x-x_2}{d_b}\right)} \tag{2 - 16}$$

Where, $\tau_b(x)$ = the shear stress along the embedment length, Pa; s_r = the residual strength, Pa; ω = the ratio between the residual and peak shear strength; α = the coefficient; and d_b = the bolt diameter, m. Although this model considered the decoupling behaviour of the bolt/grout interface and was validated by experimental results, no attempt was conduct to predict the load transfer performance of rockbolts.

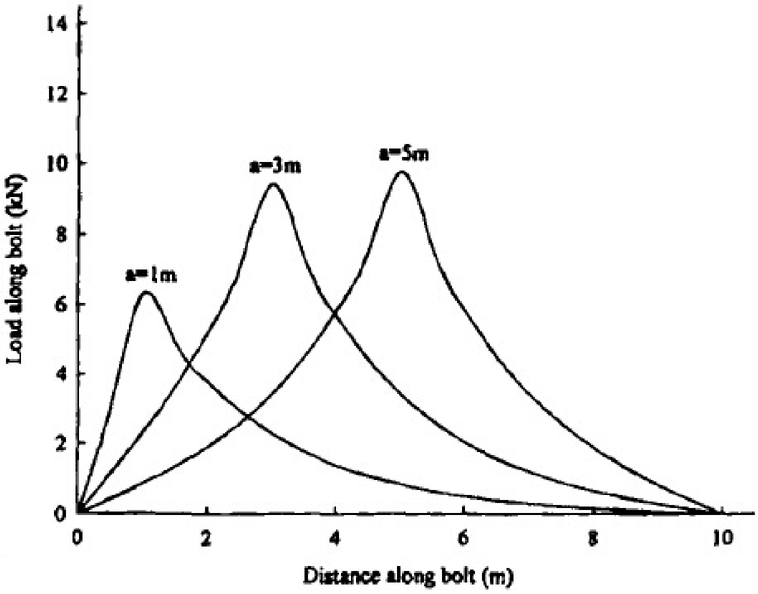

Figure 2 - 56 Load distribution along the full length of cable bolts (Hyett *et al.*, 1996)

Moosavi (1999) proposed an analytical solution to study the pull-out load versus displacement relationships of fully grouted cable bolts. The peak capacity the cable/grout interface was obtained with Equation (2 - 17):

$$\tau_{peak} = C_1 e^{-mu_a} + C_2 \quad (2 - 17)$$

Where, C_1 and C_2 = grout property parameters, Pa; u_a = pull-out displacement; and m = an empirical parameter. However, this model assumed a uniform shear stress distribution along the cable/grout interface, which is not valid when a long embedment length was used.

Ruest and Martin (2002) used the cable bolt structural element in Fast Lagrangian Analysis of Continua (FLAC) to study the load distribution along the embedment length.

In this simulation, the cable/grout interface was treated as the spring-slider system, as shown in Figure 2 - 58. However, an elastic-perfectly plastic model was used in this analysis, neglecting the softening behaviour in pull-out tests.

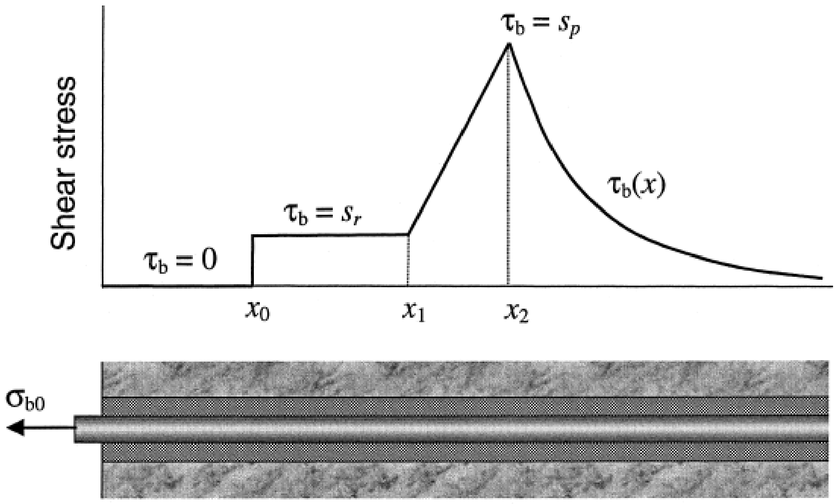

Figure 2 - 57 Shear stress distribution along the bolt/grout interface (Li and Stillborg, 1999)

Cai *et al.* (2004a) studied the load transfer performance of rockbolts used in soft rock mass. The bolt/grout interfacial property was depicted in Figure 2 - 59. The shear strength of the interface was defined with Equation (2 - 18):

$$\tau_{peak} = c_i + \sigma_{nb} \tan \phi_i \tag{2 - 18}$$

Where, c_i =cohesive strength of the grout medium, Pa; Φ_i = friction angle of the grout medium; and σ_{nb} = the normal stress applied on the rockbolt. This model was applied to evaluate the performance of rockbolts installed in a jointed rock mass, showing that the stability of the jointed rock mass around an excavation was significantly improved by rockbolting (Cai *et al.*, 2004b). However, this model had to the softening process.

Xiao and Chen (2008) used a tri-linear model to simulate the pull-out behaviour of an anchor from soil materials. A schematic diagram of the pull-out anchor is shown in

Figure 2 - 60. This model was generally composed of three parts, namely elastic, elasto-plastic and residual segments. However, Cao (2012) indicated that the equation in the elasto-plastic part was a transcendental formula and treated as a closed form.

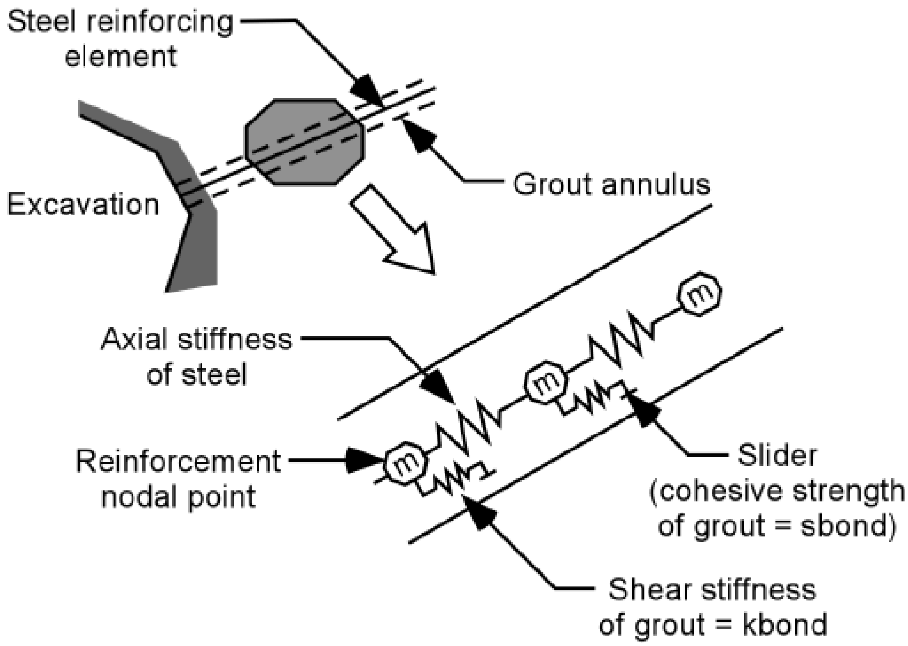

Figure 2 - 58 Shear model of fully reinforced system (Ruest and Martin, 2002)

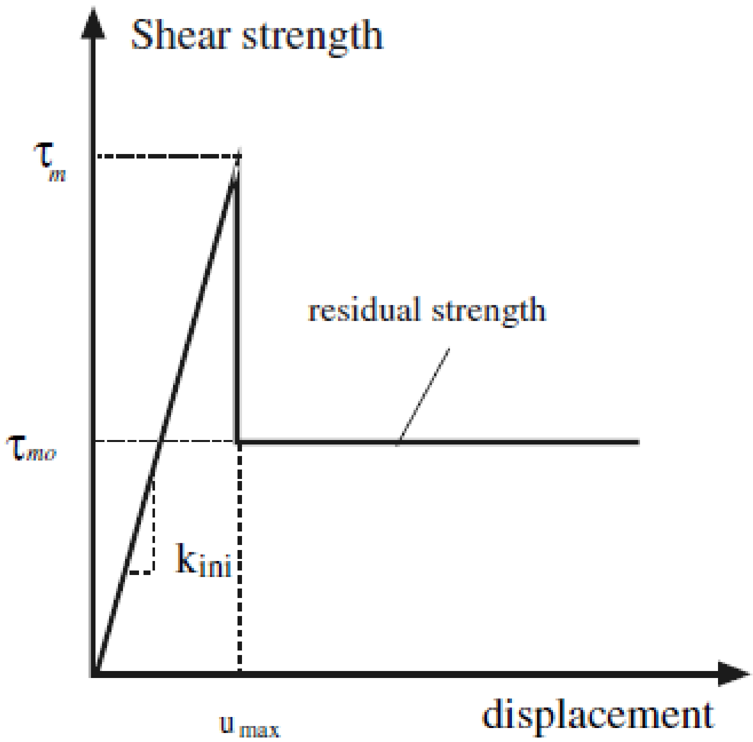

Figure 2 - 59 Shear stress model for the cable/grout interface (Cai *et al.*, 2004a)

Ren *et al.* (2010) modified the model proposed by Yuan *et al.* (2007), using a tri-linear model to study the load transfer behaviour of fully grouted rockbolts. Based on the analytical solution, the bolt/grout interface experienced five different stages, namely elastic, elastic-softening, elastic-softening-debonding softening-debonding and debonding, as shown in Figure 2 - 61. However, the user had to pre-define the different pull-out stages artificially.

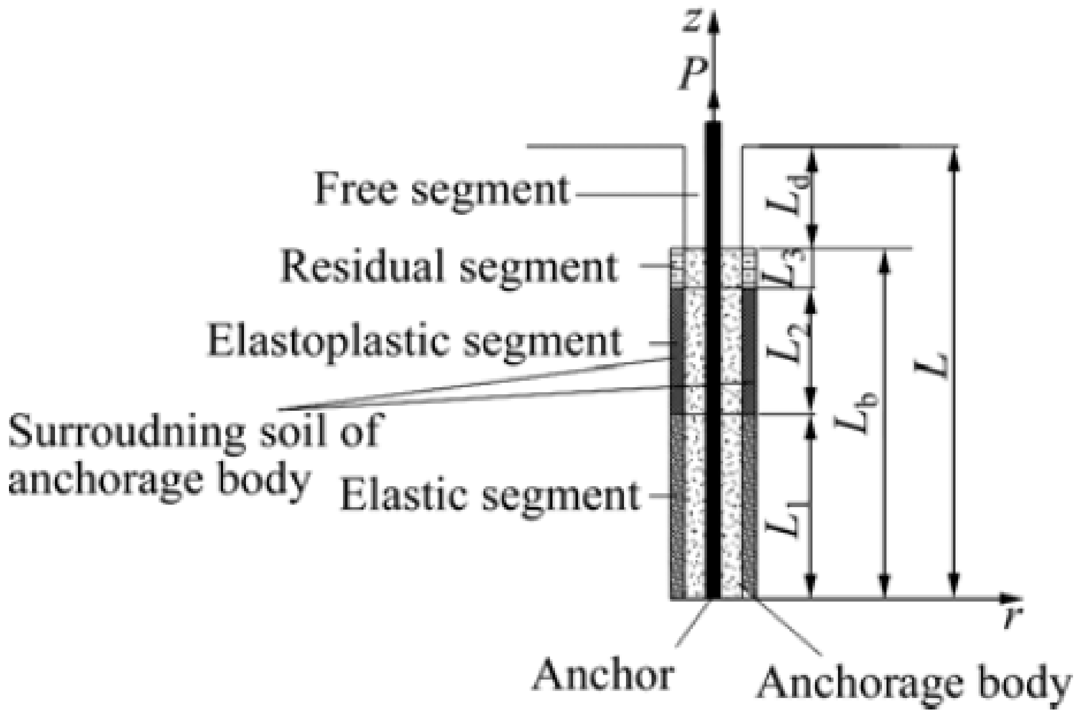

Figure 2 - 60 Schematic diagram of a pull-out model (Xiao and Chen, 2008)

The tri-linear model was also adopted by Blanco Martín *et al.* (2010) to simulate the pull-out load versus displacement behaviour of rockbolts. The innovation of their research was solving the pull-out performance of rockbolts independent of the boundary condition at the loaded end.

A load distribution model was put forward by Jalalifar (2011) to evaluate the performance of rockbolts in an elasto-plastic rock mass. The results showed that the axial load along rockbolts increased with higher initial stress. However, this work is limited to the coupling period.

Zhao and Yang (2011) studied the axial performance of imperfectly bonded rockbolts subjected to tensile loads. This solution was confirmed with numerical modelling results. No laboratory or *in-situ* tests were used to validate this theoretical model.

An analytical study was performed by Cao *et al.* (2013a) to study the bolt profile, especially the rib face angle (Figure 2 - 62) on performance of rockbolts. The rib face angle is the angle between the rib inclination and the long axis of a rock bolt (Cao *et al.*, 2013a). It was recommended to use rockbolts with smaller face angles in hard rock mines and rockbolts with large rib face angles for soft rock environments.

Blanco Martín *et al.* (2013) analysed the shear stress propagation process for a bolt/grout interface, indicating that a pure softening stage could occur if the embedment length was not long enough. However, no experimental work was performed to validate the shear stress assumption.

Ma *et al.* (2013) introduced the slip distribution equation proposed by Zhou *et al.* (2010) to study the bond-slip performance of the bolt/grout interface. The slippage along the bolt/grout interface was determined by the Equation (2 - 19):

$$s(x) = a \ln\left(1 + e^{\frac{x - x_0}{b}}\right) \tag{2 - 19}$$

Where, $s(x)$ = the slip of the bolt/grout interface at a position of x, m; a, b and x_0 = coefficients. Later, this model was improved to analyse the performance of rockbolts reaching free end slip and simulate the failure propagation of the bolt/grout interface (Ma *et al.*, 2014b; Nemcik *et al.*, 2014; Ma *et al.*, 2015). However, this model cannot be used to predict the influence of factors such as grout quality and rock mass strength on the load transfer performance of rock tendons.

Ma *et al.* (2014a) used the bolt structure in FLAC to study the interaction between rockbolts and the rock mass in a stope. Laboratory push tests were used to acquire the interface bond-slip performance and the interfacial shear stress was computed with the Equation (2 - 20):

$$\tau = \frac{cs\_scoh}{\pi d_b} \tag{2 - 20}$$

Where, cs_scoh = the cohesive strength, Pa. The simulation results showed that the maximum axial stress occurred at the rock joint position and might lead to rockbolt rupture.

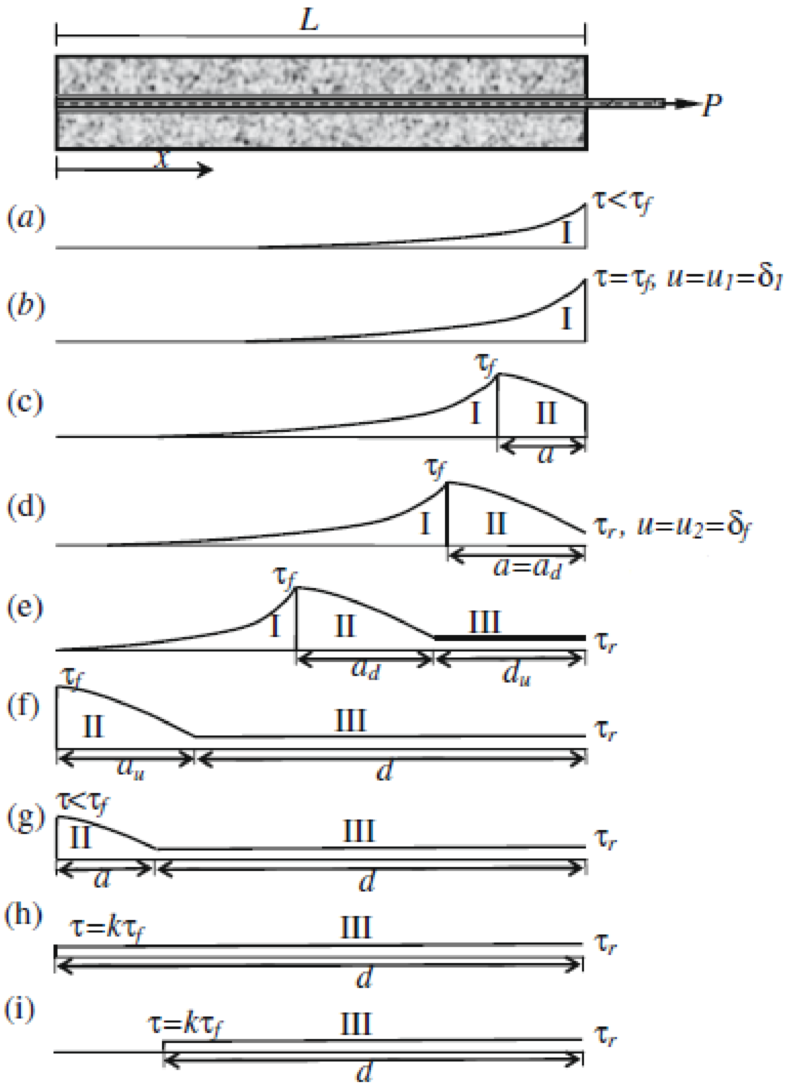

Figure 2 - 61 Shear stress propagation process along the embedment length. (a, b) elastic stage; (c, d) elastic-softening stage; (e, f) elastic-softening-debonding stage; (g) softening-debonding stage; (h, i) debonding stage (Ren *et al.*, 2010)

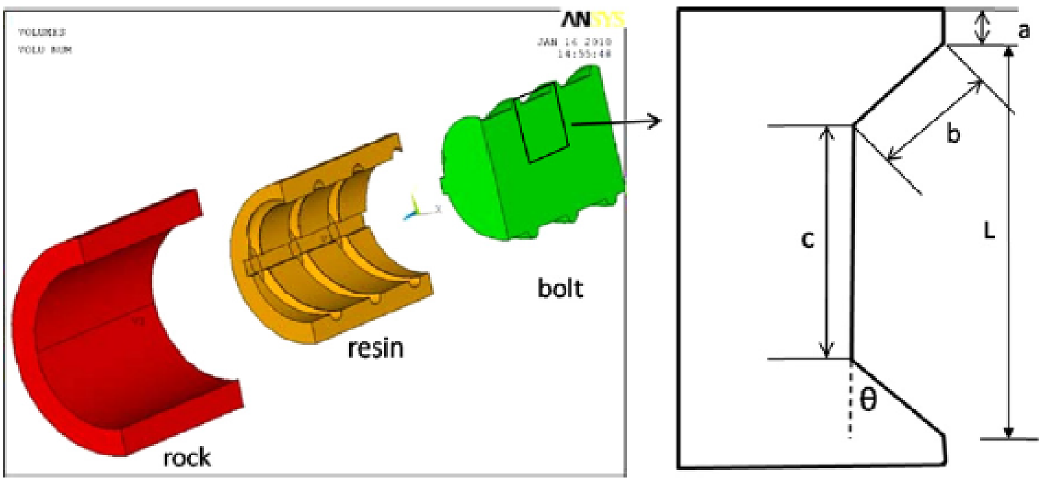

Figure 2 - 62 Bolt profile configuration (Cao *et al.*, 2013a)

2.11 Summary

Fully grouted cable bolts have been used in the underground mining industry for more than fifty years, becoming more popular in rock reinforcement design. The main purpose of cable bolting is to increase the stability of the rock mass surrounding excavations, thus providing a safe working environment.

Generally, two types of cable bolts, namely plain strands and modified cable bolts, are commonly used. Standard plain strands have a smooth surface and a small axial load bearing capacity. Consequently, they are usually used for temporary reinforcement. On the other hand, modified cable bolts have more superior performance and are commonly installed for permanent reinforcement.

Both cementitious and resin-based grouts are used as bonding materials. Nevertheless, cementitious grout is more widely used in cable bolting due to its low cost and convenient installation. Furthermore, cable bolts grouted with cement-based grout are being used in most underground excavations, such as cut-and-fill stopes, open stopes and drawpoints.

In the field, there are basically five different failure modes for cable bolts. Among them, failure along the cable/grout interface is more frequent, determined by the interface shear strengths. The load transfer of cable bolts mainly relies on the shear resistance at the cable/grout interface, which is composed of three parts, namely chemical adhesion, mechanical interlock and friction. However, chemical adhesion plays a minor role in the determination of the interfacial shear strength. Mechanical interlock and friction are more important, especially the friction, playing a paramount role in determining the pull-out capacity of cable bolts.

Much research has been undertaken on the axial performance of cable bolts. Since there is no common test standard, various approaches have been used, with differing results. Compared with the SEPT, SPPT and DEPT, the LSEPT is a better procedure to study the performance of cable bolts subjected to tensile load since it can overcome the problems occurring in previous test methods. Nevertheless, there are still some problems with the current LSEPT, especially in testing high performance modified cable bolts. Therefore it is necessary to propose a new test approach to evaluate the performance of cable bolts.

The influence of many diverse parameters on load transfer of cable bolts was studied. The results showed that the bearing capacity of cable bolts can be improved by various methods, such as installation of buttons along the strand, and adding epoxy coated materials. These experiments were beneficial to better understanding the cable bolting mechanism. However, most of them focused on performance of cable bolts under strong rock environments by using steel, aluminium or concrete blocks with high strength to simulate the rock. Moreover, little research has been performed on the axial performance of cable bolts in weak rock mass conditions.

Since the shear strength of cement grout has a significant effect on deciding the load transfer behaviour of cable bolts, the shear behaviour of cement grout under CNL condition has been studied. However, no research has been performed on the shear performance of cement grout under CNS environment.

Numerous analytical works have been executed on rock tendons. It is commonly accepted that there is shear failure propagation along the bolt/grout interface in a pull-out process, which is especially apparent for cable bolts with long embedment length. Consequently, the shear stress along the bolt/grout interface is non-uniform. However, most constitutive laws for cable bolts assumed a uniform shear stress distribution along the interface, which is only appropriate for short embedment length condition. A few analytical models evaluated the pull-out performance of cable bolts with long embedment length but are limited to only the coupling period and plain strands. Thus, it is valuable to propose a new analytical model to study the load transfer mechanism of both plain and modified cable bolts with different embedment lengths.

Finally, the load transfer mechanism of fully grouted cable bolts has not been fully understood. In this thesis, a new experimental approach is proposed for axial testing cable bolts. Furthermore, with the designed test apparatus, the load transfer behaviour of both plain and modified cable bolts is studied under weak rock conditions. The shear behaviour of the Stratabinder grout which is used in cable bolt tests is investigated via the direct shear test. Based on the experimental results, a new analytical model is put forward to study the peak capacity and shear stress propagation along the cable/grout interface in the full pull-out process.

CHAPTER THREE

MECHANICAL PROPERTIES OF CEMENT-BASED GROUT

3.1 Introduction

Two types of cement-based grout were used in the test programme. This included bulk material and a packaged material. The bulk material was mixed and delivered by cement mixer and poured directly into casings used to cast the confining medium. The rock materials were not used in this study because it is difficult to guarantee the consistence of the rock material sourced from the field, especially in coal. Therefore, packaged material was used to bond the cable bolt and the confining medium together.

To simulate rocks with different strength, three different mixes of material were used, as being grout mixtures. Strength tests were conducted on these materials. Following the current standards recommended by the International Society for Rock Mechanics (ISRM), to determine the UCS, Young's Modulus and Poisson's Ratio, cylindrical test specimens were used. Cubic test specimens were also prepared for strength tests as used in the determination of the mechanical properties of cement-based materials in the mining industry in Australia.

The product used was Stratabinder supplied by Orica Australia Pty. Ltd.. A cement-based material having low viscosity and high flow was used for grouting the cable bolt in the confining medium. A number of UCS tests were conducted on specimens with different w/c ratios to evaluate the influence of w/c ratio on the UCS of

Stratabinder grout. Both cylindrical and cubic specimens were tested and the results were compared. Furthermore, several Brazilian tensile tests were conducted to measure the tensile strength of Stratabinder grout at two different w/c ratios.

3.2 Properties of the Hanson grout

3.2.1 Components of Hanson grout

Three types of Hanson grout, namely the GS32250 grout, the YN1.5MPA grout and the GS40250 grout, were tested in this study. The components of each grout are shown in Table 3 - 1.

Table 3 - 1 Components of three types of cement-based grout

Materials	Source	Unit	GS32250	YN1.5MPA	GS40250
Cement	ex CA Goliath	kg/m^3	650	365	455
Flyash	ex CA Mt Piper	kg/m^3	150	-	195
Man. sand	ex Kulnura	kg/m^3	-	-	514
Fine sand	ex Maroota	kg/m^3	1025	1000	701
Admixture	WRDAPN20(WR) ex Grace	ml/m^3	1600	-	1300
Admixture	AEA(AEA) ex Grace	ml/m^3	-	1000	-
Admixture	ADVA-650(HWR) ex Grace	ml/m^3	3520	-	2600
Water	Water	l/m^3	300	400	300

3.2.2 UCS tests with GS32250 grout

3.2.2.1 Tests on cylindrical specimens

Based on the current ISMR standard, cylindrical specimens were prepared (ISRM, 2014). To prepare the casting moulds, PVC pipes with a diameter of 54 mm were cut into sections with a length of 135 mm. The casting mould was glued into a cardboard base, using silicon material, as shown in Figure 3 - 1.

After GS32250 grout was mixed uniformly, it was poured into the moulds. After the grout set for 24 hours, the plastic mould was removed. And the sample was placed in a water bath to cure for 28 days. Five specimens were cast at the same time, as shown in Figure 3 - 2.

Figure 3 - 1 The casting mould preparation. a) Lateral view (left), and b) vertical view (right)

Figure 3 - 2 Preparation of cylindrical specimens

After the specimens fully cured, all specimens were ground to ensure flat surfaces of the top and bottom ends. Then, the dimensions of each specimen were measured, including the length (L) and the diameter (D). The MTS machine was used to apply axial load on the specimen at a constant displacement speed of 0.003 mm/s. A load cell was installed in the lower platen to measure the axial load, as shown in Figure 3 - 3. The Young's Modulus (E) was calculated based on the axial stress - strain curve and it equals the slope of the linear portion of the stress - strain curve.

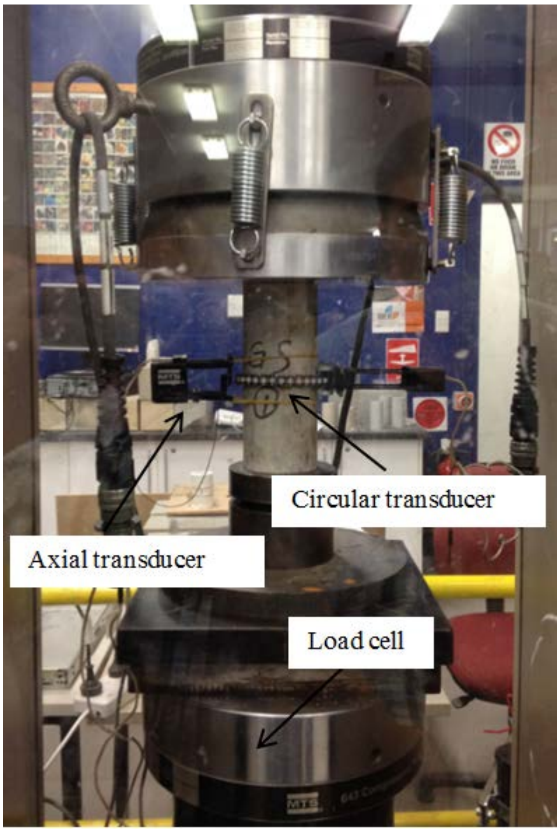

Figure 3 - 3 UCS test on the cylindrical specimen

To acquire the Poisson's Ratio (v), two transducers were attached in the middle of the specimen. The axial transducer measured the vertical deformation of the specimen with a length of 25 mm and the circular transducer measured the perimeter deformation of the specimen. Therefore, v can be acquired with Equation (3 - 1).

$$v = -\frac{E_1}{E_2} \tag{3 - 1}$$

Where, v = Poisson's Ratio; E_1 = slope of axial stress - strain curve measured with the axial strain gauge, Pa; and E_2 = slope of diametric stress - strain curve measured with the circular transducer, Pa.

The results of each specimen test are tabulated in Table 3 - 2 and the stress versus strain relationship is shown in Figure 3 - 4. In the fifth test, the axial transducer failed to record the axial deformation of the specimen and the Poisson's Ratio was not acquired. Nevertheless, the test results were still consistent.

Table 3 - 2 UCS test results of cylindrical specimens

List	*L* (mm)	*D* (mm)	*L*/*D*	UCS (MPa)	*E* (GPa)	*ν*
1	131.6	53.9	2.4	62.3	11.6	0.26
2	131.4	54.0	2.4	63.4	12.0	0.24
3	134.1	54.1	2.5	62.3	11.9	0.27
4	127.6	53.4	2.4	64.7	12.5	0.31
5	134.5	54.0	2.5	61.1	12.1	-
Mean	131.8	53.9	2.4	62.7	12.0	0.27

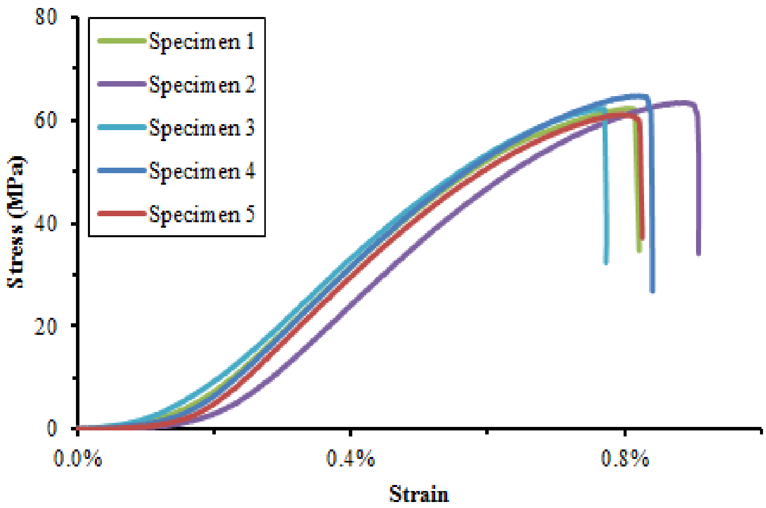

Figure 3 - 4 The stress - strain relationship of cylindrical specimens

The fourth test had the highest UCS while the fifth test had the smallest UCS value. These two test results were ignored and the remaining three were reserved as the final results. Therefore, the UCS values of cylindrical specimens are shown in Table 3 - 3 and Figure 3 - 5. The results show that the cylindrical specimens had an average UCS of 62.7 MPa, Young's Modulus of 11.8 GPa and Poisson's Ratio of 0.26. This processing method was always used in the following tests and only the average of the results was given.

The failure mode of cylindrical specimens was dominated by the shear failure in the specimen, as shown in Figure 3 - 6.

Table 3 - 3 UCS results of cylindrical specimens

No.	*L* (mm)	*D* (mm)	*L*/*D*	UCS (MPa)	*E* (GPa)	*v*
1	131.6	53.9	2.4	62.3	11.6	0.26
2	131.4	54.0	2.4	63.4	12.0	0.24
3	134.1	54.1	2.5	62.3	11.9	0.27
Mean	132.3	54	2.4	62.7	11.8	0.26

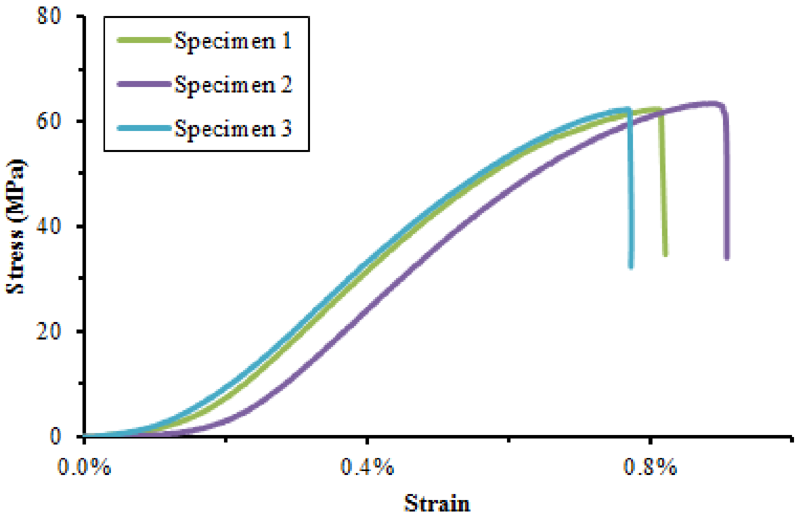

Figure 3 - 5 The stress - strain relationship of cylindrical specimens

Figure 3 - 6 Failure modes of cylindrical specimens. a) Specimen 1, and b) Specimen 2

3.2.2.2 Tests on cubic specimens

Cubic specimens with an edge length of 50 mm were also cast and prepared, following the current Australian Standards (Standard Australia, 2014). The cubic mould was provided by the Jennmar Australia Pty. Ltd., as shown in Figure 3 - 7.

Figure 3 - 7 The cubic mould

GS32250 grout was poured into the cubic moulds. After setting for 24 hours, the test specimens were removed from the moulds, as show in Figure 3 - 8. Then all cubic specimens were put into a water basin to cure for 28 days.

Figure 3 - 8 Preparation of cubic specimens

UCS tests were performed, as shown in Figure 3 - 9. The test results are shown in Table 3 - 4 and Figure 3 - 10. The results show that the cubic specimens had an average

UCS of 68.5 MPa. The failure mode of a cubic specimen is shown in Figure 3 - 11. The results show that failure occurred along a horizontal plane in each test specimen.

Figure 3 - 9 UCS test on the cubic specimen

Table 3 - 4 UCS results of cubic specimens

No.	*L* (mm)	*W* (mm)	*H* (mm)	UCS (MPa)
1	50.0	49.9	50.0	71.3
2	50.3	50.0	50.1	67.2
3	50.2	50.0	50.2	66.9
Mean	50.2	50.0	50.1	68.5

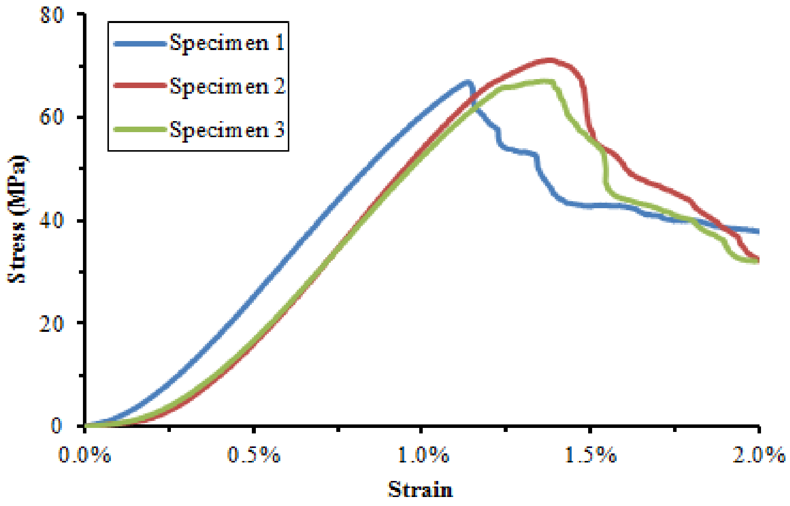

Figure 3 - 10 The stress - strain relationship of cubic specimens

Figure 3 - 11 Failure mode of the cubic specimen

3.2.2.3 Result comparison between cylindrical and cubic specimens

The UCS test results based on cylindrical and cubic specimens were compared, as shown in Figure 3 - 12. The UCS of cylindrical specimens was 62.7 MPa and the UCS of cubic specimens was 68.5 MPa, indicating that the shape of the specimen had an effect on determination of the UCS of the material. And the UCS of the cubic specimen was relatively higher than cylindrical specimens. Furthermore, the strain of cylindrical specimens where peak stress occurred was apparently smaller than cubic specimens, indicating that cylindrical specimens were more brittle than cubic specimens. As GS32250 grout was found to have the highest strength, it was selected to cast the confining medium in cable bolt pull-out tests, simulating strong rock.

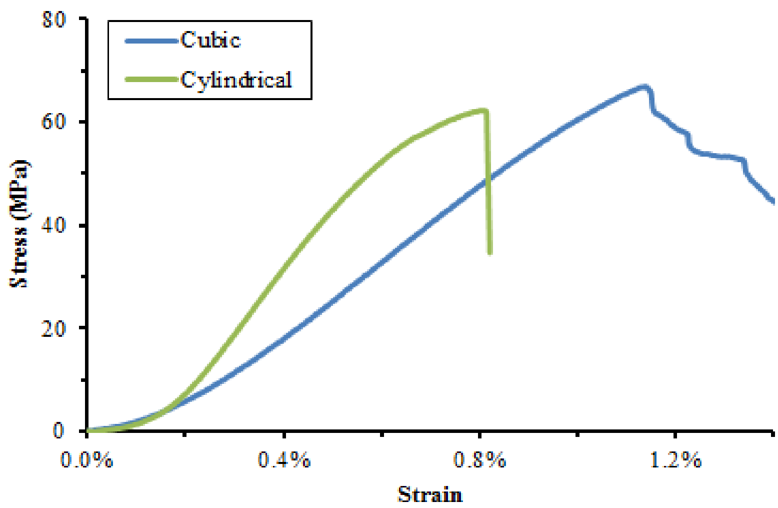

Figure 3 - 12 Comparison between UCS test results

3.2.3 UCS tests with YN1.5MPA grout

3.2.3.1 Tests on cylindrical specimens

UCS tests were conducted on cylindrical specimens cast with YN1.5MPA grout, as shown in Figure 3 - 13. The test results acquired from cylindrical specimens are shown in Table 3 - 5 and Figure 3 - 14. The table shows that the cylindrical specimens cast with YN1.5MPA grout had an average UCS of 8.8 MPa, Young's Modulus of 3.2 GPa and Poisson's Ratio of 0.10. A typical shear failure mode in the test specimen is shown in Figure 3 - 15.

Figure 3 - 13 UCS test on the cylindrical specimen

Table 3 - 5 UCS results of cylindrical specimens

No.	*L* (mm)	*D* (mm)	*L*/*D*	UCS (MPa)	*E* (GPa)	*v*
1	131.1	53.2	2.5	8.9	3.4	0.08
2	133.5	53.8	2.5	8.7	3.2	0.11
3	130.6	53.7	2.4	8.9	3.0	0.12
Mean	131.7	53.6	2.5	8.8	3.2	0.10

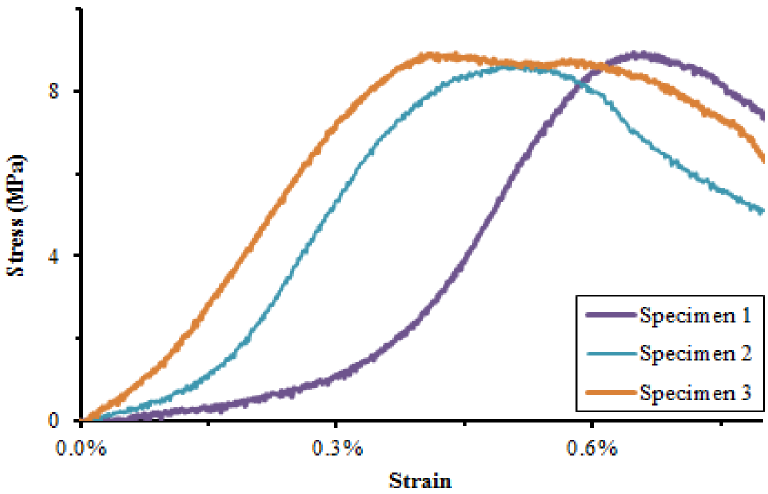

Figure 3 - 14 The stress - strain relationship of cylindrical specimens

Figure 3 - 15 Shear failure in the specimen

3.2.3.2 Tests on cubic specimens

Cubic specimens were also prepared and tested, as shown in Figure 3 - 16. The UCS results of cubic specimens are shown in Table 3 - 6 and Figure 3 - 17. The results show that the cubic specimens had a UCS of 11.5 MPa.

Figure 3 - 16 UCS test on the cubic specimen

Table 3 - 6 UCS results of the cubic specimens

No.	*L* (mm)	*W* (mm)	*H* (mm)	UCS (MPa)
1	49.8	50.3	50.2	11.5
2	49.9	50.3	49.8	11.8
3	50.3	50.2	50.2	11.3
Mean	50.0	50.3	50.1	11.5

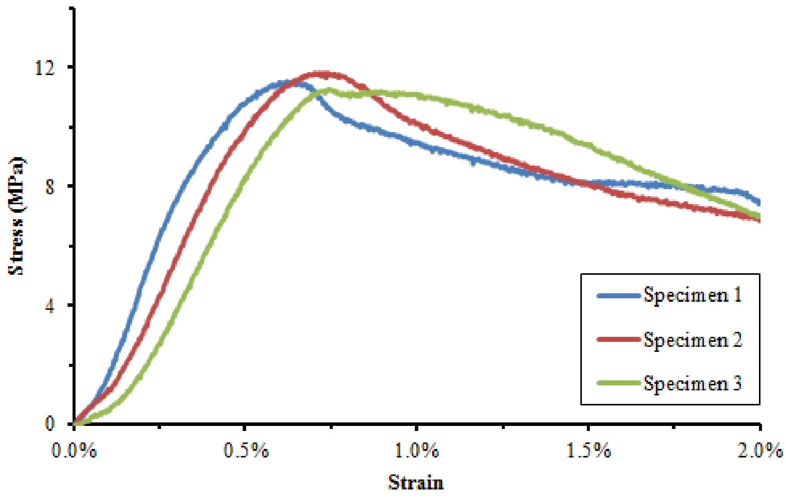

Figure 3 - 17 The stress - strain relationship of cubic specimens

The failure mode of the cubic specimens cast with YN1.5MPA material is shown in Figure 3 - 18. Clearly, a horizontal failure plane occurred along the middle of the specimen.

Figure 3 - 18 Failure mode of the cubic specimen

3.2.3.3 Result comparison between cylindrical and cubic specimens

The comparison between UCS results tested with cubic and cylindrical specimens is depicted in Figure 3 - 19. The results show that the UCS of cubic specimens was relatively higher than cylindrical specimens, which is consistent with the above findings. Generally, YN1.5MPA grout had a UCS around 10 MPa and this material was selected to cast the confining medium in cable bolt pull-out tests, simulating the weak rock.

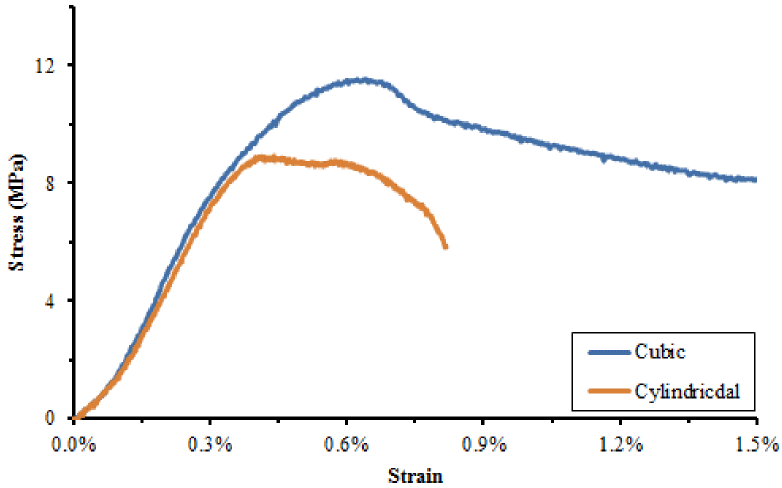

Figure 3 - 19 Comparison between UCS test results

3.2.4 UCS tests with GS40250 grout

3.2.4.1 Tests on cylindrical specimens

Cylindrical specimens were cast and prepared with GS40250 grout and UCS tests were conducted. The test results of cylindrical specimens are shown in Table 3 - 7 and Figure 3 - 20. The results show that cylindrical specimens had an average UCS of 22.5 MPa and Young's Modulus of 7.9 GPa.

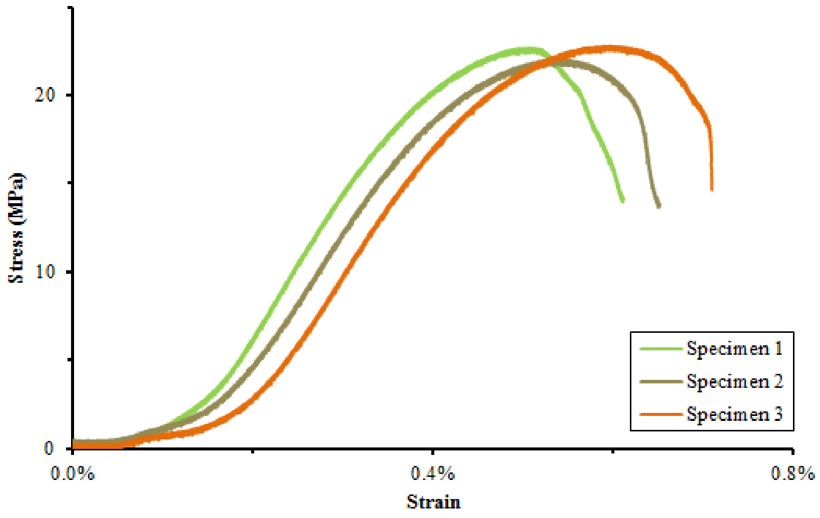

Figure 3 - 20 The stress - strain relationship of cylindrical specimens

Table 3 - 7 UCS results of cylindrical specimens

No.	*L* (mm)	*D* (mm)	*L*/*D*	UCS (MPa)	*E* (GPa)
1	141.8	53.9	2.6	22.7	8.2
2	143.0	53.9	2.7	22.0	7.7
3	143.6	53.9	2.7	22.8	7.8
Mean	142.8	53.9	2.7	22.5	7.9

3.2.4.2 Tests on cubic specimens

UCS tests were also conducted on cubic specimens and the test results are shown in Table 3 - 8 and Figure 3 - 21. The results show that the cubic specimens had a UCS of 27.1 MPa.

Table 3 - 8 UCS results of GS40250 grout tested with cubic specimens

No.	*L* (mm)	*W* (mm)	*H* (mm)	UCS (MPa)
1	50.1	50.1	50.1	27.7
2	50.2	50.1	50.5	26.9
3	50.3	50.1	50.3	26.6
Mean	50.2	50.1	50.3	27.1

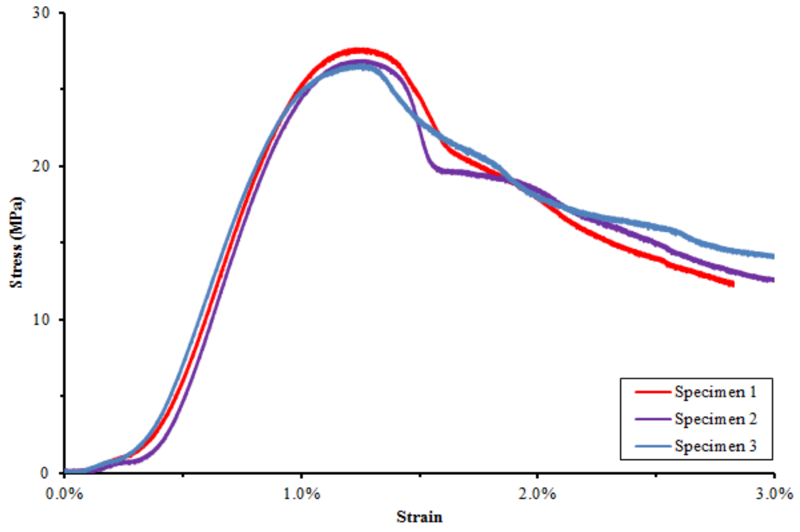

Figure 3 - 21 The stress - strain relationship of cubic specimens

3.2.4.3 Result comparison between cylindrical and cubic specimens

The UCS test results conducted on cubic and cylindrical specimens were compared together, as shown in Figure 3 - 22. The results show that the UCS of cubic specimens was generally larger than cylindrical specimens. Also, the cubic specimens behaved more ductile than cylindrical specimens.

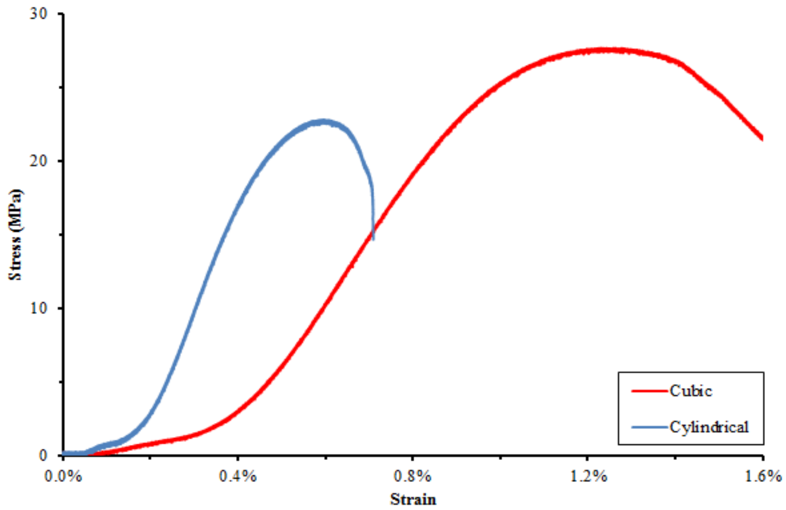

Figure 3 - 22 Comparison between UCS test results

3.3 Properties of the Orica grout

Stratabinder grout provided by Orica Australia Pty. Ltd. is widely used in the underground mining industry in Australia. A number of UCS and Brazilian tests were conducted to better understand the mechanical properties of this grout.

3.3.1 UCS tests

In the field, the grout poured into the borehole usually has a UCS close to 60 MPa. To be consistent with this, Stratabinder grout used in the laboratory should also have a UCS around 60 MPa. A number of UCS tests were conducted on specimens to evaluate the influence of w/c ratio on the UCS of Stratabinder grout.

3.3.1.1 Tests on cylindrical specimens

Four different w/c ratios, namely 0.35, 0.38, 0.42 and 0.45, were tested. The test specimens are shown in Figure 3 - 23. Both the Young's Modulus and Poisson's Ratio were measured in the test, as shown in Figure 3 - 24.

Figure 3 - 23 Specimens prepared with Stratabinder grout

Figure 3 - 24 UCS test on a cylindrical specimen

The UCS results of cylindrical specimens with a w/c ratio of 0.35 are shown in Table 3 - 9 and Figure 3 - 25. The results show that when a low w/c ratio of 0.35 was used, cylindrical specimens had a mean UCS of 63.1 MPa. When a w/c ratio of 0.38 was used, the stress versus strain relationship of cylindrical specimens is shown in Figure 3 - 26 and Table 3 - 10. When the w/c ratio was increased to 0.42, the UCS, Young's Modulus and Poisson's Ratio are shown in Table 3 - 11 and Figure 3 - 27. Last, when the w/c ratio was further increased to 0.45, the stress versus strain relationship of cylindrical specimens is shown in Table 3 - 12 and Figure 3 - 28.

Then, the performance of cylindrical specimens with four different w/c ratios was compared, as shown in Table 3 - 13 and Figure 3 - 29. The results show that the w/c ratio had an apparent influence on deciding the UCS of the specimens. Increasing the w/c ratio resulted in a reduction of both the UCS and the Young's Modulus.

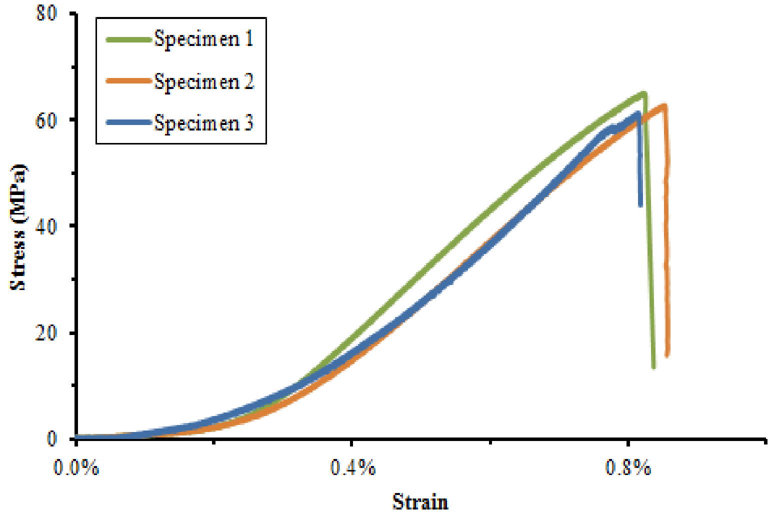

Figure 3 - 25 The stress - strain relationship of cylindrical specimens with a w/c ratio of 0.35

Table 3 - 9 UCS results of cylindrical specimens with a w/c ratio of 0.35

No.	*L* (mm)	*D* (mm)	*L*/*D*	UCS (MPa)	*E* (GPa)	*v*
1	141.0	53.3	2.6	65.1	12.0	0.20
2	141.1	53.3	2.6	62.8	11.4	0.23
3	141.4	53.7	2.6	61.4	12.1	0.25
Mean	141.2	53.4	2.6	63.1	11.8	0.23

Table 3 - 10 UCS results of cylindrical specimens with a w/c ratio of 0.38

No.	*L* (mm)	*D* (mm)	*L*/*D*	UCS (MPa)	*E* (GPa)	*v*
1	141.8	53.2	2.7	58.5	11.6	0.14
2	140.9	53.3	2.6	52.9	10.0	0.23
3	141.2	53.6	2.6	64.6	11.0	0.24
Mean	141.3	53.4	2.6	58.6	10.8	0.20

Table 3 - 11 UCS results of cylindrical specimens with a w/c ratio of 0.42

No.	*L* (mm)	*D* (mm)	*L*/*D*	UCS (MPa)	*E* (GPa)	*v*
1	139.3	53.3	2.6	53.9	9.4	0.18
2	138.9	53.2	2.6	55.4	10.4	0.28
3	139.7	53.3	2.6	53.5	10.0	0.18
Mean	139.3	53.3	2.6	54.3	9.9	0.21

Table 3 - 12 UCS results of cylindrical specimens with a w/c ratio of 0.45

No.	*L* (mm)	*D* (mm)	*L*/*D*	UCS (MPa)	*E* (GPa)	*v*
1	141.0	53.9	2.6	42.2	8.5	0.38
2	139.6	53.3	2.6	41.7	9.2	0.26
3	141.1	53.9	2.6	46.4	8.5	0.37
Mean	140.6	53.7	2.6	43.4	8.7	0.34

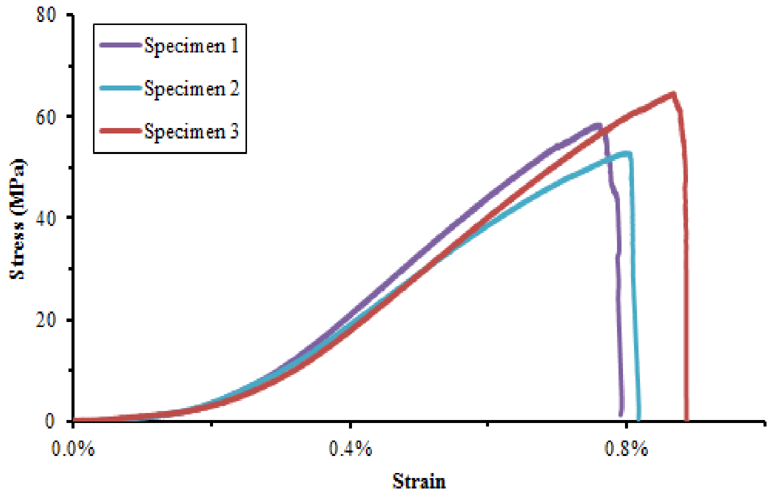

Figure 3 - 26 The stress - strain relationship of cylindrical specimens with a w/c ratio of 0.38

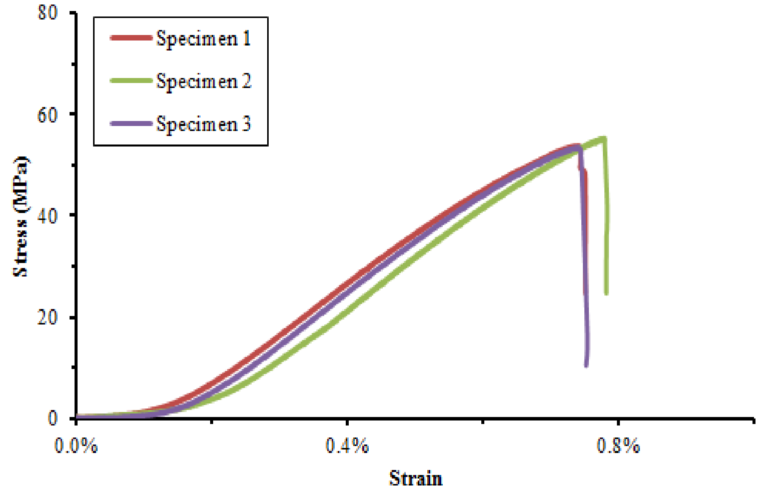

Figure 3 - 27 The stress - strain relationship of cylindrical specimens with a w/c ratio of 0.42

The failure modes of cylindrical specimens with different w/c ratios are shown in Figure 3 - 30. The results show that cylindrical specimens always failed along an inclined plane regardless of w/c ratios.

Sometimes, failure also occurred near the top section of cylindrical specimens and the grout in that area was ejected, as shown in Figure 3 - 31. However, this is probably due to the fact that the surface on one side of specimens was not smooth and stress concentration existed within unsmooth area in the loading process. Consequently, this stress concentration broke the grout in the top region.

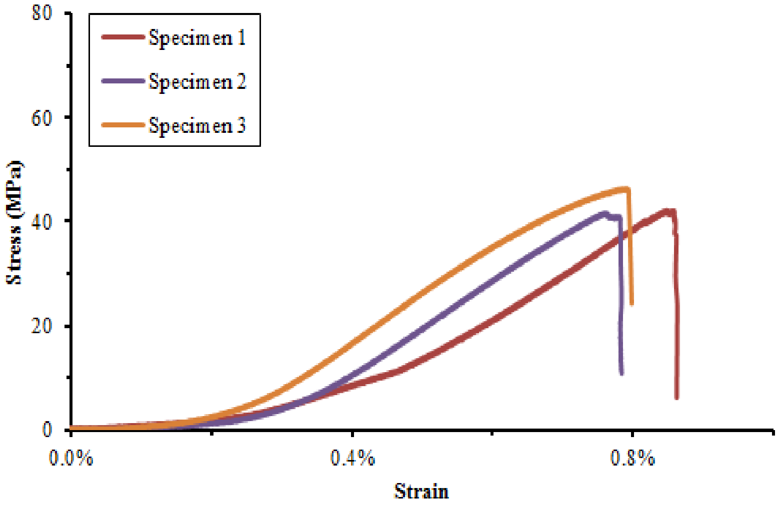

Figure 3 - 28 The stress - strain relationship of cylindrical specimens with a w/c ratio of 0.45

Table 3 - 13 Impact of w/c ratio on performance of cylindrical specimens

List	w/c ratio	UCS (MPa)	*E* (GPa)	*v*
1	0.35	63.1	11.8	0.23
2	0.38	58.6	10.8	0.20
3	0.42	54.3	9.9	0.21
4	0.45	43.4	8.7	0.34

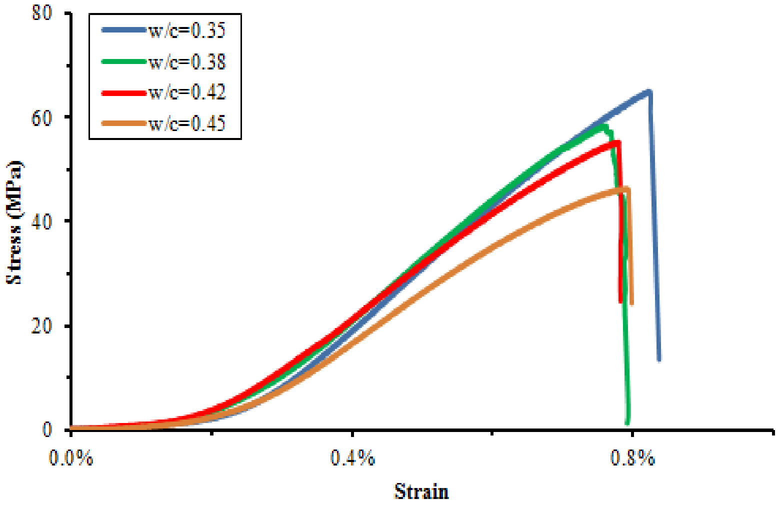

Figure 3 - 29 Influence of w/c ratio on stress - strain performance of cylindrical specimens

Figure 3 - 30 Failure modes of cylindrical specimens with different w/c ratios

Figure 3 - 31 Failure around the top section of cylindrical specimens

3.3.1.2 Tests on cubic specimens

UCS tests were also performed on cubic specimens of Stratabinder grout. The results of cubic specimens with the w/c ratio ranging from 0.35 to 0.45 are tabulated in Table 3 - 14, Table 3 - 15, Table 3 - 16 and Table 3 - 17. The stress versus strain relationship of the cubic specimens with the w/c ratio increasing from 0.35 to 0.45 are depicted in Figure 3 - 32, Figure 3 - 33, Figure 3 - 34 and Figure 3 - 35 separately.

The UCS results of cubic specimens are compared together, as shown in Figure 3 - 36. The results show that decreasing the w/c ratio was beneficial to improving the UCS of specimens.

Table 3 - 14 UCS results of cubic specimens with a w/c ratio of 0.35

No.	*L* (mm)	*W* (mm)	*H* (mm)	UCS (MPa)
1	50.3	49.9	49.9	71.5
2	50.5	50.1	50.0	69.6
3	50.3	50.2	50.3	64.7
Mean	50.4	50.1	50.1	68.6

Table 3 - 15 UCS results of cubic specimens with a w/c ratio of 0.38

No.	*L* (mm)	*W* (mm)	*H* (mm)	UCS (MPa)
1	50.4	50.3	50.4	60.7
2	50.3	50.3	50.2	63.9
3	50.2	50.2	50.1	67.8
Mean	50.3	50.3	50.2	64.1

Table 3 - 16 UCS results of cubic specimens with a w/c ratio of 0.42

No.	*L* (mm)	*W* (mm)	*H* (mm)	UCS (MPa)
1	50.4	50.1	50.3	63.6
2	50.3	50.3	50.2	56.7
3	50.5	50.2	50.2	60.3
Mean	50.4	50.2	50.2	60.2

Table 3 - 17 UCS results of cubic specimens with a w/c ratio of 0.45

No.	*L* (mm)	*W* (mm)	*H* (mm)	UCS (MPa)
1	50.4	50.1	50.3	52.7
2	50.3	50.2	50.2	50.1
3	50.5	50.2	50.2	46.7
Mean	50.4	50.2	50.2	49.8

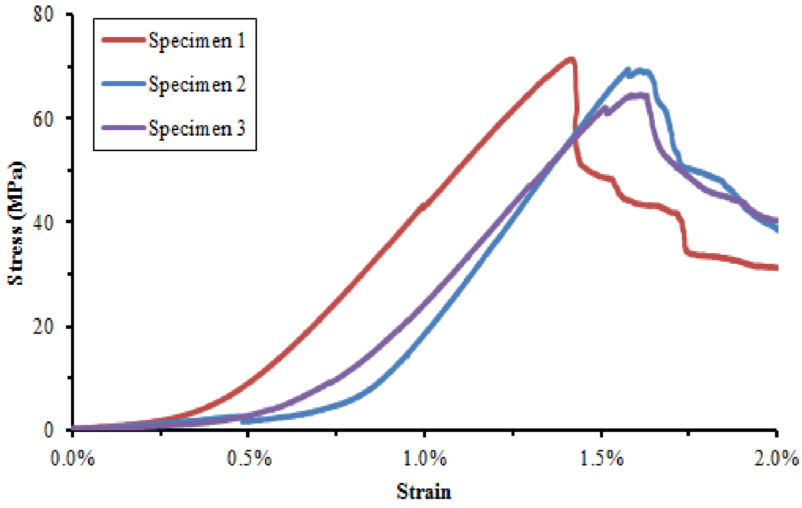

Figure 3 - 32 The stress - strain relationship of cubic specimens with a w/c ratio of 0.35

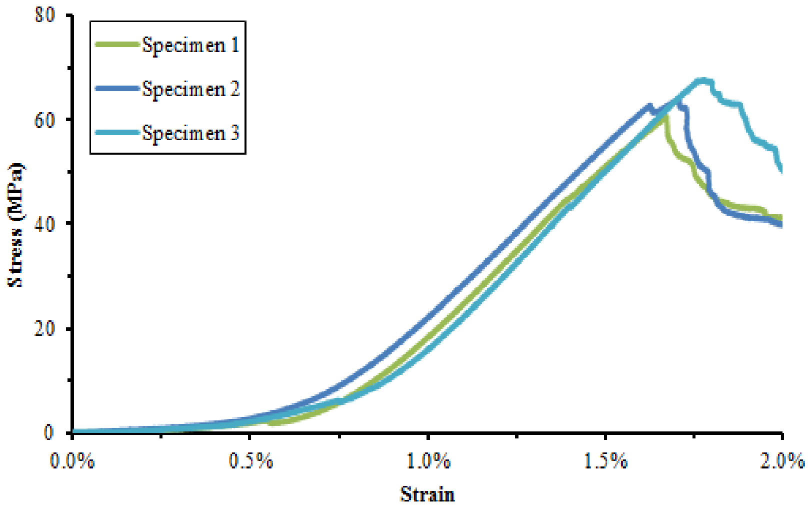

Figure 3 - 33 The stress - strain relationship of cubic specimens with a w/c ratio of 0.38

Typical failure modes are shown in Figure 3 - 37. It is clear to see that a horizontal failure plane occurred in the middle of the specimens and that thus was the dominant failure mode. The shear failure along an inclined plane was also found, as shown in Figure 3 - 38. However, this type of failure behaviour was less frequent.

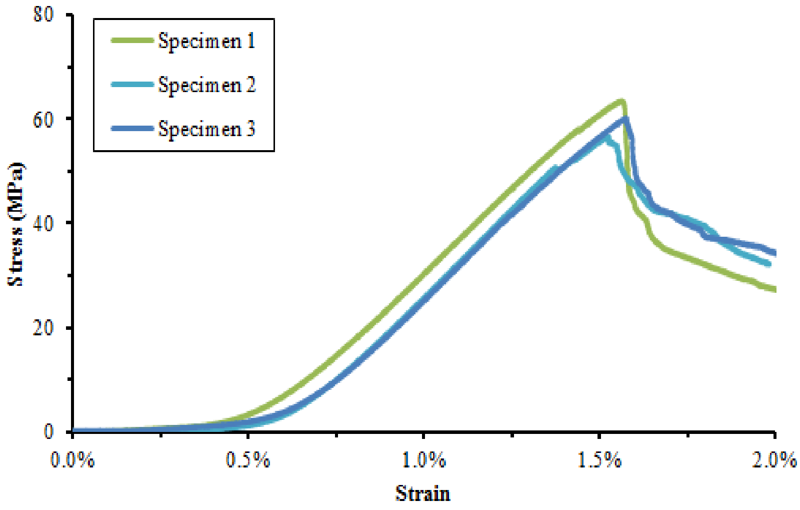

Figure 3 - 34 The stress - strain relationship of cubic specimens with a w/c ratio of 0.42

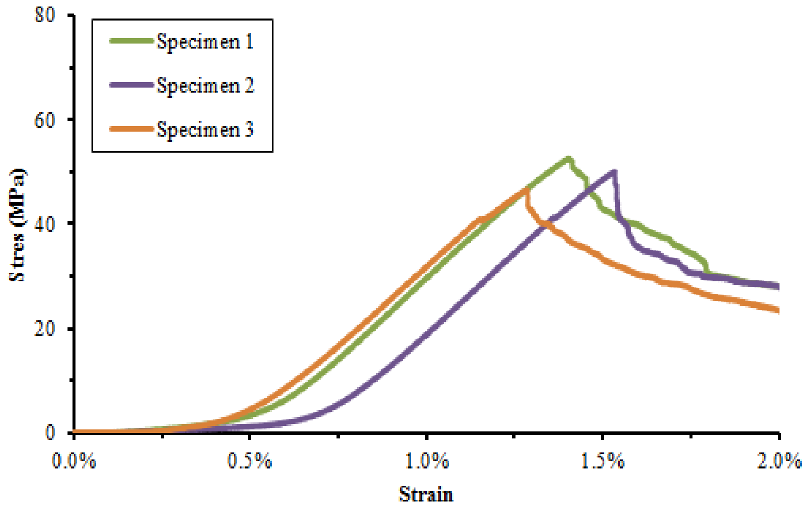

Figure 3 - 35 The stress - strain relationship of cubic specimens with a w/c ratio of 0.45

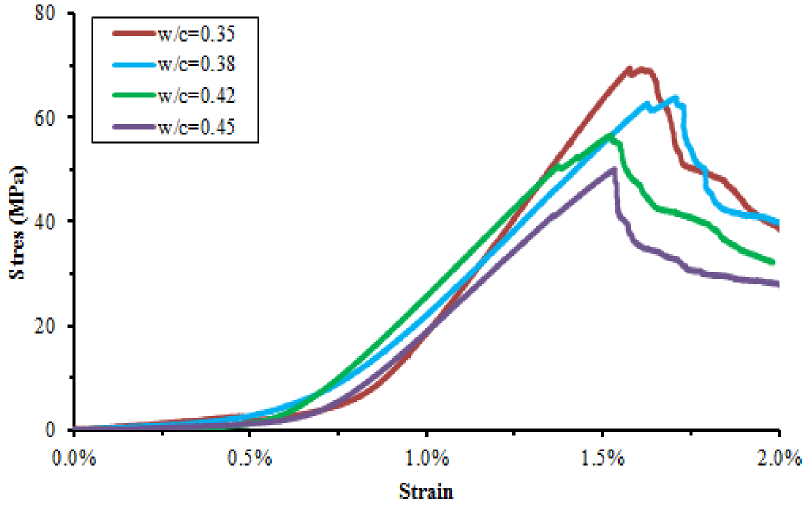

Figure 3 - 36 Influence of w/c ratio on axial performance of cubic specimens

Figure 3 - 37 Failure along a horizontal plane in cubic specimens

Figure 3 - 38 Shear failure of cubic specimens along an inclined plane

3.3.1.3 Result comparison between cylindrical and cubic specimens

The influence of specimen shape on axial performance of Stratabinder grout is shown in Figure 3 - 39, Figure 3 - 40, Figure 3 - 41 and Figure 3 - 42. The results show that in different w/c ratio conditions, cubic specimens were more ductile than cylindrical specimens. Furthermore, the UCS of cubic specimens was always higher than cylindrical specimens.

The influence of w/c ratio on the UCS of Stratabinder grout is shown in Table 3 - 18 and Figure 3 - 43. As would be expected, the w/c ratio had a significant effect on determining the strength of the grout and decreasing the w/c ratio effectively increased the UCS of Stratabinder grout. It was also found that when a w/c ratio of 0.42 was used, the UCS of Stratabinder grout was close to 60 MPa. Thus, the w/c ratio of 0.42 was always used for the embedment section in the cable bolt pull-out tests. Furthermore, to prevent the bond failure in the anchor section and make sure the bond strength in the anchor section was higher than the embedment section, the w/c ratio of 0.35 was used to bond the cable bolt and the anchor tube together, which will be illustrated in detail in the next chapter.

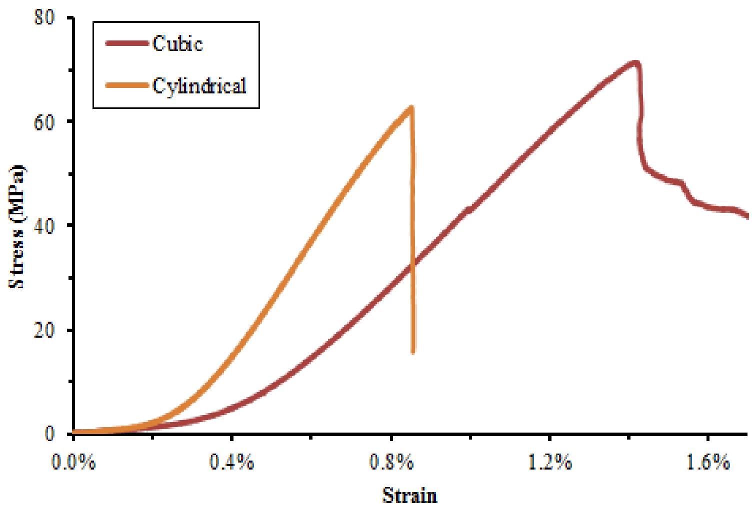

Figure 3 - 39 Comparison between UCS test results with a w/c ratio of 0.35

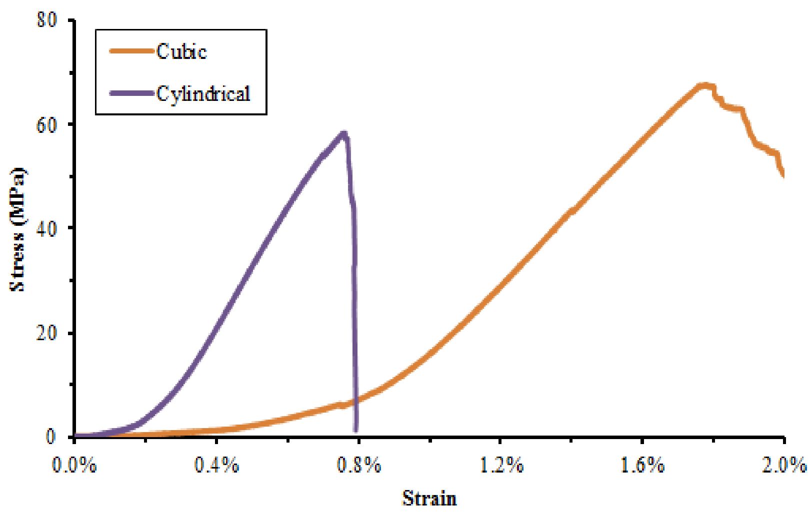

Figure 3 - 40 Comparison between UCS test results with a w/c ratio of 0.38

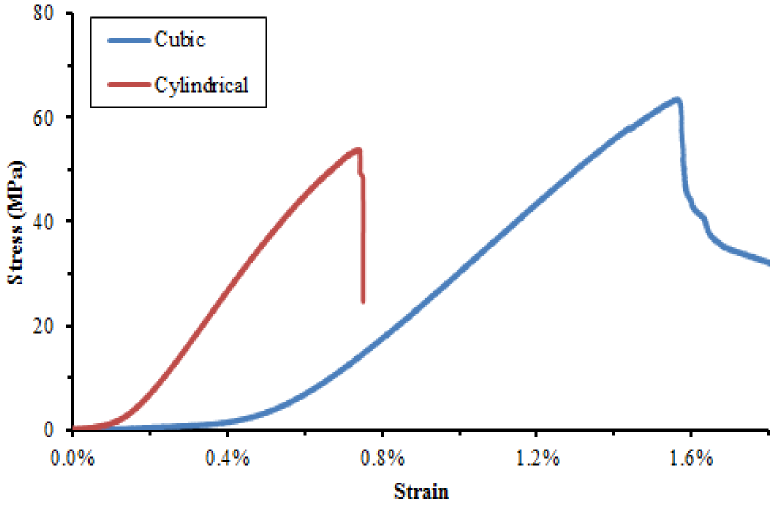

Figure 3 - 41 Comparison between UCS test results with a w/c ratio of 0.42

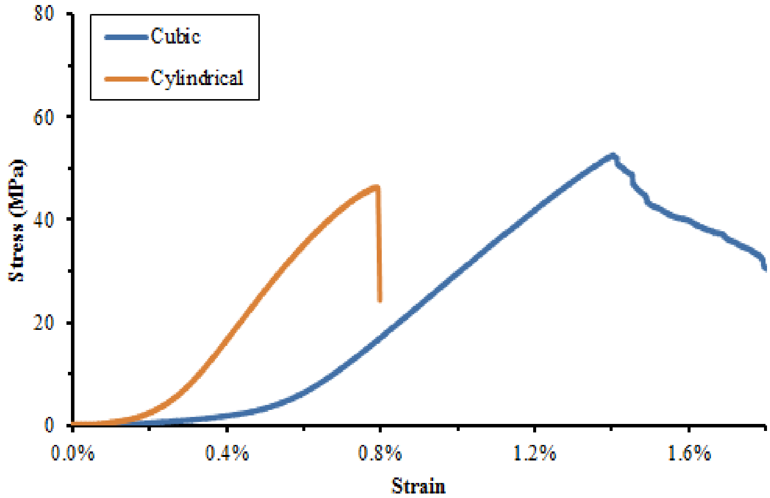

Figure 3 - 42 Comparison between UCS test results with a w/c ratio of 0.45

Table 3 - 18 UCS of Stratabinder grout tested with cylindrical and cubic specimens

List	w/c ratio	UCS of cylindrical specimens (MPa)	UCS of cubic specimens (MPa)
1	0.35	63.1	68.6
2	0.38	58.6	64.1
3	0.42	54.3	60.2
4	0.45	43.4	49.8

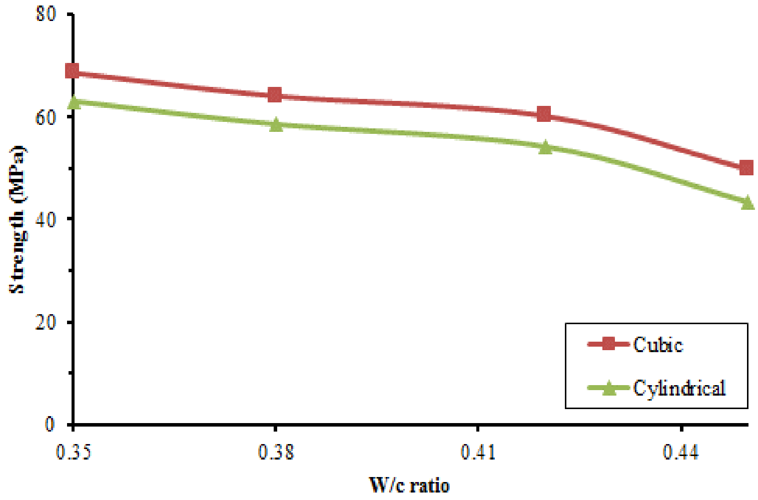

Figure 3 - 43 Influence of w/c ratio on UCS of cylindrical and cubic specimens

3.3.2 Brazilian tests

Brazilian tests were conducted to evaluate the tensile strength of Stratabinder grout in different w/c ratio conditions. Two w/c ratios, namely 0.35 and 0.42, were tested. When the w/c ratio of 0.35 was used, a photo of specimens is shown in Figure 3 - 44.

The MTS machine was used to conduct the Brazilian test and the test process is depicted in Figure 3 - 45. A tensile failure mode in the specimen is shown in Figure 3 - 46.

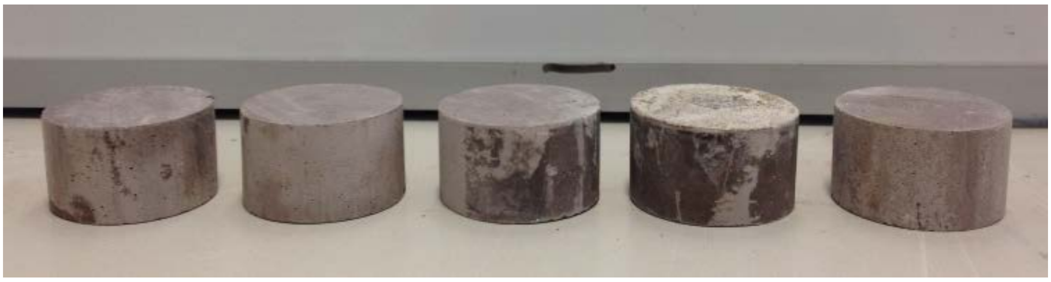

Figure 3 - 44 Test specimen preparation for Brazilian testing

The bearing capacity was recorded during the test. The dimensions of specimens including the specimen thickness (*T*) and results are tabulated in Table 3 - 19. The results show that when the w/c ratio of 0.35 was used, the specimens had a tensile strength of 1.9 MPa.

Figure 3 - 45 Brazilian test on the specimen

Figure 3 - 46 Tensile failure in the specimen

Brazilian tests were also conducted on specimens cast with a w/c ratio of 0.42 and the results are shown in Table 3 - 20. The results show that when the w/c ratio increased to

0.42, the tensile strength decreased to 1.5 MPa, indicating that the w/c ratio had an impact on the tensile strength of the grout. However, this impact was less sensitive.

Table 3 - 19 Test results of specimens cast with a w/c ratio of 0.35

List	*T* (mm)	*D* (mm)	Load (kN)	Stress (MPa)
1	24.4	42.3	2.6	1.6
2	25.6	41.0	3.5	2.1
3	24.3	41.5	3.0	1.9
Mean	24.8	41.6	3.0	1.9

Table 3 - 20 Test results of specimens cast with a w/c ratio of 0.42

List	*T* (mm)	*D* (mm)	Load (kN)	Stress (MPa)
1	25.0	42.1	3.0	1.8
2	24.9	41.9	2.2	1.3
3	25.1	42.1	2.3	1.4
Mean	25.0	42.0	2.5	1.5

3.4 Summary

Two types of cement-based grout of which one is Hanson grout and the other is Orica grout were tested. Hanson grout is used to cast the confining medium in the cable bolt pull-out tests, simulating rocks with different strength. UCS tests were conducted on three different materials, namely GS32250 grout, YN1.5MPa grout and GS40250 grout. Both cylindrical and cubic specimens were prepared and tested. It was found that the cubic specimens always had a higher UCS than cylindrical specimens. Also, cubic specimens showed ductile behaviour while cylindrical specimens displayed brittle behaviour. Furthermore, when the cubic specimens were tested, failure occurred along a horizontal plane in the specimen or an inclined plane. However, for cylindrical specimens, shear failure along an inclined plane always occurred. In the following chapters, the mechanical properties of the grout were analysed based on cylindrical specimen testing results.

GS32250 grout had a UCS of 62.7 MPa, Young's Modulus of 11.8 GPa and Poisson's Ratio of 0.26. This material had high strength and was selected to simulate strong rock in cable bolt pull-out tests. YN1.5MPA grout had a much lower UCS of 8.8 MPa, Young's Modulus of 3.2 GPa and Poisson's Ratio of 0.10. And this grout was used to represent weak rock. As for GS40250 grout, it had a medium UCS of 22.5 MPa and Young's Modulus of 7.9 GPa.

Stratabinder grout supplied by Orica Australia Pty. Ltd. was selected as the cable bonding material. A number of UCS tests were conducted on both cylindrical and cubic specimens to evaluate the influence of w/c ratio on axial performance of the grout. It was found that when cylindrical specimens were tested, the UCS of Stratabinder grout decreased from 63.1 MPa to 43.4 MPa with the w/c ratio increasing from 0.35 to 0.45. Meanwhile, increasing the w/c ratio had an adverse impact on the Young's Modulus of the grout which decreased from 11.8 GPa to 8.7 GPa. Two w/c ratios were selected in the following cable bolt pull-out tests. Specifically, the w/c ratio of 0.42 was used in the embedment section and the w/c ratio of 0.35 was used in the anchor section.

Brazilian tests were performed on Stratabinder grout with two w/c ratios, namely 0.35 and 0.42. It was found that when the w/c ratio of 0.35 was used, Stratabinder grout had a tensile strength of 1.9 MPa. When the w/c ratio was increased to 0.42, the tensile strength decreased to 1.5 MPa.

CHAPTER FOUR

THE SHEAR BEHAVIOUR OF THE PORTLAND CEMENT GROUT WITH DIRECT SHEAR TEST

4.1 Introduction

The shear behaviour of the cement-based materials can be evaluated via either a tri-axial test or direct shear test. However, the shear failure in tri-axial tests always occurs on an arbitrary plane. It is not a true reflection of the cable bolting failure mode because bond failure usually occurs along a pre-defined plane or the cable/grout interface, as proved by Thomas (2012), Blanco Martín *et al.* (2011), Cao *et al.* (2012) and Ma (2014). Therefore, the direct shear test which can induce the shear failure along a pre-determined plane can better reflect the shear performance of the grout used in cable bolt applications. Furthermore, Moosavi and Bawden (2003) compared the tri-axial test and direct shear test results on Type 10 Portland cement, finding tri-axial tests were more likely to overestimate the shear strength, as shown in Figure 4 - 1.

The shear behaviour of the Stratabinder grout was studied with direct shear tests. Intact cubic samples with an edge length of 100 mm were cast with a w/c ratio of 0.42. After fully cured, all samples were ground to ensure that they had flat surfaces. A direct shear box test machine with a maximum shear capacity of 300 kN was used. Two different boundary conditions, namely constant normal stress and constant normal stiffness, were applied on the samples. In each boundary condition, five different normal stresses, namely 0.1 MPa, 0.5 MPa, 1.5 MPa, 3 MPa and 6 MPa, were applied. Furthermore, in the constant normal stiffness condition, a low stiffness of 10 kN/mm was applied. The shear stress, dilation and shear displacement were recorded. After testing, the shear strength failure envelope of the grout was acquired. A Mohr - Coulomb model was used to fit the shear strength failure envelope to determine the cohesive strength and the internal friction angle. Finally, the shear behaviour of the grout in the constant normal stress and constant normal stiffness conditions was compared.

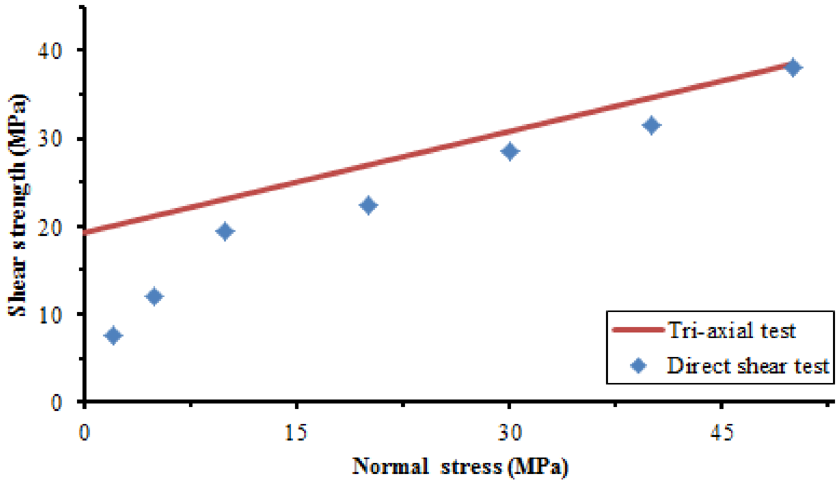

Figure 4 - 1 Comparison between results acquired from tri-axial tests and direct shear tests on Type 10 Portland cement with a w/c ratio of 0.4, after Moosavi and Bawden (2003)

4.2 Direct shear test preparation

4.2.1 The direct shear box test machine

The direct shear box RDS-300 manufactured by Geotechnical Consulting and Testing Systems (GCTS) was used. The front view of the direct shear box is shown in Figure 4 - 2. The direct shear box is a servo control machine, mainly composed of two parts, namely the shear loading section and the normal loading section. The shear loading actuator can provide a maximum shear capacity of 300 kN and the normal loading actuator can provide a maximum normal load of 500 kN. Two different boundary conditions, namely the constant normal stress and constant normal stiffness, can be applied. Additionally, since the sample mould can be regarded as rigid, the boundary between the sample and the mould is identical with the boundary between the mould and the shear box. During testing, the GCTS software package automatically calculates shear stress, normal deformation and shear deformation. Different components of the direct shear box are shown in Figure 4 - 3.

Figure 4 - 2 The outline of the direct shear box (GCTS, 2010)

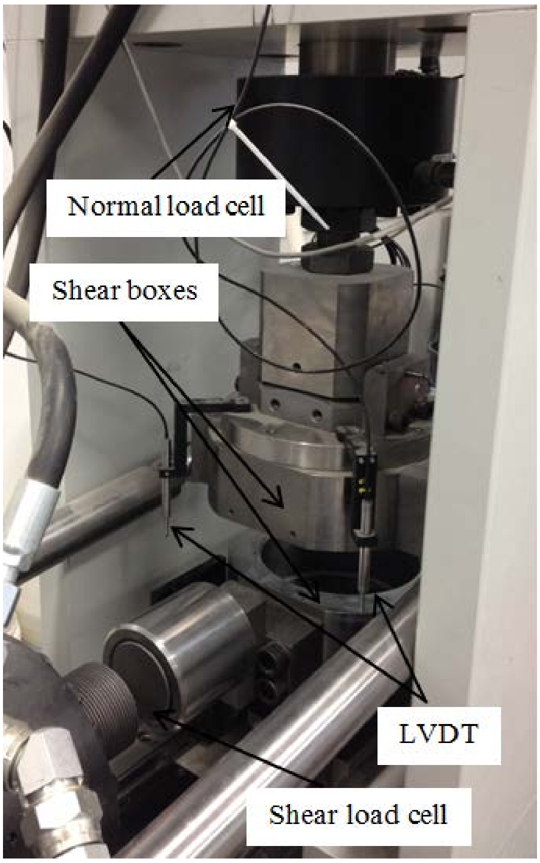

Figure 4 - 3 Main components of the direct shear box

4.2.2 Sample preparation

Currently, there is no standard in specifying the geometry and dimensions of samples for shear tests of cement grout. The ISRM recommends using cubic samples for the direct shear test (ISRM, 2007). However, it is mainly applicable to tests for jointed rock masses. Although little work was conducted on the shear behaviour of the cement paste via direct shear test, more work has been done on the direct shear tests of concrete materials, such as by Sonnenberg *et al.* (2003), and Wong *et al.* (2007), and cubic samples were always used, as shown in Figure 4 - 4.

Thus, cubic samples were cast and used in this study. First, a plastic mould was prepared, as shown in Figure 4 - 5. Then, the grout was mixed and poured into the mould. A w/c ratio of 0.42 was selected because this w/c ratio was used in the embedment section of the following cable bolt pull-out tests. After setting for 24 hours, the plastic mould was removed. The samples were put into the water basin, curing for at least 28 days. Then the samples were ground to ensure that they have flat parallel surfaces.

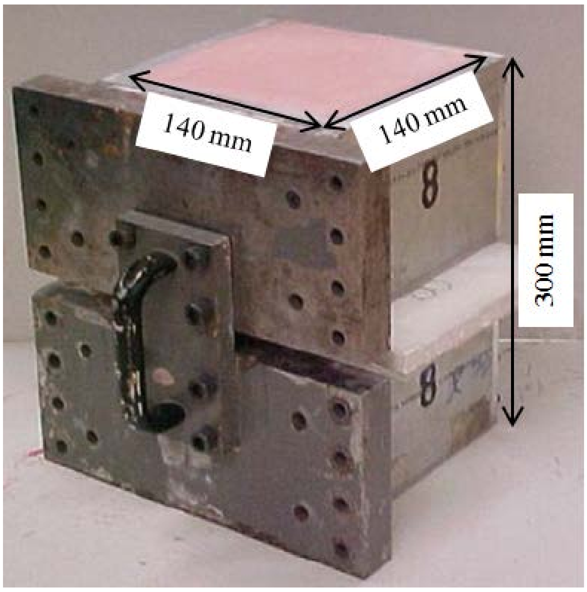

Figure 4 - 4 Cubic samples used in direct shear tests on concrete materials, after Wong *et al.* (2007)

Figure 4 - 5 Cubic sample mould preparation

4.3 Shear behaviour of the grout in the constant normal stress condition

4.3.1 Direct shear test process in the constant normal stress condition

The first series of tests was conducted in the constant normal stress condition. Specifically, the bottom shear box was pulled out before testing. Then the assembled sample and sample holder were installed in the bottom of the shear box, as shown in Figure 4 - 6.

The top sample holder was installed, as shown in Figure 4 - 7. The top shear box was moved down until a low normal force of 0.5 kN was applied on the sample. The relative position of the top and bottom of shear boxes is shown in Figure 4 - 8.

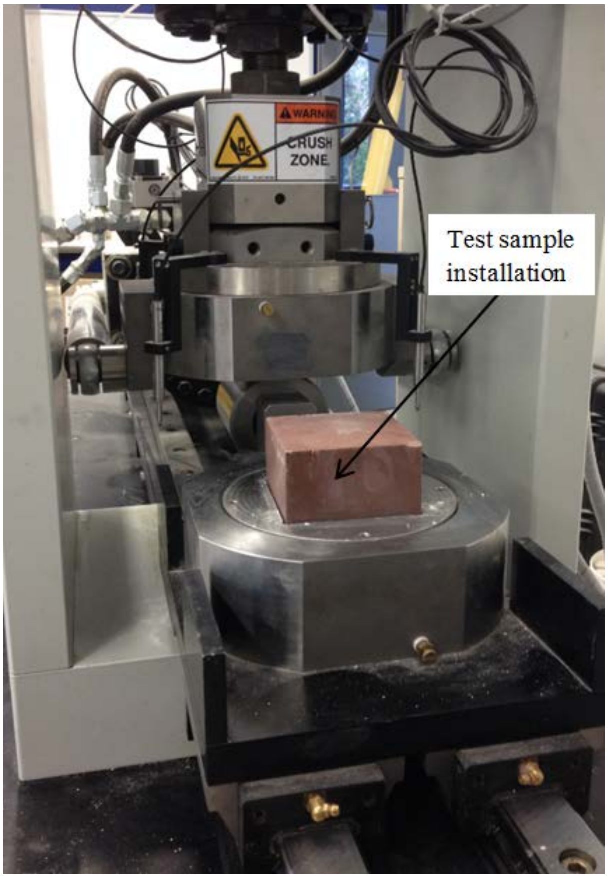

Figure 4 - 6 Sample installation in the direct shear box

Figure 4 - 7 Making the sample holder in line with the shear box

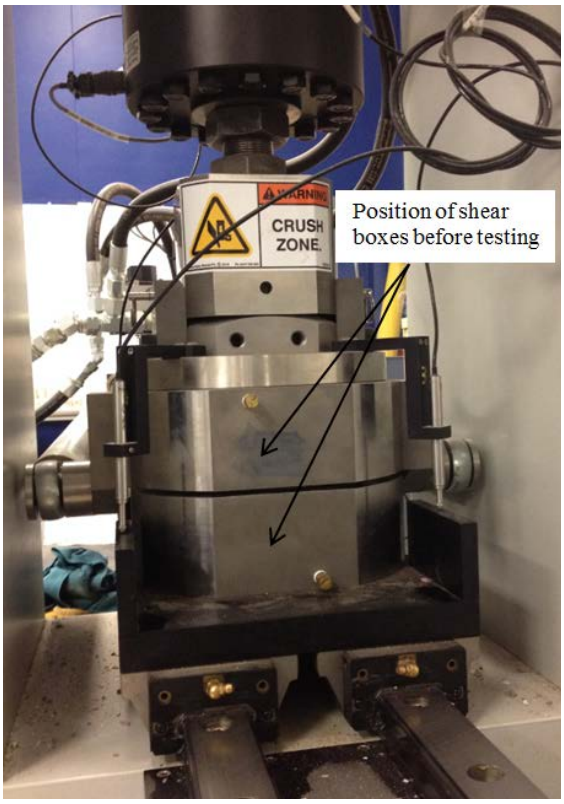

Figure 4 - 8 Relative positioning of the shear boxes before testing

To acquire the shear strength envelope of the grout, a series of different normal stresses should be applied. Furthermore, the normal stresses should be larger than zero and smaller than the UCS of the sample. Therefore, in the first series of tests, a low normal stress of 0.1 MPa was applied on the sample. The feedback of the normal actuator was set as stress control. After the normal load cell was able to record a stable stress of 0.1 MPa, the normal actuator was set up accordingly.

Then, the connector between the shear load cell and the bottom shear box was tightened, as shown in Figure 4 - 9. After the load cell and displacement transducers were zeroed, the shear specimen was ready for testing.

In the direct shear test, the shearing speed can be chosen within the range between 0 and 1 mm/min (ISRM, 2007). Thus, a constant shearing speed of 0.5 mm/min was applied on the sample, as shown in Figure 4 - 10. During testing, the dilation or normal displacement, shear stress and displacement were recorded. The shear stress versus displacement relationship of the sample is shown in Figure 4 - 11. The results show that there was no variation of the shear stress until a shear displacement of 1.4 mm. The reason is that there was a small gap between the sample and the mould after the sample was installed. In the initial loading stage, the gap was squeezed. And after the side of the sample fully contacted with the mould, the shear stress started to increase apparently. At a shear displacement of 6.7 mm, the shear stress reached a peak value to 12.2 MPa. Meanwhile, the dilation reached a maximum value of 0.7 mm. After the peak, there was a sudden drop of the shear stress, which was the result of the brittle failure of the grout.

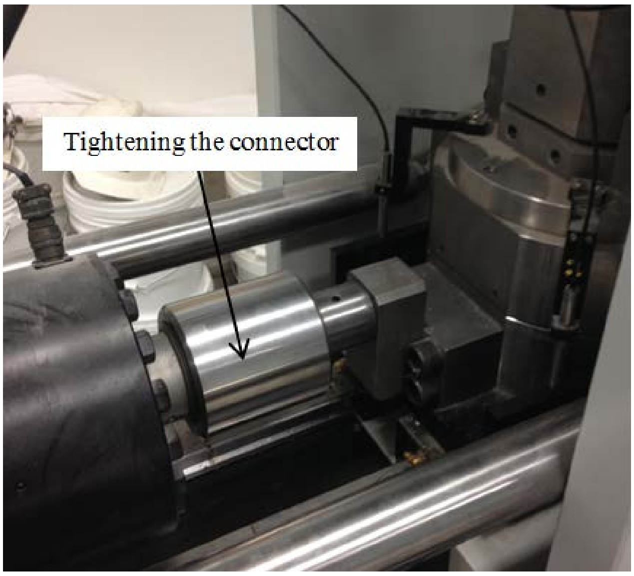

Figure 4 - 9 Tightening the connector between the load cell and the bottom shear box

After the test, the connector was released and the top shear box was lifted up, as shown in Figure 4 - 12 and Figure 4 - 13. Then, the sample holders were removed to check the failure mode, as shown in Figure 4 - 14. An apparent shear failure plane occurred in the middle of the sample. Also, it was found that the shear failure plane was not perfectly horizontal. This uneven shear failure plane resulted in dilation during the shear loading process.

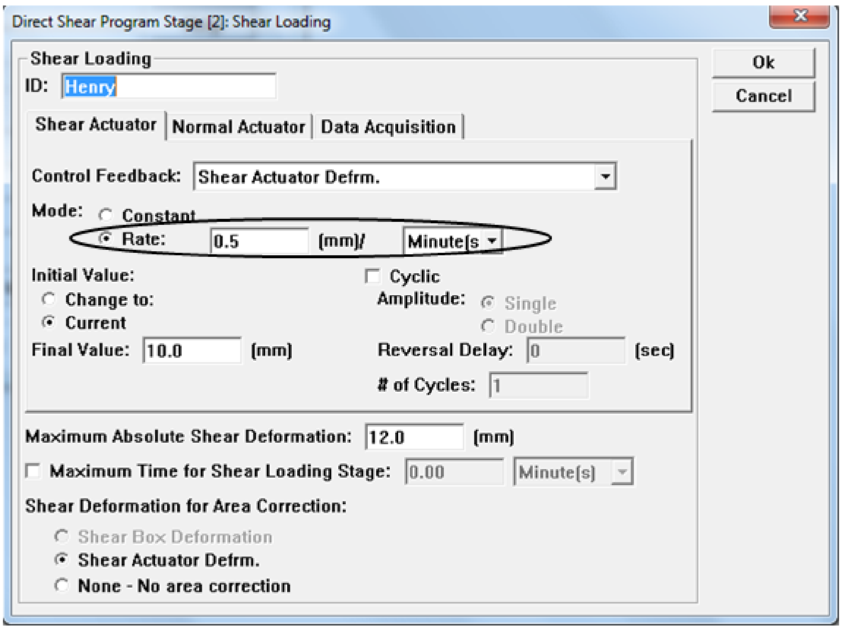

Figure 4 - 10 Constant shearing speed configuration in the software

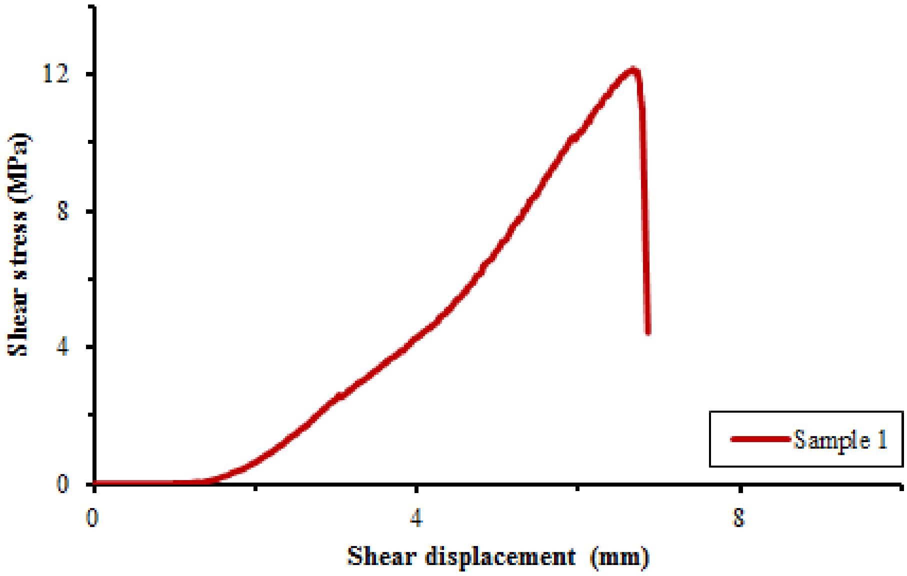

Figure 4 - 11 Shear stress variation of the sample with displacement

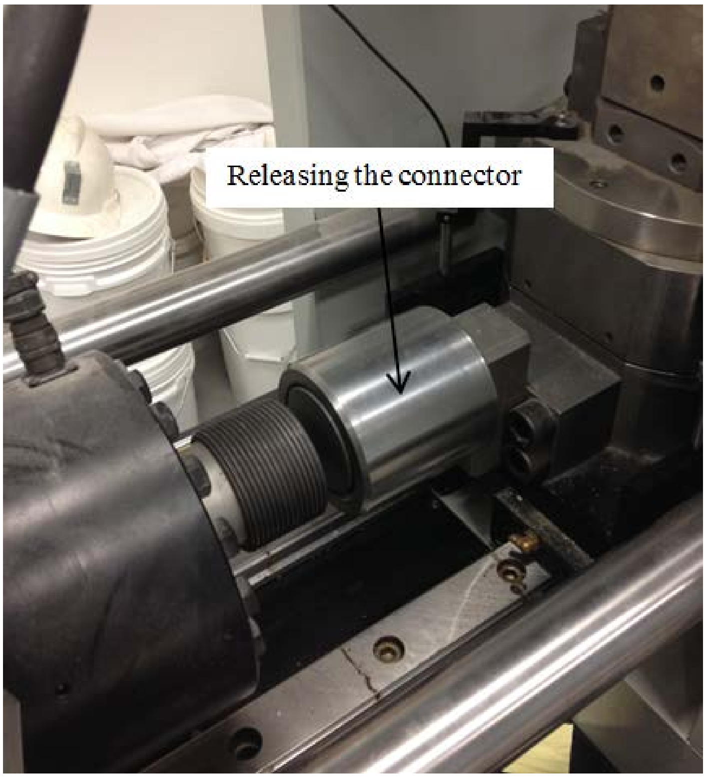

Figure 4 - 12 The connector was released after testing

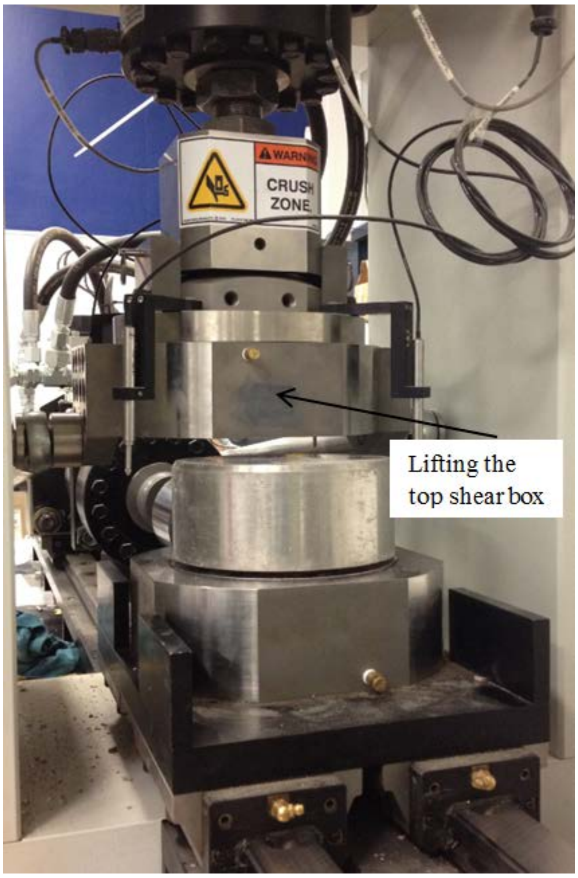

Figure 4 - 13 The top shear box was lifted up to remove the sample

Figure 4 - 14 Shear failure in the middle of the sample

4.3.2 Test results in the constant normal stress condition

Each test was replicated three times. After the results were acquired, two tests that have close results were regarded as the best. As for the third one, it was discarded. The best two were averaged as final results. With a normal stress of 0.1 MPa, the relationship between the shear stress and displacement is shown in Figure 4 - 15 and Table 4 - 1. The results show that at a shear displacement of 3.8 mm, the shear stress of the Sample 2 decreased momentarily and then the shear stress increased again. This is because an initial crack occurred in the sample after a small shear displacement. With the shear displacement increasing, the mechanical interlocking was enhanced and the shear stress increased again until the peak.

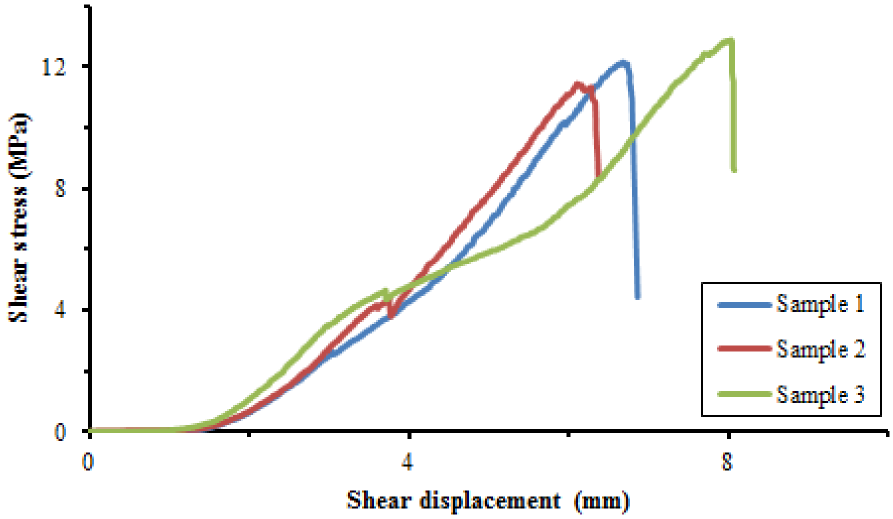

Figure 4 - 15 Shear behaviour of the grout with a normal stress of 0.1 MPa

Table 4 - 1 Selected test results of the grout with a normal stress of 0.1 MPa

Sample number	Length (mm)	Width (mm)	Shear strength (MPa)	Dilation limit (mm)
1	100.1	99.1	12.2	0.7
2	99.3	99.3	11.4	0.6
Mean	99.7	99.2	11.8	0.6

Then the normal stress was increased to 0.5 MPa, the relationship between the shear stress and displacement is shown in Figure 4 - 16 and Table 4 - 2.

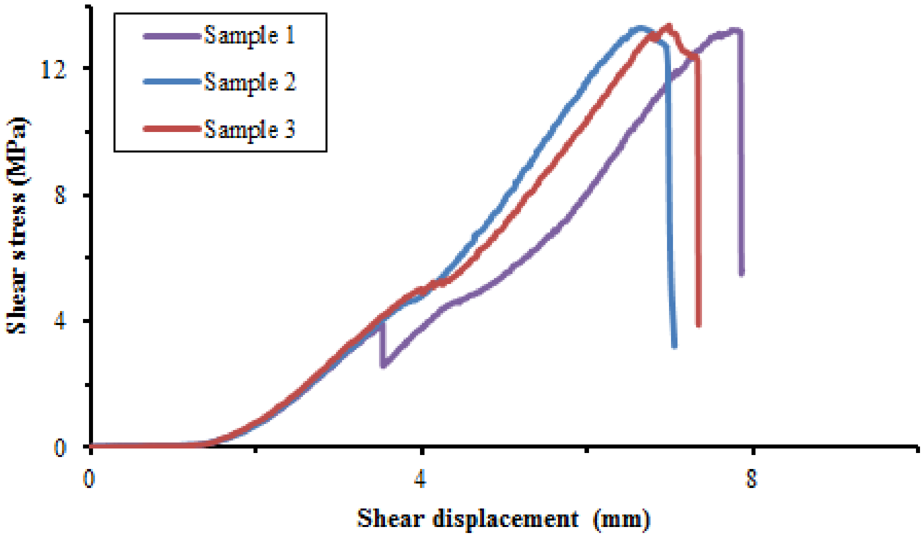

Figure 4 - 16 Shear behaviour of the grout with a normal stress of 0.5 MPa

Table 4 - 2 Selected test results of the grout with a normal stress of 0.5 MPa

Sample number	Length (mm)	Width (mm)	Shear strength (MPa)	Dilation limit (mm)
2	99.7	99.6	13.3	0.7
3	99.2	98.8	13.4	0.7
Mean	99.4	99.2	13.4	0.7

When the normal stress was increased to 1.5 MPa, the relationship between the shear stress and displacement is shown in Figure 4 - 17 and Table 4 - 3.

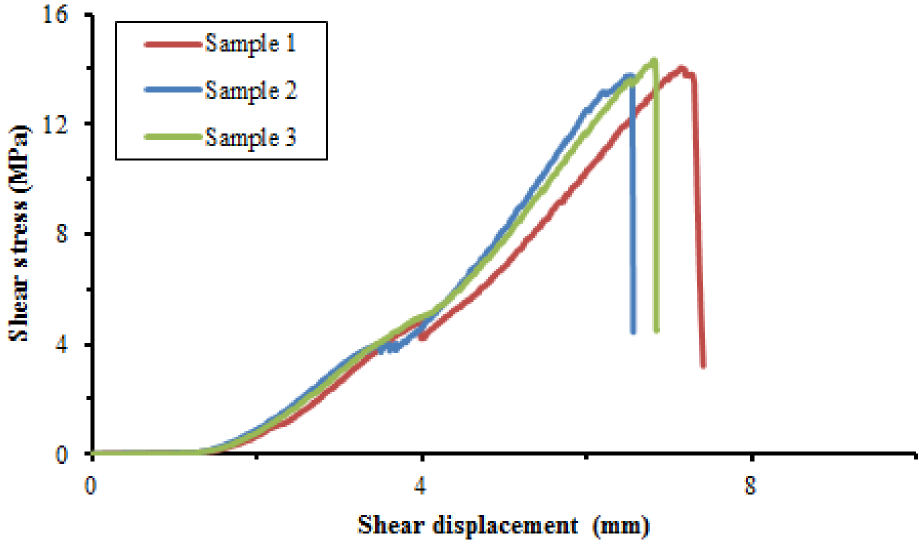

Figure 4 - 17 Shear behaviour of the grout with a normal stress of 1.5 MPa

Table 4 - 3 Selected test results of the grout with a normal stress of 1.5 MPa

Sample number	Length (mm)	Width (mm)	Shear strength (MPa)	Dilation limit (mm)
2	99.8	98.9	13.8	0.4
3	99.0	98.8	14.4	0.6
Mean	99.4	98.9	14.1	0.5

With a normal stress of 3 MPa, the relationship between the shear stress and displacement is shown in Figure 4 - 18 and Table 4 - 4.

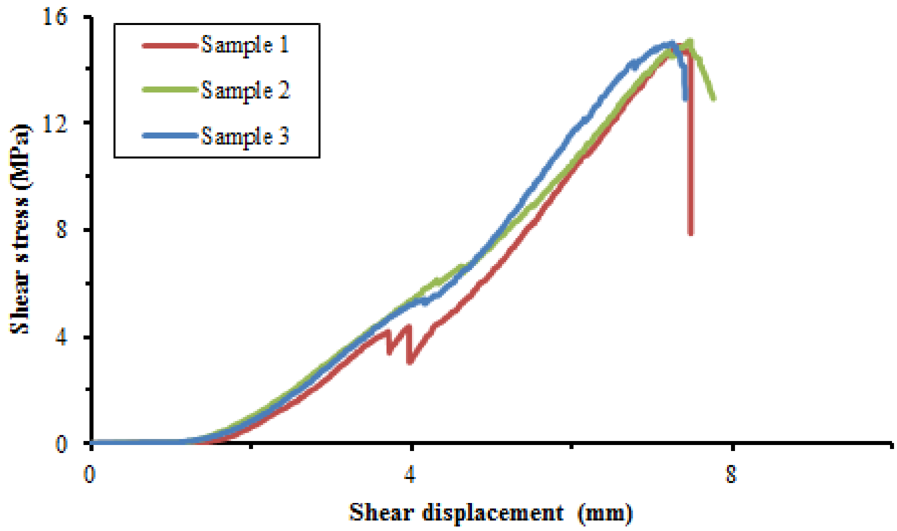

Figure 4 - 18 Shear behaviour of the grout with a normal stress of 3 MPa

Table 4 - 4 Selected test results of the grout with a normal stress of 3 MPa

Sample number	Length (mm)	Width (mm)	Shear strength (MPa)	Dilation limit (mm)
2	99.5	99.1	15.1	0.6
3	98.9	98.6	15.0	0.7
Mean	99.2	98.9	15.1	0.6

Finally, the normal stress was increased up to 6 MPa, the relationship between the shear stress and displacement is shown in Figure 4 - 19 and Table 4 - 5.

The shear performance of the grout in different normal stress conditions is shown in Figure 4 - 20 and Table 4 - 6. The results show that the shear strength of the grout increased with the normal stress. The shear displacement where shear strength occurred also increased with the normal stress. The influence of normal stress on the dilation of the grout is shown in Figure 4 - 21, which shows that the dilation limit was less sensitive to the different normal stresses.

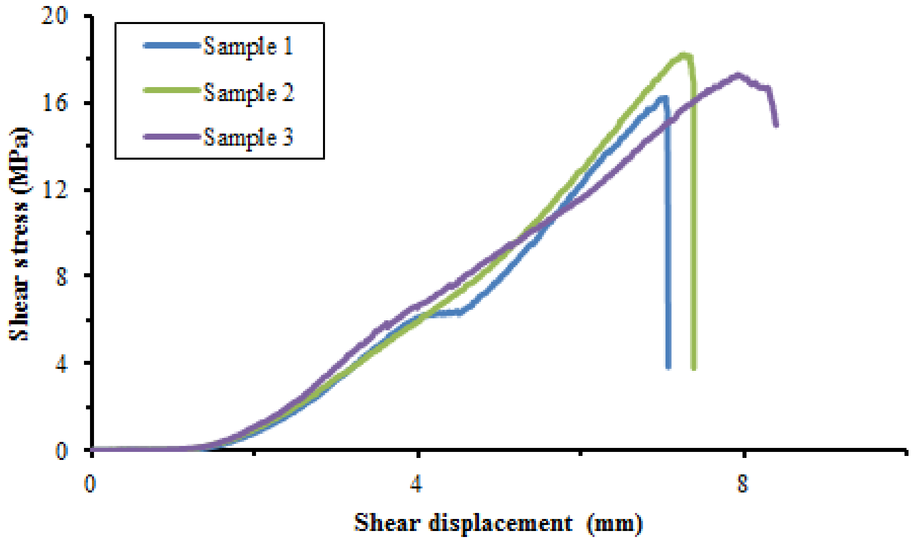

Figure 4 - 19 Shear behaviour of the grout with a normal stress of 6 MPa

Table 4 - 5 Selected test results of the grout with a normal stress of 6 MPa

Sample number	Length (mm)	Width (mm)	Shear strength (MPa)	Dilation limit (mm)
2	99.6	98.8	18.2	0.7
3	99.6	99.1	17.3	0.6
Mean	99.6	98.9	17.7	0.6

The shear strength failure envelope of the grout in the constant normal stress condition is shown in Figure 4 - 22. A linear Mohr - Coulomb model was used to fit the shear strength failure envelope, as shown in Equation (4 - 1). Then cohesion and the friction angle, which are 12.4 MPa and 42.3°, were acquired, as tabulated in Table 4 - 7.

$$\tau = 12.4 + 0.91\sigma \qquad (4 - 1)$$

Where, τ = shear strength of the material, Pa; and σ = normal stress, Pa.

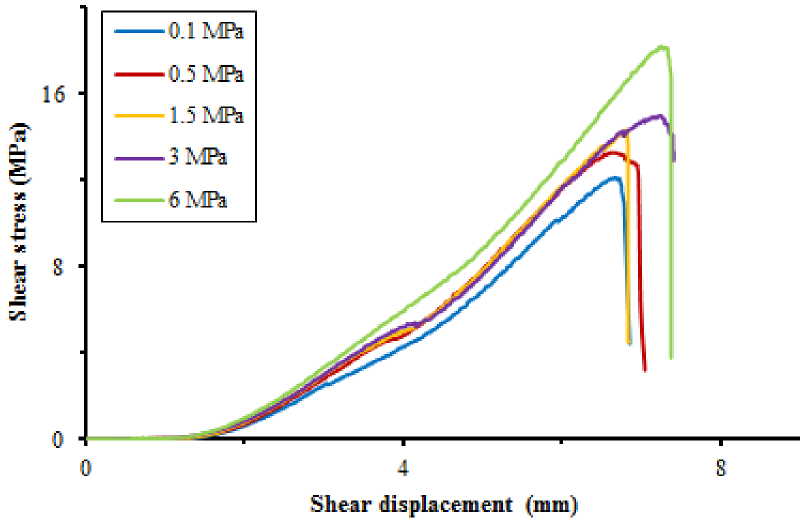

Figure 4 - 20 Shear stress variation of the grout in different normal stress conditions

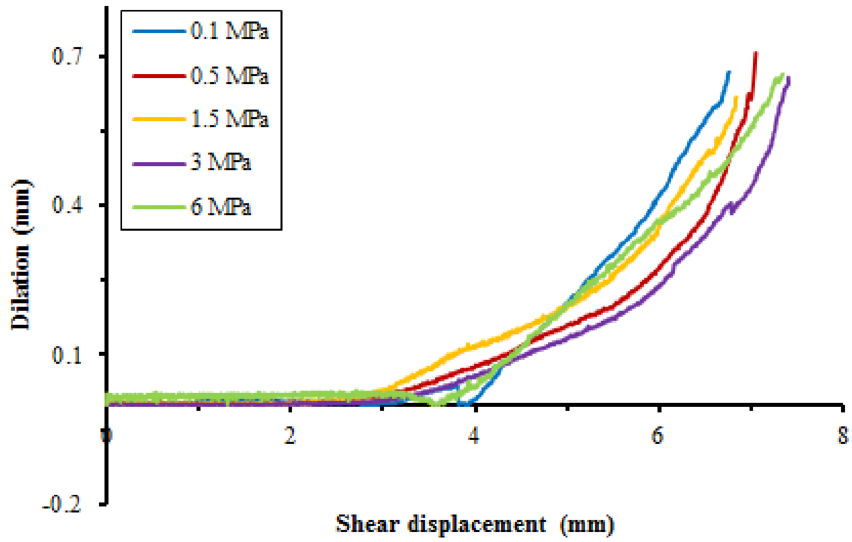

Figure 4 - 21 Dilation variation of the grout in different normal stress conditions

Table 4 - 6 Shear performance of the grout in the constant normal stress condition

List number	Normal stress (MPa)	Shear strength (MPa)	Dilation limit (mm)
1	0.1	11.8	0.6
2	0.5	13.4	0.7
3	1.5	14.1	0.5
4	3.0	15.1	0.6
5	6.0	17.7	0.6

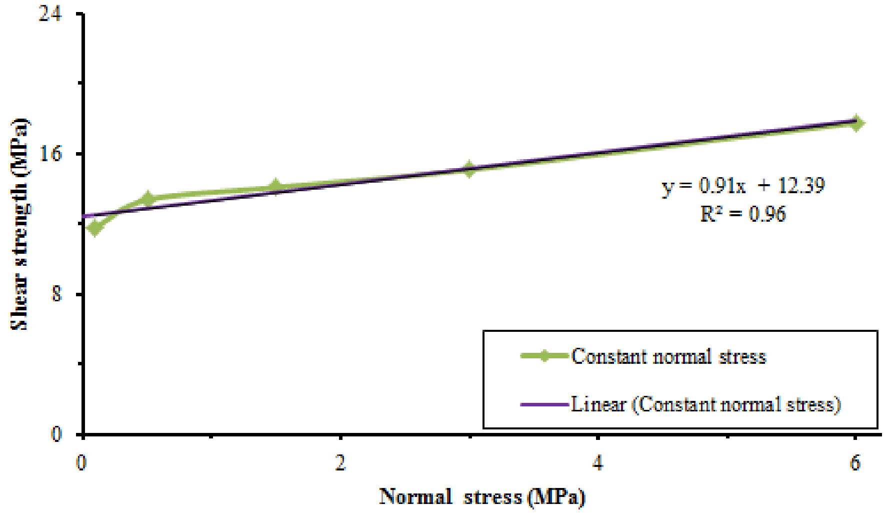

Figure 4 - 22 Shear strength failure envelope of the grout in the constant normal stress condition

Table 4 - 7 Cohesion and friction angle of the grout

Grout type	w/c ratio	Boundary condition	Cohesion (MPa)	Friction angle (°)
Stratabinder	0.42	constant normal stress	12.4	42.3

4.4 Shear behaviour of the grout in constant normal stiffness condition

4.4.1 Direct shear test process in constant normal stiffness condition

Since no research has been conducted on the shear behaviour of the grout under a constant normal stiffness condition, the second series of tests was conducted in the constant normal stiffness environment. The test process was generally consistent with the previous process except the normal actuator was set as stiffness control and a normal stiffness of 10 kN/mm was applied, as shown in Figure 4 - 23. In the constant normal stiffness condition, the normal stress applied on the sample was variable, yielding to Equation (4 - 2).

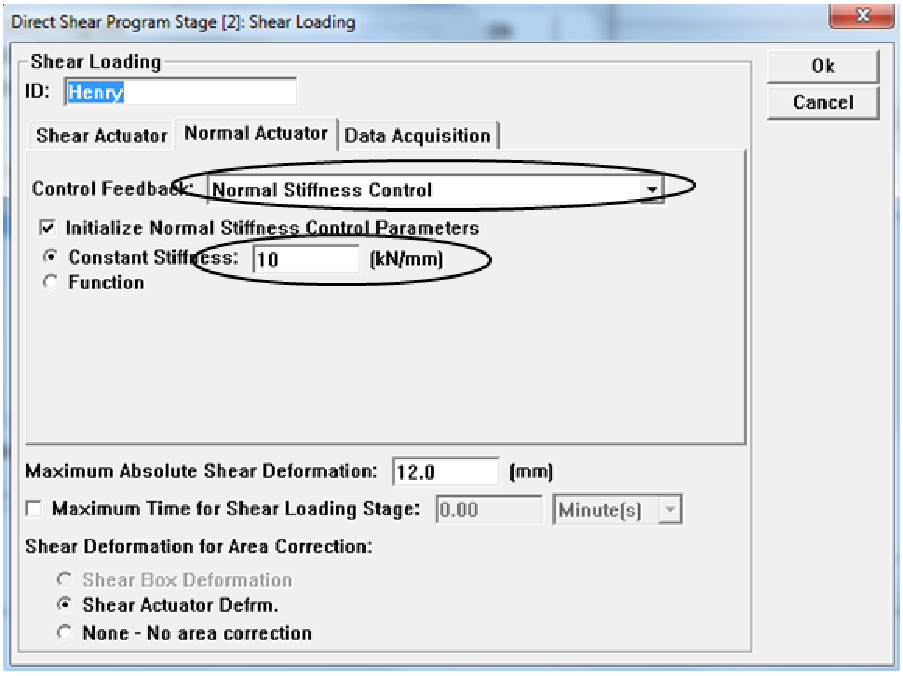

Figure 4 - 23 Constant normal stiffness configuration

$$\sigma_n = \sigma_{n0} + k_n \frac{d}{A_s} \qquad (4 - 2)$$

Where, σ_{n0} = initial normal stress applied on the sample, Pa; k_n = normal stiffness, N/m; d = dilation in the test process, m; and A_s = shearing area of the sample, m^2.

4.4.2 Direct shear test results in the constant normal stiffness condition

When the initial normal stress was 0.1 MPa, the relationship between the shear stress and displacement is shown in Figure 4 - 24 and Table 4 - 8. The shear failure mode for the sample is shown in Figure 4 - 25.

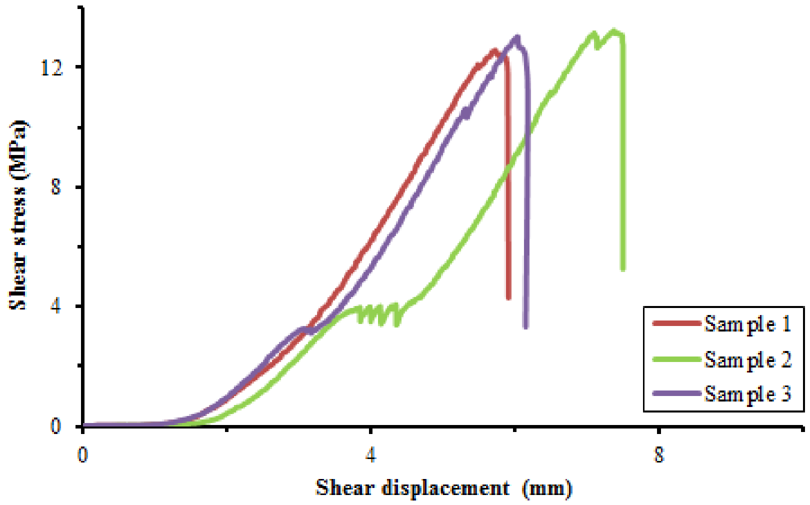

Figure 4 - 24 Shear behaviour of the grout with an initial normal stress of 0.1 MPa in the constant normal stiffness condition

Table 4 - 8 Selected test results of the grout with an initial normal stress of 0.1 MPa in the constant normal stiffness condition

Sample number	Length (mm)	Width (mm)	Shear strength (MPa)	Dilation limit (mm)
1	99.5	98.7	12.6	0.6
3	99.2	98.9	13.0	0.7
Mean	99.3	98.8	12.8	0.7

Figure 4 - 25 Shear failure in the middle of the sample

When the initial normal stress was increased to 0.5 MPa, and the relationship between the shear stress and displacement is shown in Figure 4 - 26 and Table 4 - 9.

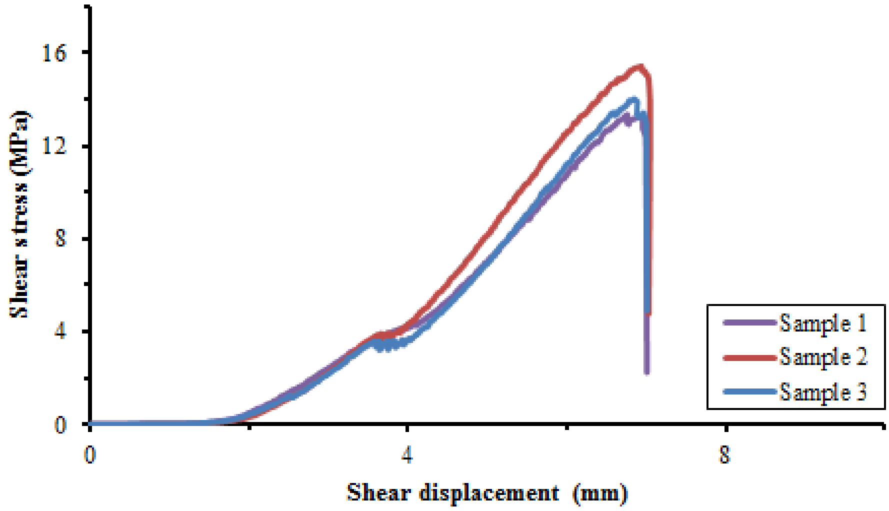

Figure 4 - 26 Shear behaviour of the grout with an initial normal stress of 0.5 MPa in the constant normal stiffness condition

Table 4 - 9 Selected test results of the grout with an initial normal stress of 0.5 MPa in the constant normal stiffness condition

Sample number	Length (mm)	Width (mm)	Shear strength (MPa)	Dilation limit (mm)
1	99.6	98.9	13.4	0.7
3	99.3	99.2	14.0	0.7
Mean	99.5	99.0	13.7	0.7

As the initial normal stress was increased to 1.5 MPa, the relationship between the shear stress and displacement is shown in Figure 4 - 27 and Table 4 - 10.

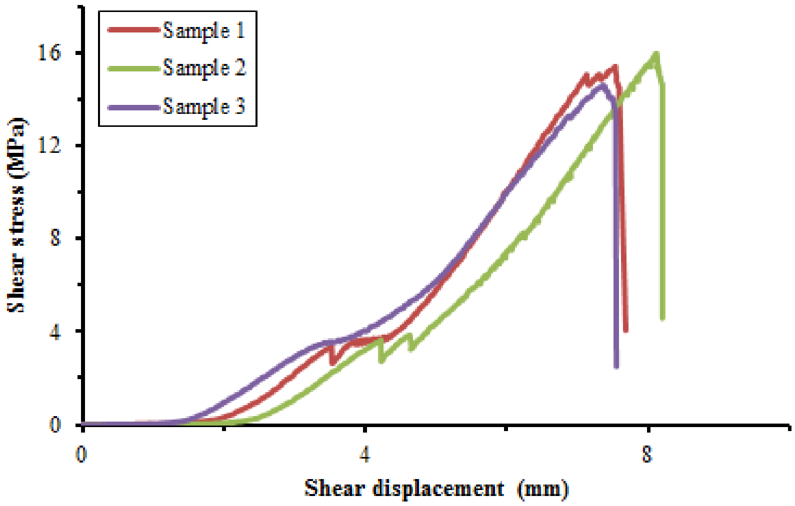

Figure 4 - 27 Shear behaviour of the grout with an initial normal stress of 1.5 MPa in the constant normal stiffness condition

Table 4 - 10 Selected test results of the grout with an initial normal stress of 1.5 MPa in the constant normal stiffness condition

Sample number	Length (mm)	Width (mm)	Shear strength (MPa)	Dilation limit (mm)
1	99.2	99.0	15.4	0.6
3	99.8	99.5	14.6	0.6
Mean	99.5	99.2	15.0	0.6

With an initial normal stress of 3 MPa, the relationship between the shear stress and displacement is shown in Figure 4 - 28 and Table 4 - 11.

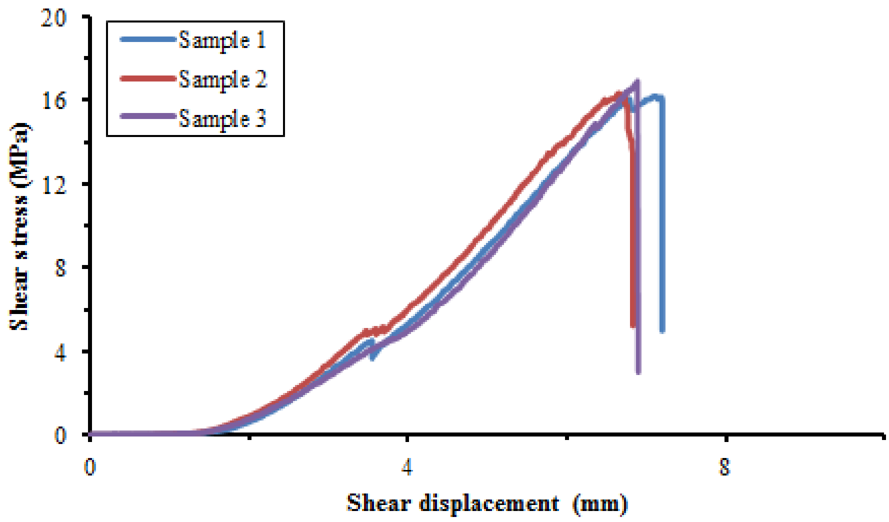

Figure 4 - 28 Shear behaviour of the grout with an initial normal stress of 3 MPa in the constant normal stiffness condition

Table 4 - 11 Test results of the grout with an initial normal stress of 3 MPa in the constant normal stiffness condition

Sample number	Length (mm)	Width (mm)	Shear strength (MPa)	Dilation limit (mm)
2	99.5	98.7	16.3	0.7
3	100.0	98.2	16.9	0.6
Mean	99.7	98.5	16.6	0.6

Finally, the initial normal stress was increased up to 6 MPa, the relationship between the shear stress and displacement is shown in Figure 4 - 29 and Table 4 - 12.

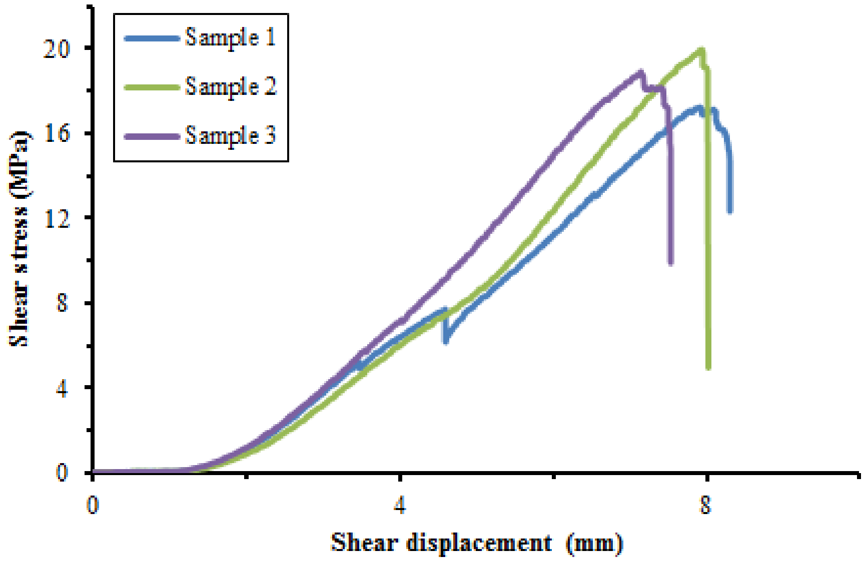

Figure 4 - 29 Shear behaviour of the grout with an initial normal stress of 6 MPa in the constant normal stiffness condition

Table 4 - 12 Test results of the grout with an initial normal stress of 6 MPa in the constant normal stiffness condition

Sample number	Length (mm)	Width (mm)	Shear strength (MPa)	Dilation limit (mm)
2	99.1	99.5	19.9	0.6
3	99.9	99.3	18.9	0.8
Mean	99.5	99.4	19.4	0.7

The shear performance of the grout in constant normal stiffness condition is shown in Figure 4 - 30 and Table 4 - 13. The results show that with the initial normal stress increasing, shear strength of the grout and shear displacement where peak occurred increased. This was consistent with shear behaviour of the grout under constant normal stress condition. The influence of the normal stress on the dilation of the grout is shown in Figure 4 - 31. The results show that the different normal stress condition had little effect on determining the dilation limit.

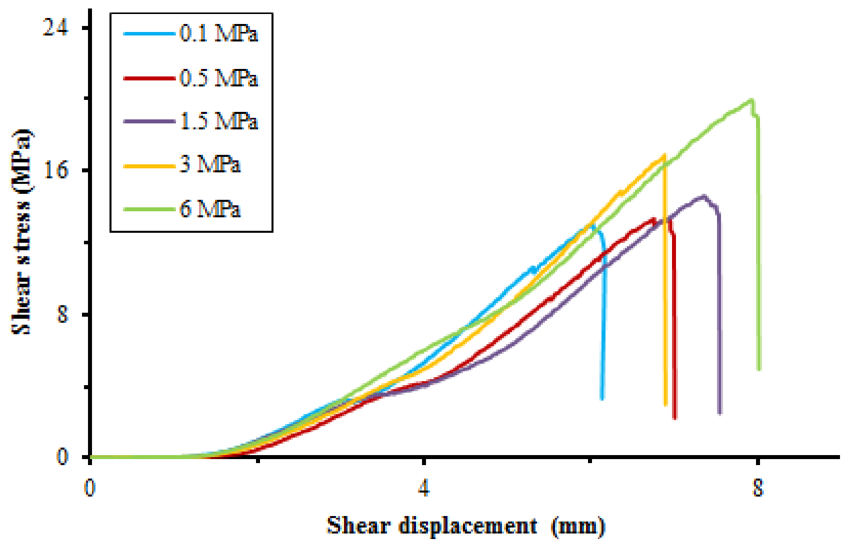

Figure 4 - 30 Shear stress variation of the grout in the constant normal stiffness condition

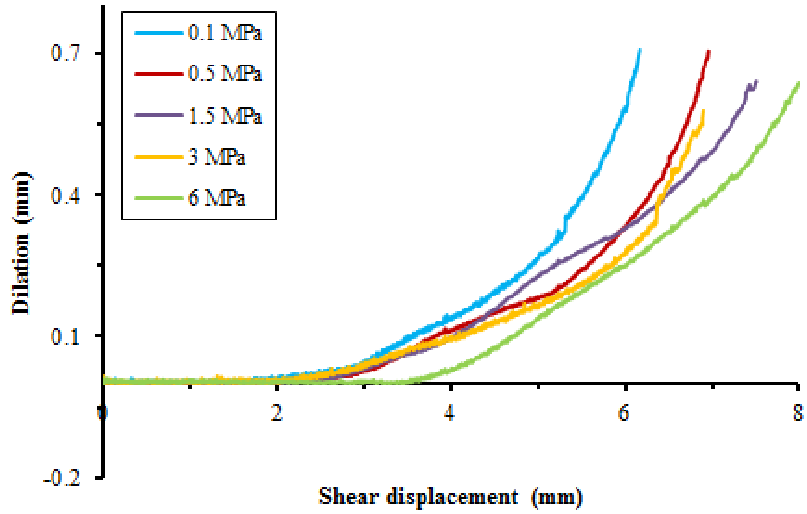

Figure 4 - 31 Dilation variation of the grout in the constant normal stiffness condition

Table 4 - 13 Shear performance of the grout in the constant normal stiffness condition

List number	Initial normal stress (MPa)	Shear strength (MPa)	Dilation limit (mm)
1	0.1	12.8	0.7
2	0.5	13.7	0.7
3	1.5	15.0	0.6
4	3.0	16.6	0.6
5	6.0	19.4	0.7

The shear strength failure envelope of the grout in the constant normal stiffness condition is shown in Figure 4 - 32. The Mohr - Coulomb model was used to fit the shear strength failure envelope, as shown in Equation (4 - 3). Then, the cohesion and the friction angle were acquired, which are 13.1 MPa and 47.5°, as tabulated in Table 4 - 14.

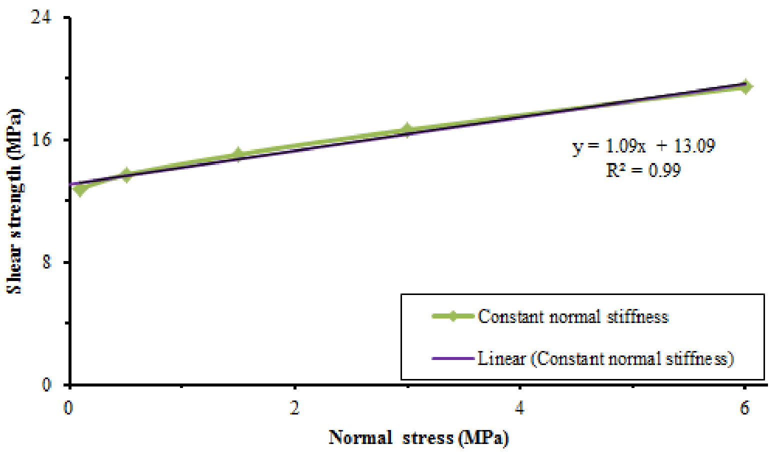

Figure 4 - 32 Shear strength failure envelope of the grout in the constant normal stiffness condition

$$\tau = 13.1 + 1.09\sigma \tag{4 - 3}$$

Table 4 - 14 Cohesion and friction angle of the grout

Grout type	w/c ratio	Boundary condition	Cohesion (MPa)	Friction angle (°)
Stratabinder	0.42	constant normal stiffness	13.1	47.5

4.5 Comparison between the shear behaviour of the grout in the constant normal stress and constant normal stiffness conditions

The shear behaviour of the Stratabinder grout in the constant normal stress and constant normal stiffness conditions was compared, as shown in Figure 4 - 33. It is found that the shear strength of the grout in the constant normal stiffness condition was slightly larger than constant normal stress condition, as a result of the different boundary condition. Specifically, in the constant normal stiffness condition, the normal stress increased gradually because of the sample dilation.

However, it is also found that the difference between the shear strength in constant normal stress and constant normal stiffness conditions was negligible. This was due to the fact that a low stiffness was applied on the boundary. Consequently, during the test, there was a small difference of the normal stress under the constant normal stress and constant normal stiffness conditions.

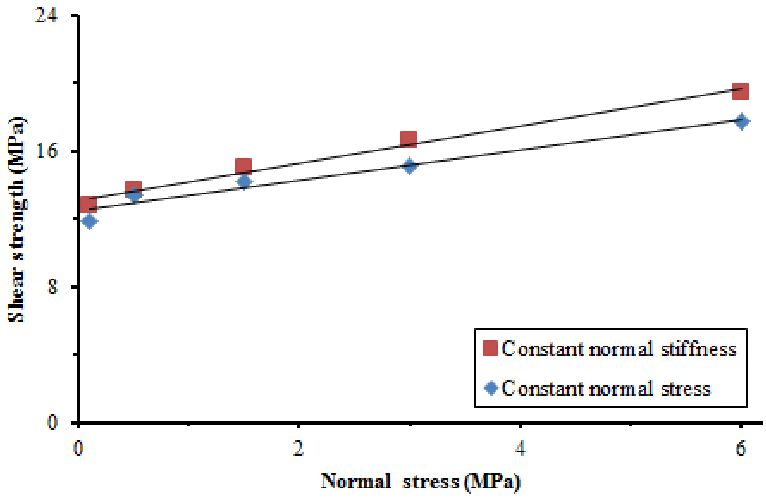

Figure 4 - 33 Shear behaviour of the grout in the constant normal stress and constant normal stiffness conditions

The influence of boundary condition on the shear performance of the grout was analysed. As shown in Table 4 - 15, the low stiffness boundary condition had little effect on improving the cohesion of the grout. On the other hand, the friction angle of the grout in the constant normal stiffness condition was slightly higher than the constant normal stress condition.

Table 4 - 15 Comparison of the cohesion and friction angle of the grout in different boundary conditions

Grout type	w/c ratio	Boundary condition	Cohesion (MPa)	Friction angle (°)
Stratabinder	0.42	constant normal stress	12.4	42.3
		constant normal stiffness	13.1	47.5

4.6 Summary

A number of direct shear tests were conducted on the Stratabinder grout to determine the material properties of Portland cement subjected to shear. This understanding is important as this material can often fail in shear either at the cable/grout or grout/rock interface when it is used to grout a cable bolt into the borehole. Furthermore, the mechanical properties of the Stratabinder grout acquired from the direct shear test will be used in the numerical simulation work in Chapter Eight.

Intact cubic samples with an edge length of 100 mm were prepared. The direct shear tests were performed under constant normal stress and constant normal stiffness conditions. In the constant normal stress condition, five different normal stresses, 0.1 MPa, 0.5 MPa, 1.5 MPa, 3 MPa and 6 MPa, were applied, and in the constant normal stiffness condition, an additional normal stiffness of 10 kN/mm was applied.

The results show that the shear strength of the grout and the displacement where peak shear strength occurred increased with the normal stress in both the constant normal stress and constant normal stiffness conditions. In the post-failure stage, there was a sudden drop of the shear stress with no residual shear stress, indicating that the Stratabinder grout mixed with a w/c ratio of 0.42 was brittle. Furthermore, the dilation limit was less sensitive to the normal stress. It should also be noted that apparent shear failure in the middle of the sample occurred in each test.

The shear strength failure envelope of the grout was acquired in both the constant normal stress and constant normal stiffness conditions. The results show that the shear strength in constant normal stiffness was relatively higher than in the constant normal stress condition. This was a result of higher normal stress in constant normal stiffness condition. However, since the applied stiffness was small, the difference between the shear strengths in the constant normal stress and constant normal stiffness was not apparent.

The Mohr - Coulomb model was used to fit the shear strength failure envelopes of the grout. The results show that the cohesion of the grout was 12.4 MPa and the friction angle was 42.3° in the constant normal stress condition. As for the constant normal stiffness condition, the cohesion was 13.1 MPa and the friction angle was 47.5°. This indicates that the low stiffness boundary condition had little effect on improving the cohesion of the grout material.

CHAPTER FIVE

A NEW LABORATORY SHORT ENCAPSULATION PULL TEST APPARATUS DESIGN

5.1 Introduction

In the field, a grouted cable bolt can be divided into two parts, namely the pick-up or embedment length and the anchor length, as shown in Figure 5 - 1. Conceptually, these two different segments are separated by the rock joint.

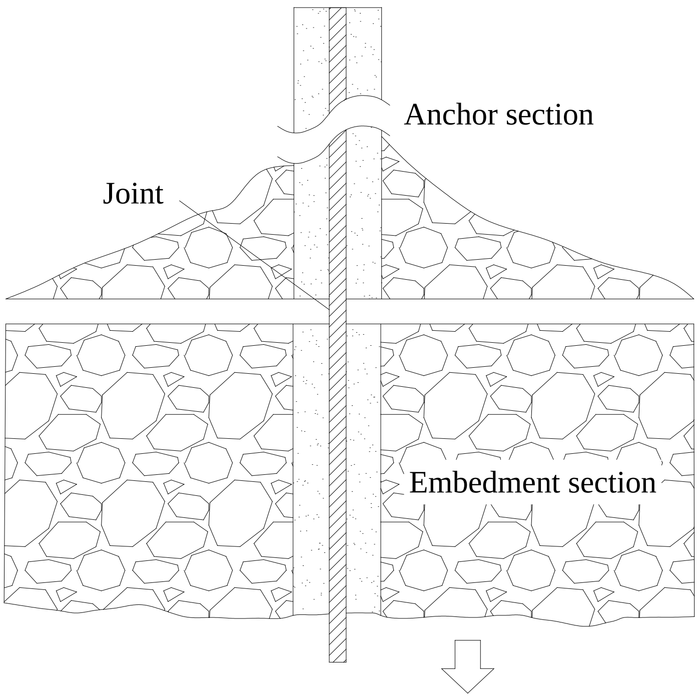

Figure 5 - 1 The load transfer concept of cable bolts, after Hutchinson and Diederichs (1996)

To be consistent with this scenario, a new LSEPT rig was developed, which is outlined in this chapter. The apparatus is fundamentally composed of two parts, namely the embedment section and anchor section. For the embedment section, the influence of confining medium diameter on the bond capacity of cable bolts was studied. In the anchor length, an internally threaded anchor tube was designed to confine the cable bolt.

The method of using a locking key and two locking nuts to prevent the cable bolt from rotating was used.

5.2 LSEPT apparatus design

5.2.1 Components of the test rig

The axis of the equipment is vertically aligned as shown in Figure 5 - 2.

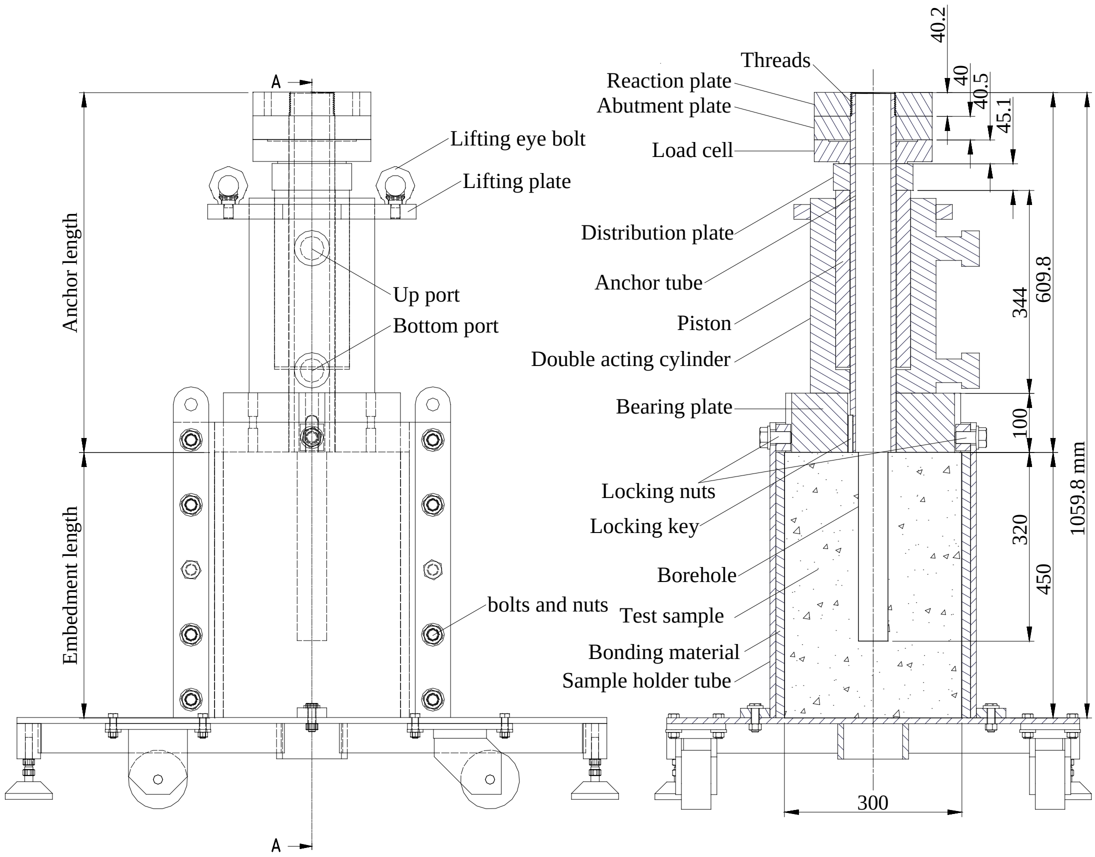

Figure 5 - 2 Test rig configuration. a) Front view showing the new LSEPT facility (left), and b) side view illustrating dimensions of the various components (right)

The test unit is comprised of the followings elements: embedment section, bearing plate, and anchor section. A double-acting hollow cylinder with a capacity of 931 kN and specially designed electrically actuated hydraulic power pack with the frequency ranged from 0 to 50 Hz are used to apply a load near the mid-point of the embedded cable bolt adjacent to the bearing plate. A load cell with a capacity of 1000 kN measures the actual load and three displacement transducers measure displacement. More detailed information regarding the parts of this rig is given in the following sections.

5.2.2 Test confining medium

In cable bolt tests, the cylindrical confining medium made up of cement-based or concrete material were commonly used to simulate the rock. Since there is no common standard in the size of the confining medium, some researchers used different confining medium diameters, varying from 142 mm to 300 mm (Stillborg, 1984; Farah and Aref, 1986b; Farah and Aref, 1986a; Hassani and Rajaie, 1990; Benmokrane *et al.*, 1995; Altounyan and Clifford, 2001; Bigby, 2004; Bigby and Reynolds, 2005; Blanco Martín, 2012). The variation in confining medium size made it difficult to compare the performance of different cable bolt tests.

To provide a stable bond capacity, Rajaie (1990) recommended a confining medium diameter of 200 mm for cable bolt testing. However, only plain strands were tested in his research. Little research has been reported regarding the influence of confining medium size on bond capacity of modified cable bolts. To evaluate this effect, a number of pull-out tests were performed as part of this study.

A Sumo strand, which is a modified cable bolt design manufactured by Jennmar Australia was selected, because it is one of the largest load capacity cable bolts used in Australian underground coal mining and represents the worst cases in terms of stresses induced in the rock during a pull-out test (Brown *et al.*, 2013). Therefore, when lower load transfer cable bolts are used, the optimised confining medium diameter can also be applicable. The Sumo cable bolt has a diameter of 28.5 mm and a bulbed section with a diameter of 35 mm. The full length of the strand is 900 mm, in which the section of 280 mm was fully embedded in the borehole of the test confining medium. The bulb with a diameter of 36.5 mm was located mid-way in the borehole. The cement confining medium used had different diameters ranging from 150 mm to 508 mm, as shown in Figure 5 - 3.

Figure 5 - 3 The confining medium with different diameters ranging from 150 mm to 508 mm

The approach of SEPT test was adopted. Specifically, a bearing plate was mounted on the top surface of the confining medium. Then, a hollow cylinder with a maximum bearing capacity of 900 kN was placed over the cable bolt. The top of the cable bolt was gripped and fixed by the barrel and wedge system. A load cell was used to measure the pull-out load and an LVDT recorded axial displacement. Each test was replicated three times.

Two series of tests were conducted. In the initial series, all confining media were unconfined. While in the second series of tests, holder tubes with a thickness of 10 mm were used to restrict the confining medium to provide a constant normal stiffness boundary. During testing, the pull-out load and displacement were recorded.

After testing, the resultant variation in bond capacity versus confining medium diameter at the two different boundary conditions is shown in Figure 5 - 4. The figure shows that the confining medium size has an apparent influence on determining bond capacity. A bi-linear relationship was adopted to illustrate the relationship between bond capacity and confining medium size in unconfined condition. Specifically, as the confining medium diameter increased from 150 mm up to approximately 360 mm, the bond capacity increased linearly from 30 kN to 100 kN. Above 360 mm, there was little further change in bond capacity with confining medium diameter.

A similar relationship between bond capacity and confining medium size was found in the confined confining medium, however, bond capacity became stable slightly higher at 112 kN, once a confining medium diameter of approximately 300 mm was reached. This indicates a threshold level of confining medium size beyond which diameter no longer influences the bond capacity in confined conditions.

Furthermore, the bond capacity in the confined condition was always larger than the unconfined environment. This is assumed to be a result of the bulbed geometry under load causing distinct dilation at the cable/grout interface. When the confining medium was enclosed by the steel tube, it increased the effective strength of the confining medium and the dilation was partly suppressed, generating more confining pressure on the confining medium and resulting in a larger bond capacity. To minimise the influence of confining medium size, all subsequent confining media were prepared with a diameter of 300 mm.

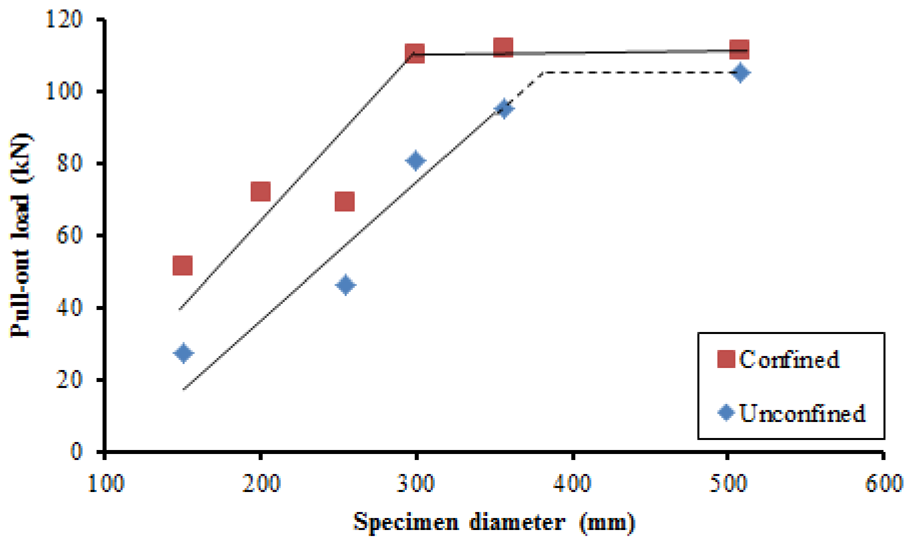

Figure 5 - 4 Comparison between bond capacity in different boundary conditions

5.2.3 Confinement tube

In the field, the cable bolt is typically confined within an infinite rock mass. To simulate this confinement effect, previous research had either a CNL or a Constant Normal Stiffness (CNS) boundary condition. The CNL is achieved by using a bi-axial cell to apply a level of confinement stress to the confining medium (Altounyan and Clifford, 2001). However, in field situation, the confinement in a rock mass is variable during cable bolts' service life, which is not reflected in the CNL condition. It is felt that the CNS better simulates field conditions (Clifford *et al.*, 2001; Kent and Bigby, 2001; Reynolds, 2006; Thomas, 2012).

In this study, a CNS condition is used. Specifically, a cylindrical steel tube with a thickness of 10 mm is used to contain the confining medium in the embedment section, as shown in Figure 5 - 5. To ensure that the confining medium can be removed easily after testing, this confining medium holder tube is split in the middle. During installation, bolts and nuts are secured to assemble the pair of steel tubes together.

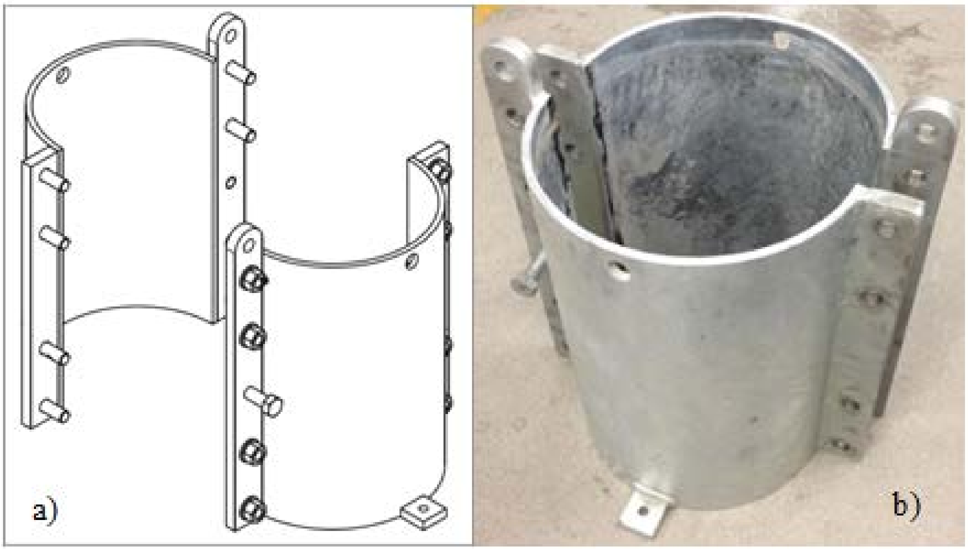

Figure 5 - 5 a) The schematic diagram of the confinement tube (left), and b) A pair of the confining medium holder tubes in practice (right)

5.2.4 Anchor tube

An anchor tube with a length of 608 mm was used to secure the free-end of the cable bolt. The anchor tube grips the cable bolt, preventing it from rotating during the pull-out process. The anchor tube has an internal diameter of 50 mm, which is sufficient to contain all types of cable bolts. In addition, the very steady Stratabinder grout with low w/c ratio is used to fill the annulus between the internal surface of the anchor tube and the cable bolt. It should be noted that the internal surface of this anchor tube is threaded with a pitch of 2 mm and a depth of 1 mm to ensure good bonding contact between the anchor tube and the cable bolt, as depicted in Figure 5 - 6.

Figure 5 - 6 End view of internal section of the threaded anchor tube

5.2.5 Bearing plate

The bearing plate is an important element in the test unit. Its purpose is to evenly distribute the axial pull-out load from the hydraulic cylinder across the full surface of the confining medium. Importantly, the borehole size in the middle of the bearing plate has a crucial role in determining the failure mode of this cable bolting system. It is not uncommon to see in some tests that the internal diameter of the bearing plate is of a similar size as the rock tendon outsider diameter (Blanco Martín *et al.*, 2011; Blanco Martín, 2012). As a result, the grout annulus within the borehole is constrained by the bearing plate and failure must occur at the bolt/grout interface. This does not simulate reality where there is no confinement around the cable bolt at the surface of a discontinuity when the ground separates, as indicated by Thomas (2012). Hence the bearing plate used in the laboratory should have a larger internal hole diameter as compared to the borehole size.

On the other hand, Khan (1994) had earlier suggested that if the internal hole of the bearing plate was too large (over 100 mm bigger than the cable bolt diameter), it would have an adverse impact on the results as shown in Figure 5 - 7.

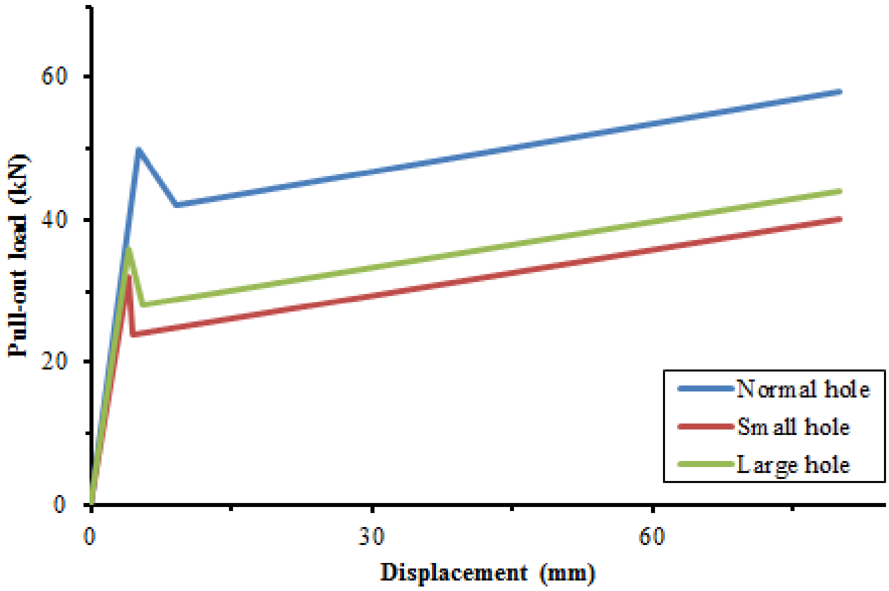

Figure 5 - 7 Effect of hole diameter in the bearing plate on pull-out load, after Khan (1994)

Considering these problems, a bearing plate with an internal diameter of 70.4 mm is used, as shown in Figure 5 - 8. Since the largest borehole within all tests is limited to 52 mm, there is a minimum difference of 18 mm between the borehole diameter and the internal hole diameter of the bearing plate, allowing the grout column and confining medium material surrounding the borehole to be liberated. By this means, the different failure modes of the cable bolting system that commonly occur in the field can be studied, as suggested by Jeremic and Delaire (1983).

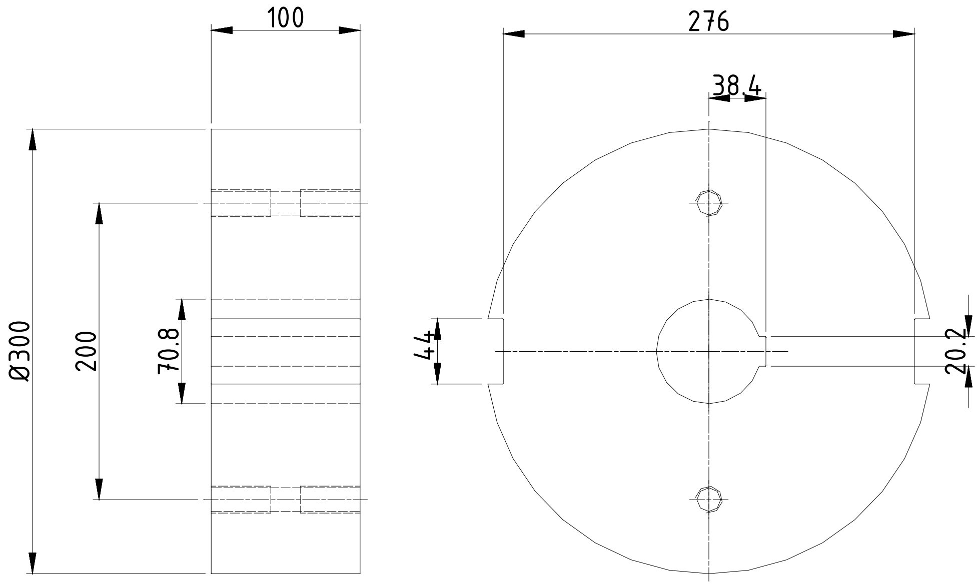

Figure 5 - 8 a) Front view of the bearing plate (left), and b) side view showing the dimension (right)

5.2.6 Anti-rotation devices

Manufacturing of a cable bolt involves the winding of individual wires around each other, except for some specific non-rotating cables. Hence, there is a tendency for cable bolts to unwind when stretched. However, in the field, a fully grouted cable is constrained from rotation by its surrounding rock mass. In some previous test designs, there was no provision made for anti-rotation, which had an adverse impact on the performance of some cable bolts. In other test designs, there has been provision made to prevent unscrewing of the cable bolt at the joint during loading. For example, in DEPT, cylindrical steel rods were welded to pipes to constrain movement only in the pull-out direction (Satola, 2007). When it comes to LSEPT, little information is provided in relation to cable rotation behaviour within the current British Standard (BS7861-1, 2007). In the work conducted by Blanco Martín *et al.* (2013), round metal pins were inserted into the confining medium, connecting it with the biaxial cell upper piston and preventing any relative rotation from occurring. However, whether the inserted pin would be harmful to the integrity of the confining medium was not discussed.

Based on this, a new approach was developed (Figure 5 - 9). In detail, a key slot was machined in the lower end of the anchor tube and in the internal hole of the bearing plate. A longitudinal steel key was used to lock them together. Two locking nuts were used to couple the bearing plate and the confining medium holder tube together. This design allowed for axial movement during the pull-out process and prevented any rotation. The locking key assembly enabled a pull-out displacement of 100 mm, and hence was able to study of the post-failure behaviour of cable bolts.

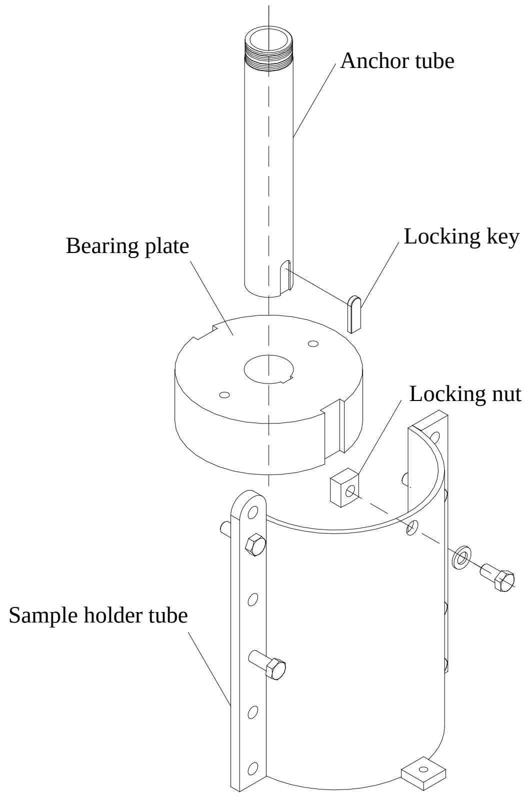

Figure 5 - 9 Locking key and nuts were used to couple the anchor tube, the bearing plate and confinement tube

5.2.7 Hydraulic control

Both load control and displacement control can be used to provide axial pulling force. However, a displacement control was used in this study, because it has been successfully used in previous research, such as Hyett *et al.* (1992b), Reichert *et al.* (1992), Hyett *et al.* (1993) and Hyett and Bawden (1994), and it is the simpler of the two options.

A constant displacement rate of 0.26 mm/s was applied in each test so that failure should occur within an approximately 15 minute period. To achieve this, a constant displacement pump and controller unit is used, as shown in Figure 5 - 10.

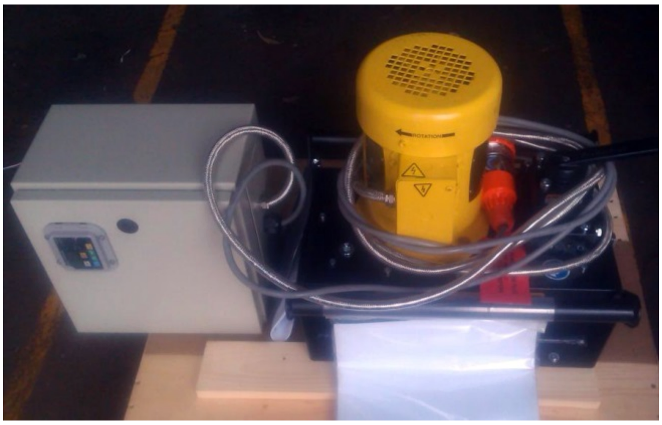

Figure 5 - 10 Constant displacement hydraulic powerpack and controller

5.2.8 Monitoring system

After the test specimen, confining medium holder tube, bearing plate and the anchor tube were installed together, a double acting hydraulic cylinder was seated on the bearing plate, followed by the distribution plate, load cell, abutment plate and finally the reaction plate, as shown in Figure 5 - 11. The load cell was used to record the variation in pull-out load.

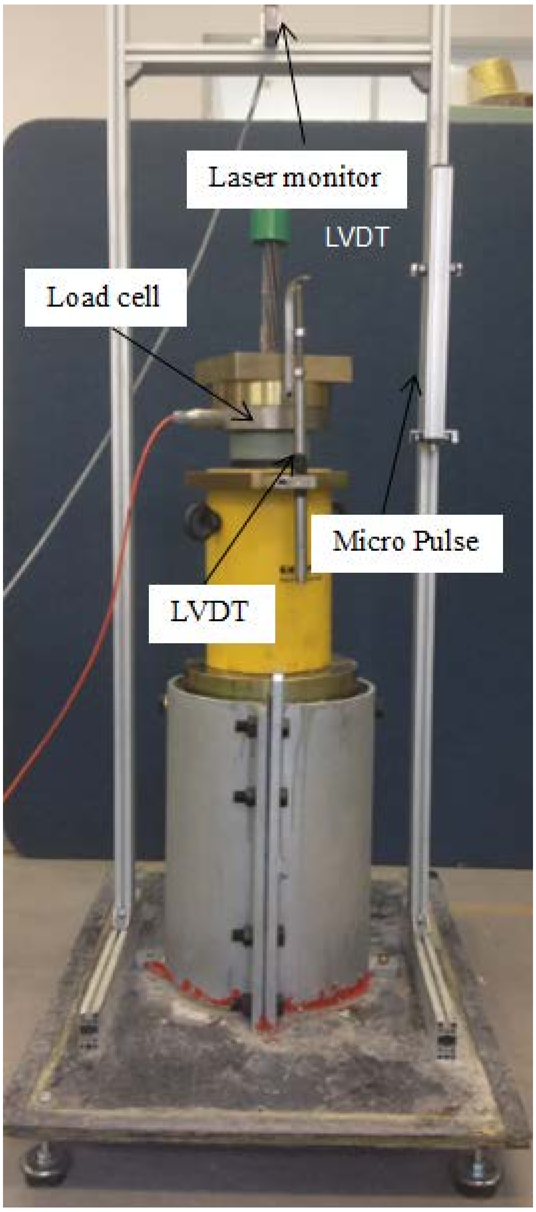

Figure 5 - 11 Front view of the test rig showing the monitoring system

Three displacement transducers were adopted to monitor the pull-out displacement. Specifically, a Micro Pulse transducer was installed on the test frame to measure the displacement of the anchor tube relative to the ground, as shown in Figure 5 - 11. Meanwhile, a laser radiation instrument was attached on the top of the frame, recording the relative displacement between the cable bolt and the ground. Therefore, if there was no bond failure between the anchor tube and the cable bolt, the displacement recorded by the laser transducer should equal the value monitored by the Micro Pulse. A LVDT fixed on the hydraulic cylinder was used to monitor the movement of the piston for backup purpose. Dimensions of the LSEPT apparatus is shown in Table 5 - 1.

Table 5 - 1 Technical data about the test rig

Component	Dimension	Value
Confining medium holder tube	length	450 mm
	thickness	10 mm
	internal diameter	330 mm
Confining medium	length	450 mm
	diameter	300 mm
	borehole length	320 mm
	borehole diameter	variable
Bearing plate	outside diameter	300 mm
	internal diameter	70 mm
	thickness	100 mm
Anchor tube	length	608 mm
	thickness	10 mm
	internal diameter	50 mm
	internal groove	1 mm in depth and 2 mm in pitch
Locking key	length	70 mm
	width	19.8 mm
	thickness	8 mm
Hydraulic ram jack	stroke	153 mm
	max. capacity	950 kN
Load cell	capacity	1000 kN
Abutment plate	height	40 mm
Reaction plate	height	40 mm
LVDT	stroke	100 mm
Micro Pulse	stroke	160 mm
Laser transducer	stroke	200 mm

5.3 Test specimen preparation and installation

5.3.1 Cementitious confining medium casting and curing

Cardboard cylinders were used as moulds to prepare the confining medium. Each cylinder had a length of 450 mm and an outside diameter of 310 mm, as shown in

Figure 5 - 12. The thickness of the cardboard is 5 mm, providing sufficient stiffness to resist deformation of the moulds in confining medium casting.

Figure 5 - 12 a) Profile of a cardboard mould (left), and b) vertical view of the mould (right)

The cylinder was glued to a wooden base plate using silicon to provide a waterproof seal. The board also provided a flat surface during testing for the bearing plate. In the centre of each cylinder, a hollow plastic pipe was placed. It should be mentioned that a plastic tube with an outside diameter of 5 mm and a pitch of 20 mm was wound around the middle pipe, creating a rifled borehole within the confining medium as shown in Figure 5 - 13.

Figure 5 - 13 a) Plastic tube wound around outside of the plastic pipe (left), and b) corresponding rifled borehole (right)

A foam mix was used to fill the internal space of the tube as shown in Figure 5 - 14 and fasten the tube to the base plate. The fully assembled casting mould with rifling tube can be seen in Figure 5 - 15.

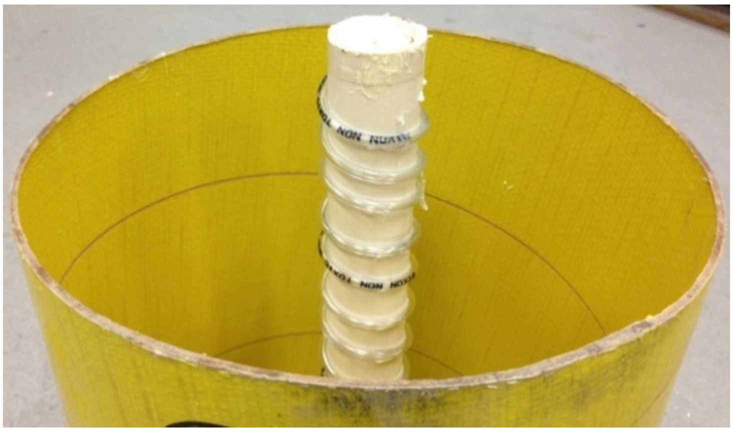

Figure 5 - 14 Fill & fix foam material within the rifling tube

Figure 5 - 15 Profile of the fully assembled casting mould prior to pouring

A 5 m^3 mixer or truck was used to cast all confining media, as shown in Figure 5 - 16. Two batches of cement-based mortar, in which one was the YN1.5MPA grout, simulating weak rock and the other was the GS32250 grout, representing strong rock, were used.

Figure 5 - 16 Pouring the pre-mixed cement based mortar into casting moulds

The confining medium were placed on a pallet and moved to an area to set, as shown in Figure 5 - 17.

Figure 5 - 17 Newly casted confining media

Figure 5 - 18 a) shows a picture of all casted confining media. After curing for 24 hours, the rifling tube was extracted from each confining medium. The outer casing cardboard

was also removed and each confining medium was placed in a large plastic bag filled with untreated tap water to cure for 28 days, as shown in Figure 5 - 18 b). Full immersion in water ensures a more consistent level of cement hydration during the curing process and consistent material properties between each confining medium.

Figure 5 - 18 a) Confining media after mass pouring, and b) confining media in plastic bags filled with water for curing

As the rifling tube was fixed to the base plate during casting of the confining medium, the rifling borehole consequently extended for the full height of each confining medium. After the rifling tube was extracted, the borehole was back-filled using General Purpose Cement, having similar strength to the confining medium material, to reduce it to the pre-determined embedment length of 320 mm for cable bolt testing as shown in Figure 5 - 19 a). To ensure that the rifling spirals in the upper section of the borehole were not filled during the pouring process, the cement was poured down via a plastic tube that was lowered into the borehole. During the backfilling, the borehole length was measured to confirm that sufficient cement had been added to achieve the required borehole length as shown in Figure 5 - 19 b).

Figure 5 - 19 a) Backfilling of a rifled borehole with cement paste, and b) confirming the level of backfilling has achieved the required embedment length

5.3.2 Cable bolt and anchor tube installation

After all confining media were fully cured, they were placed together for cable bolt installation, as shown in Figure 5 - 20.

Figure 5 - 20 Fully cured confining media

Two types of cable bolts, namely an MW9, a modified cable bolt and a Superstrand, which is a plain cable bolt, were tested. The MW9 cable bolt is a flexible rock tendon with a diameter of 28.5 mm, manufactured by twisting nine spirally indented steel wires together with a nut added (Megabolt, 2012). And the Superstrand cable bolt is a plain cable tendon, having a diameter of 21.8 mm. It is fabricated by twisting nine steel smooth wires together (Jennmar, 2014). It should be mentioned that for all cable bolts tested, a special bulb was manufactured in the anchor section to improve the bond capacity between the cable bolt and the anchor tube.

Prior to cable bolt installation, the top surface was checked to confirm that it was flat level, as shown in Figure 5 - 21.

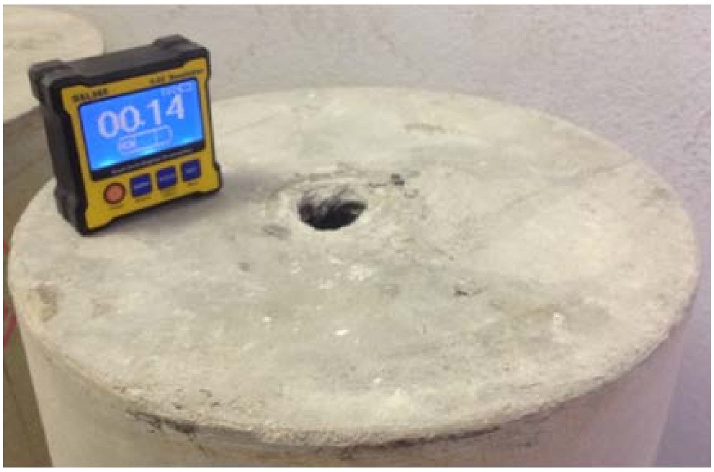

Figure 5 - 21 Using a digital level checker to adjust the position of the confining medium

The Stratabinder grout having a w/c ratio of 0.42 was poured into the borehole close to the top section, as shown in Figure 5 - 22. Then the cable bolt was inserted into the borehole and rotated to mix and ensure good coverage between the cable bolt, grout and confining medium, as shown in Figure 5 - 23.

Figure 5 - 22 Borehole filled with Stratabinder grout prior to insertion of the cable bolt

Figure 5 - 23 Cable bolt installation in the confining medium

After the cable bolt was installed, a special clamp made of angle iron welded to a heavy base was added to clamp the cable bolt and ensure the cable remained in the middle of the borehole during curing as shown in Figure 5 - 24. After the Stratabinder grout had set for 12 hours, the clamps were removed.

Figure 5 - 24 A pair of clamps designed to ensure alignment of the cable bolt

The anchor tube was installed over the exposed cable bolt after the Stratabinder grout had set for at least 24 hours. The top section of the anchor tube was wrapped with a plastic tape to prevent the threads around the top of the anchor tube being fouled by the grout as shown in Figure 5 - 25. To prevent bond failure occurring in the anchor length, the w/c ratio of the Stratabinder grout poured into the anchor tube was slightly reduced to 0.38 to increase grout strength.

Figure 5 - 25 Pouring Stratabinder grout into top section of the anchor tube

Similar to the method of securing the cable bolt in the confining medium, clamps were used to secure the anchor tube and ensure alignment parallel to the borehole axis, as illustrated in Figure 5 - 26.

Figure 5 - 26 Clamps were used to keep the anchor tube straight

It should be noted that the MW9 cable bolt has a hollow tube in the middle as shown in Figure 5 - 27. Considering that the middle tube is always filled with grout in field applications, the Stratabinder grout with the same w/c ratio of 0.42 used in the embedment section was poured into the middle hollow tube through a funnel as shown in Figure 5 - 28. It should also be noted that the Superstrand cable bolts have no middle tube and no additional treatment was required.

After the grout was poured into the anchor tube, the assembled specimens were left for 28 days to fully cure as shown in Figure 5 - 29.

Figure 5 - 27 Hollow middle tube of the MW9 cable bolt

Figure 5 - 28 Filling the middle tube with a funnel

Figure 5 - 29 Fully assembled test specimens

5.4 Preliminary tests

5.4.1 Test with a MW9 cable bolt

To confirm the workability of the newly established apparatus, a test was conducted on a specimen installed with a MW9 cable bolt. After the test, the pull-out load versus displacement curve measured by the LVDT is shown in Figure 5 - 30. It can be seen that the pull-out load increased quickly up to 378 kN within a small displacement of 9 mm. Then, there is a reduction of the pulling load. After 50 mm of pull-out displacement, the residual load of the MW9 cable bolt reached 295 kN and stably decreased.

To further check the failure mode of this cable bolting system, the confining medium holder tube was removed and the confining medium was split in two, in which one piece is shown in Figure 5 - 31. The results show that there was even contact between the cable and grout and between the grout and confining medium. The grout column had firmly adhered to the confining medium and slippage was evident along the cable/grout interface.

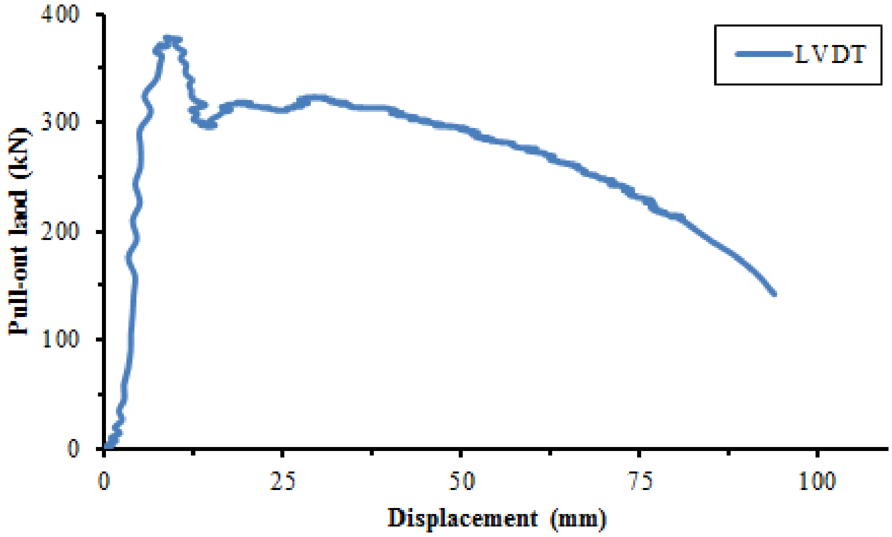

Figure 5 - 30 Load/displacement relationship of the MW9 cable bolt recorded by the LDVT

Figure 5 - 31 Shear failure along the cable/grout interface

Figure 5 - 32 and Figure 5 - 33 depict the load versus displacement relationship of the MW9 cable bolt recorded by the Micro Pulse and Laser transducer respectively.

A comparison between the results acquired by the LVDT, Micro Pulse and Laser transducer is shown in Figure 5 - 34. The results show that there was reasonable correlation among the three displacement measurement systems. However, since the LVDT was fixed on the hydraulic cylinder and because of vibration of the cylinder, more noise occurred in the result recorded by the LVDT. Although there was less vibration in the signal with the Micro Pulse, like the LVDT, it was physically tied to the apparatus, which limited its measurement range. The Laser being a non-contact unit was both unaffected by vibration and also had a much larger measurement range, making it more suited in this application. Therefore, in subsequent tests, the results measured by the laser transducer were used.

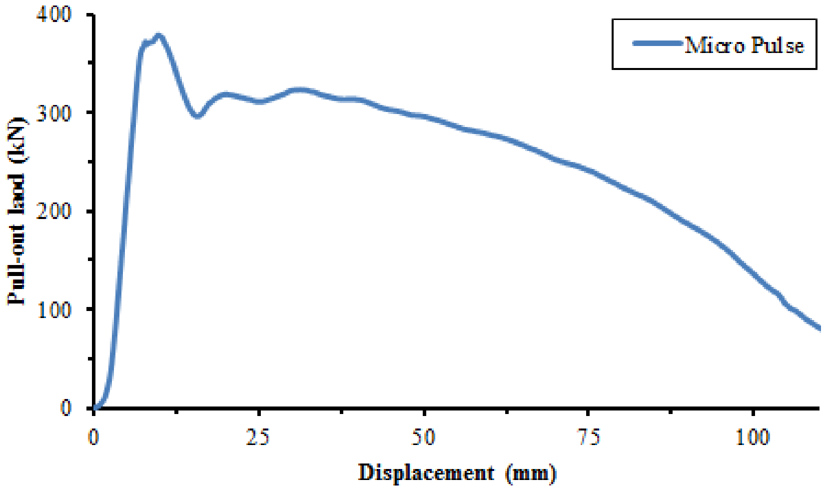

Figure 5 - 32 Load/displacement relationship of the MW9 cable bolt recorded by the Micro Pulse

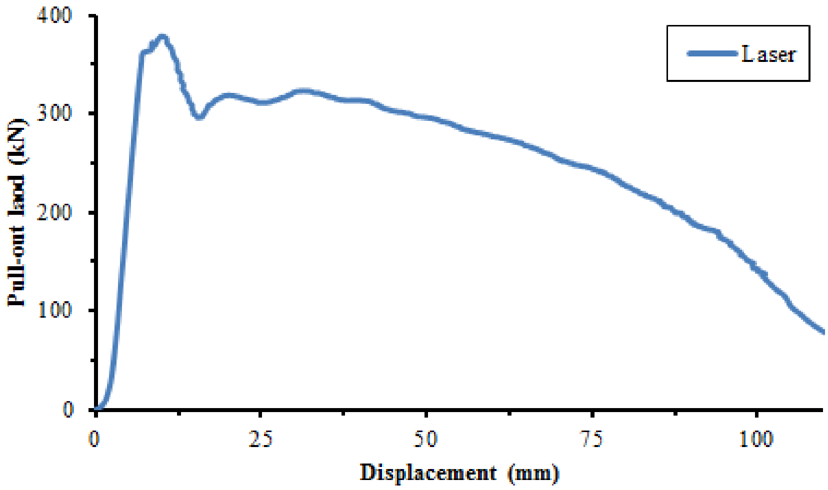

Figure 5 - 33 Load/displacement relationship of the MW9 cable bolt recorded by the Laser transducer

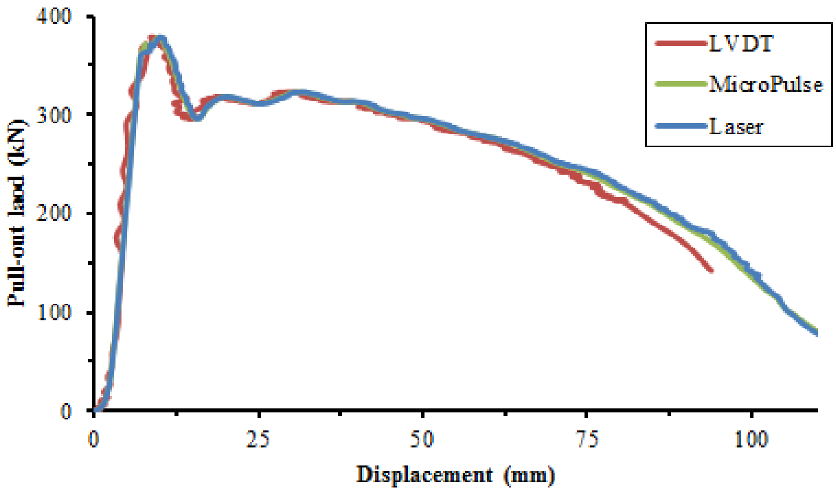

Figure 5 - 34 Comparison in resolution between the LVDT, Micro Pulse and Laser transducer

Also, the consistency between the results obtained from Micro Pulse and Laser transducer indicated that there was no relative movement between the anchor tube and the cable bolt. This can also be seen from Figure 5 - 35, showing that there was good bond contact between the MW9 cable bolt and the anchor tube.

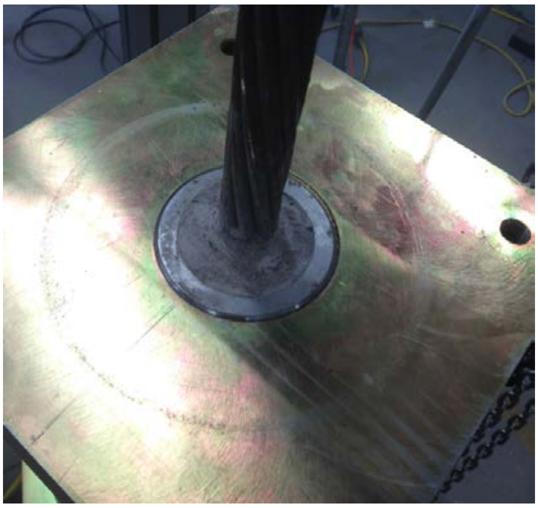

Figure 5 - 35 The relative position of the MW9 cable bolt, grout and anchor tube after testing

5.4.2 Test with a Superstrand cable bolt

The other test was performed on a Superstrand cable bolt. The pull-out load versus displacement relationship of the Superstrand cable is shown in Figure 5 - 36. It can be seen that within the initial 3 mm displacement, the pull-out force rapidly increased to 120 kN. After that, there was a small decrease of the pull-out load, due to a crack induced within the confining medium. Then, load increased with displacement until a peak value of 158 kN at a displacement of 64.7 mm. Beyond the maximum value, the pull-out force decreased gradually to 130 kN at 100 mm.

After the test, the bearing plate was removed and it was found that the whole cable bolt was pulled from the grout column, as shown in Figure 5 - 37, indicating that shear failure occurred at the cable/grout interface.

During this test, the anchor tube performed well with no slippage. As seen in Figure 5 - 38, there is a no relative movement between the anchor tube, grout column and the Superstrand cable bolt.

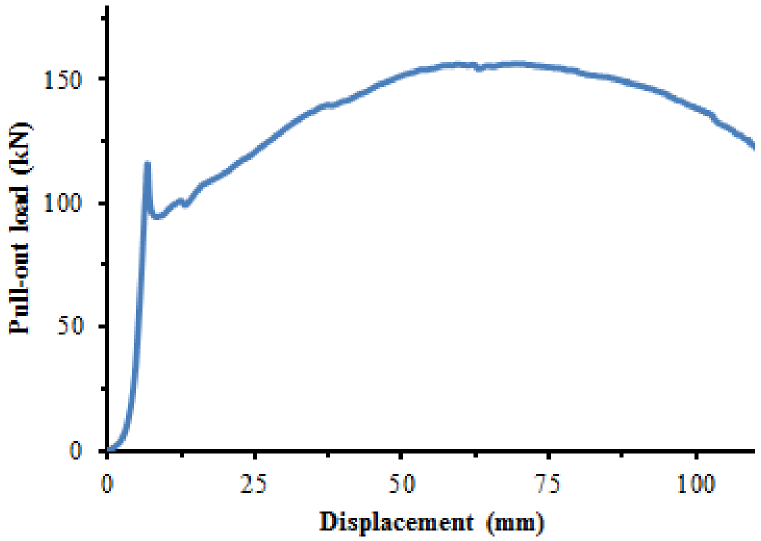

Figure 5 - 36 Load/displacement relationship of the Superstrand cable bolt

Figure 5 - 37 The Superstrand cable bolt was extracted leaving a column of grout material fixed to the confining medium

Figure 5 - 38 View of cable bolt at top of anchor tube after testing

5.4.3 Influence of borehole roughness

The effect of borehole roughness on the performance of rock tendons was evaluated by Blanco Martín (2012), using the confining medium with a UCS strength of 60 MPa. The effect though in weaker rock types such as coal is unclear. Therefore, several weak confining media made of the YN1.5MPA grout with rifled and smooth boreholes were tested, using both the modified (MW9) and the plain (Superstrand) cable bolts.

The performance of MW9 cable bolts pulled from rifled and smooth boreholes is compared in Figure 5 - 39 and Table 5 - 2. Surprisingly, roughening of the borehole had little impact on the maximum pull-out load. In the post failure region, the smooth borehole provided more consistent results whereas load fell away quickly in the rifled borehole.

With respect to the failure mode, although shear slippage was evident at the grout/rock interface in both cases, as shown in Figure 5 - 40 and Figure 5 - 41, the failure process was different. In the rifled borehole, the material between the grout ribs was detached (Figure 5 - 40). This reduced the resistance between the detached and surrounding medium. In the case of the smooth boreholes, no material was detached and shear slippage occurred along the grout/rock interface.

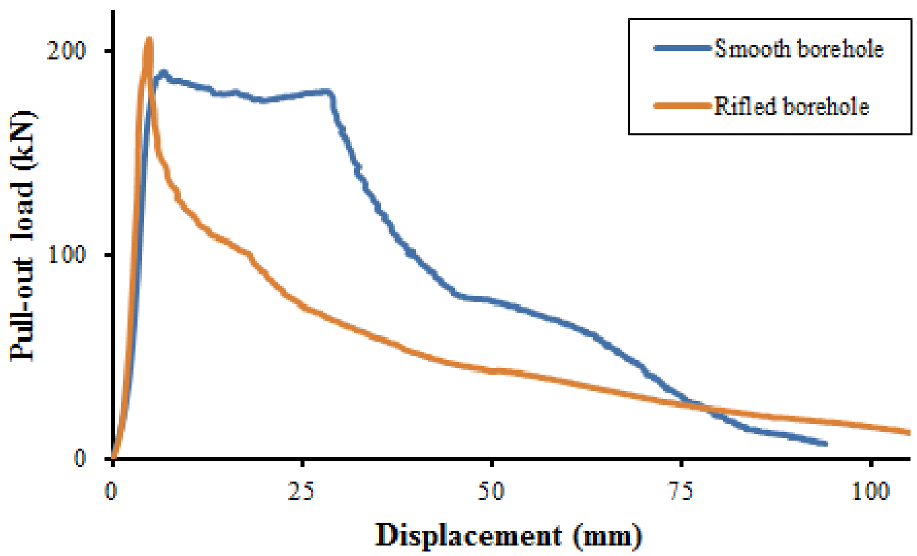

Figure 5 - 39 Borehole roughness effect on performance of MW9 cable bolts

Figure 5 - 40 Failure of the MW9 cable bolt in a rifled borehole

Figure 5 - 41 Failure of the MW9 cable bolt in a smooth borehole

Table 5 - 2 Peak load of MW9 cable bolts pulled from rifled and smooth boreholes

Cable name	Borehole roughness	Peak load (kN)	Averaged load (kN)
MW9	Rifled	208	208
		210	
		206	
	Smooth	206	202
		210	
		190	

The influence of borehole roughness on performance of plain strands is shown in Figure 5 - 42 and Table 5 - 3. As seen, there is no apparent difference between them.

On the other hand, with the Superstrand, different failure modes occurred. As shown in Figure 5 - 43 and Figure 5 - 44, failure always occurred at the cable/grout interface independent of borehole roughness. Also, the load transfer capacity of Superstrand bolts installed in those two borehole roughness conditions was almost identical.

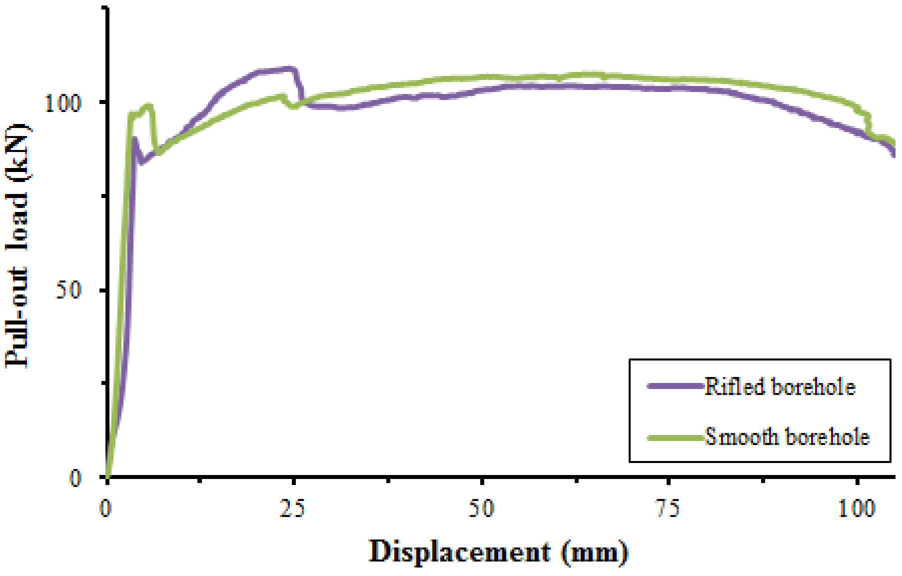

Figure 5 - 42 Borehole roughness effect on performance of the Superstrand cable bolt

Table 5 - 3 Peak load of Superstrand cable bolts pulled from rifled and smooth boreholes

Cable name	Borehole roughness	Peak load (kN)	Averaged load (kN)
Superstrand	Rifled	109	112
		118	
		110	
	Smooth	110	111
		116	
		107	

Figure 5 - 43 Failure of the Superstrand cable bolt in a rifled borehole

Figure 5 - 44 Failure of the Superstrand cable bolt in a smooth borehole

It was determined that the borehole roughness can influence the load transfer performance of cable bolts particularly when failure occurs at the grout/rock interface. Furthermore, when bond failure occurs along the grout/rock interface, the borehole roughness has an influence on the post-peak performance of cable bolts. To be consistent with spiral boreholes in the field, rifled boreholes were used in all tests.

5.4.4 Influence of pre-confinement of the confining medium

The steel cylinder was adopted as a means of providing passive confinement to the confining medium. The cylinder is formed by bolting together a pair of cylinder plates. Before each test, a foam pad was inserted between the face plates of each half cylinder to create a flexible gap of approximately 5 mm thickness. The confining medium was placed within the assembled cylinder and grout was added to fill the small annulus between the confining medium and cylinder. After the grout cured, the bolts were tightened using a torque wrench to a predetermined fixed level of torque. This effectively provided confinement to the confining medium as shown in Figure 5 - 45. The level of confinement is a function of the torque applied. This ensured a consistent level of contact between the confining medium and cylinder.

To study the effect of this pre-confinement on the pull-out behaviour of cable bolts, a number of tests were undertaken with torque ranging from 0 to 200 N•m on MW9 cable bolts reinforced in strong confining media. The pull-out load versus displacement characteristics was recorded and compared as shown in Figure 5 - 46 and Table 5 - 4. The graph shows that the pre-confinement torque had little or no impact on the initial stiffness of the grouted cable bolting system but does influence the peak load of cable bolts. To illustrate this effect, the peak loads for each level of torque are shown in Figure 5 - 47.

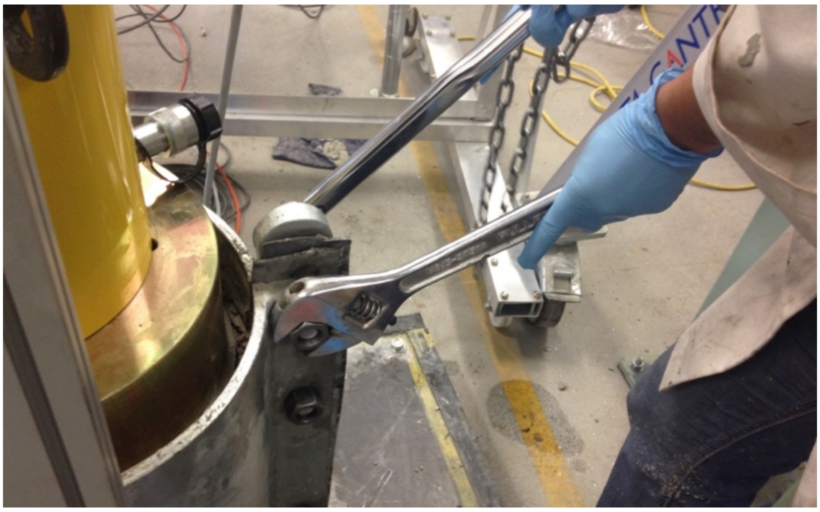

Figure 5 - 45 Tightening the bolts joining the two halves of the steel cylinder to a constant torque ensures a consistent level of confinement

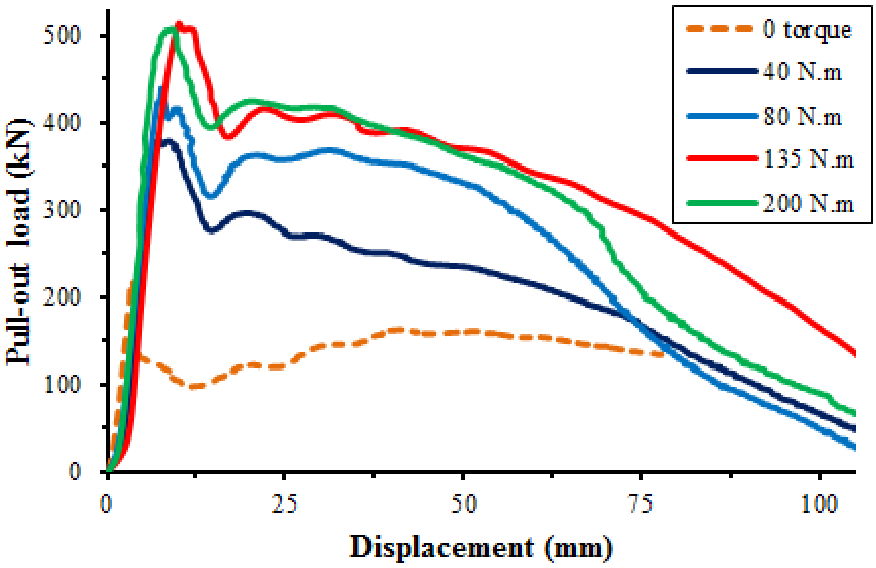

Figure 5 - 46 Pull-out performance of MW9 cable bolts at different levels of torque

The graph shows that the maximum pull-out load increased with the pre-confinement torque rising up to approximately 150 N·m beyond which there was little further change. The likely reason for this is that the grout bonding the confining medium and the confinement tube yielded and underwent plastic deformation.

Table 5 - 4 Pull-out results of MW9 cable bolts with different levels of torque

Test number	Pre-confinement torque (N·m)	Peak load (kN)
1	0	218
2	40	381
3	80	439
4	135	514
5	200	507

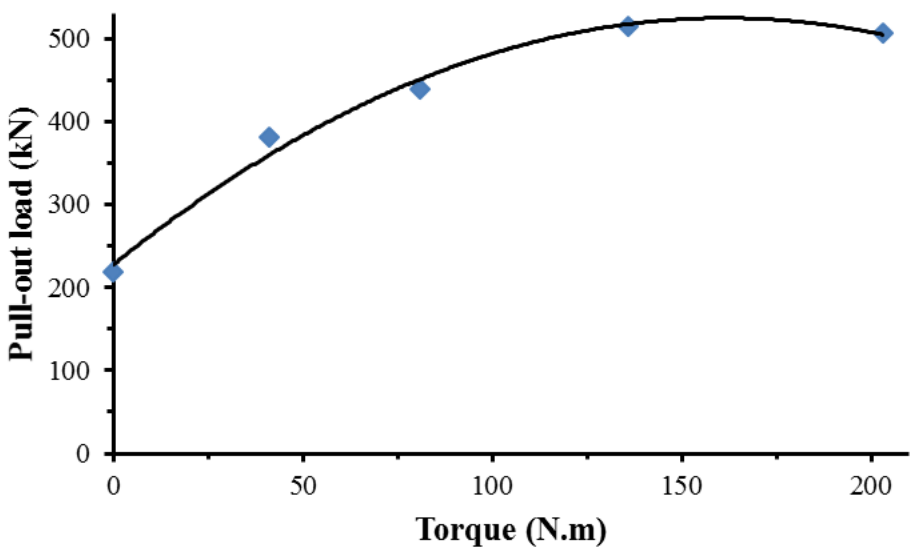

Figure 5 - 47 Peak load of MW9 cable bolts at different levels of torque

Hence pre-confinement has an appreciable effect on the load transfer capacity of cable bolts. To ensure a constant test environment and minimise any potential of cable bolt rupture, a lower level of pre-confinement torque of 40 N·m was always used in the following tests. Low torque was desired to minimise the impact of confinement that might otherwise have a different impact with different cable bolt types on pull-out performance.

5.4.5 Further study of cable termination methods

In previous LSEPT, end fittings, such as the barrel and wedge system (Figure 5 - 48), were used to prevent slippage in the anchor section (Reynolds, 2006; Thomas, 2012).

However, different termination fittings are currently used for cable bolts in the market. For example, Figure 5 - 49 shows a termination plate used in MW9 cable bolts.

To minimise the impact of different end fittings on pull-out behaviour of cable bolts, the designed anchor tube aims at eliminating reliance on end fittings. Several pull-out tests were performed on MW9 cable bolts installed in strong confining media with three different termination methods, namely no termination device, the barrel and wedge system and the termination plate, were used. When a pre-confinement torque of 40 N·m was applied, the results are shown in Figure 5 - 50, indicating that different termination methods had little effect on the cable bolts' performance.

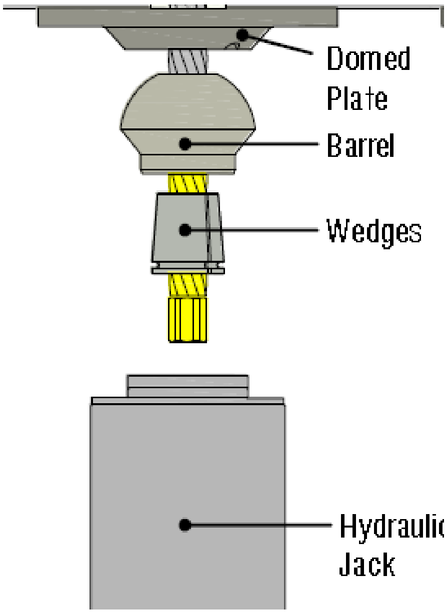

Figure 5 - 48 System of cable termination using barrel and wedge (Megabolt, 2012)

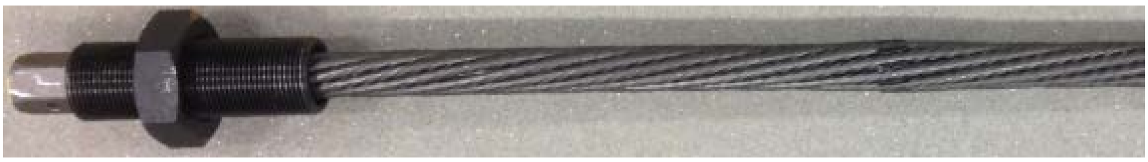

Figure 5 - 49 The termination plate for Megabolt cable bolts

Based on the test results, it is further confirmed that the designed internally threaded anchor tube works just as effectively in firmly gripping the cable bolt as any of the other termination devices. Therefore, in the following tests, no termination device was applied on the end of the anchor tube.

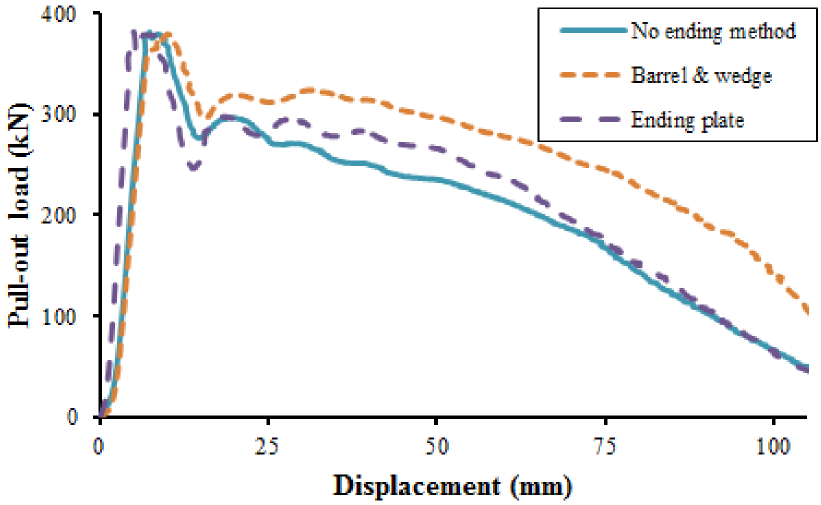

Figure 5 - 50 Comparison between different termination methods

5.5 Summary

A new design of an axial test rig based on the original LSEPT was developed. To reflect the load transfer situation of reinforcement tendons in the field, this apparatus incorporates two sections, namely the embedment and the anchor sections. In the embedment section, the confining medium was confined by a split-tube. As for the anchor section, the bearing plate, anchor tube, hydraulic cylinder, distribution plate, load cell, abutment plate and finally the reaction plate were installed in sequence.

A number of pull-out tests were conducted to evaluate the influence of confining medium size on the bond capacity of cable bolts. The diameter of the confining medium ranged from 150 mm to 508 mm and a high capacity cable bolt that would induce the largest stress in the confining medium as a result of load transfer from the cable bolt was used. Two different boundary conditions, unconfined and confined, were applied. It was found that the bond capacity varied significantly with confining medium diameter. Furthermore, the peak load of cable bolts in confined situation is always higher than unconfined. An embedment section diameter of 300 mm was used in following tests to ensure consistent confinement conditions, eliminating any effect of confining medium size on performance.

A locking key and two locking nuts were designed to couple the confinement tube, bearing plate and anchor tube together. These were effective in preventing the cable bolts from rotating over a large axial displacement range up to 100 mm so that both the peak and residual behaviour of cable bolts could be studied.

Two types of confining media, in which one was made of the YN1.5MPA grout, simulating weak rock, while the other was mixed with GS32250 grout, representing strong rock, were cast. Stratabinder grout was used to bond the cable bolt with the surrounding confining medium. In the embedment section, a w/c ratio of 0.42 was used and in the anchor section, a lower w/c ratio of 0.38 was adopted.

Three displacement transducers were used to monitor the movement of the cable bolt. A consistent result occurred between all three of transducers: the LVDT, Micro Pulse and Laser. However, the results acquired by the LVDT were apparently influenced by the vibration of the hydraulic cylinder. The non-contact Laser instrument could record a smooth result and then in following tests, the displacement result obtained by the Laser transducer was always used.

Initially, two pull-out tests with the new apparatus were performed on modified and plain cable bolts. The results show that there was no bond failure occurring in the anchor tube, indicating that the designed anchor tube can bear the capacity of cable bolts.

The influence of borehole roughness on performance of modified and plain cable bolts installed in the weak confining medium was studied. Both smooth and rifled boreholes were tested. The results show that the borehole roughness has little effect on determining the peak capacity of cable bolts. However, the borehole roughness makes a difference in deciding the residual behaviour of cable bolts only when failure occurs along the grout/rock interface.

Several pull-out tests were conducted on modified cable bolts with the pre-confinement torque varying from 0 to 200 N·m. The results show that the pre-confinement torque has almost no influence on determining the initial stiffness of the cable bolting system. However, with the pre-confinement torque increasing, the peak load of cable bolts increased. To ensure a uniform test environment, a pre-confinement torque of 40 N·m was used in all subsequent tests.

Three different termination methods, namely no termination device, a barrel and wedge system and the special termination plate, were used on modified cable bolts to test the impact of the termination method on the behaviour of the cable bolts. The results show that the performance of cable bolts is independent of the different termination methods, further proving that the designed anchor tube is able to bear the load capacity of the cable bolts. Therefore, in all following tests, no termination device is applied on the end of the anchor tube.

CHAPTER SIX

LOAD TRANSFER BEHAVIOUR OF FULLY GROUTED CABLE BOLTS

6.1 Introduction

Two types of fully grouted cable bolts, namely plain cable bolts and modified cable bolts, are currently used in the mining industry. Plain cable bolts were first introduced to complement rigid rockbolts in rock reinforcement applications. Their inherent flexibility offered the advantage that they could be anchored much deeper into a rock mass than rigid steel rockbolts. They also have an axial strength comparable to rockbolts (Thompson *et al.*, 2012). Over recent decades, modifications have been made to the design and construction of the cable bolt to improve its strength and load transfer capacity. This chapter reports on a study comparing the performance of two cable bolts representative of both types of cable bolts. Specifically, MW9 and Superstrand cable bolts, which are widely used in the Australian underground coal mining industry, were selected.

Considering that the grout poured into the borehole usually has a UCS around 60 MPa in field applications, the Stratabinder grout with a w/c ratio of 0.42 and a measured strength of 54.3 MPa was used.

The influence of different parameters on the load transfer behaviour of cable bolts was studied. Specifically, to study the performance of cable bolts in the weak rock condition, YN1.5MPA grout with a UCS of 8.8 MPa was used to prepare the confining medium in which the cable bolts were anchored. Both MW9 and Superstrand cable bolts were pulled from the weak confining medium to check their workability. Two types of bearing plates, in which one is the standard bearing plate with a normal hole diameter of 70.3 mm and the other one has a larger hole with a diameter of 140 mm, were used. By comparing the results of cable bolts in those two conditions, the influence of bearing plate dimension on load transfer behaviour of both modified and plain cable bolts was analysed.

The borehole size effect on the performance of fully grouted cable bolts installed in the weak confining medium was studied. Two types of borehole diameters were tested. In detail, the diameter recommended by the cable bolt manufacturer is termed as the “standard” borehole size while an oversized hole diameter is called as the “larger” boreholes. For example, in the case of the MW9 cable bolt, the hole diameter of 42 mm, recommended by manufacturers, was used as the standard size and compared against the performance in an oversized hole with a diameter of 52 mm. During the test, the failure mode, peak and residual load bearing capacity were evaluated and compared.

To investigate the influence of confining medium strength on the performance of cable bolts, GS32250 grout with a UCS of 62.7 MPa was used to cast the strong confining medium. Pull-out tests were conducted on both MW9 and Superstrand cable bolts embedded in these strong confining media.

The impact of embedment length on axial behaviour of the modified cable bolts was also studied. Specifically, the MW9 cable bolts were tested and the embedment length increased from 320 mm to 380 mm.

Finally, the cable surface geometry influence was investigated. The performance of MW9 and Superstrand cable bolts embedded in the same condition was compared.

6.2 Load transfer of modified cable bolts

6.2.1 Dimensions of MW9 cable bolts

To enhance the mechanical interlock between the cable bolt and the grout column, the nutcage geometry with a diameter of 37.9 mm was fabricated along the cable bolt, as shown in Figure 6 - 1. The full length of the cable bolt used in tests was 1180 mm, in which 320 mm was encapsulated in the confining medium. It should be mentioned that the nutcage geometry was contained in the anchor length to increase the bond strength of anchor section. The dimensions of the MW9 cable bolt is tabulated in Table 6 - 1.

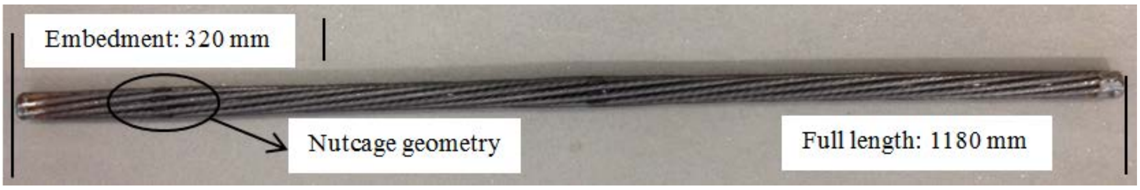

Figure 6 - 1 MW9 cable bolt geometry

Table 6 - 1 MW9 cable bolt dimensions

Cable type	Wires	Length (mm)	Diameter (mm)	Perimeter (mm)	Nutcage geometry	
					Length (mm)	Diameter (mm)
MW9 cable bolt	9	1180	28.5	125.5	180	37.9

6.2.2 Bearing plate effect

The first series of pull-out tests was conducted in the weak confining medium. YN1.5MPA grout with a UCS of 8.8 MPa was used to cast the confining medium. A standard borehole diameter of 42 mm was prepared. After the confining medium fully cured for 28 days, pull-out tests were conducted. During the test, it was found that the cable bolt and the grout column were extruded from the confining medium, as shown in Figure 6 - 2.

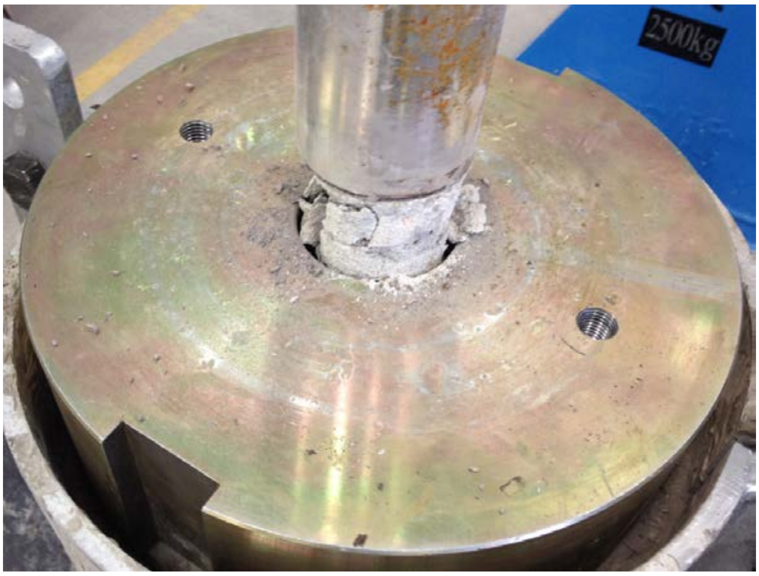

Figure 6 - 2 The cable bolt and the grout column that were pulled from the confining medium

The pull-out load and displacement were recorded, as shown in Figure 6 - 3. Apparent brittle behaviour was exhibited by the MW9 cable bolt. Pull-out load increased linearly to a peak value of 205 kN when displacement reached 4.8 mm. Then the pull-out load rapidly reduced to 100 kN. When the pull-out displacement reached 50 mm, the MW9 cable bolt displayed a residual load of approximately 43 kN.

After the test, the confining medium was split to observe the failure mode, as seen in Figure 6 - 4. Shear slippage occurred at the grout/rock interface. In detail, the confining medium material between the spiral “grout ribs” was sheared off, as shown in Figure 6 - 5**.** The reason is that the confining medium material had much lower strength compared to the Stratabinder grout. During testing, the shear strength of cable/grout interface increased because of the cable’s special nutcage geometry.

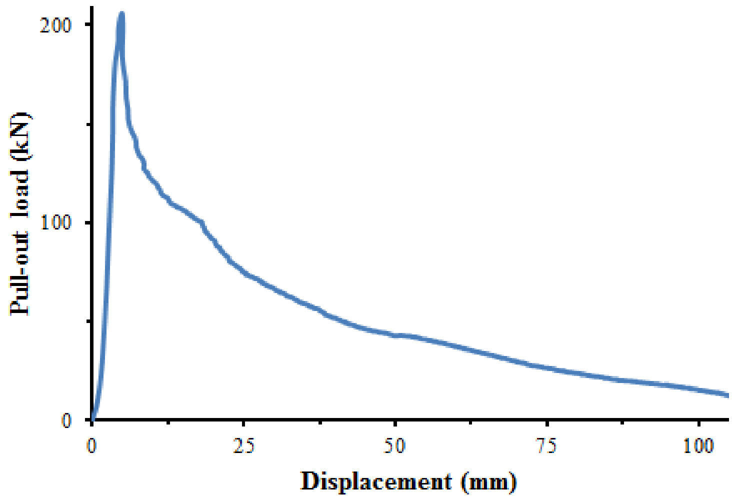

Figure 6 - 3 Performance of the MW9 cable bolt tested with a standard bearing plate

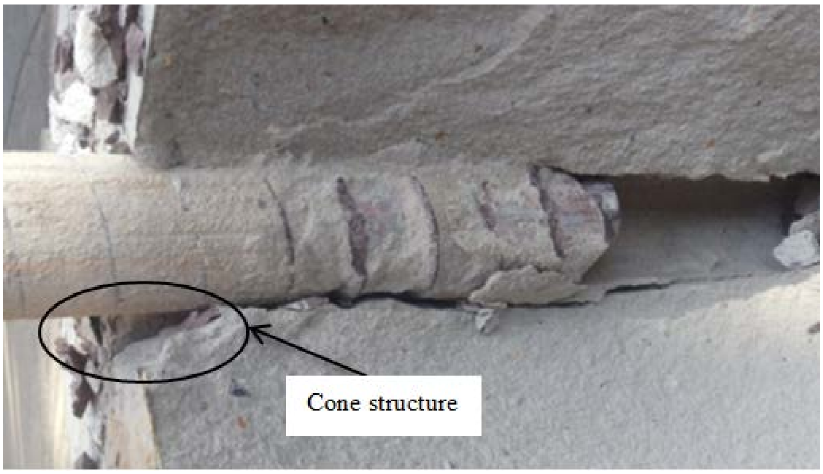

Figure 6 - 4 Failure at the grout/rock interface

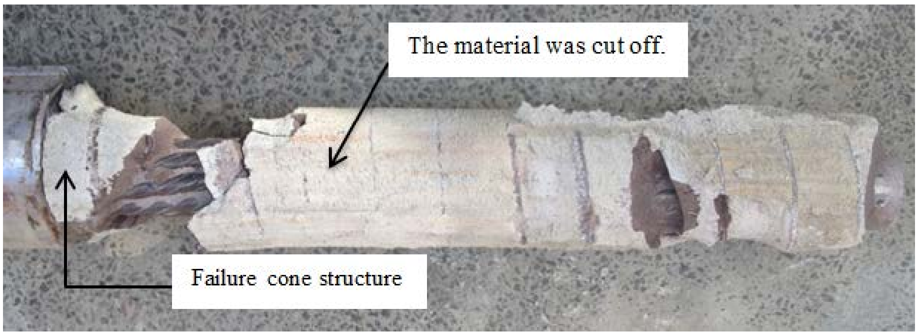

Figure 6 - 5 The material between rifled ribs was cut off.

It is also found that near the “joint”, a crater failure at the surface of the borehole collar occurred. However the size of this crater was likely to be limited by the hole diameter in the bearing plate. To further confirm this, a second bearing plate with an internal hole diameter of 140 mm (termed the larger bearing plate) was designed and used, as shown in Figure 6 - 6.

Figure 6 - 6 The MW9 cable bolt was tested with a larger bearing plate.

As shown in Figure 6 - 7, when this plate was used, the crater was much larger than the previous one. To determine the crater size, plaster material was poured into the cone. It was found that the crater had a depth of 43 mm and inclination close to 45 degrees (Figure 6 - 8).

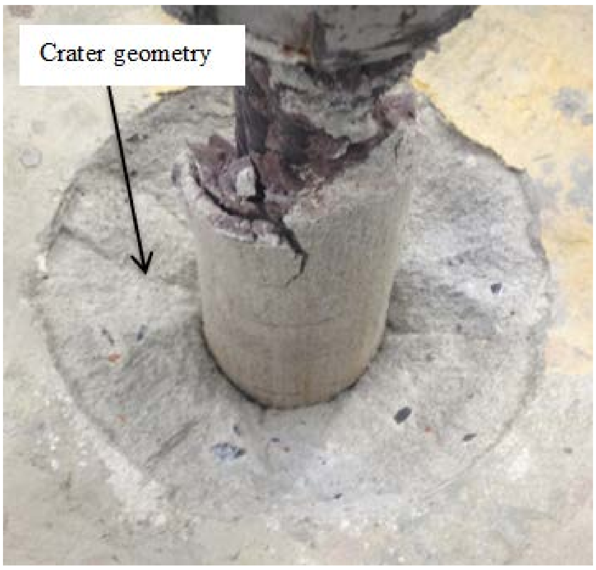

Figure 6 - 7 The crater geometry

Figure 6 - 8 Inclination angle of the crater geometry

A comparison between the performance of MW9 cable bolts with normal and larger bearing plates is shown in Figure 6 - 9, indicating that the bearing plate has a marked impact on the peak capacity, as depicted in Table 6 - 2.

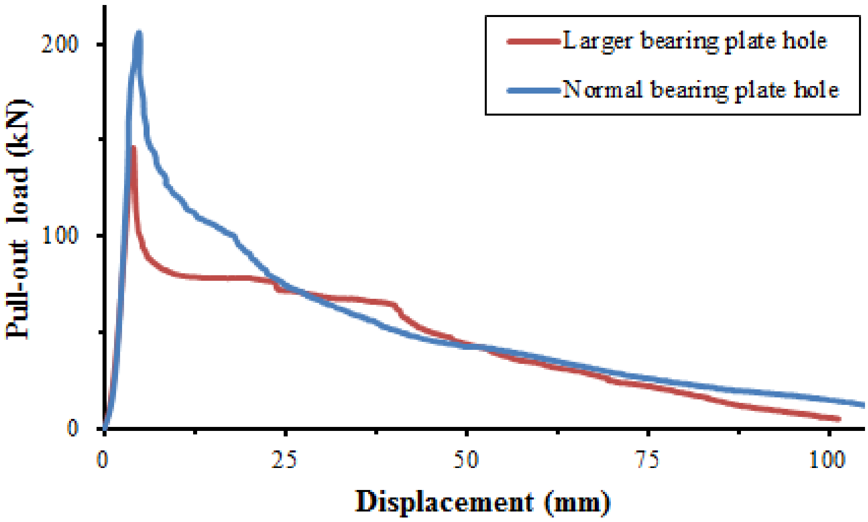

Figure 6 - 9 Influence of bearing plate hole size on performance of MW9 cable bolts

Table 6 - 2 Peak and residual capacities of MW9 cable bolts

Bearing plate hole size \ Performance	Peak load (kN)	Residual load (kN)
Normal plate hole	206	43
Larger plate hole	146	43

The performance of MW9 cable bolts with two bearing plates is primarily determined by different failure modes. Specifically, when a normal bearing plate was used, the main part of the confining medium was compressed. Failure was restricted to shear slippage along the grout/rock interface for the full embedment length of 320 mm. By contrast, with the larger plate hole, tensile failure of the confining medium took place and shear slippage occurred along grout/rock interface over a smaller embedment length of 277 mm, as shown in Figure 6 - 10.

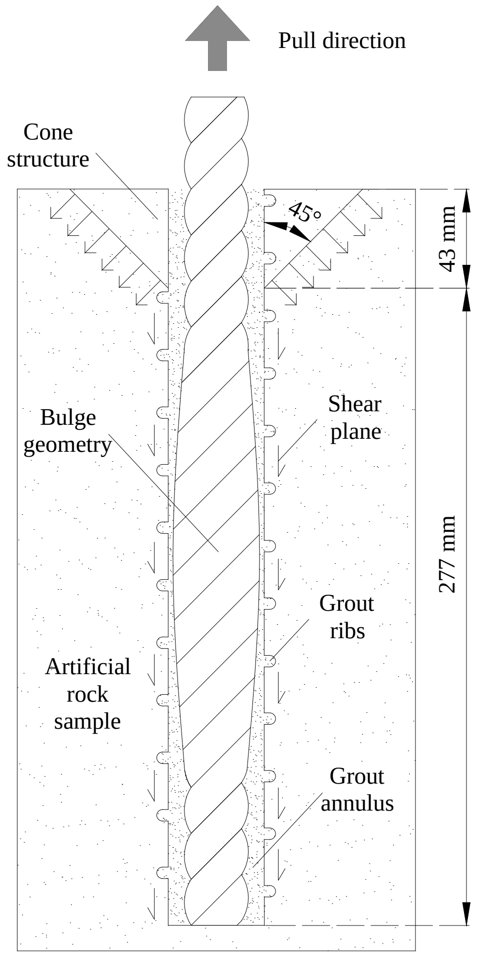

Figure 6 - 10 Cone structure was removed on the top of the confining medium.

To study the bond performance of MW9 cable bolts, the bearing plate with a standard hole was used in the following tests. The performance of MW9 cable bolts installed in weak the confining medium is tabulated in Table 6 - 3.

Table 6 - 3 Results of MW9 pulled from the weak confining medium

No.	Borehole size (mm)	Peak load (kN)	Residual load (kN)
1	42	208	136
2	42	210	144
3	42	206	43
	Mean	208	108

6.2.3 Borehole size effect

Although the cable bolt manufacturer always recommends a particular borehole size for cable bolt products, operators prefer to use larger boreholes in the field because it is easier to install the cable bolts. However, the influence of increasing borehole size on the performance of cable bolts in the weak confining medium has not been studied. Thus, a relatively larger borehole diameter of 52 mm was used to evaluate the borehole size effect on load transfer behaviour of modified cable bolts. The confining medium was still cast with YN1.5MPA grout. During the test, the MW9 cable bolt was pulled from the confining medium, as shown in Figure 6 - 11.

The test was replicated five times (Figure 6 - 12). During the test, the pull-out load and displacement were recorded. It should be mentioned that when the third test was conducted, the data logging system failed to record the results because of a power failure. Nevertheless, the results obtained from the remaining four tests were consistent. The second, fourth and fifth tests were selected as the final results. The first test result was not selected because its residual load was apparently much higher than the other tests. The method of selecting best three results from five tests was always used in following tests.

Figure 6 - 11 The cable bolt was pulled from the larger borehole.

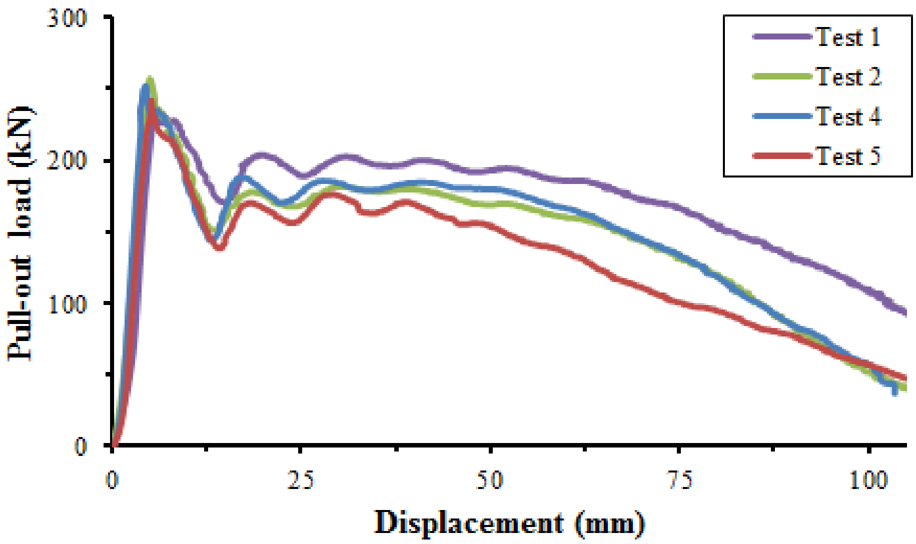

Figure 6 - 12 Replication tests of MW9 cable bolts

The load transfer behaviour of MW9 cable bolts installed in larger boreholes is shown in Figure 6 - 13 and Table 6 - 4. The results show that after a short pull-out displacement of 5 mm, the bearing capacity of this cable bolting system reached a peak load of 250 kN. The residual load was approximately 167 kN at a pull-out displacement of 50 mm.

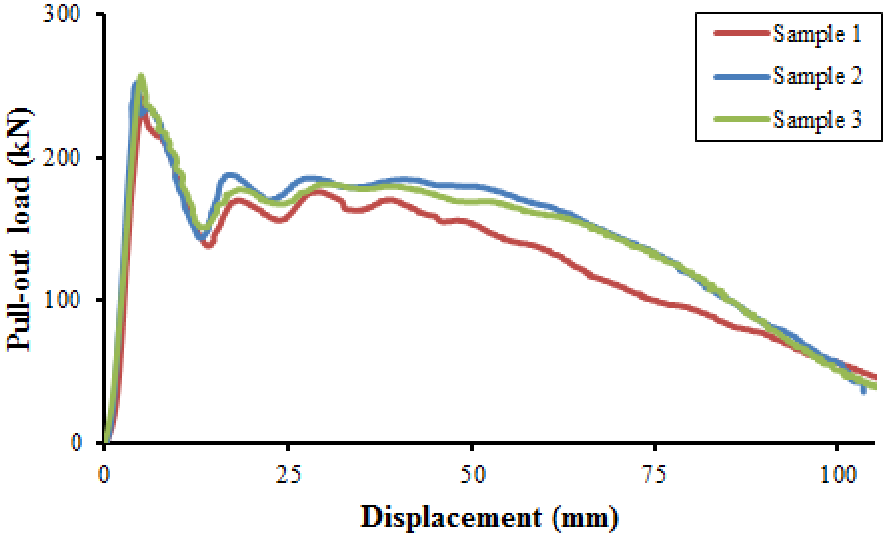

Figure 6 - 13 Performance of MW9 cable bolts pulled from larger boreholes

Table 6 - 4 Results of MW9 cable bolts pulled from larger boreholes

No.	Borehole size (mm)	Peak load (kN)	Residual load (kN)
1	52	257	170
2	52	252	180
3	52	242	152
	Mean	250	167

After the test, the confining medium was split to check the failure mode. Figure 6 - 14 shows that shear failure occurred along the cable/grout interface. After a short pull-out displacement of only 5 mm, the chemical adhesion was damaged. Further checking the failure status showed that the grout material close to the bulb location was almost removed, indicating that the mechanical interlock around the cable bolt nutcage geometry was broken. At this point, the MW9 had achieved its maximum load bearing capacity. However, at a pull-out displacement of 12 mm, the nutcage geometry re-engaged with the intact grout ridges and resistance of MW9 began to rise again. At 18 mm the grout ridges were sheared and the bearing capacity of MW9 dropped off once again. This cyclic phenomenon was maintained until a pull-out displacement of 60 mm, at which point the nutcage was only 10 mm extracted from the borehole. This is described as the slip-lock mechanism as the cable bolt slips along the cable/grout interface before re-gripping. After a pull-out displacement of 60 mm, the load transfer capacity of the MW9 decreased linearly, being a function of pure friction between the cable and the grout annulus.

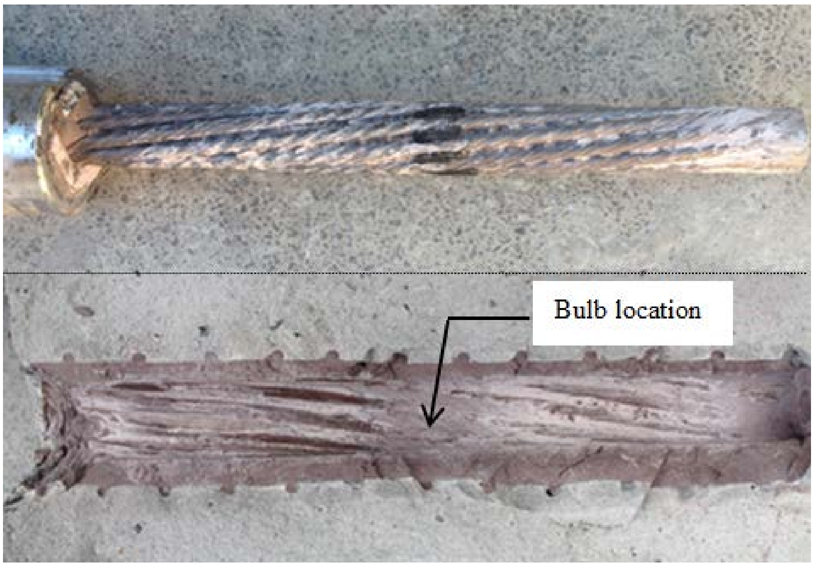

Figure 6 - 14 Shear failure at the cable/grout interface showing a) view of the modified cable bolt (top), and b) borehole surface condition (bottom)

In the weak confining medium, the influence of the oversized borehole diameter on MW9 cable bolts is shown in Figure 6 - 15. The borehole size has a significant effect on deciding the performance of MW9 cable bolts. Both the peak and residual load were significantly improved, as shown in Table 6 - 5.

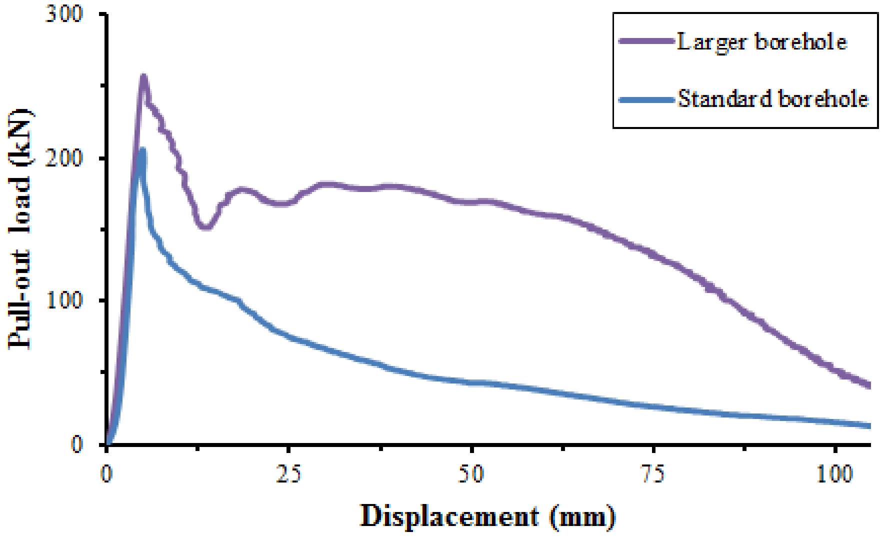

Figure 6 - 15 The effect of increasing borehole size on performance of MW9 cable bolts

Table 6 - 5 Bearing capacities of MW9 cable bolts in different boreholes

Borehole size \ Load	Peak load (kN)	Residual load (kN)
Standard borehole	206	108
Larger borehole	250	167
Percentage change	+21.4%	54.6%

6.2.4 Confining medium strength effect

The GS32250 grout was used to cast the strong confining medium. A standard borehole of 42 mm was used. During the test, it was found that the cable bolt was extruded from the grout column, as shown in Figure 6 - 16.

After the test, the load transfer performance of MW9 cable bolts is shown in Figure 6 - 17 and Table 6 - 6. The strong material provided a higher level of resistance, resulting in a stiff tendon having a large pull-out load of nearly 380 kN after a displacement of only 10 mm. After the peak load, the load bearing capacity in the post-failure region fell quickly. After 100 mm displacement, the capacity of the cable bolt reduced to less than 80 kN.

Figure 6 - 16 The MW9 cable bolt which was pulled from the grout column

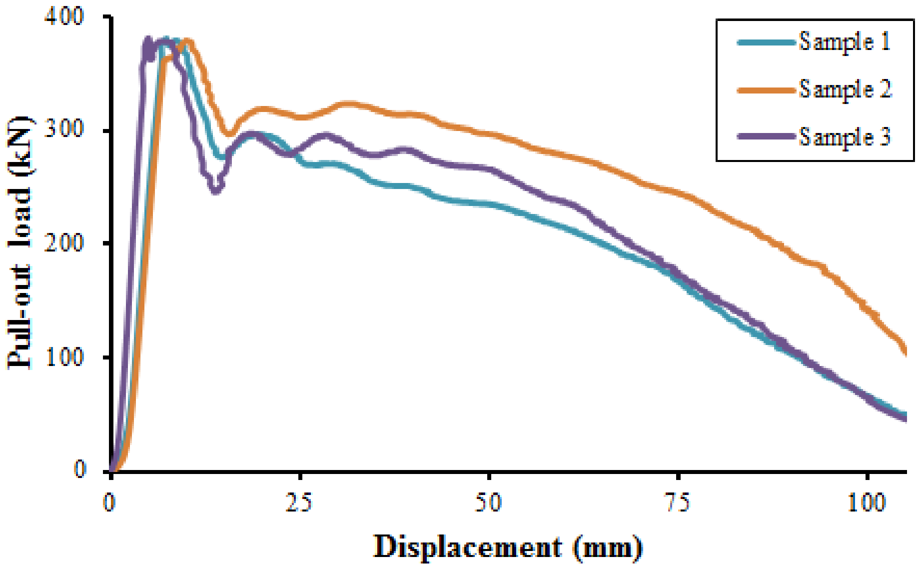

Figure 6 - 17 Performance of MW9 cable bolts pulled from the strong confining medium

Table 6 - 6 Results of MW9 cable bolts pulled from the strong confining medium

No.	Borehole size (mm)	Peak load (kN)	Residual load (kN)
1	42	381	234
2	42	379	296
3	42	381	263
	Mean	380	264

The failure mode in the embedment section is shown in Figure 6 - 18 and Figure 6 - 19 respectively. These indicated good contact at the grout/rock interface. During the pull-out process, failure initially occurred at the loaded end of the cable/grout interface. Then it propagated to the far end when the whole cable/grout interface was broken.

Figure 6 - 18 The MW9 cable bolt after testing

Figure 6 - 19 Shear failure at the cable/grout interface

The slip-lock phenomenon occurred within a short displacement between 13 to 60 mm for the MW9 cable bolt in the strong confining medium, as highlighted in Figure 6 - 20. Beyond this zone there was a uniform reduction of load.

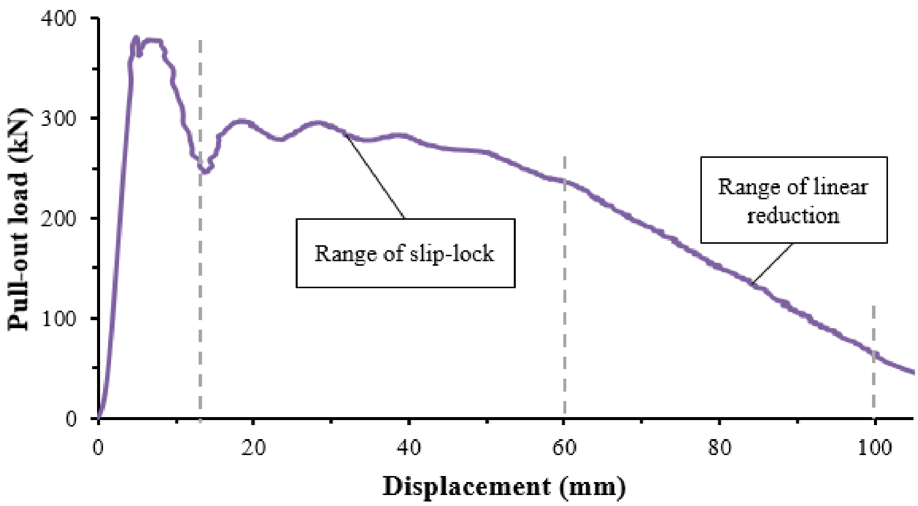

Figure 6 - 20 Typical performance of a MW9 cable bolt pulled from the strong confining medium

The load transfer performance of MW9 cable bolts installed in weak and strong confining media is compared, as shown in Figure 6 - 21. The confining medium strength had an obvious influence on the performance of the MW9 cable bolts. In the weak confining medium, shear failure occurred at the grout/rock interface. Consequently, after the peak load, the bearing capacity of the modified cable bolting system dropped gradually. However, when the MW9 cable bolt was pulled from the strong confining medium, failure occurred at the cable/grout interface. The nutcage geometry re-engaged with the confining grout column periodically, resulting in oscillation of the pull-out load. Furthermore, both the peak load and residual load of MW9 cable bolts installed in the strong confining medium were much higher than when installed in the weak confining medium, as shown in Table 6 - 7.

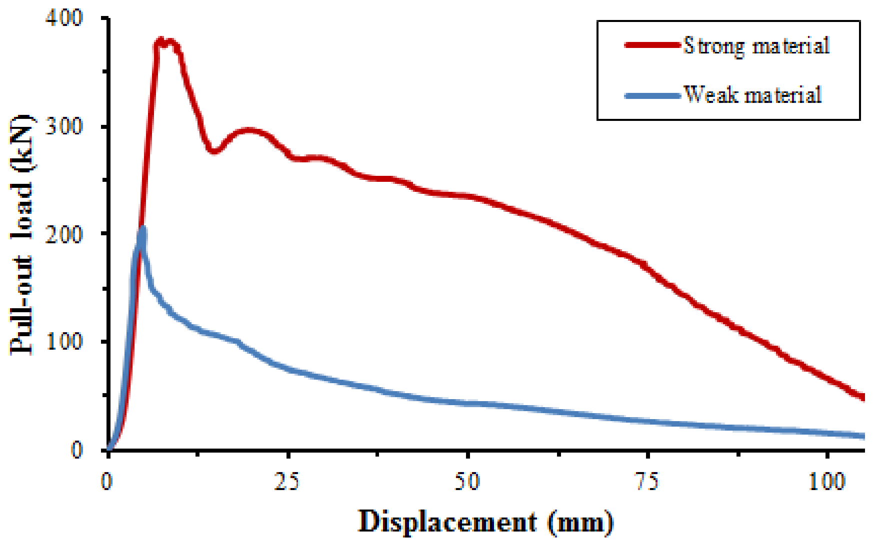

Figure 6 - 21 The effect of confining medium strength on performance of MW9 cable bolts

Table 6 - 7 Bearing capacities of MW9 cables pulled from different confining media

Load / Confining medium strength	Peak load (kN)	Residual load (kN)
Weak	208	108
Strong	380	264

6.2.5 Embedment length effect

In the field, the embedment length can be varied depending on joint intervals. To study the influence of embedment length on the performance of modified cable bolts, MW9 cable bolts were installed in the strong confining medium with different embedment lengths: 340 mm, 360 mm and 380 mm.

MW9 cable bolts with the same configuration were used. Sketches of the tests are shown in Figure 6 - 22, Figure 6 - 23 and Figure 6 - 24. It is clear that the distance between the lower end of the nutcage geometry and the bottom of the borehole was constant at 70 mm. And, the distance between the upper section of the nutcage geometry and the borehole collar increased from 90 mm to 130 mm.

After testing, all failure occurred along the cable/grout interface in the embedment section. No bond failure was observed between the cable bolt, the grout column and the anchor tube. This further certified that the designed anchor tube is able to bear the capacity of cable bolts with longer embedment length.

The load performance of MW9 cable bolts with the embedment length ranging from 320 mm to 380 mm is shown in Figure 6 - 25. The trend of the load-displacement curves were consistent and different embedment length had almost no impact on deciding the initial stiffness of the cable bolting system. However, increasing the embedment length was beneficial to improving both the peak and residual bearing capacity of the cable bolts. Furthermore, the slip-lock phenomenon is more apparent when a longer embedment length was used.

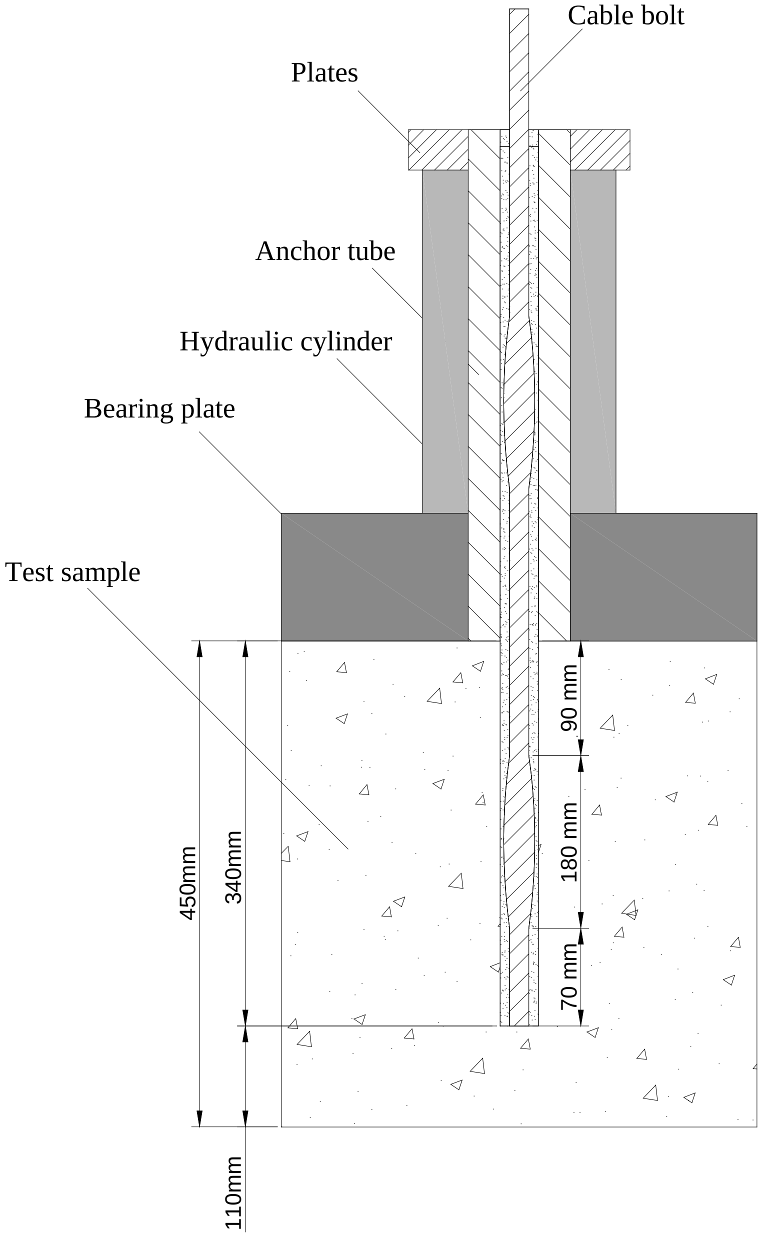

Figure 6 - 22 An embedment length of 340 mm

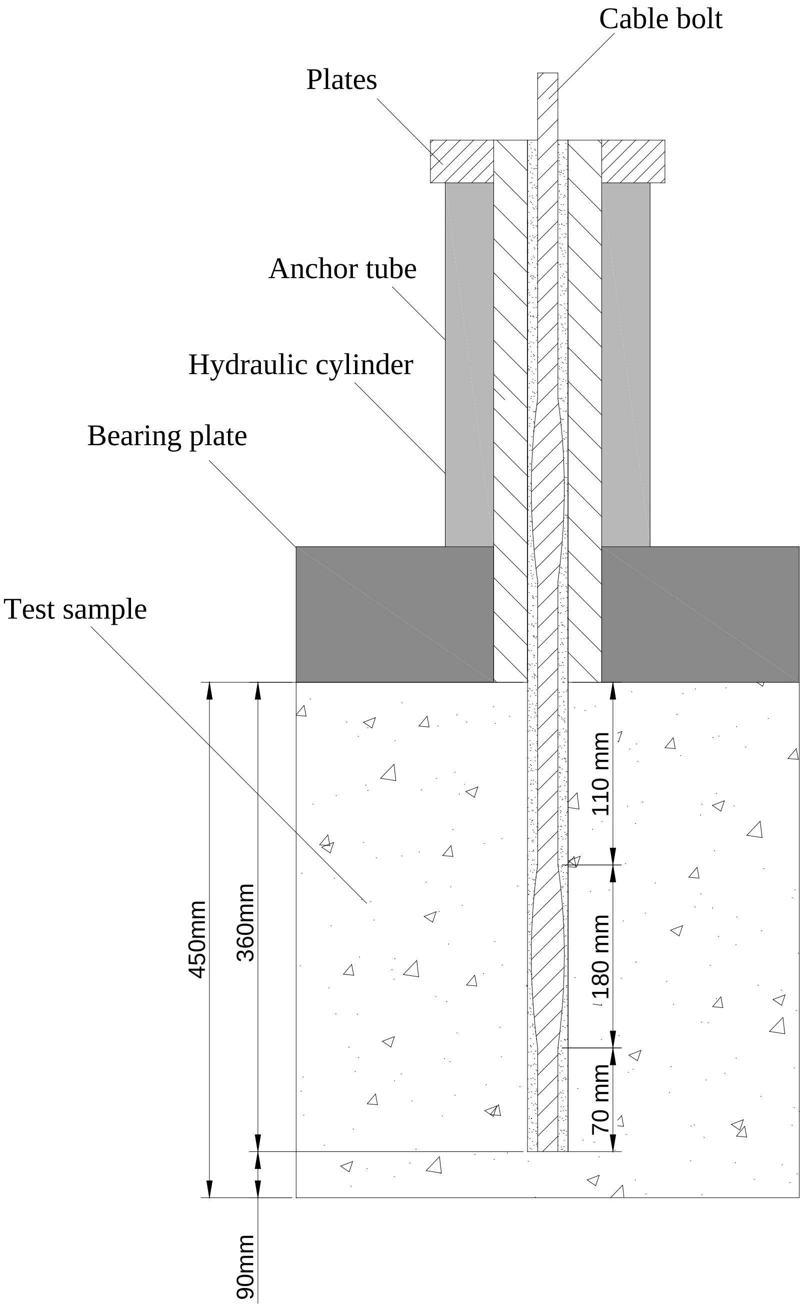

Figure 6 - 23 An embedment length of 360 mm

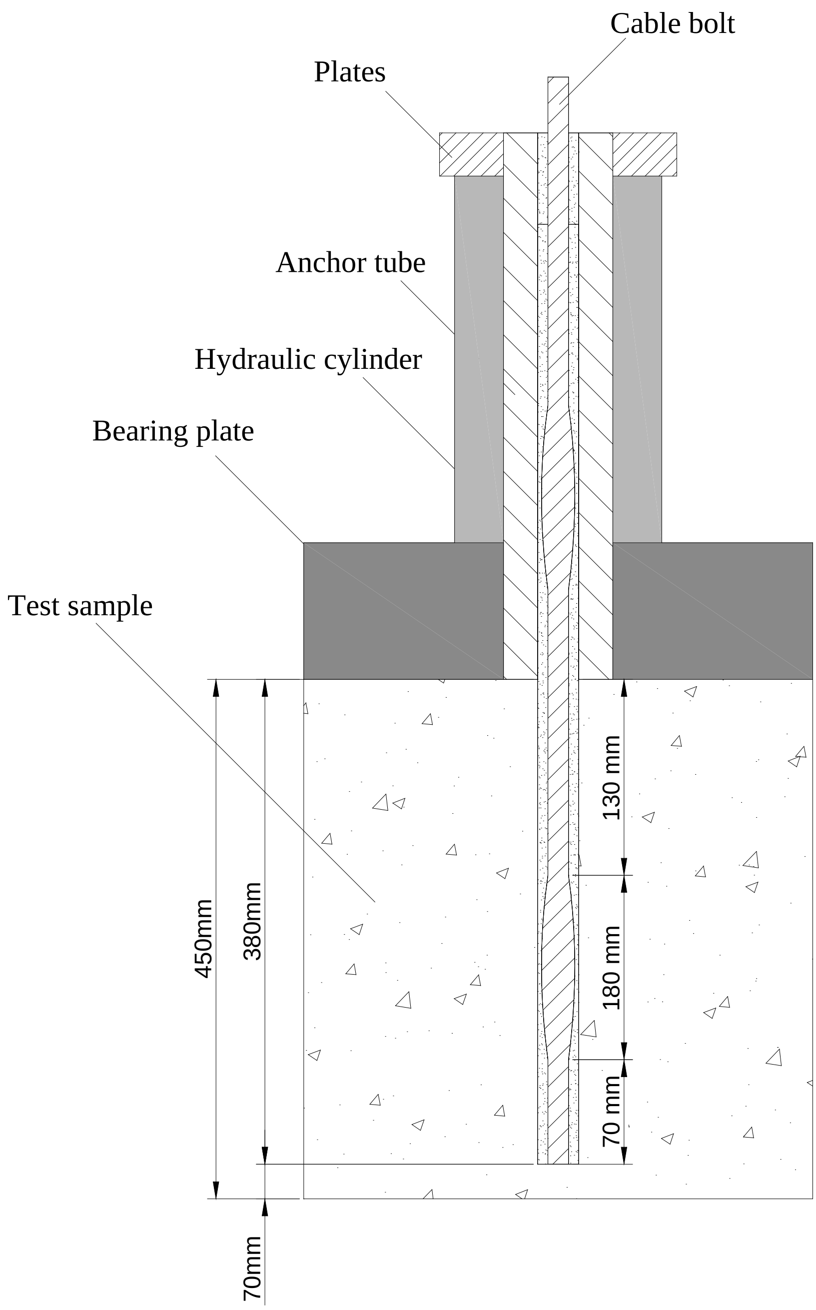

Figure 6 - 24 An embedment length of 380 mm

The relationship between the peak capacity of MW9 cable bolts and the embedment length is shown in Figure 6 - 26. There was almost a linear relationship between the peak capacity of MW9 cable bolts and embedment length within a short range of 360 mm. However, once the embedment length is longer than that, the maximum bearing capacity of the cable bolts was still rising but with a much lower slope. The reason for this is when the embedment length was short enough (less than 12.6 times of the cable diameter), the shear stress along the MW9 cable/grout interface could be regarded uniform. However, once the embedment length was longer than that, a non-uniform shear stress variation was more apparent, resulting in the bearing capacity increasing non-linearly.

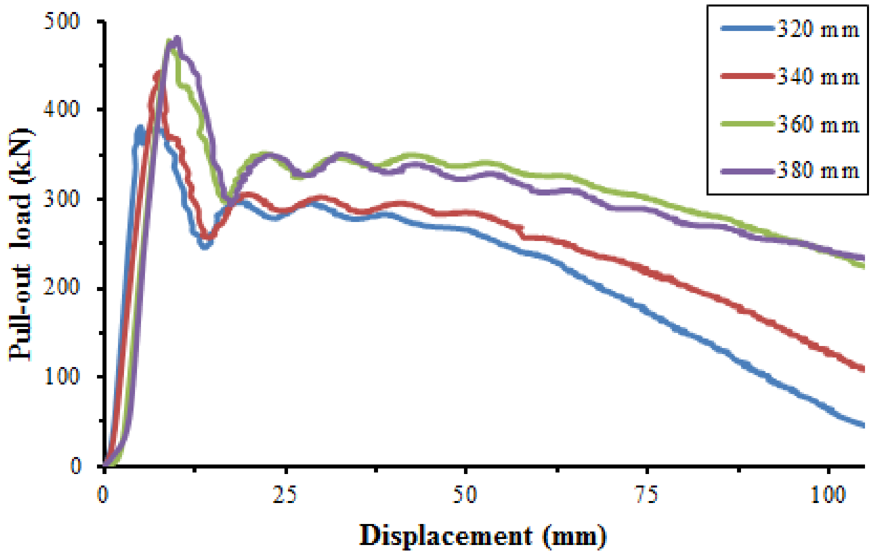

Figure 6 - 25 The effect of embedment length on performance of MW9 cable bolts

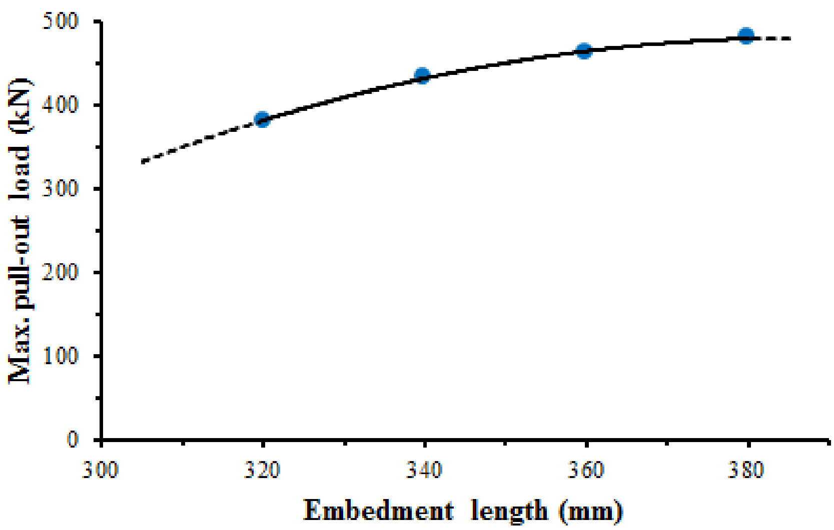

Figure 6 - 26 Effect of embedment length on peak capacity of MW9 cable bolts

6.3 Load transfer of plain cable bolts

6.3.1 Dimensions of Superstrand cable bolts

The full length of the Superstrand used in this study was 1180 mm, of which 320 mm was embedded in the confining medium. To ensure that the bond strength in the anchor section was higher than the embedment section, a special bulb geometry was placed in the anchor section, as shown in Figure 6 - 27. The dimension of the Superstrand is tabulated in Table 6 - 8.

Figure 6 - 27 Superstrand cable bolt geometry

Table 6 - 8 Superstrand cable bolt dimensions

Cable name	Type	Wires	Length (mm)	Diameter (mm)	Perimeter (mm)
Superstrand	Plain	9	1180	21.8	96

6.3.2 Bearing plate effect

The first series of pull-out tests was conducted on Superstrand cable bolts installed in the weak confining medium. YN1.5MPA grout was used to cast the confining medium and a borehole diameter of 27 mm used. Two different bearing plates, namely a standard bearing plate with an internal hole of 70.4 mm and a second bearing plate with an internal hole of 140 mm, were tested. The load transfer performance of Superstrand cable bolts tested with these two bearing plates is shown in Figure 6 - 28. The size of the bearing plate in this instance had almost no significant influence on performance of the plain cable bolts, which is largely different from the influence of bearing plate size on behaviour of modified cable bolts in the weak confining medium.

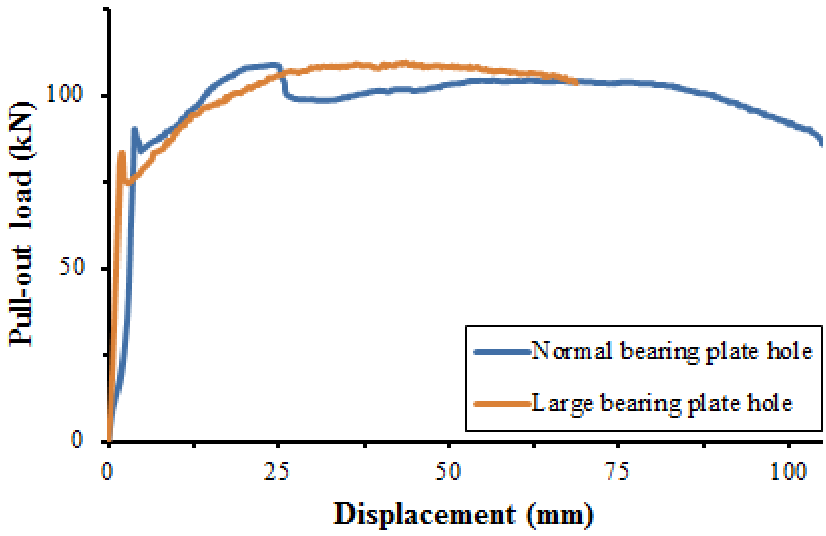

Figure 6 - 28 Performance of Superstrand cable bolts pulled from the weak confining medium

Further checking the failure mode displays that the crater outline was more discernible when the larger bearing plate was used, as shown in Figure 6 - 29. Nevertheless, the crater depth in both cases was quite small (less than 2 mm). Failure of the Superstrand was dominated by shear slippage along the cable/grout interface within the entire encapsulation length, as shown in Figure 6 - 30 a). Also, Figure 6 - 30 b) indicates that the entire length of the Superstrand cable in the embedment section was extruded from the grout column. To better study the bond failure of cable bolting systems, the standard bearing plate was used in all subsequent tests with the Superstrand cable bolts.

The load transfer behaviour of Superstrand cable bolts installed in the weak confining medium is provided in Figure 6 - 31 and Table 6 - 9. The results show that the Superstrand cable bolts behaved in an elastic, perfectly-plastic behaviour. Specifically, there was a linear relationship between the pull-out load and displacement when the displacement was less than 3 mm. Then, the bearing capacity of Superstrand cable bolts decreased a little. This is probably due to the bond failure between the cable bolt and the grout column near the borehole collar. With the pull-out displacement increasing, the bearing capacity rose again. The peak load was achieved at a large pull-out displacement around 30 mm. In the residual period, the bearing capacity of Superstrand cable bolts remained largely unchanged at a high level around 100 kN.

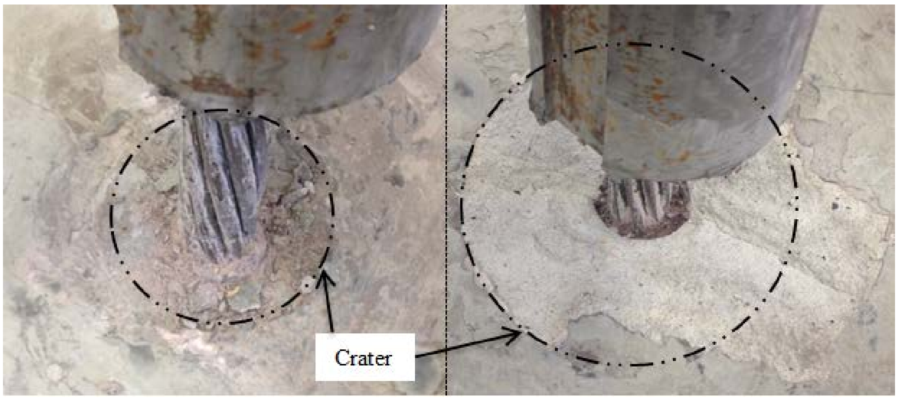

Figure 6 - 29 Confining medium status. a) standard bearing plate with an internal hole diameter of 70.4 mm (left), and b) a second bearing plate with an internal hole diameter of 140 mm (right)

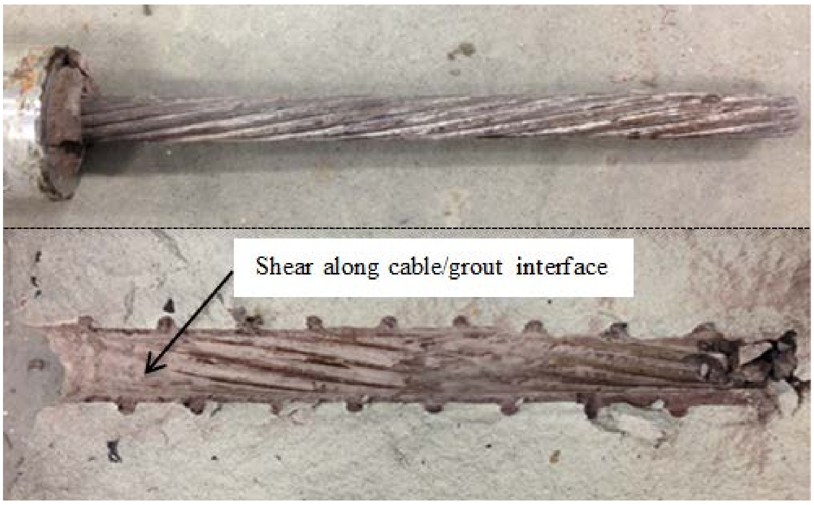

Figure 6 - 30 Shear slippage along the cable/grout interface for Superstrand cable bolts showing a) view of cable bolt (top), and b) borehole surface condition (bottom)

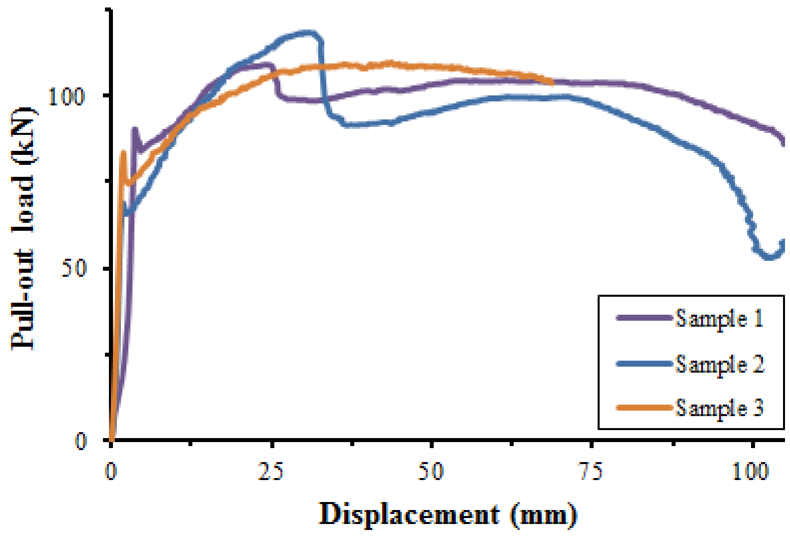

Figure 6 - 31 Performance of Superstrand cable bolts pulled from the weak confining medium

Table 6 - 9 Results of Superstrand cable bolts pulled from the weak confining medium

No.	Borehole size (mm)	Peak load (kN)	Residual load (kN)
1	27	109	103
2	27	118	96
3	27	110	108
	Mean	112	102

6.3.3 Borehole size effect

To study the influence of borehole size on load transfer performance of plain cables in the weak confining medium, pull-out tests were conducted on Superstrand cable bolts installed in larger boreholes with a diameter of 37 mm. The confining medium was cast using the weak YN1.5MPA grout.

The axial performance of Superstrand cable bolts installed in larger boreholes in the weak confining medium is shown in Figure 6 - 32. The average peak and residual loads are tabulated in Table 6 - 10. In the test, the Superstrand was directly pulled from the confining medium, as shown in Figure 6 - 33. Apparently, shear failure occurred along the cable/grout interface, as shown in Figure 6 - 34.

The borehole size had almost no effect on the load versus displacement trend of Superstrand cable bolts and the failure mode. However, it did make a difference in the bearing capacity of Superstrand cable bolts in the weak confining medium. A comparison between the load transfer performance of Superstrand cable bolts installed in different boreholes is shown in Figure 6 - 35 and Table 6 - 11. These indicate that increasing the borehole diameter was beneficial to improving both the peak and residual bearing capacities of Superstrand cable bolts with the weak confining medium.

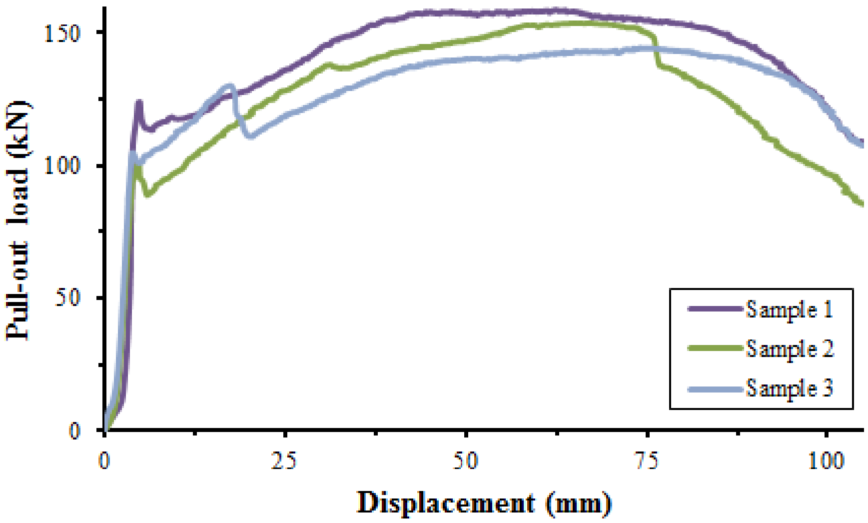

Figure 6 - 32 Performance of Superstrand cable bolts pulled from larger boreholes

Table 6 - 10 Results of Superstrand cable bolts pulled from larger boreholes

No.	Borehole size (mm)	Peak load (kN)	Residual load (kN)
1	37	159	157
2	37	154	148
3	37	144	140
	Mean	152	148

Figure 6 - 33 The cable was pulled from the confining medium.

Figure 6 - 34 Shear failure along the cable/grout interface in a larger borehole

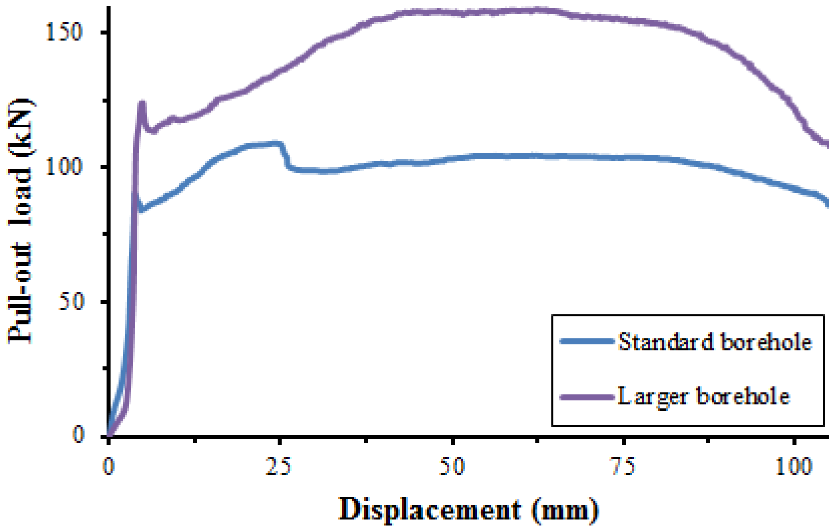

Figure 6 - 35 The effect of increasing borehole size on the performance of Superstrand cable bolts

It should be mentioned that the borehole size effect on the performance of cable bolts installed in the strong confining medium has been previously studied. For example, Rajaie (1990) conducted pull-out tests on plain cable bolts installed in concrete blocks with higher strength than 30 MPa, finding that the borehole size had almost no influence on load transfer performance of cable bolts. This was later confirmed by Martin *et al.* (1996), Chen and Mitri (2005) and Mosse-Robinson and Sharrock (2010). As for the cause of this different performance, it is likely that in the weak confining medium, the confinement provided by the surrounding medium including both the grout annulus and confining medium material was limited. When the borehole size was increased, the larger diameter for the same size cable bolt meant that the annulus of the high strength grout was larger, effectively increasing its stiffness. This provided more confinement on the cable bolt. Hence when mining activities encounter the weak confining medium, it is recommended to use relatively larger boreholes to improve the performance of fully grouted cable bolts.

Table 6 - 11 Bearing capacities of Superstrand cable bolts in different boreholes

Borehole size \ Load	Peak load (kN)	Residual load (kN)
Standard borehole	112	102
Larger borehole	152	148
Percentage change	+35.7%	+45.1%

6.3.4 Confining medium strength effect

To study the influence of confining medium strength on the performance of plain cable bolts, GS32250 grout was used to cast the confining medium. A standard borehole diameter of 27 mm was used. The performance of Superstrand cable bolts installed in the strong confining medium is shown in Figure 6 - 36 and Table 6 - 12. These show that the pull-out load increased linearly with the displacement when the displacement was less than 3 mm. Then, the pull-out load still increased but with a decreasing slope. When the pull-out displacement increased to 35 mm, the bearing capacity arrived at the peak value of 265 kN. Failure of the Superstrand cable bolting system occurred along the cable/grout interface, as shown in Figure 6 - 37 and Figure 6 - 38.

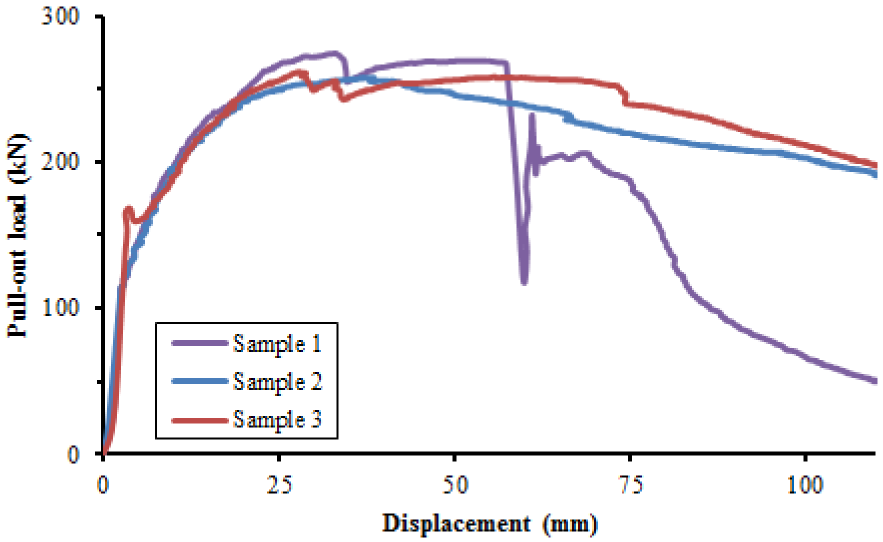

Figure 6 - 36 Performance of Superstrand cable bolts pulled from the strong confining medium

Table 6 - 12 Results of Superstrand cable bolts pulled from the strong confining medium

No.	Borehole size (mm)	Peak load (kN)	Residual load (kN)
1	27	275	269
2	27	258	245
3	27	262	257
	Mean	265	257

The influence of confining medium strength on the load transfer performance of Superstrand cable bolts was evaluated, as shown in Figure 6 - 39 and Table 6 - 13. The results show that the confining medium strength had a significant effect on deciding the load bearing capacity of Superstrand cable bolts. With the confining medium strength increasing from 8.8 MPa to 62.7 MPa, the peak capacity of Superstrand cable bolts rose from 112 kN to 265 kN. As for the residual behaviour, Superstrand cable bolts installed in the weak confining medium maintained a pull-out load of 102 kN within a large pull-out displacement of 100 mm. However, when the strong confining medium were used, after the peak capacity, the bearing capacity of Superstrand cable bolts decreased gradually.

Figure 6 - 37 The Superstrand cable bolt was pulled from the grout column.

Figure 6 - 38 Shear failure along the cable/grout interface

Table 6 - 13 Bearing capacities of Superstrand cable bolts with different confining medium strength

Load / Confining medium strength	Peak load (kN)	Residual load (kN)
Weak	112	102
Strong	265	257

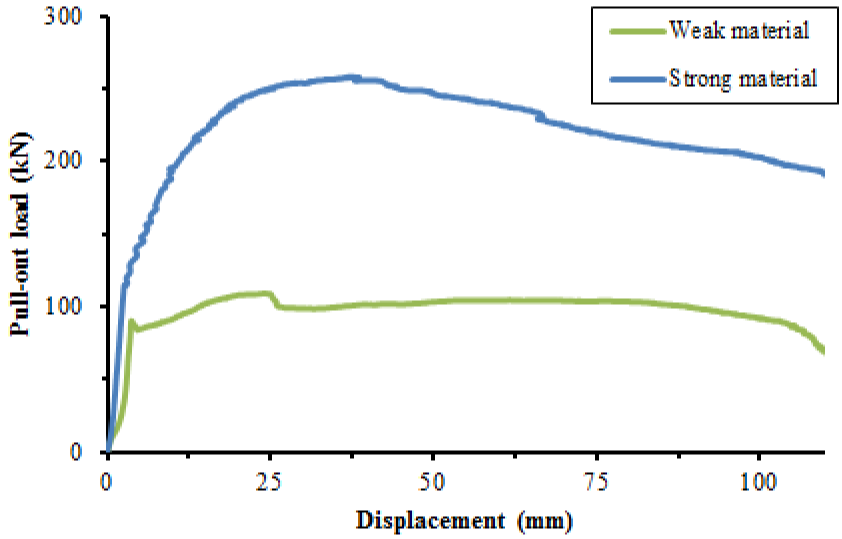

Figure 6 - 39 The effect of confining medium strength on performance of Superstrand cable bolts

6.4 Comparison between two types of cable bolts

6.4.1 Cable surface geometry effect in the weak confining medium

To evaluate the impact of cable surface geometry on the load transfer performance of cable bolts in the weak confining medium, the load versus displacement curves of the Superstrand and MW9 cable bolt were compared, as presented in Figure 6 - 40. The results show that in the weak confining medium, the MW9 cable bolt had much higher peak capacity than the Superstrand cable bolt, as depicted in Table 6 - 14, indicating that the nutcage geometry was quite effective in improving the maximum load bearing capacity of cable bolts.

However, after the peak load, there was a sudden drop of the load bearing capacity of the MW9 cable bolt. As for the Superstrand cable bolt, the bearing capacity almost levelled off within a large pull-out displacement of 100 mm. It is apparent that the residual load of the Superstrand cable bolt was higher than the MW9 cable bolt, indicating that the Superstrand is more appropriate for the situation where large displacement of rock mass can occur.

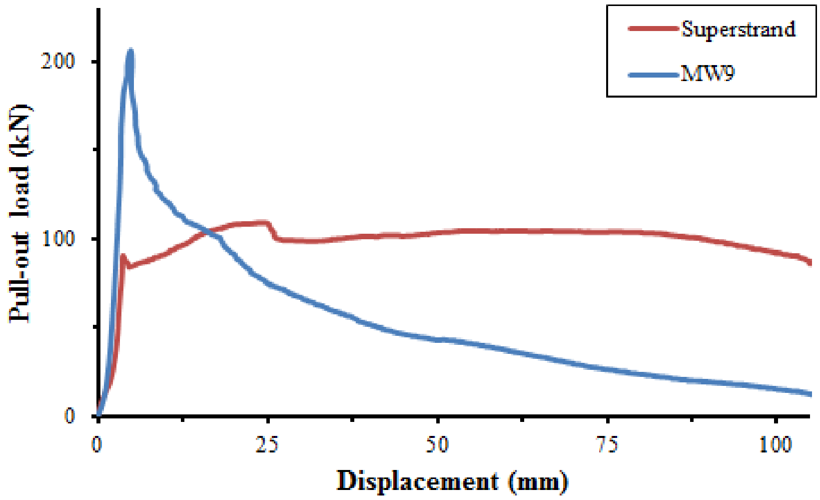

Figure 6 - 40 Comparison of Superstrand and MW9 cable bolts pulled from the weak confining medium

Table 6 - 14 Bearing capacities of Superstrand and MW9 cable bolts pulled from the weak confining medium

Load / Confining medium strength	Peak load (kN)	Residual load (kN)
Superstrand	112	102
MW9	208	108

The cable surface geometry also had an impact on the failure mode of the cable bolting systems in the weak confining medium. As shown in Figure 6 - 41 a), when the MW9 cable bolt was tested, apparent shear failure occurred along the grout/rock interface. However, when the Superstrand cable bolt was tested, bond failure occurred along the cable/grout interface, as shown in Figure 6 - 41 b). This difference was mainly a result of the modified or nutcage geometry. Specifically, when the MW9 cable bolt was pulled from the weak confining medium, the mechanical interlock and friction between the cable bolt and grout column was enhanced. Since the confining medium had a low strength, the shear strength of the grout/rock interface was lower than the cable/grout interface. Consequently, bond failure occurred along the grout/rock interface.

Figure 6 - 41 A comparison between cable bolting failure modes in the weak confining medium. a) MW9 cable (left), and b) Superstrand cable (right)

6.4.2 Cable surface geometry effect in the strong confining medium

The influence of cable surface geometry on axial performance of cable bolts in the strong confining medium is shown in Figure 6 - 42. The figure demonstrates that the peak capacity of the MW9 cable bolt was still much higher than the Superstrand cable bolt, as depicted in Table 6 - 15. However, the displacement where peak load occurred was much different. For the MW9 cable bolt, after a short pull-out displacement of 8 mm, the bearing capacity reached the peak value of 380 kN while for the Superstrand cable bolt, the peak capacity of 257 kN occurred when the pull-out displacement arrived at 38 mm.

After the peak load, there was a sudden drop of the bearing capacity of the MW9 cable bolt. Furthermore, an oscillation of the pull-out load occurred within a pull-out displacement range from 13 mm to 60 mm. As for the Superstrand, the bearing capacity maintained within a large pull-out displacement up to 100 mm.

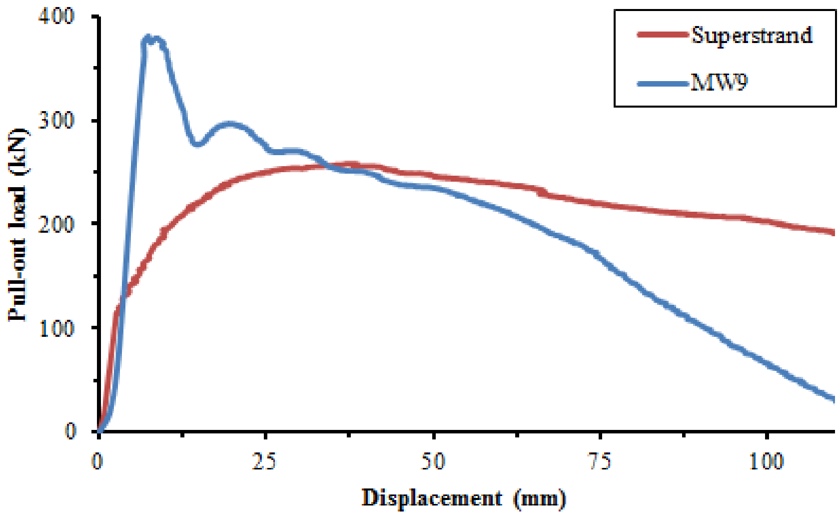

Figure 6 - 42 A Comparison of Superstrand and MW9 cable bolts pulled from the strong confining medium

Table 6 - 15 Bearing capacities of Superstrand and MW9 cable bolts pulled from the strong confining medium

Load / Confining medium strength	Peak load (kN)	Residual load (kN)
Superstrand	265	257
MW9	380	264

It was also found that the cable surface geometry had no influence on deciding the failure mode of cable bolting systems in the strong confining medium. As shown in Figure 6 - 43, shear failure always occurred along the cable/grout interface, independent of the cable type.

Figure 6 - 43 A comparison between failure modes of cable bolting systems pulled from the strong confining medium. a) MW9 cable bolt (left), and b) Superstrand cable bolt (right)

6.5 Post-failure behaviour

6.5.1 MW9 cable bolt

In earlier test work reported by Thomas (2012), measurements were truncated soon after the peak load was reached. This was typically within a total displacement of 15 mm. Little post-failure behaviour of the cable bolts was measured in each case.

Significantly, with this new test facility, the post-failure behaviour of the MW9 cable bolt could be determined well beyond the peak load. As shown in Figure 6 - 44, the post-failure behaviour over a displacement range of 100 mm was consistently achieved.

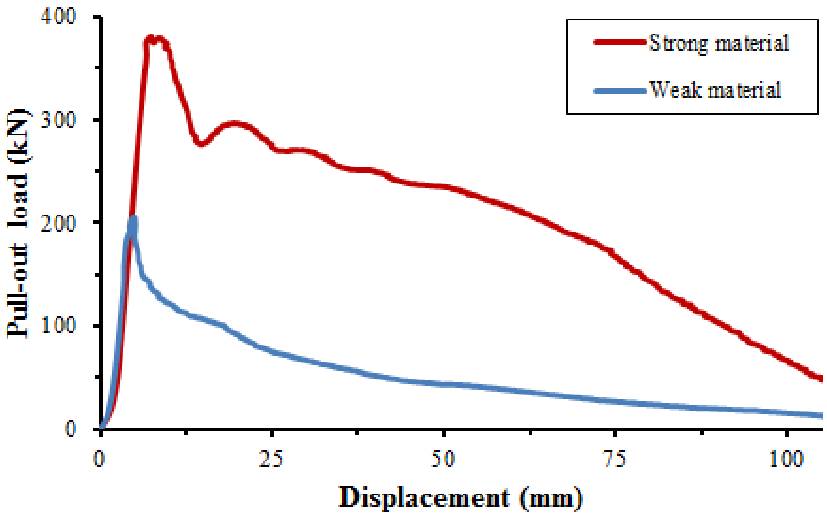

Figure 6 - 44 Performance of MW9 cable bolts pulled from strong and weak confining media

There was evidence of slip-lock mechanism with the MW9 cable bolt. This was observed when the strong confining medium was used. Furthermore, beyond a displacement of about 30 mm to 40 mm, there was a near-uniform reduction in load with displacement signifying little effective bond strength or resistance between the cable and grout. When the weak confining medium was used, the slip-lock phenomenon was only observed when MW9 cable bolts were pulled from large boreholes.

6.5.2 Superstrand cable bolt

For the Superstrand cable bolt, there was some appreciable and sustained level of load bearing capacity after the maximum load was achieved as shown in Figure 6 - 45. After 100 mm displacement, the cable bolt could still maintain a load bearing capacity of nearly 80 kN in the weak confining medium. Interestingly, the post-failure load was consistently maintained over the full range of controlled displacement in the weak confining medium. However, in the strong confining medium, there was a near 25% reduction in load bearing capacity over the final 60 mm displacement to 100 mm. Even so, the load bearing capacity after 100 mm displacement in the strong confining medium was nearly 200 kN.

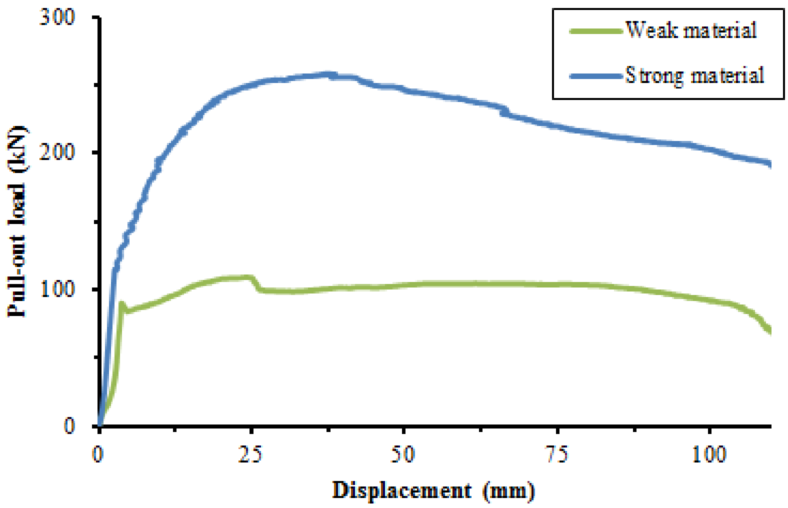

Figure 6 - 45 Performance of Superstrand cable bolts pulled from strong and weak confining media

6.6 Summary

Pull-out tests were conducted on two types of cable bolts, namely the MW9 cable bolt which is a modified cable bolt and the Superstrand cable bolt that is a plain cable.

For the MW9 modified cable bolt, it was found that:

- When the cable bolt was pulled from the weak confining medium, bond failure occurred along the grout/rock interface. Furthermore, the dimension of the bearing plate had a significant effect on deciding the performance of cable bolts. When the bearing plate with a larger hole was used, the surrounding confining medium material was also pulled out and a combination of bond failure with crater failure occurred. In contrast, when the bearing plate with a hole size comparable to the borehole diameter was used, failure only occurred along the grout/rock interface. The effect of the bearing plate with the smaller hole was to constrain the material surrounding the cable bolt and grout, increasing its strength and resistance to failure. The peak capacity of the cable bolt pulled from the bearing plate with a larger hole was smaller than the plate with a standard hole.
- Increasing the borehole size had a significant effect on improving the performance of cable bolts in the weak confining medium. Both the peak load and residual load were higher when a larger borehole was used. This is assumed to be due to the fact that the grout column in the borehole had a much higher strength than the confining medium and when larger boreholes were used, more confinement could be provided by the confining medium, resulting in larger pulling load. Furthermore, when the cable bolt was pulled from larger boreholes, bond failure occurred along the cable/grout interface.
- The strength of the confining medium had a significant effect on the load transfer performance of the cable bolting system. In the strong confining

medium, bond failure only occurred at the cable/grout interface whereas in the weaker confining medium, failure was more likely to occur at the grout/rock interface. Furthermore, the peak and residual load of cable bolts installed in the strong confining medium were much higher than those installed in the weak confining medium.

- Several pull-out tests were conducted on cable bolts installed in the strong confining medium. Within an embedment length of less than 360 mm, there was a linear relationship between the embedment length and peak capacity. Beyond this value, the bearing capacity increased but with a much lower slope. This was assumed to be the non-uniform shear stress distribution along the cable/grout interface, especially when long embedment length was used.

For the Superstrand or plain cable bolt, it was found that:

- Failure of the cable bolting system always occurred along the cable/grout interface independent of the confining medium strength.
- The dimension of the bearing plate had little effect on deciding the performance of the cable bolts. There was no crater failure of the cable bolting system when the bearing plate with the larger hole was used.
- Increasing the borehole size was beneficial to improving the peak and residual capacity of cable bolts installed in the weak confining medium.
- Strength of the confining medium had an influence on cable bolt performance. When the cable was pulled from the strong confining medium, there was

apparent reduction in the bearing capacity in the residual stage. However, when the weak confining medium was tested, the bearing capacity of the cable bolt maintained throughout a large pull-out displacement of 100 mm.

The influence of cable surface geometry on load transfer performance of cable bolts was analysed. The cable surface geometry influenced the failure modes of cable bolts when installed in the weak confining medium. Specifically, the modified surface geometry resulted in bond failure occurring along the grout/rock interface when the weak confining medium was used. For cable bolts installed in the strong confining medium, bond failure always occurred along the cable/grout interface, independent on the cable surface geometry. Nevertheless, the cable surface geometry had a significant effect on deciding the peak capacity. With the modified geometry, the peak capacity of cable bolts more than doubled. As for the residual load, the modified cable bolts decreased quickly with displacement. However, for plain cable bolts, the residual load could be maintained over a large displacement.

The post-failure behaviour of modified cable bolts was largely different from plain cable bolts. When the modified cable bolts were pulled from the confining medium and failure occurred along the cable/grout interface, oscillation of the pull-out load occurred, which was a result of the re-engagement of the modified cable surface geometry and the grout column. However, for plain cable bolts, after the peak load, there was a steady reduction of the bearing capacity of cable bolts with the pull-out displacement.

CHAPTER SEVEN

AN ANALYTICAL MODEL TO STUDY LOAD TRANSFER BEHAVIOUR OF FULLY GROUTED CABLE BOLTS

7.1 Introduction

An analytical model was proposed to study the load transfer mechanism of fully grouted cable bolts with particular focus on maximum load bearing capacity. This model assumed that the cable bolting system was composed of three parts, namely the cable bolt, the grout column and the cylindrical confining medium. Considering that the shear slip along the cable/grout interface is the major failure mode in cable bolting applications, this model focused on the bond failure at the cable/grout interface. The mechanical equilibrium equation was established to determine the relationship between the axial stress in the cable bolt and shear stress along the cable/grout interface. The shear slip of the cable/grout interface was expressed in terms of the axial movement of the cable bolt and the confining medium. A tri-linear relationship was adopted to model the behaviour between the shear stress and shear slip of the cable/grout interface. The shear stress propagation was analysed in different pull-out stages including: the elastic, elastic-softening, elastic-softening-debonding, softening-debonding, pure softening and debonding. This analytical model was used to predict the maximum load bearing capacity of cable bolting systems with different embedment length. Specifically, the peak capacity of standard cable bolts with the embedment length ranging between 150 mm and 700 mm was analysed. For the modified cable bolts, the embedment length ranged from 320 mm to 380 mm. Laboratory pull-out tests using these two types of cable bolts were used to validate this analytical model, which resulted in a good correlation between analytical modelling and laboratory test results. The shear stress distribution state of cable bolts when peak capacity reached was also analysed. Finally, the analytical model was used to evaluate the shear stress propagation process in the full pull-out process of cable bolts.

7.2 Analytical modelling of the fully grouted cable bolts

7.2.1 Governing equation

The fully grouted cable bolting system in the embedment section is mainly composed of three parts, namely the cable bolt with a diameter of *D*, the grout column having an annulus thickness of *t* and the confining medium with a thickness of *b*. This creates two interfaces, namely the cable/grout interface and the grout/confining medium interface, as shown in Figure 7 - 1. In this study, the shear failure along the cable/grout interface was studied as this is the most commonly encountered failure mode in both laboratory and field tests (Cao *et al.*, 2013b; Ma *et al.*, 2013; Wang *et al.*, 2015). Therefore, when the cable bolt is subjected to axial load, shear stress along the cable/grout interface is induced as a result of the differential axial stress.

During the pull-out process, the resultant force on the bolt should equal the shear resistance induced along the bolt/grout interface (Blanco Martín *et al.*, 2011; Ma *et al.*, 2014b):

$$\tau(x)\pi D dx = \left(\sigma_b(x) + d\sigma_b(x) - \sigma_b(x)\right)\frac{\pi D^2}{4} \qquad (7 - 1)$$

Therefore, the relationship between the axial stress and shear stress can be expressed as:

$$\tau(x) = \frac{D}{4}\frac{d\sigma_b(x)}{dx} \qquad (7 - 2)$$

Where, τ (x) = the shear stress along the cable/grout interface at a longitudinal position x, Pa; and σ_b (x) = the axial stress of the cable bolt, Pa.

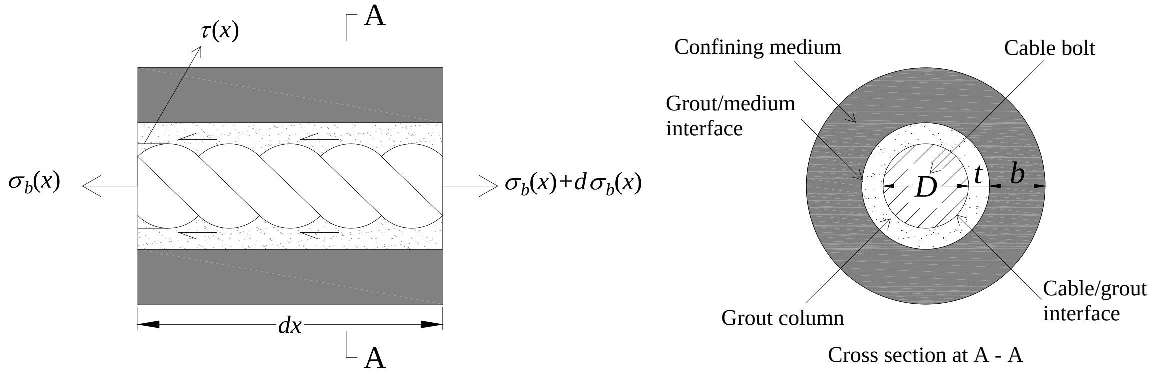

Figure 7 - 1 a) Stress state within an elementary length dx, and b) geometry of a cable bolting system

As shown in Figure 7 - 2, the shear stress along the diametrical direction in the grout column at a radius of r can be calculated (Cai *et al.*, 2004a):

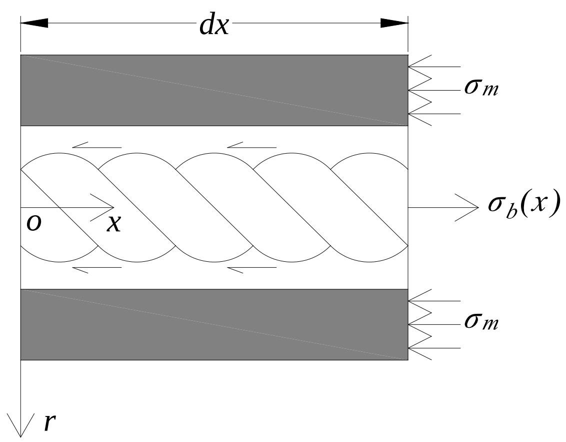

Figure 7 - 2 Shear stress distribution within the cable bolting system

$$\tau_r = \frac{D}{2r}\tau(x) \tag{7 - 3}$$

In most instances, performance of the cable bolting system is primarily dependent on the properties of the cable/grout interface whereas the grout and confining medium are essential in providing confinement. Hence the grout and confining medium are treated as elastic materials. If the thickness of the grout column t is thin, the shear stress in the grout can be calculated with the material shear modulus G (Farmer, 1975; Dunham, 1976):

$$\tau_r = -G\frac{du}{dr} \tag{7 - 4}$$

Where, u = the longitudinal displacement of the grout, m. Since G can be calculated via the grout Young's Modulus E_g and Poisson's Ratio v_g, τ_r can be further expressed as:

$$\tau_r = -\frac{E_g}{2(1+v_g)}\frac{du}{dr} \tag{7 - 5}$$

Then the displacement of grout at the radius of r can be acquired by substituting Equation (7 - 3) into Equation (7 - 5) and integrating it from the cable/grout interface to the grout/medium interface:

$$u_r = u_0 + \frac{D\tau(1+v_g)}{E_g}\ln\frac{D}{2r} \tag{7 - 6}$$

Where, u_0 = axial displacement of the cable/grout interface, m. Then, the displacement of the grout/medium interface u_m can be obtained by substituting $r = t + D/2$ into Equation (7 - 6):

$$u_m = u_0 + \frac{D\tau\left(1+v_g\right)}{E_g}\ln\frac{D}{D+2t} \tag{7 - 7}$$

On the condition that u_b represents axial displacement of the cable, the shear slip of the cable/grout interface δ can be calculated from the equation of $\delta = u_b - u_0$. Through substituting δ into Equation (7 - 7), the interface slip is:

$$\delta = u_b - u_m + \frac{D\tau\left(1+v_g\right)}{E_g}\ln\frac{D}{D+2t} \tag{7 - 8}$$

Equations (7 - 2) and (7 - 8) can be solved once the relationship between τ and δ is determined. In the following context, the method of using a tri-linear model to evaluate mechanical properties of fiber-reinforced plastic (FRP) proposed by Wu *et al.* (2010) was adopted as appropriate to describe the axial loading behaviour of fully grouted cable bolts. However, they only considered three stages. In this study, the tri-linear model is extended to analyse the load transfer behaviour of cable bolts within the full pull-out stages.

7.2.2 The tri-linear model of the cable/grout interface

A tri-linear model is basically composed of three segments as shown in Figure 7 - 3: (I) a linear elastic section from the origin to peak load, Point (δ_1, τ_p); (II) a stress softening section until the Point (δ_2, τ_f); and, (III) a residual load section. It should be mentioned that Wu *et al.* (2010) assumed a perfect bonding between the confining medium (in their case a steel tube) and the grout. This assumption is also applicable to cable bolts, because the medium/grout interface usually remains intact during the pull-out process.

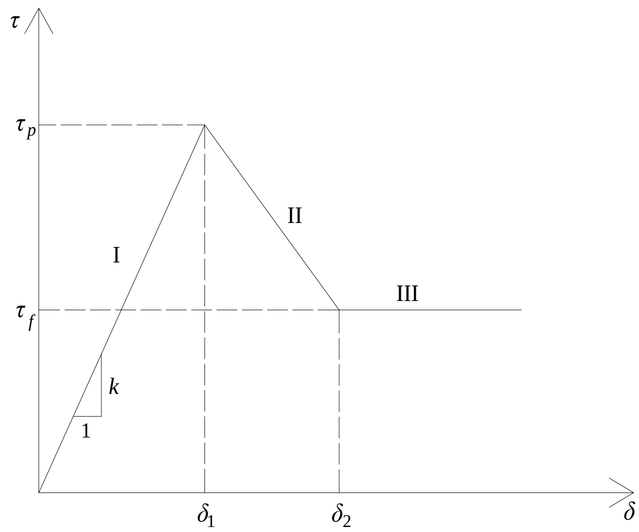

Figure 7 - 3 A tri-linear law with characteristic parameters, after Wu *et al.* (2010)

The shear stress along the cable/grout interface can be calculated based on the following equations:

$$\tau = k\delta \quad \left(0 \le \delta \le \delta_1\right) \tag{7 - 9a}$$

$$\tau = \frac{\tau_p \delta_2 - \tau_f \delta_1}{\delta_2 - \delta_1} - \frac{\tau_p - \tau_f}{\delta_2 - \delta_1}\delta \quad \left(\delta_1 < \delta \le \delta_2\right) \tag{7 - 9b}$$

$$\tau = \tau_f \quad \left(\delta > \delta_2\right) \tag{7 - 9c}$$

Where, δ = the interface shear slip, m; k = the stiffness in elastic stage, Pa/m; τ_p = the interfacial shear strength, Pa, and τ_f = the interfacial frictional or residual strength, Pa.

7.2.3 Pull-out stages of cable bolts

Under an axial loading condition, the fully grouted rock tendon may undergo different stages including elastic, elastic-softening, elastic-softening-debonding, softening-debonding and debonding (Ballivy and Martin, 1983; Nemcik *et al.*, 2014). Blanco Martín *et al.* (2013) indicated that pure softening rather than elastic-softening-debonding may occur, if the embedment length is not long enough. This study analyses the load transfer performance of cable bolts under the two scenarios.

To validate this analytical model, the modelling peak load was compared with laboratory test results. Considering peak load can only occur in either the elastic-softening or elastic-softening-debonding stages, the maximum pull-out load is derived from those two stages (Ren *et al.*, 2010).

7.2.3.1 Elastic stage

When an axial load is applied at one end of a fully grouted cable bolt, the cable/grout interface first deforms elastically, and the shear stress along the interface can be calculated by combining Equation (7 - 9a) with (7 - 8):

$$\tau = \frac{kE_g}{E_g + Dk\left(1+v_g\right)\ln\frac{D+2t}{D}}\left(u_b - u_m\right) \tag{7 - 10}$$

Through differentiating Equation (7 - 10) with regard to x, the following equation can be obtained:

$$\frac{d\tau}{dx} = \frac{kE_g}{E_g + Dk\left(1+v_g\right)\ln\frac{D+2t}{D}}\left(\frac{\sigma_b}{E_b} - \frac{\sigma_m}{E_m}\right) \tag{7 - 11}$$

Where, E_b = the Young's Modulus of cable bolts, Pa, and E_m = the Young's Modulus of the confining medium, Pa. Based on the mechanical equilibrium in the longitudinal direction, the axial stress on the confining medium σ_m can be expressed as:

$$\sigma_m = -\frac{D^2}{4\mathrm{b}\left(D+b+2t\right)}\sigma_b \tag{7 - 12}$$

Substituting Equations (7 - 2) and (7 - 12) into Equation (7 - 11) results in:

$$\frac{D}{4}\frac{d^2\sigma_b}{dx^2} = \frac{kE_g}{E_g + Dk\left(1+v_g\right)\ln\frac{D+2t}{D}}\left[\frac{\sigma_b}{E_b} + \frac{D^2}{4b\left(D+b+2t\right)}\frac{\sigma_b}{E_m}\right] \tag{7 - 13}$$

Since only σ_b is unknown, Equation (7 - 13) can be further expressed as:

$$\frac{d^2\sigma_b}{dx^2} - \frac{4kE_g}{D\left(E_g + Dk\left(1+v_g\right)\ln\frac{D+2t}{D}\right)}\left[\frac{1}{E_b} + \frac{D^2}{4b\left(D+b+2t\right)E_m}\right]\sigma_b = 0 \tag{7 - 14}$$

Therefore, the following equation can be obtained:

$$\frac{d^2\sigma_b}{dx^2} - \alpha^2\sigma_b = 0 \tag{7 - 15}$$

Where,

$$\alpha^2 = \frac{4kE_g}{D\left(E_g + Dk\left(1+v_g\right)\ln\frac{D+2t}{D}\right)}\left[\frac{1}{E_b} + \frac{D^2}{4E_m b\left(D+b+2t\right)}\right] \tag{7 - 16}$$

In this state, for a fully grouted cable bolt with an embedment length of L, assuming the axial load at the loaded end is F, the boundary conditions are:

$$\sigma_b\left(x=0\right) = 0 \tag{7 - 17}$$

$$\sigma_b\left(x=L\right) = \frac{4F}{\pi D^2} \tag{7 - 18}$$

Through substituting Equations (7 - 17) and (7 - 18) into Equation (7 - 15), $\sigma_b\,(x)$ and $\tau\,(x)$ can be acquired:

$$\sigma_b\left(x\right) = \frac{4F}{\pi D^2}\frac{e^{\alpha x} - e^{-\alpha x}}{e^{\alpha L} - e^{-\alpha L}} \tag{7 - 19}$$

$$\tau\left(x\right) = \frac{F\alpha}{\pi D}\frac{e^{\alpha x} + e^{-\alpha x}}{e^{\alpha L} - e^{-\alpha L}} \tag{7 - 20}$$

With the pull-out load increasing, the shear stress at the loaded end, or τ_l, gradually reaches the interfacial shear strength. In this state, the pulling force is defined as the initial cracking load and can be calculated as:

$$F_{ini} = \frac{\tau_p \pi D}{\alpha} \frac{e^{\alpha L} - e^{-\alpha L}}{e^{\alpha L} + e^{-\alpha L}} \tag{7 - 21}$$

In the elastic stage, F is always less than or equal to F_{ini}. Therefore, the domain for F is $\left[0, \frac{\tau_p \pi D}{\alpha} \frac{e^{\alpha L} - e^{-\alpha L}}{e^{\alpha L} + e^{-\alpha L}}\right]$.

7.2.3.2 Elastic-softening stage

Once the pull-out load is larger than F_{ini}, the cable/grout interface at the loaded end (right side in Figure 7 - 4) starts softening and a softening length, a_s, occurs from the loaded end.

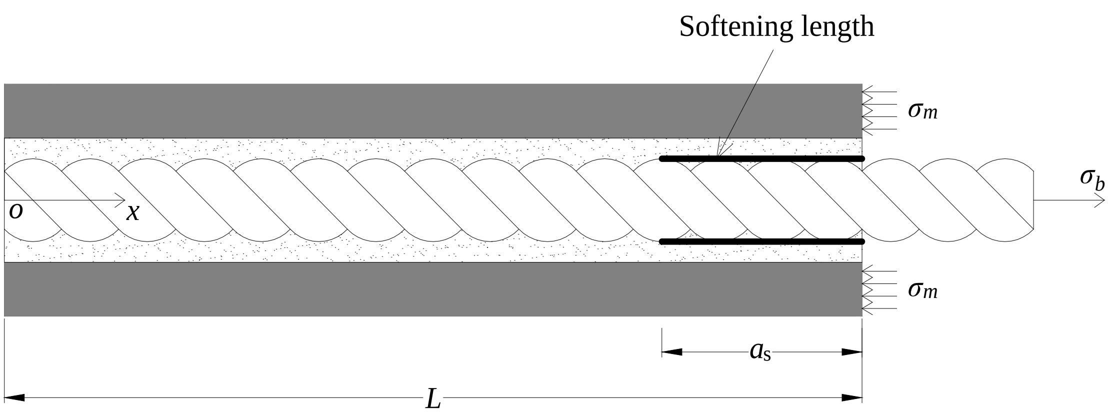

Figure 7 - 4 Softening length propagation along the cable/grout interface

Within the range $0 \leq x \leq L - a_s$, the interface still remains elastic. And the shear stress at the position $x = L - a_s$ equals the interfacial shear strength, i. e.,

$$\tau\left(x = L - a_s\right) = \tau_p \tag{7 - 22}$$

The σ_b and τ can be acquired by solving Equation (7 - 15) with conditions of Equations (7 - 17) and (7 - 22).

$$\sigma_b(x) = \frac{4\tau_p}{D\alpha} \frac{e^{\alpha x} - e^{-\alpha x}}{e^{\alpha(L-a_s)} + e^{-\alpha(L-a_s)}} \tag{7 - 23}$$

$$\tau(x) = \tau_p \frac{e^{\alpha x} + e^{-\alpha x}}{e^{\alpha(L-a_s)} + e^{-\alpha(L-a_s)}} \tag{7 - 24}$$

In this stage, a_s is always smaller than L. Thus, the domain for a_s is (0, L). As for the range $L - a_s < x \leq L$, the interface softens. Through combining Equations (7 - 9b) and (7 - 8) together, τ can be obtained as:

$$\begin{aligned} \tau = &-\frac{E_g(\tau_p - \tau_f)}{E_g(\delta_2 - \delta_1) + D(\tau_p - \tau_f)(1+v_g)\ln\frac{D}{D+2t}}(u_b - u_m) + \\ &\frac{E_g(\tau_p\delta_2 - \tau_f\delta_1)}{E_g(\delta_2 - \delta_1) + D(\tau_p - \tau_f)(1+v_g)\ln\frac{D}{D+2t}} \end{aligned} \tag{7 - 25}$$

Differentiating τ with regard to x can get:

$$\frac{d\tau}{dx} = -\frac{E_g(\tau_p - \tau_f)}{E_g(\delta_2 - \delta_1) + D(\tau_p - \tau_f)(1+v_g)\ln\frac{D}{D+2t}}\left(\frac{\sigma_b}{E_b} - \frac{\sigma_m}{E_m}\right) \tag{7 - 26}$$

Substituting Equations (7 - 2), (7 - 12) into (7 - 26) yields:

$$\frac{d^2\sigma_b}{dx^2} + \omega^2\sigma_b = 0 \tag{7 - 27}$$

Where,

$$\omega^2 = \frac{4E_g\left(\tau_p-\tau_f\right)}{DE_g\left(\delta_2-\delta_1\right)+D^2\left(\tau_p-\tau_f\right)\left(1+v_g\right)\ln\frac{D}{D+2t}} \left[\frac{1}{E_b}+\frac{D^2}{4E_m b\left(D+\mathrm{b}+2t\right)}\right] \tag{7 - 28}$$

Considering σ_b and τ should be continuous at the position $x = L - a_s$, σ_b and τ can be expressed as:

$$\sigma_b\left(x\right)=\left[\begin{array}{l}\frac{4\tau_p}{D\alpha}\tanh\left(\alpha\left(L-a_s\right)\right)\cos\left(\omega\left(L-a_s\right)\right)-\\ \frac{4\tau_p}{D\omega}\sin\left(\omega\left(L-a_s\right)\right)\end{array}\right]\cos\left(\omega x\right)+ \left[\begin{array}{l}\frac{4\tau_p}{D\alpha}\tanh\left(\alpha\left(L-a_s\right)\right)\sin\left(\omega\left(L-a_s\right)\right)+\\ \frac{4\tau_p}{D\omega}\cos\left(\omega\left(L-a_s\right)\right)\end{array}\right]\sin\left(\omega x\right) \tag{7 - 29}$$

$$\tau\left(x\right)=-\tau_p\left[\begin{array}{l}\frac{\omega}{\alpha}\tanh\left(\alpha\left(L-a_s\right)\right)\cos\left(\omega\left(L-a_s\right)\right)-\\ \sin\left(\omega\left(L-a_s\right)\right)\end{array}\right]\sin\left(\omega x\right)+ \tau_p\left[\begin{array}{l}\frac{\omega}{\alpha}\tanh\left(\alpha\left(L-a_s\right)\right)\sin\left(\omega\left(L-a_s\right)\right)+\\ \cos\left(\omega\left(L-a_s\right)\right)\end{array}\right]\cos\left(\omega x\right) \tag{7 - 30}$$

Substituting the boundary condition of Equation (7 - 18) into Equation (7 - 29), the pull-out load F can be expressed as:

$$F=\frac{\tau_p\pi D}{\alpha}\tanh\left(\alpha\left(L-a_s\right)\right)\cos\left(\omega a_s\right)+\frac{\tau_p\pi D}{\omega}\sin\left(\omega a_s\right) \tag{7 - 31}$$

Through solving $\mathrm{d}F/\mathrm{d}a_s = 0$, the critical softening length a_{sc} can be acquired. Then, the maximum load transfer capacity can be calculated by substituting a_{sc} into Equation (7 - 31). In this state, τ_l can be acquired by substituting $a_s = a_{sc}$ and $x = L$ into Equation (7 - 30):

$$\tau_l = \tau_p \cos\left(\omega a_{sc}\right) - \frac{\tau_p \omega}{\alpha} \tanh\left(\alpha\left(L - a_{sc}\right)\right) \sin\left(\omega a_{sc}\right) \quad (7 - 32)$$

In Equation (7 - 32), τ_l should always be larger than or equal to τ_f. However, if the calculated τ_l is smaller than τ_f, debonding occurs and the interface proceeds into elastic-softening-debonding stage.

7.2.3.3 Elastic-softening-debonding stage

It should be mentioned that after the elastic-softening stage, pure softening can also occur. Nevertheless, the elastic-softening-debonding stage is analysed ahead, because the maximum pull-out load, which is calculated and compared with physical test results, occurs in this period. In this stage, a frictional length a_f develops from the loaded end, as depicted in Figure 7 - 5.

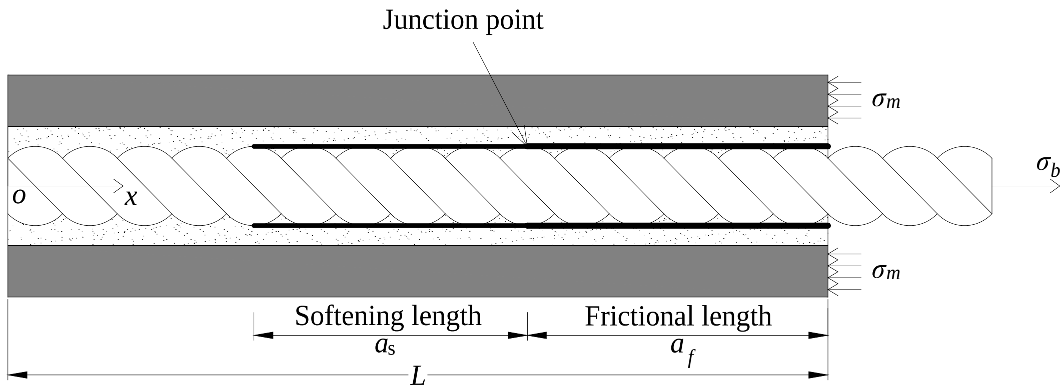

Figure 7 - 5 Softening length and frictional length propagation along the cable/grout interface

For the range $0 \leq x \leq L - a_s - a_f$, the cable/grout interface remains elastic. At the position $x = L - a_s - a_f$, the shear stress equals the interfacial shear strength:

$$\tau\left(x = L - a_s - a_f\right) = \tau_p \quad (7 - 33)$$

The σ_b and τ can be acquired by calculating Equations (7 - 15) , (7 - 17) and (7 - 33):

$$\sigma_b\left(x\right)=\frac{4\tau_p}{D\alpha}\frac{e^{\alpha x}-e^{-\alpha x}}{e^{\alpha(L-a_s-a_f)}+e^{-\alpha(L-a_s-a_f)}} \tag{7 - 34}$$

$$\tau\left(x\right)=\tau_p\frac{e^{\alpha x}+e^{-\alpha x}}{e^{\alpha(L-a_s-a_f)}+e^{-\alpha(L-a_s-a_f)}} \tag{7 - 35}$$

When it comes to the range L - a_s - $a_f < x \leq L$ - a_f, σ_b and τ can be solved by calculating Equation (7 - 27) with the continuity conditions of σ_b and τ at the position $x = L$ - a_s - a_f.

$$\begin{aligned}\sigma_b\left(x\right)=&\begin{bmatrix}\frac{4\tau_p}{D\alpha}\tanh(\alpha(L-a_s-a_f))\cos(\omega(L-a_s-a_f))-\\ \frac{4\tau_p}{D\omega}\sin(\omega(L-a_s-a_f))\end{bmatrix}\cos\left(\omega x\right)+\\ &\begin{bmatrix}\frac{4\tau_p}{D\alpha}\tanh(\alpha(L-a_s-a_f))\sin(\omega(L-a_s-a_f))+\\ \frac{4\tau_p}{D\omega}\cos(\omega(L-a_s-a_f))\end{bmatrix}\sin\left(\omega x\right)\end{aligned} \tag{7 - 36}$$

$$\begin{aligned}\tau\left(x\right)=&-\tau_p\begin{bmatrix}\frac{\omega}{\alpha}\tanh(\alpha(L-a_s-a_f))\cos(\omega(L-a_s-a_f))-\\ \sin(\omega(L-a_s-a_f))\end{bmatrix}\sin\left(\omega x\right)+\\ &\tau_p\begin{bmatrix}\frac{\omega}{\alpha}\tanh(\alpha(L-a_s-a_f))\sin(\omega(L-a_s-a_f))+\\ \cos(\omega(L-a_s-a_f))\end{bmatrix}\cos\left(\omega x\right)\end{aligned} \tag{7 - 37}$$

Then, for the frictional range L - $a_f < x \leq L$, τ keeps a constant value of τ_f, i. e.,

$$\tau\left(x\right)=\tau_f \tag{7 - 38}$$

As for σ_b, it can be acquired by solving Equation (7 - 2) with the continuity condition of σ_b at $x = L$ - a_f.

$$\begin{aligned}\sigma_b\left(x\right)=&\frac{4\tau_f}{D}x+\frac{4\tau_p}{D\alpha}\tanh\left(\alpha\left(L-a_s-a_f\right)\right)\cos\left(\omega a_s\right)+\\ &\frac{4\tau_p}{D\omega}\sin\left(\omega a_s\right)-\frac{4\tau_f}{D}\left(L-a_f\right)\end{aligned} \tag{7 - 39}$$

Through substituting Equation (7 - 18) into (7 - 39), F is derived in terms of a_s and a_f:

$$F=\tau_f \pi D a_f+\frac{\tau_p \pi D}{\alpha}\tanh\left(\alpha\left(L-a_s-a_f\right)\right)\cos\left(\omega a_s\right)+\frac{\tau_p \pi D}{\omega}\sin\left(\omega a_s\right) \tag{7 - 40}$$

The maximum load transfer capacity can be calculated once the relationship between a_s and a_f is determined. By substituting the condition $\tau\,(x = L - a_f) = \tau_f$ into Equation (7 - 37), the subsequent equation can be derived:

$$\cos\left(\omega a_s\right)-\frac{\omega}{\alpha}\tanh\left(\alpha\left(L-a_s-a_f\right)\right)\sin\left(\omega a_s\right)-\frac{\tau_f}{\tau_p}=0 \tag{7 - 41}$$

Combining Equations (7 - 40) and (7 - 41) together, and solving for dF / da_s = 0, a_{sc} can be obtained. According to Equation (7 - 41), the critical debonding length a_{fc} can also be acquired. Substituting a_{sc} and a_{fc} into Equation (7 - 40), the maximum load transfer capacity can be obtained.

7.2.3.4 Pure softening stage

The pure softening behaviour occurs when the a_s in the elastic-softening stage increases up to the full embedment length, i. e., $a_s = L$ and τ_l is still larger than τ_f. In this case, the full cable/grout interface experiences softening behaviour, as shown in Figure 7 - 6.

For the range $0 \leq x \leq L$, assuming that the shear stress at the unloaded end is τ_u, τ can be solved by calculating Equation (7 - 27) with the boundary conditions of (7 - 17) and $\tau\,(x = 0) = \tau_u$.

$$\tau\left(x\right)=\tau_u\cos\left(\omega x\right) \tag{7 - 42}$$

In Equation (7 - 42), τ_u mobilises in the pull-out process. However, it is possible to determine the proper range in which τ_u is involved. When the pure softening stage starts,

τ_u reaches the maximum value, equalling τ_p. Then τ_u decreases gradually until the τ_l drops to τ_f. Meanwhile, τ_u reaches the minimum value in this stage, which can be solved by substituting τ ($x = L$) = τ_f into Equation (7 - 42):

$$\tau_{u\min} = \frac{\tau_f}{\cos(\omega L)} \tag{7 - 43}$$

Therefore, the domain for τ_u is [$\frac{\tau_f}{\cos(\omega L)}$,τ_p].

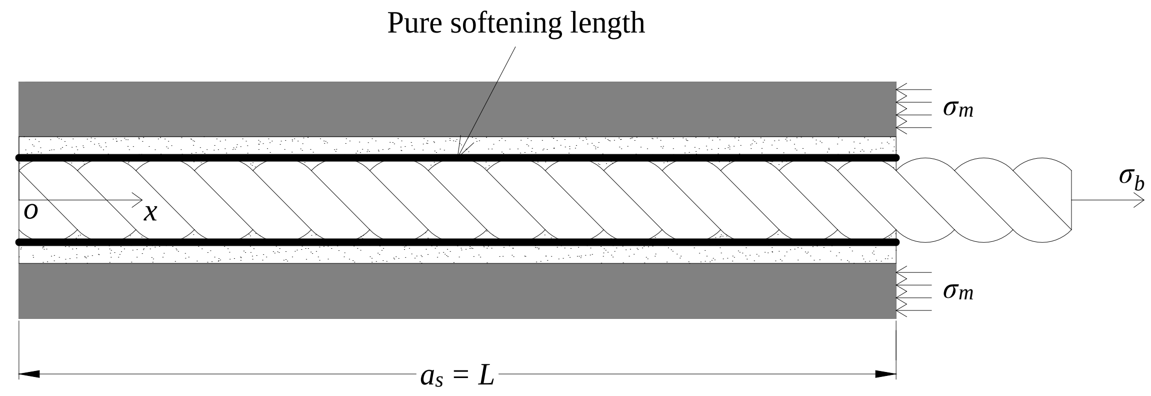

Figure 7 - 6 Softening along the full length of the cable/grout interface

7.2.3.5 Softening-debonding stage

As the pull-out process continues, both the elastic-softening-debonding and pure softening stages will proceed into the softening-debonding period. In this phase, the full embedment length is divided into two parts, namely a softening length a_s and a debonding length a_f, as shown in Figure 7 - 7.

The shear stress at the junction point equals τ_f:

$$\tau(x = a_s) = \tau_f \tag{7 - 44}$$

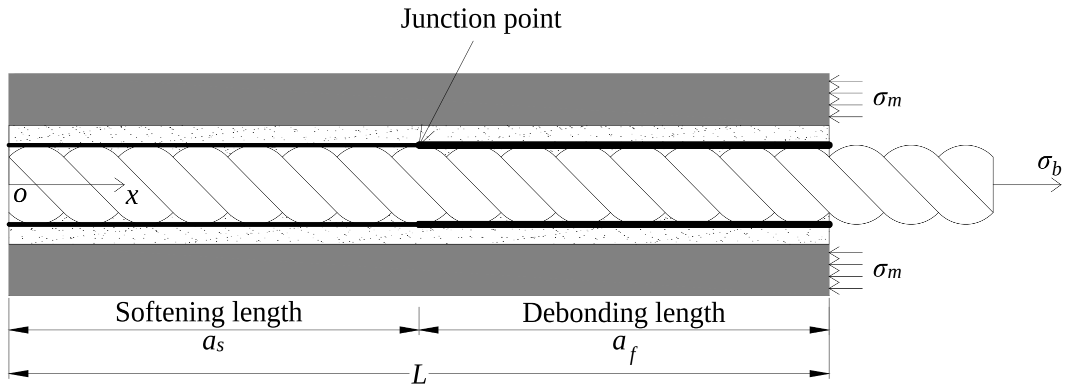

Figure 7 - 7 Softening-debonding stage

Within the range $0 \le x \le a_s$, τ can be solved by calculating Equation (7 - 27) with boundary conditions (7 - 17) and (7 - 44):

$$\tau(x) = \tau_f \frac{\cos(\omega x)}{\cos(\omega a_s)} \tag{7 - 45}$$

In the above equation, a_s is flexible but can be determined within a proper range. Since the softening-debonding stage following the elastic-softening-debonding stage (Type Ⅰ) and the softening-debonding stage following pure softening stage (Type Ⅱ) have different boundary conditions, these two cases were analysed separately.

For Type Ⅰ, when a_s equals the maximum softening length a_{smax}, τ_u equals τ_p. Substituting $\tau_u = \tau_p$ into Equation (7 - 45), a_{smax} can be derived:

$$a_{s\max} = \frac{\arccos\left(\frac{\tau_f}{\tau_p}\right)}{\omega} \tag{7 - 46}$$

Therefore, the domain for a_s is (0, $\frac{\arccos\left(\frac{\tau_f}{\tau_p}\right)}{\omega}$].

While for Type Ⅱ, a_{smax} equals the full length L and the domain for a_s is (0, L).

As for the τ in the debonding range $a_s \le x \le L$, it always equals τ_f, i. e.,

$$\tau(x) = \tau_f \tag{7 - 47}$$

7.2.3.6 Debonding stage

Finally, the debonding stage occurs when τ_u decreases to τ_f. And the full interface length experiences debonding, which is shown in Figure 7 - 8.

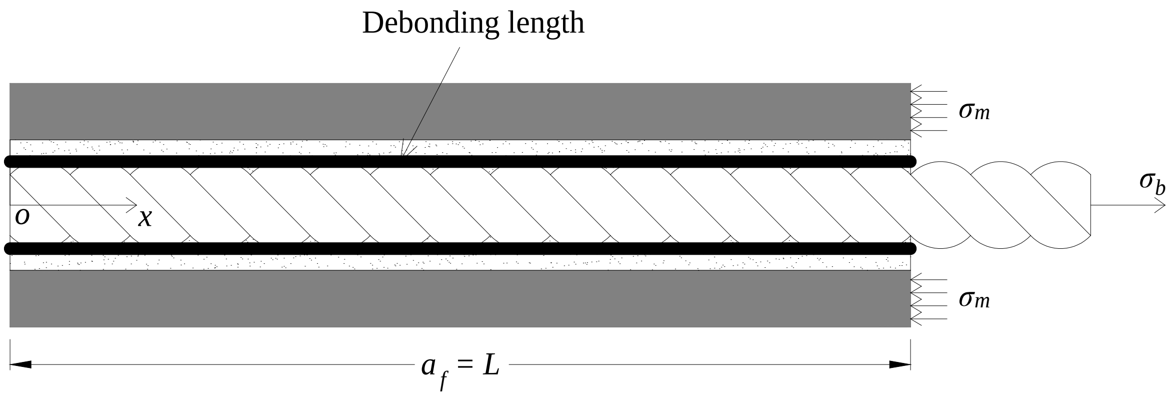

Figure 7 - 8 Debonding propagates along the full cable/grout interface

Within this period, the shear stress along the full embedment length equals τ_f, namely:

$$\tau(x) = \tau_f \tag{7 - 48}$$

7.3 Validation of the analytical model

A number of pull-out test results were undertaken to validate this analytical model. Both plain cables and modified cable bolts were tested. The maximum pull-out load in axial tests of the cable bolts was calculated using this model and compared with laboratory test results. Specifically, Equations (7 - 16) and (7 - 28) were used to calculate the parameters including α and ω. Then Equation (7 - 32) was used to calculate τ_l. If τ_l was larger than τ_f, the peak load occurred in the elastic-softening stage and it could be calculated with Equation (7 - 31). Otherwise, the maximum load transfer capacity occurred in the elastic-softening-debonding stage and it could be computed with Equation (7 - 40).

7.3.1 Pull-out tests on plain cable bolts

Rajaie (1990) performed a vast array of SEPT using conventional plain cable bolts with a diameter of 15.2 mm. Concrete cylinders with a UCS of 35 MPa were used as the confining medium. A plain cementitious grout with a w/c ratio of 0.3 was selected when installing the cable bolts. The embedment length was varied from 150 mm to 700 mm. Detailed information regarding relevant parameters are listed in Table 7 - 1.

Table 7 - 1 Technical data of relevant parameters (Rajaie, 1990)

No.	D (mm)	t (mm)	b (mm)	L (mm)	E_g (GPa)	v_g	E_b (GPa)	E_m (GPa)
1	15.2	17.9	99.5	150	21.2	0.19	194	19
2	15.2	17.9	99.5	200	21.2	0.19	194	19
3	15.2	17.9	99.5	300	21.2	0.19	194	19
4	15.2	17.9	99.5	400	21.2	0.19	194	19
5	15.2	17.9	99.5	500	21.2	0.19	194	19
6	15.2	17.9	99.5	600	21.2	0.19	194	19
7	15.2	17.9	99.5	700	21.2	0.19	194	19

Pull tests using cable bolts with a short embedment length of 200 mm were used to determine the interfacial shear properties. Corresponding values of the tri-linear model are shown in Table 7 - 2.

Table 7 - 2 Shear properties of the cable/grout interface

δ_1 (mm)	i_p (MPa)	k (MPa/mm)	δ_2 (mm)	i_f (MPa)
9.9	5.84	0.6	19.9	2.81

Substituting these parameters into the analytical model, the maximum load transfer capacity of cable bolts with different embedment length can be determined. The analytical modelling results for F_{amax} were compared with the test results F_{tmax}, as shown in Table 7 - 3. The relationship between the peak capacity and embedment length in physical tests and analytical modelling is shown in Figure 7 - 9. It can be seen that there is little significant difference between the modelling results and the test results, indicating that the analytical solution is able to reasonably predict the maximum load transfer capacity of plain cable bolts.

Table 7 - 3 Comparison between laboratory test results and modelling results

No.	1	2	3	4	5	6	7
F_{tmax} (kN)	43.4	55.8	85.2	115.6	145.6	168.6	187.2
F_{amax} (kN)	41.8	55.7	83.2	110.4	137.3	163.6	189.3
$(F_{amax} - F_{tmax})/ F_{tmax}$	-3.8%	-0.3%	-2.4%	-4.5%	-5.7%	-3.0%	1.1%

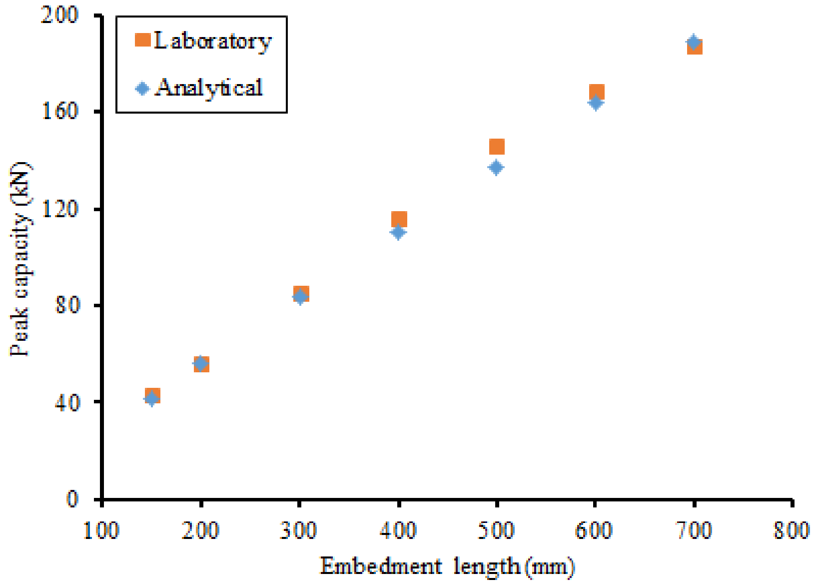

Figure 7 - 9 Comparison between analytical and physical results

Reichert (1991) conducted split-pipe pull tests on plain cable bolts. A PVC pipe with a Young’s Modulus of 3 GPa was used to simulate weak rock. A plain cable bolt with a short embedment length of 250 mm was tested. Detailed information regarding parameters is tabulated in Table 7 - 4.

Table 7 - 4 Technical data of relevant parameters (Reichert, 1991)

No.	D (mm)	t (mm)	b (mm)	L (mm)	E_g (MPa)	v_g	E_b (MPa)	E_m (MPa)
1	15.9	20.55	6.6	250	9600	0.18	196000	3000

A tri-linear model was used to represent the interfacial shear behaviour and the corresponding parameters are listed in Table 7 - 5.

Table 7 - 5 Shear properties of the cable/grout interface (after Reichert, 1991)

δ_1 (mm)	i_p (MPa)	k (MPa/mm)	δ_2 (mm)	i_f (MPa)
2.6	2.82	1.1	3.4	2.11

With parameters listed in Table 7 - 4 and Table 7 - 5, a modelling peak load of 31.5 kN was obtained. Compared with the test result of 35.2 kN, there was only an error of -10.5% between analytical results and laboratory results, further confirming the usefulness of this analytical solution.

7.3.2 Pull-out tests on modified cable bolts

Modified cable bolts were also tested to verify this analytical model. A number of pull-out tests were conducted on MW9 cable bolts. During these tests, cable bolts were installed in boreholes with a diameter of 42 mm. Stratabinder grout with a UCS of 54 MPa was used as the bonding agent. More information about relevant parameters is given in Table 7 - 6.

Pull-out tests on cable bolts with a short length of 320 mm were used to measure the shear performance of the cable/grout interface, and a tri-linear model was used to describe the bond-slip performance of the cable/grout interface. Corresponding values such as peak shear strength and residual shear strength are given in Table 7 - 7.

Using the analytical model, the maximum load bearing capacity of cable bolts with embedment lengths varying from 320 mm to 380 mm were acquired. These bearing capacities were compared with laboratory test results, depicted in Table 7 - 8 and Figure 7 - 10. The results show that the modelling results were consistent with the test results. Thus, this analytical solution appears to also be applicable to modified cable bolts.

Table 7 - 6 Parameter data of the LSEPTs

No.	D (mm)	t (mm)	b (mm)	L (mm)	E_g (GPa)	v_g	E_b (GPa)	E_m (GPa)
1	28.5	6.75	154	320	9.94	0.21	201	11.82
2	28.5	6.75	154	340	9.94	0.21	201	11.82
3	28.5	6.75	154	360	9.94	0.21	201	11.82
4	28.5	6.75	154	380	9.94	0.21	201	11.82

Table 7 - 7 Shear properties of the cable/grout interface

δ_1 (mm)	i_p (MPa)	k (MPa/mm)	δ_2 (mm)	i_f (MPa)
5.0	13.50	2.7	12.0	11.00

Table 7 - 8 Comparison between laboratory test results and modelling results

No.	1	2	3	4
F_{tmax} (kN)	381.3	432.9	462.6	479.1
F_{amax} (kN)	385.0	408.8	432.6	456.3
$(F_{amax} - F_{tmax})/ F_{tmax}$	1.0%	-5.6%	-6.5%	-4.8%

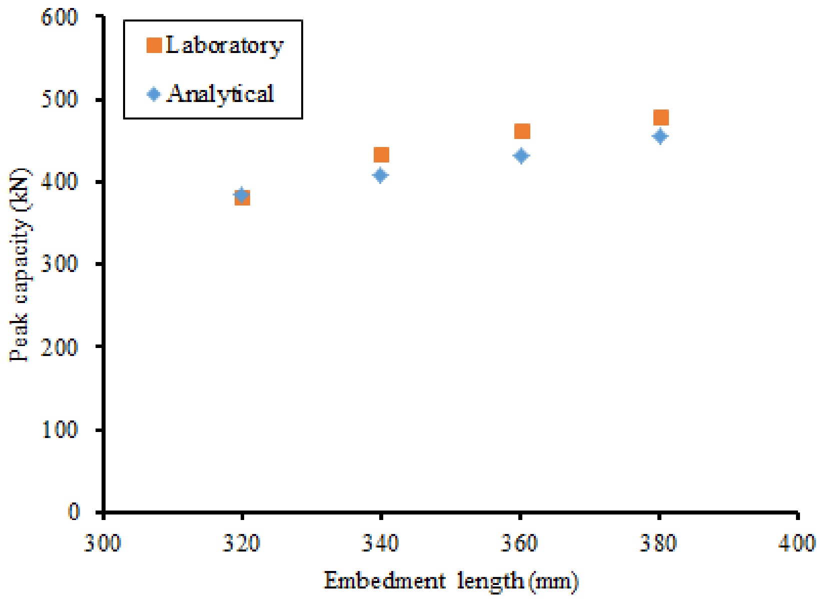

Figure 7 - 10 Peak load of MW9 cable bolts with varying embedment length

7.4 Shear stress distribution of the cable/grout interface in the peak load state

This analytical model is able to analyse the shear stress distribution along the full length when peak load occurs. For plain cable bolts, as the results are summarised in Figure 7 - 11, peak load occurred in the elastic-softening stage. Equations (7 - 24) and (7 - 30) were used to calculate the shear stress distribution shown in Figure 7 - 11. It can be seen that when the embedment length was short enough (less than 200 mm); there was no obvious shear stress variation along the full length. In this case, the interfacial shear stress could be assumed uniform. However, as the embedment length increased, the non-uniform shear stress distribution became more apparent.

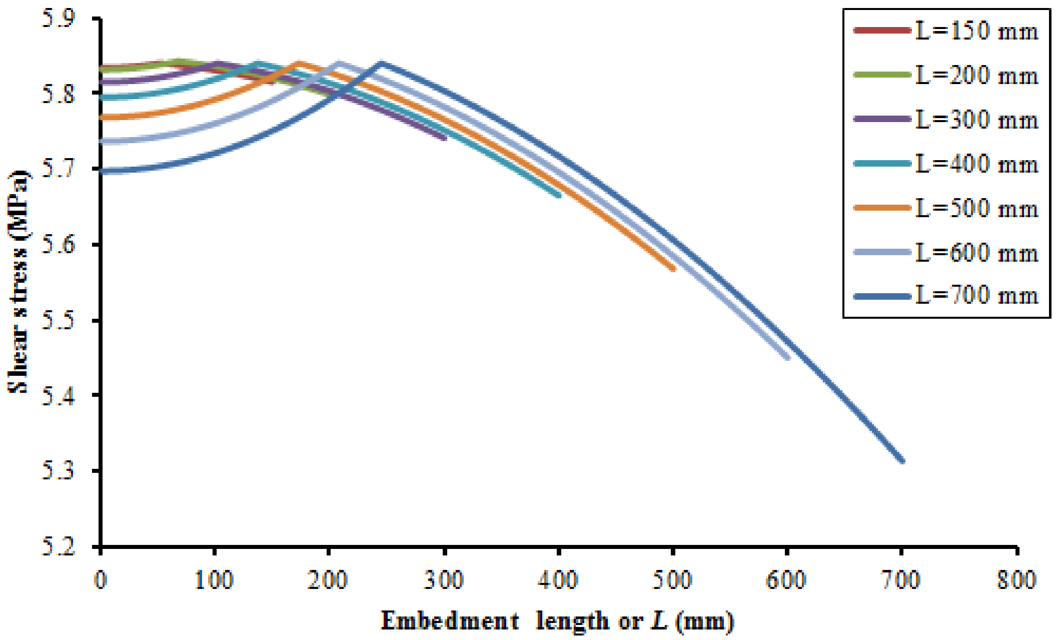

Figure 7 - 11 Shear stress distribution along cable bolts

In cable bolts confined with a PVC pipe, peak load occurred in the elastic-softening-debonding stage, as shown in Figure 7 - 12. Thus, Equations (7 - 35), (7 - 37) and (7 - 38) were used to evaluate the shear stress distribution. The results show that when peak load occurred, debonding started to propagate from the loaded end.

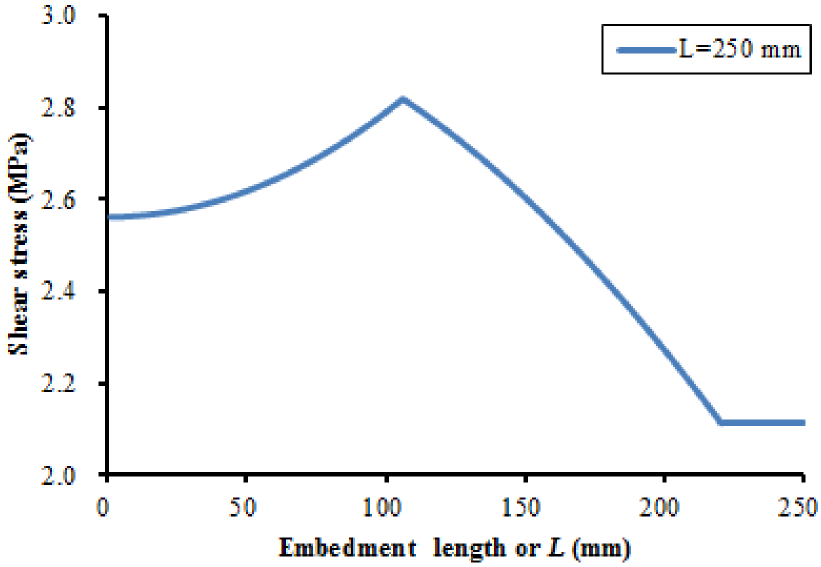

Figure 7 - 12 Shear stress distribution along a plain cable

7.5 Interfacial shear stress propagation with pull-out stages

This analytical model can also be adopted to evaluate the shear stress propagation in the pull-out process. For the plain cables listed in Table 7 - 1, the interface shear stress successively experienced five different stages. Specifically, Equation (7 - 20) was used to illustrate the shear stress distribution in the elastic stage and Equations (7 - 24) and (7 - 30) were adopted to evaluate the shear stress state in elastic-softening stage. As for pure softening, Equation (7 - 42) was used. Then in the softening-debonding stage, Equations (7 - 45) and (7 - 47) were selected. Lastly, in the debonding stage, Equation (7 - 48) was used. The shear stress distribution for a plain cable bolt with an embedment length of 700 mm is shown in Figure 7 - 13.

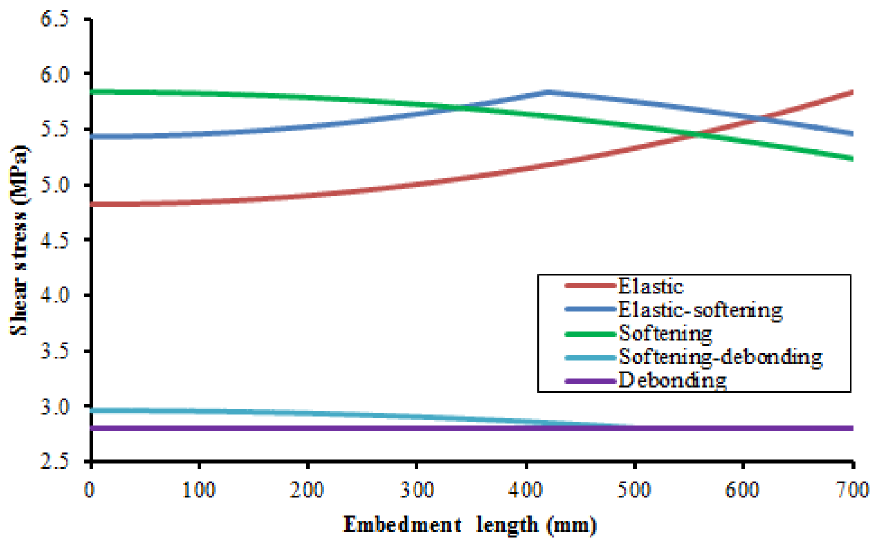

Figure 7 - 13 Shear stress propagation of the 700 mm cable bolt in the pull-out test

In the elastic stage, the shear stress decreased exponentially from the loaded end along the full embedment length. Then, the peak shear stress propagated towards the direction of the unloaded end until the shear stress at the unloaded end reached interfacial shear strength. In the pure softening stage, the shear stress decreased gradually from the unloaded end to the loaded end. When the shear stress at the loaded end decreased to the interfacial residual strength, a debonding length started to propagate. As the debonding length occupied the full embedment length, the debonding stage started.

As for the cable bolt shown in Table 7 - 4, there are also five stages within the whole pull-out process. The difference is that the elastic-softening-debonding rather than the pure softening occurred. And Equations (7 - 35), (7 - 37) and (7 - 38) were used to analyse the shear stress distribution in the elastic-softening-debonding period. The shear stress propagation process of a cable bolt with an embedment length of 250 mm is shown in Figure 7 - 14. After the elastic stage, the elastic-softening stage occurred. Then, the elastic-softening-debonding stage started to work, followed by the softening-debonding stage. Lastly, debonding occurred along the whole cable/grout interface.

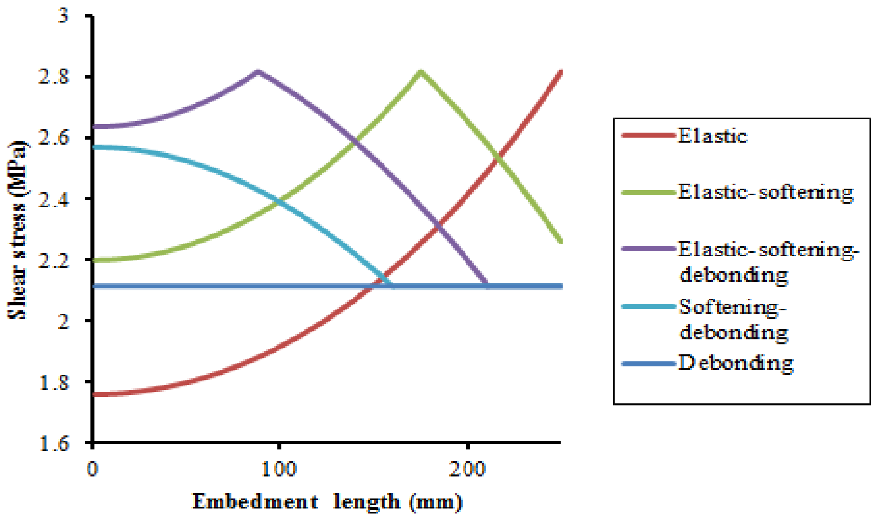

Figure 7 - 14 Shear stress propagation in a full pull-out process

7.6 Summary

To better understand the behaviour of the load transfer mechanism of fully grouted cable bolts in axial loading condition, an analytical model was developed. A tri-linear model that best models the shear behaviour of the cable/grout interface was selected. Mechanical properties of various cable bolts, grout and confining medium were employed in the model. Laboratory test results for both plain cable bolts and modified cable bolts were used to verify this analytical model. There was a consistent correlation between laboratory test values and modelling results.

With this analytical model, the shear stress distribution at peak load state was studied on plain cable bolts. The results show that when the embedment length was short, the variation of the shear stress along the embedment length was small. However, as embedment length increased, the non-uniform shear stress distribution became more apparent. Furthermore, the maximum load transfer capacity could occur in the elastic-softening or elastic-softening-debonding stage, dependent on the mechanical properties of the confining medium.

The shear stress propagation process was also analysed. In a pull-out process, there were five different stages in a pull-out process: elastic, elastic-softening, elastic-softening-debonding, softening-debonding and debonding. In some cases, a pure softening stage may occur after the elastic-softening stage.

However, in both of these situations, the interfacial shear stress from the loaded to the unloaded end gradually reached the interfacial shear strength. The benefit of this analytical model is its capability to predict the maximum load transfer capacity of cable bolts of differing embedment lengths.

CHAPTER EIGHT

NUMERICAL SIMULATION OF THE PULL-OUT BEHAVIOUR OF FULLY GROUTED CABLE BOLTS

8.1 Introduction

The pull-out behaviour of fully grouted cable bolts was simulated with the numerical code FLAC2D. The FLAC2D software package was used because it is an effective modelling technique for geotechnical problems (Gale *et al.*, 2004; Mark *et al.*, 2007; Liu *et al.*, 2008; Carranza-Torres, 2009; Hsiao *et al.*, 2009; Ma, 2014; Nemcik *et al.*, 2014; Ma *et al.*, 2015). Furthermore, the structural elements embedded in FLAC2D are commonly used in modelling ground support tools, such as rockbolts, cable bolts and tiebacks. First, the performance of cable bolt and rockbolt elements was compared.

Then the LSEPT was simulated using FLAC2D. A strain-softening model was used to simulate the cement-based confining medium. Specifically, the UCS, Young's Modulus and Poisson's Ratio were compared and validated with the experimental test results. The pull-out behaviour of MW9 cable bolts illustrated in Chapter Six was simulated in different conditions confined by weak and strong confining media. The cohesive strength between the cable bolt and the grout, the cohesive strength between the grout and the confining medium, and the strain-softening behaviour were analysed. The confining pressure when the maximum pull-out load occurred was determined. Furthermore, the pull-out performance of the Superstrand cable bolts was simulated. All numerical pull-out results were compared and validated with experimental results.

8.2 Structural element selection

There are different structural elements in FLAC2D to be used in modelling of different support elements. The cable bolt and rockbolt elements are always used to simulate the reinforcement such as rockbolts, cable bolts and tiebacks (Itasca, 2000).

The cable bolt element is divided into a number of segments, and nodal points are located at each segment end (Li *et al.*, 2012). The axial behaviour of the rock tendon (either a bar or a cable) is simulated by a one-dimensional constitutive law, as displayed in Equation (8 - 1). Specifically, the axial stiffness of the rock tendon is represented by the reinforcement cross-sectional area and Young's Modulus.

$$\Delta F = -\frac{EA}{L}\Delta u \tag{8 - 1}$$

Where, $\Delta F =$ the incremental force in the rock tendon along the tangential or axial direction, N; E = Young's Modulus of the rock tendon, Pa; A = cross-sectional area of the rock tendon, m^2; L = embedment length, m; and Δu = the relative displacement, m.

The shear behaviour of the grout annulus is the most important part in the cable bolt element, determining the bearing capacity and failure modes of the rock reinforcement system. The shear behaviour of the grout annulus is represented by a spring-slider system. Shear failure can occur along either the bolt/grout or the grout/rock interface. The shear force in the grout annulus is calculated from the grout shear stiffness and the shear displacement, as displayed in Equation (8 - 2).

$$\frac{F_s}{L} = K_{bond}\left(u_c - u_m\right) \tag{8 - 2}$$

Where, F_s = shear force in the grout annulus, N; K_{bond} = grout shear stiffness, can be acquired from the laboratory pull-out tests, N/m/m; u_{c} = axial displacement of the rock tendon, m; and u_{m} = axial displacement of the medium (soil or rock mass), m.

The maximum shear force that the grout annulus can provide is determined by the interfacial cohesive strength and the frictional resistance, as shown in Figure 8 - 1. Furthermore, Equation (8 - 3) is used to calculate the maximum shear force.

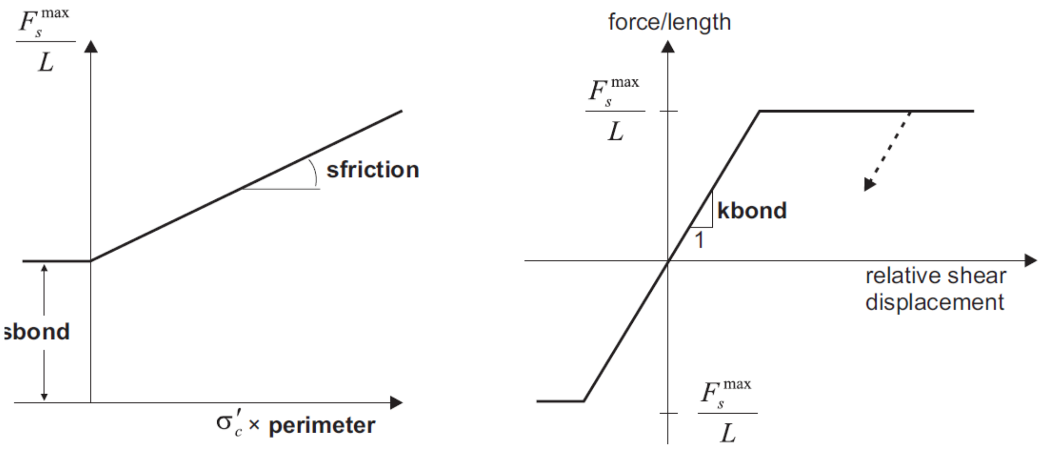

Figure 8 - 1 The mechanical behaviour of the grout annulus. a) shear strength criteria; b) relationship between the shear force and shear displacement (Itasca, 2000)

$$\frac{F_s^{\max}}{L} = S_{bond} + \sigma_c^{'} \times \tan\varphi \times c_b \tag{8 - 3}$$

Where, $F_s^{\max}$ = the maximum shear force, N; S_{bond} = cohesive strength, N/m; $\sigma_c^{'}$ = mean effective confining stress normal to the element, Pa; φ = friction angle, °; and c_b = exposed perimeter, m.

When bond failure occurs along the cable/grout interface, S_{bond} can be calculated with Equation (8 - 4).

$$S_{bond} = \pi D \mathrm{c} \mathrm{Q}_{\mathrm{B}} \tag{8 - 4}$$

Where, D = the diameter of the rock tendon, m; c = cohesion of the grout annulus and if such information is not available, one-half of the UCS can be used, Pa; and Q_B = bond quality (Q_B = 1 for perfect bonding).

For some cases, bond failure may occur at the grout/rock interface. This means that the expression D in Equation (8 - 4) should be replaced by (D+2t), in which t is the thickness of the grout annulus.

The rockbolt element uses the same constitutive laws for the rock tendon and grout annlus as the cable bolt element before the peak load occurs. However, the rockbolt element is able to simulate the strain-softening behaviour. To better reflect the pull-out behaviour, the rockbolt element was selected. Furthermore, the rockbolt element does not include the rotation behaviour of rock tendons, which is consistent with the laboratory scenario where the rotation of cable bolts was prevented.

8.3 Calibration of confining medium material

There are two different types of confining media, namely the strong and weak confining media. The important parameters such as the UCS, Young's Modulus and Poisson's Ratio were numerically calibrated.

8.3.1 Calibration of the weak confining medium material

In the laboratory, tests were conducted to measure the UCS, Young's Modulus and Poisson's Ratio. Specifically, an axial transducer was used to record the vertical deformation of the specimen with a length of 25 mm, as shown in Figure 8 - 2. And a circular transducer recorded the circular deformation of the specimen with a vertical height of 10 mm.

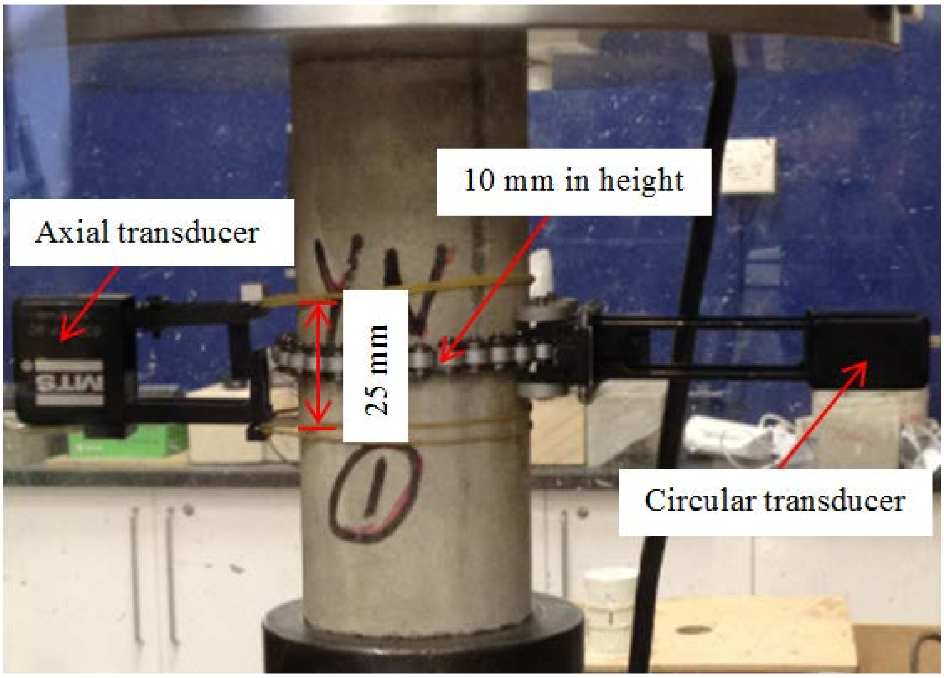

Figure 8 - 2 Axial and circular transducers attached to measure the Poisson's Ratio

To calibrate the parameters, a numerical model was established in FLAC2D. This model had a width of 54 mm and height of 134 mm, as shown in Figure 8 - 3, being consistent with the specimen dimensions used in the laboratory.

The bottom grid points were fixed in *X* and *Y* directions. Furthermore, the initial velocity of the bottom grid points was set to zero. This is used to simulate the scenario that the bottom surface of the specimen was fixed by the platen and no movement of the bottom surface was allowed in the loading process. To simulate the compressive process, an initial vertical velocity of 3.3×10^{-7} meter per step was applied on the top grid points.

A Fish function was compiled to record the vertical stress as part of FLAC2D modelling process. Specifically, during the loading process, the vertical stresses of bottom zones were summed and averaged in each step, as shown in Equation (8 - 5), being regarded as the vertical stress of this numerical model.

$$\sigma = \frac{\sum_{i=1}^{n} \sigma_i}{n} \tag{8 - 5}$$

Where, i = zone number; n = number of zones in the bottom; σ_i = vertical stress in the zone, Pa; and σ = vertical stress of the numerical model, Pa.

The vertical displacement of the top grid point was recorded. Through dividing the vertical displacement by the length of the specimen, the vertical strain of this numerical model was acquired, as shown in Equation (8 - 6).

$$\varepsilon = \frac{y_d}{l} \tag{8 - 6}$$

Where, y_d = vertical displacement of the grid point in the top, m; l = length of the specimen, m; and ε = vertical strain of the specimen.

The Poisson's Ratio is the most difficult parameter to acquire in the modelling process. First, the vertical strain in the centre with a length of 26.8 mm was monitored and calculated. Specifically, the vertical displacement of grid points A and B in Figure 8 - 3 was measured. The relative difference between them is:

$$\Delta y = y_A - y_B \tag{8 - 7}$$

Where, Δy = deformation of the specimen, m; y_A = vertical displacement of the grid point A, m; and y_B = vertical displacement of the grid point B, m.

Then, the axial strain within the middle section can be calculated with Equation (8 - 8):

$$\varepsilon_y = \frac{\Delta y}{l_{AB}} \tag{8 - 8}$$

Where, l_{AB} = length between grid points A and B, m; and ε_y = vertical strain.

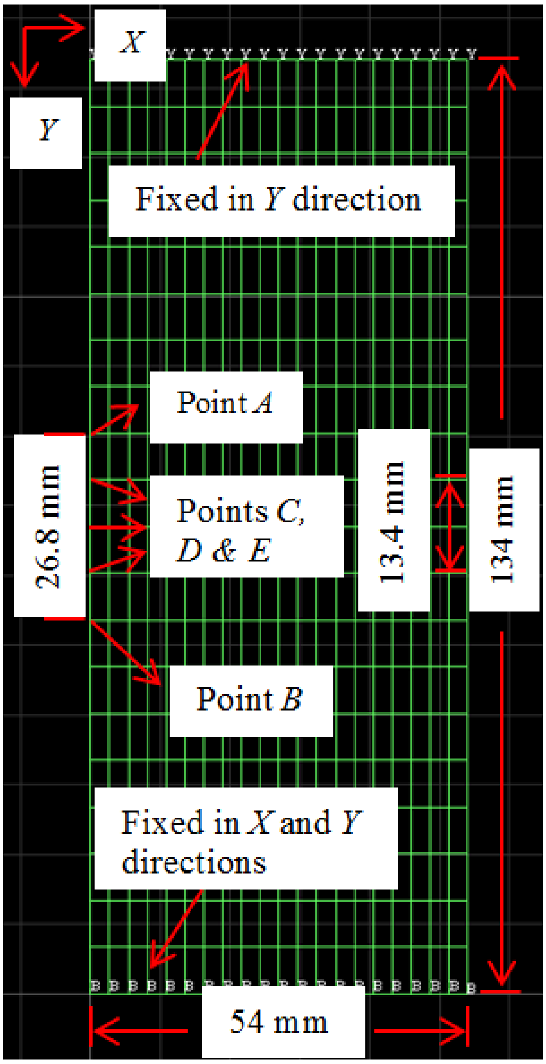

Figure 8 - 3 Establishing the numerical model for the UCS test

The circular strain of the specimen can be calculated with Equation (8 - 9):

$$\varepsilon_x = \frac{\Delta p}{p} \tag{8 - 9}$$

Where, p = the perimeter of the cylindrical specimen, equalling $2\pi r$; r = radius of the specimen, m; and ε_x = circular strain of the specimen.

Then, ε_x can be further expressed as:

$$\varepsilon_x = \frac{\Delta r}{r} \tag{8 - 10}$$

Therefore, the horizontal displacement of grid points *C*, *D* and *E* was summed and averaged as the circular deformation of the specimen in the middle section with a length of 13.4 mm, as shown in Equation (8 - 11).

$$x_d = \frac{x_{dC} + x_{dD} + x_{dE}}{3} \tag{8 - 11}$$

Where, x_{dC}, x_{dD}, and x_{dE} = horizontal displacement of grid points *C, D* and *E*, m; and x_d = horizontal displacement of the specimen centre, m.

Then, the circular strain of the specimen was calculated with Equation (8 - 12).

$$\varepsilon_x = \frac{x_d}{r} \tag{8 - 12}$$

Finally, the Poisson's Ratio can be calculated with Equation (8 - 13).

$$v = -\frac{\varepsilon_y}{\varepsilon_x} \tag{8 - 13}$$

A strain softening model was used, because it is able to simulate the post-peak behaviour of materials. The input parameters are tabulated in Table 8 - 1.

During the loading process, the vertical velocity contour in the specimen is shown in Figure 8 - 4. Apparently, the vertical velocity in the specimen was not uniform. Specifically, the vertical velocity of the specimen in the top was higher, equalling the loading speed, while the vertical velocity of the specimen in the bottom equalled zero. This was consistent with the loading condition in the laboratory environment.

Table 8 - 1 Input parameters for the weak material

Parameters	K (GPa)	G (GPa)	c (MPa)	φ (°)	σ_T (MPa)	ρ (kg/m^3)
Values	1.1	1.2	3.42	13.8	1	2100

Where, K = bulk modulus, equalling $\frac{E}{3(1-2v)}$, Pa; G = shear modulus, equalling $\frac{E}{2(1+v)}$, Pa; c = cohesion, Pa; σ_T = tensile strength, Pa; and ρ = density of the material, kg/m^3.

The relationship between the vertical stress and strain is shown in Figure 8 - 5. As seen, there is almost a linear relationship between the vertical stress and strain before the peak. At a vertical strain of 0.34%, the vertical stress reached a UCS of 8.9 MPa. Then, the vertical stress decreased, because of the softening behaviour. A linear line was drawn to fit with the linear portion, as shown in Figure 8 - 5, and the slope of the linear line was regarded as the Young’s Modulus, which is 3.0 GPa.

At a step of 1400, the numerical model reached the peak capacity and the plastic state is shown in Figure 8 - 6. Plastic deformation occurred in most zones and a shear failure occurred in the model.

The axial and circular stress - strain relationships are shown in Figure 8 - 7. The results show that at the same stress state, the diametrical strain was much smaller than the axial strain. Linear lines were drawn to fit with the linear portions in the curve. Therefore, the Poisson’s Ratio can be acquired:

$$v = -\frac{2.7}{26.8} = 0.10 \tag{8 - 14}$$

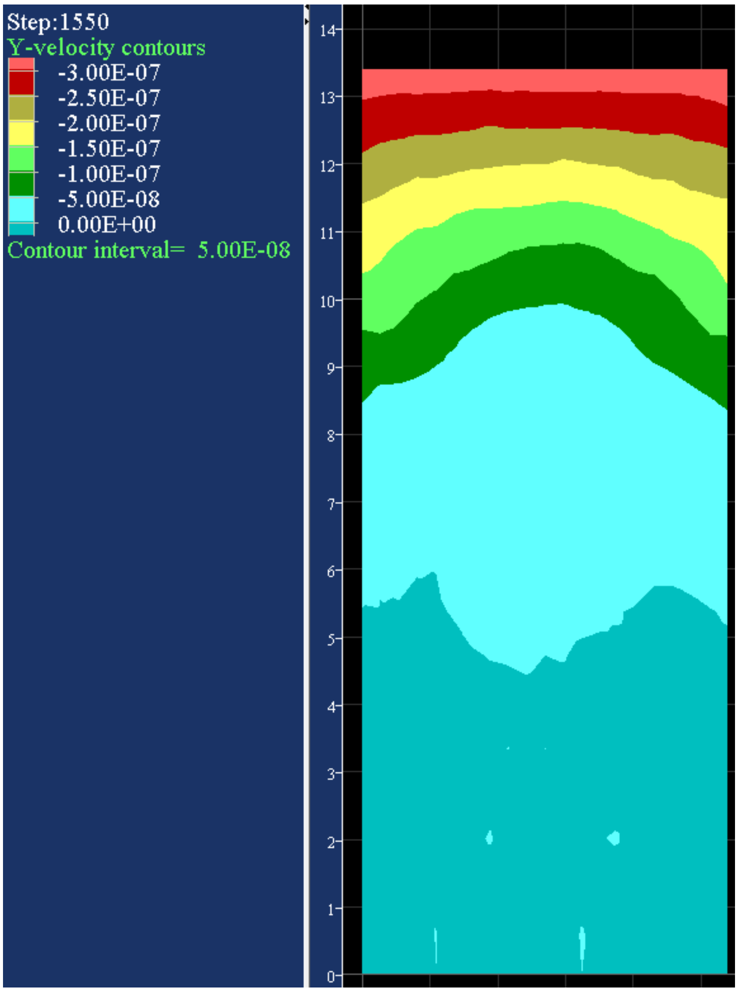

Figure 8 - 4 Vertical velocity contour in the loading process

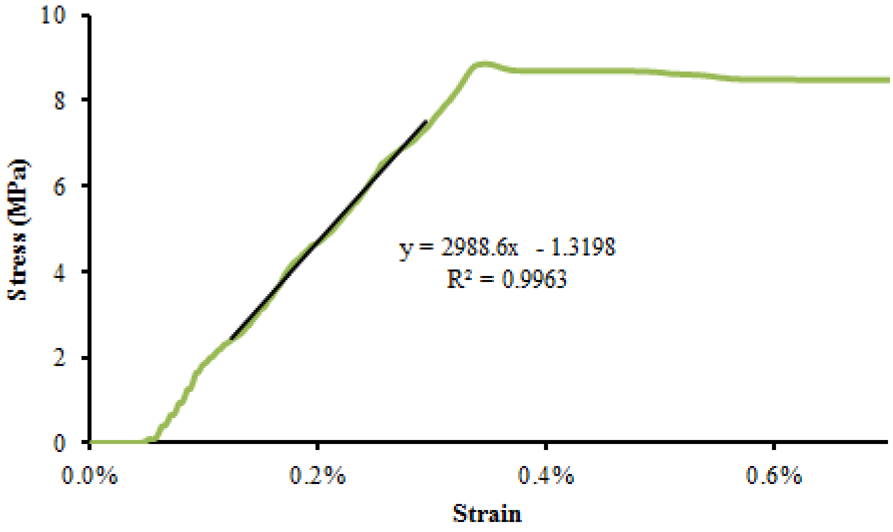

Figure 8 - 5 Stress versus strain relationship of the numerical model for the weak material in FLAC2D

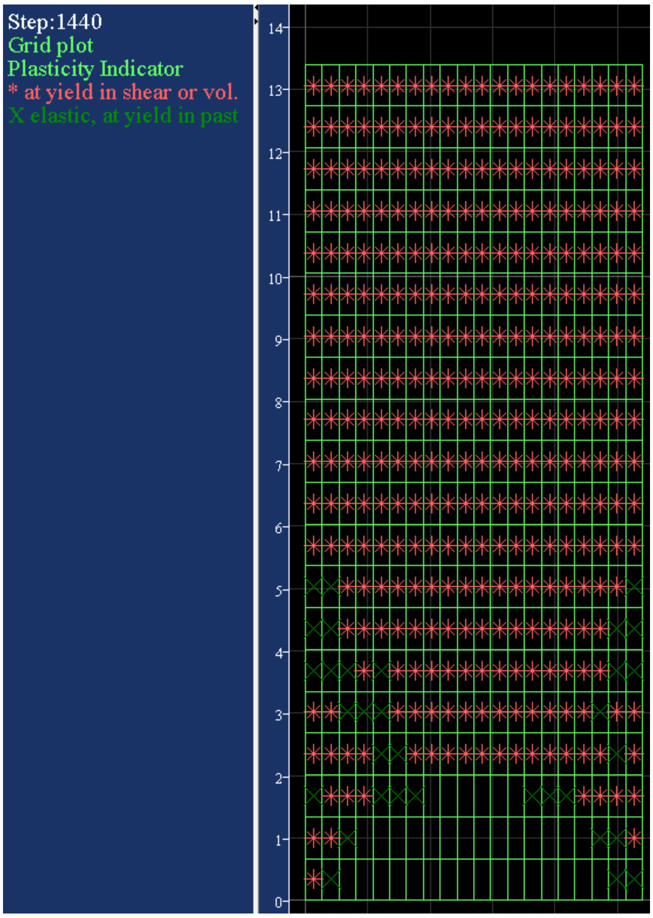

Figure 8 - 6 Elastic and plastic zones in the numerical model when the UCS was reached for the weak material

The comparison between numerical simulation and laboratory test results is shown in Figure 8 - 8 and Table 8 - 2. The results show that there was a good correlation between them. Consequently, the input parameters were appropriate to simulate the behaviour of the weak material.

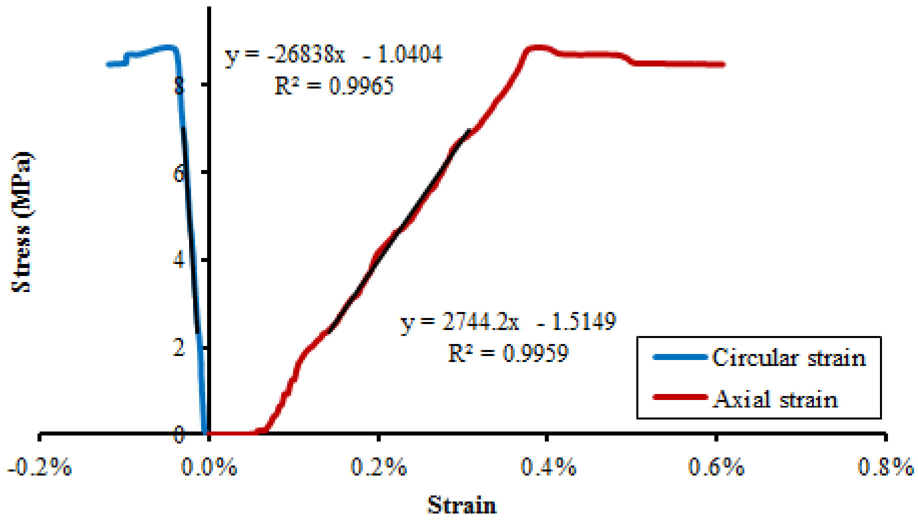

Figure 8 - 7 Axial and circular stress - strain relationships for the weak material

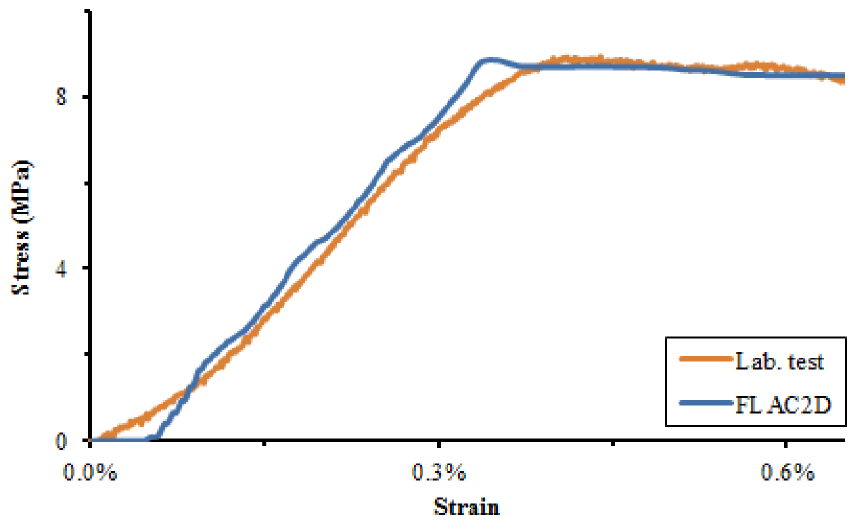

Figure 8 - 8 Comparison between numerical simulation and laboratory test results for the weak material

Table 8 - 2 Comparison between the UCS, Young's Modulus and Poisson's Ratio for the weak material

Approach	UCS (MPa)	Young's Modulus (GPa)	Poisson's Ratio
FLAC2D simulation	8.9	3.0	0.10
Lab. test	8.8	3.2	0.10

8.3.2 Calibration of the strong confining medium material

The calibration process was also conducted on the strong material. The input parameters are tabulated in Table 8 - 3.

Table 8 - 3 Input parameters for the strong material

Parameters	K (GPa)	G (GPa)	c (MPa)	φ (°)	σ_T (MPa)	ρ (kg/m^3)
Values	5.4	3.7	24.5	15.0	2	2300

The stress versus strain relationship of the numerical model is shown in Figure 8 - 9. Apparent brittle behaviour occurred. After an axial strain of 0.67%, the numerical model reached the UCS of 62.9 MPa. Meanwhile, the plastic state in the numerical model is shown in Figure 8 - 10. Then, there was a sudden drop of the bearing capacity. The Young's Modulus of the numerical confining medium was 10.6 GPa.

The axial and circular stress versus strain relationships are shown in Figure 8 - 11. Furthermore, the Poisson's Ratio can be acquired, which was 0.27.

The comparison between laboratory test and numerical modelling results is shown in Figure 8 - 12 and Table 8 - 4. There is good correlation between the modelling and laboratory test results.

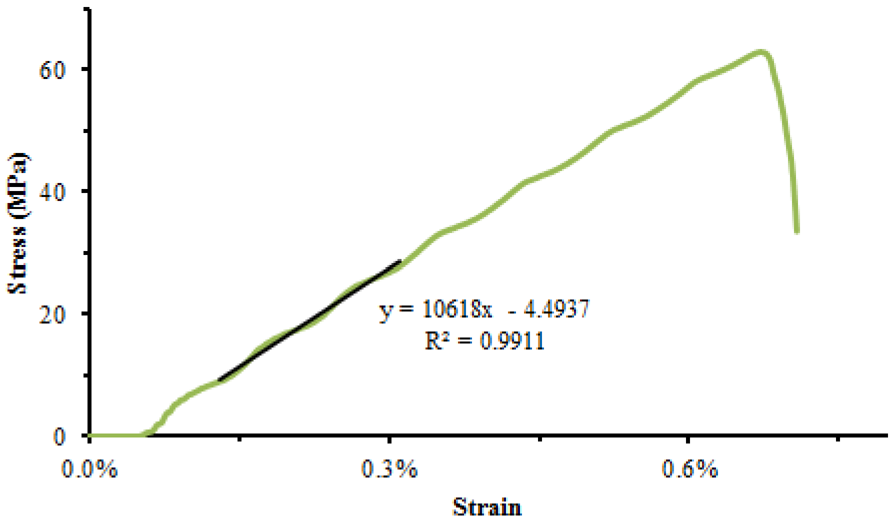

Figure 8 - 9 Stress versus strain relationship of the numerical model for the strong material

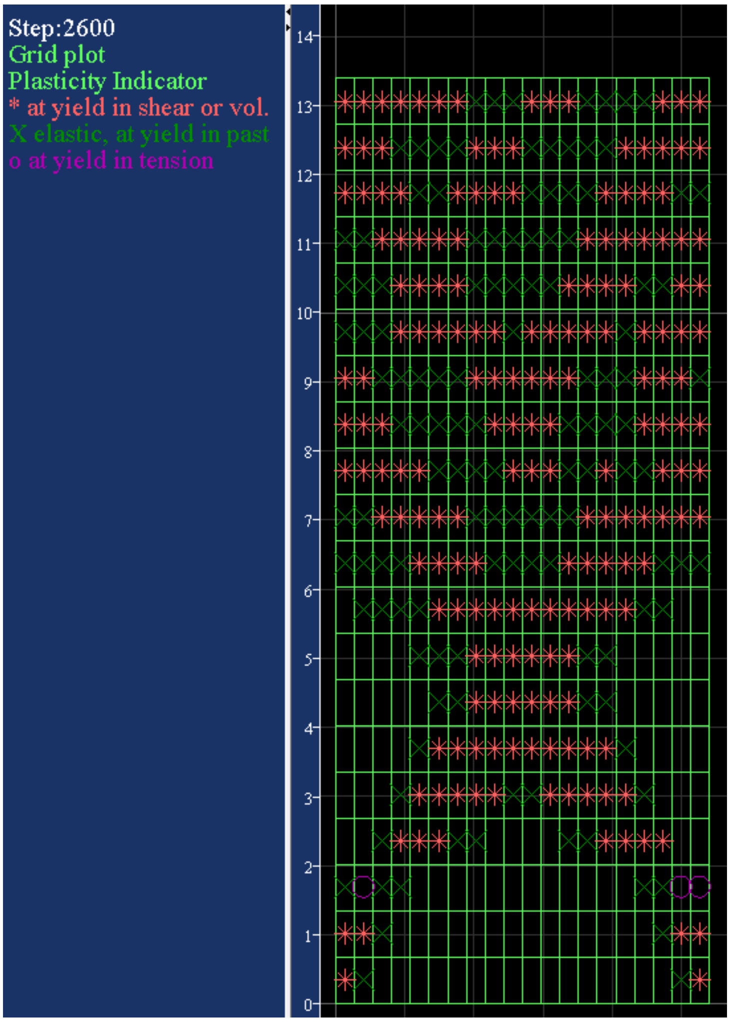

Figure 8 - 10 Elastic and plastic zones in the numerical model when the UCS was reached for the strong material

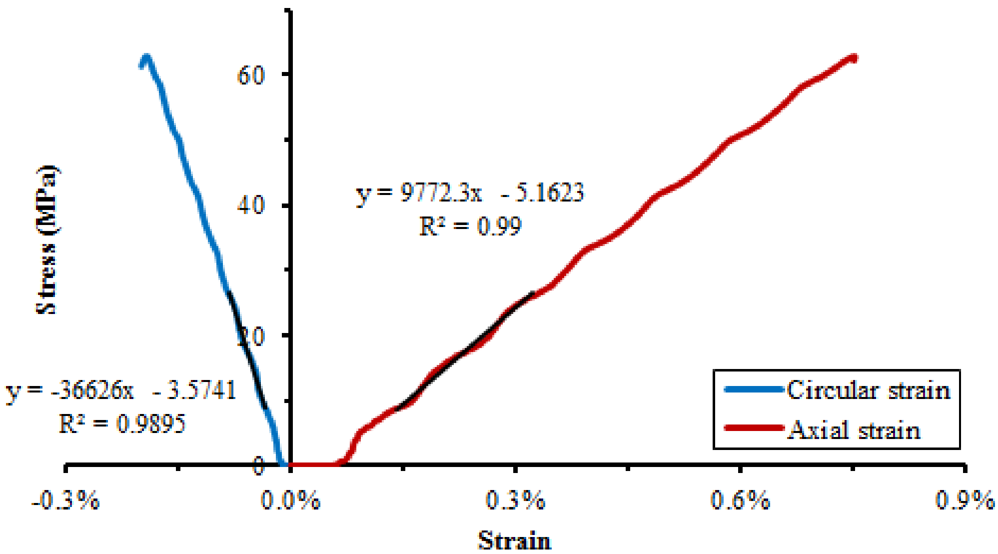

Figure 8 - 11 Axial and circular stress - strain relationships for the strong material

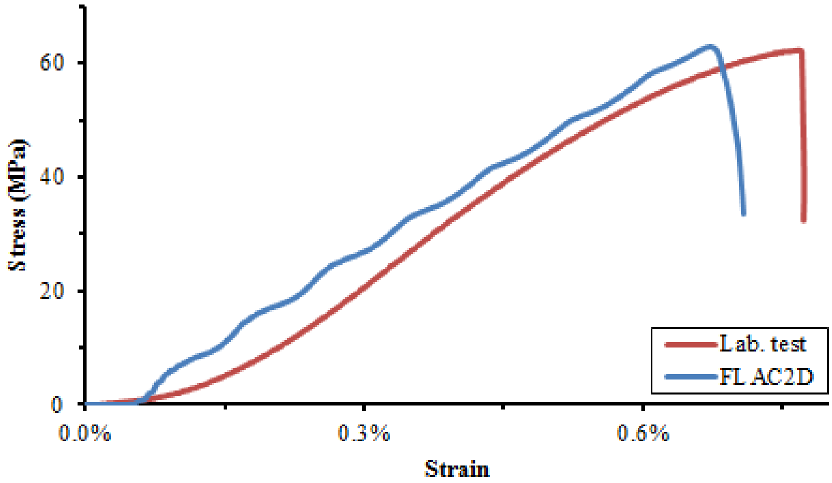

Figure 8 - 12 Comparison between numerical simulation and laboratory test results for the strong material

Table 8 - 4 Comparison between the UCS, Young's Modulus and Poisson's Ratio for the strong material

Approach	UCS (MPa)	Young's Modulus (GPa)	Poisson's Ratio
FLAC2D simulation	62.9	10.6	0.27
Lab. test	62.7	11.8	0.26

8.4 Simulation of the pull-out behaviour of Superstrand cable bolts

8.4.1 Simulation of Superstrand cables pulled from the weak confining medium with normal borehole

The pull-out behaviour of Superstrand cable bolts was simulated. Specifically, the middle cross section was selected and the geometry of the numerical model is shown Figure 8 - 13. The confining medium had a width of 300 mm and height of 450 mm, being consistent with the dimensions of the confining medium used in the laboratory. The top grid points were fixed in the *Y* direction. The structural element with an embedment length of 320 mm was installed in the confining medium. A free length of 10 mm was left above the confining medium and a constant pulling velocity of 1.0×10^{-6} meter per step was applied at the loaded end.

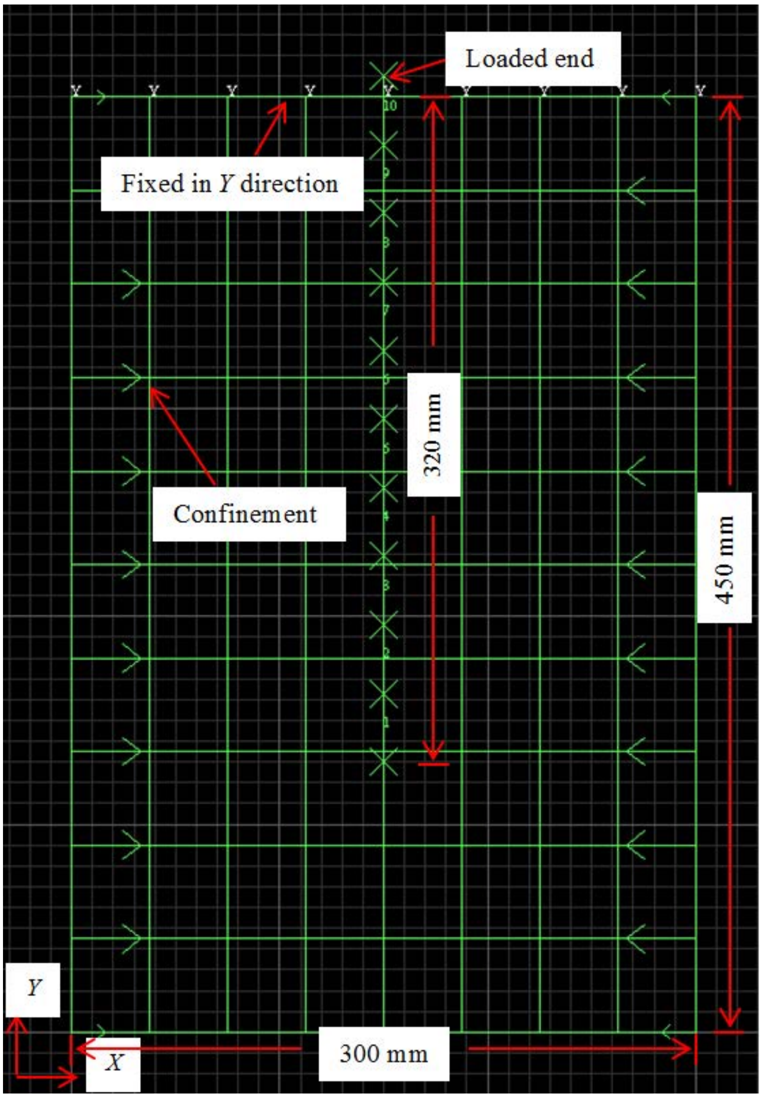

Figure 8 - 13 Geometry of the numerical model for pulling test on the Superstrand

The confining medium was simulated with the strain softening model and the input parameters were acquired through calibration. The input parameters for the Superstrand cable bolt including the Young's Modulus, tensile strength and radius are shown in Table 8 - 5.

Table 8 - 5 Input parameters for the Superstrand cable bolt (Jennmar, 2014)

Cable bolt name	E (GPa)	Yield (kN)	Radius (mm)
Superstrand	194.2	525	10.9

As for the grout column, the cohesive strength and friction angle are shown in Table 8 - 6, which were acquired from the direct shear test.

Table 8 - 6 Input parameters for the grout column

Grout name	Cohesion (MPa)	Friction angle (°)
Stratabinder	12.4	42.3

Considering that the laboratory test results showed that bond failure occurred along the cable/grout interface, Equation (8 - 4) was used to calculate the cohesive strength of the cable/grout interface. Q_B is an empirical factor, dependent on the geometry of the cable and grout property. Hutchinson and Diederichs (1996) indicated that the bond strength between the regular carbon steel and cement grout ranged from 1 to 3 MPa, with the w/c ratio varying from 0.35 to 0.5. Macsporran (1993) tested the bond strength of the cable/grout interface. The Type 10 Portland cement mixed with a w/c ratio of 0.4, having a UCS of 58.4 MPa was used. His results showed that the bond strength of the cable/grout interface was around 3.2 MPa, as shown in Figure 8 - 14.

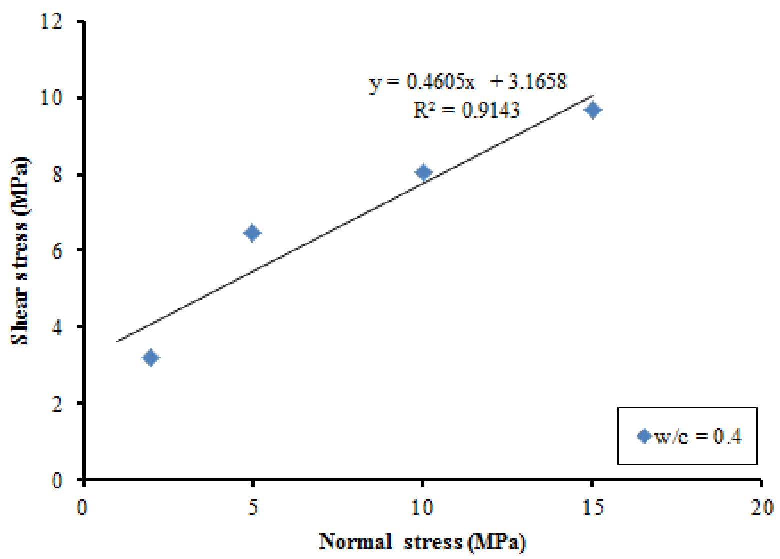

Figure 8 - 14 Bond strength of the cable/grout interface under different confining pressure conditions, after Macsporran (1993)

Since the Stratabinder grout mixed with a w/c ratio of 0.42, having a UCS of 54.3 MPa, was consistent with the grout properties used by Macsporran (1993), a bond quality of

0.27 was used. Therefore, the bond strength between the Superstrand and the grout was: 0.27×12.4 = 3.348 MPa. The S_{bond} can be calculated as:

$$S_{bond} = 3.348 \times 0.0218 \times 3.14 \times 10^{3} = 229 \tag{8 - 15}$$

The perimeter where bond failure occurred was calculated by:

$$p = 3.14 \times 21.8 = 68.5 \tag{8 - 16}$$

In FLAC2D, a normal coupling spring which is used to account for the shear behaviour of the rock tendons, was involved in the rockbolt structural element. Considering that this simulation only focused on the axial behaviour of rock tendons, the input parameters of the normal coupling spring were left blank.

A Fish function was created to record the pull-out force. Specifically, the vertical unbalanced force along the pull-out direction at each top grid point was summed, which was consistent with using a load cell to record the reaction force in the laboratory environment.

The displacement was recorded with two different approaches. In the first approach, the pull-out displacement was acquired by multiplying the pulling velocity with the time step and this was realised by the Fish function. With the second approach, the axial displacement of the loaded end in Figure 8 - 13 was recorded. A comparison was conducted on the results. As shown in Figure 8 - 15, the displacement recorded with those two different approaches is the same. Therefore, the approach of using the Fish function was selected to record the pull-out displacement of cable bolts.

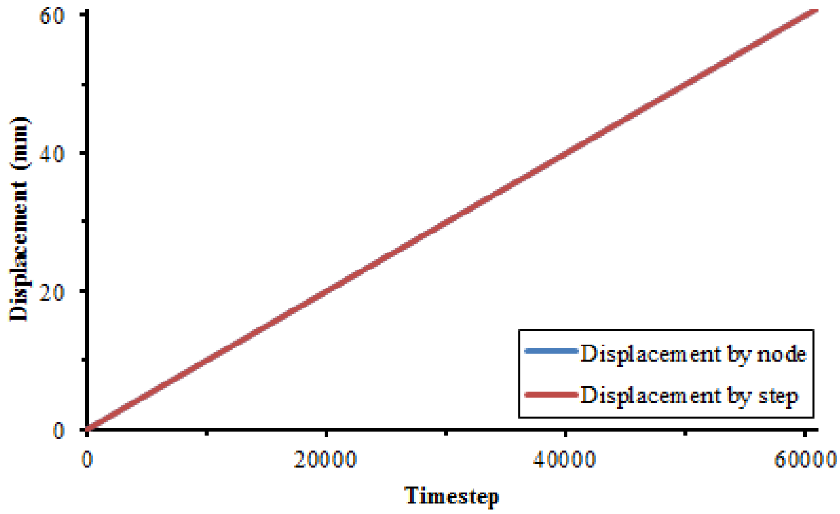

Figure 8 - 15 Displacement recording with two different approaches

During the loading process, confining pressure was applied on the confining medium, as shown in Figure 8 - 13. The confining pressure was calibrated until the maximum pull-out load in numerical simulation was consistent with the peak capacity in the laboratory tests. It was found that when a confining pressure of 2 MPa was applied, the Superstrand cable bolting system in FLAC2D had a peak capacity of 111 kN, which was consistent with the peak capacity recorded in the laboratory tests. It should be mentioned that the peak load occurred when the pull-out displacement reached 32 mm. Before the peak capacity, there was a reduction of the cable bolting system stiffness. And this was realised by decreasing the function of cs_sstiff, which determines the shear stiffness of the grout column in FLAC2D.

The post-peak behaviour was simulated through the strain softening model. Specifically, two functions, namely “cs_scohesion” and “cs_sfriction”, were used to depict the reduction of the cohesive strength and friction after the peak load. The input parameters for those two functions were calibrated until the bearing capacity in the post-peak stage was consistent with the laboratory test results. A comparison between the numerical and experimental test results is shown in Figure 8 - 16. There was good correlation between the numerical simulation and laboratory test results.

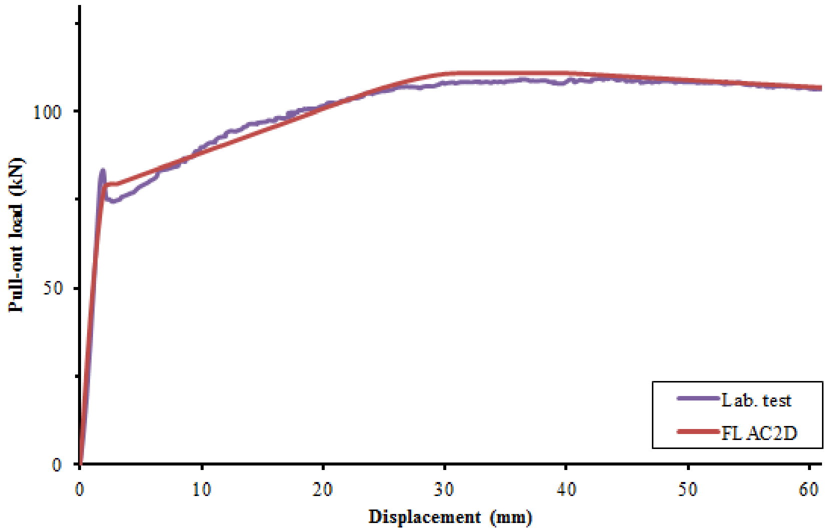

Figure 8 - 16 Comparison between numerical and laboratory test results on Superstrand cable bolts installed in the weak confining medium

When the pull-out displacement reached 60 mm, the displacement vector of the numerical confining medium is shown in Figure 8 - 17. With the cable bolt being pulled out, the confining medium had a tendency to move vertically. However, at the top of the confining medium, since the grid points were fixed in the *Y* direction, there was no vertical movement.

Figure 8 - 17 also showed that there was no lateral deformation of confining medium and the structural element in the middle. Therefore, it is assumed that leaving the input parameters of the normal coupling spring blank had no effect on the pull-out results. To validate this assumption, a pull-out simulation was conducted with the input parameters of the normal coupling spring involved.

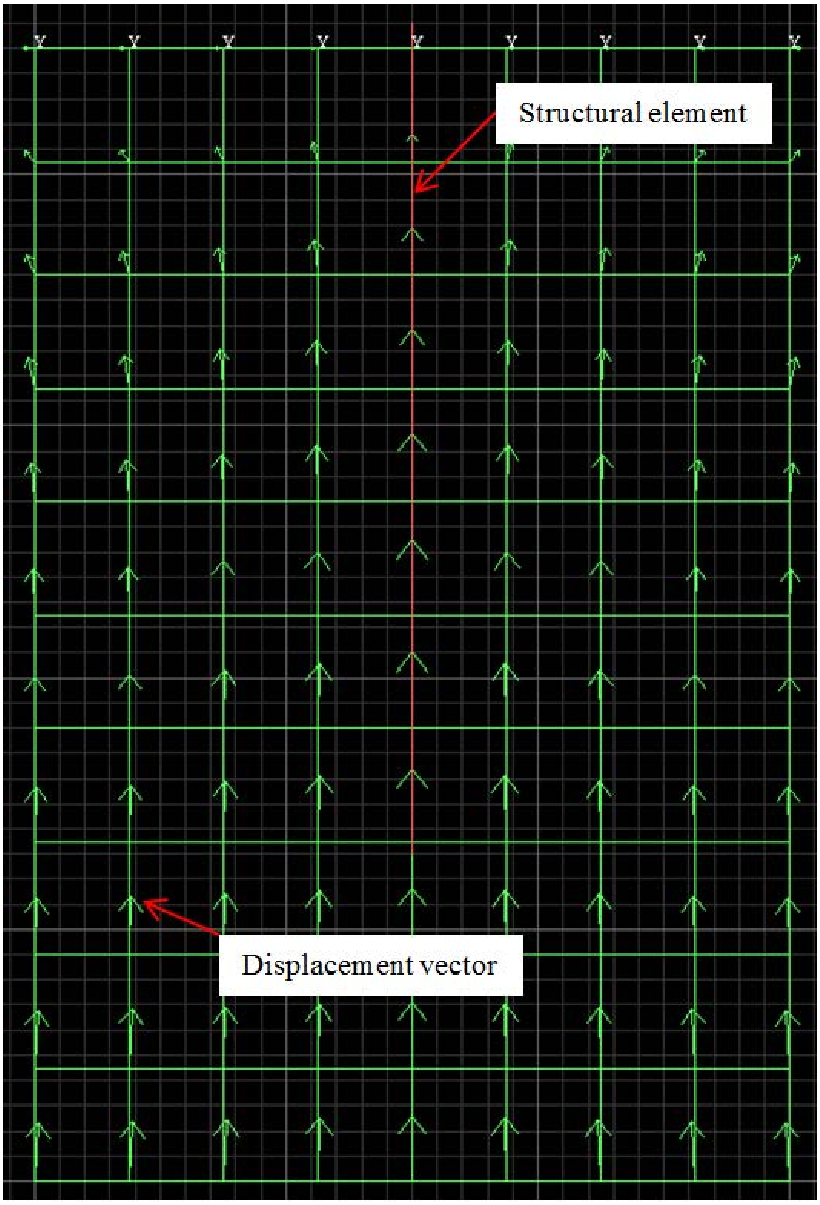

Figure 8 - 17 Displacement vector distribution in the numerical confining medium

Equation (8 - 17) was used to calculate the second moment of area or *i*, which is 1.1×10^{-8} m^4.

$$i = 0.25\pi r^4 \quad (8 - 17)$$

The stiffness, cohesive strength and friction angle of the normal coupling spring were acquired from the handbook, as tabulated in Table 8 - 7.

A comparison between the numerical simulation results is shown in Figure 8 - 18. The normal coupling spring had no effect on the result in the axial loading condition. Therefore, the input parameters of the normal coupling spring were all left blank in the following simulation.

Table 8 - 7 Input parameters for the normal coupling spring (Itasca, 2000)

Bolt type	cs_nstiff (N/m/m)	cs_ncoh (N/m)	Friction angle (°)
Cable bolt	1×10^{10}	2×10^{6}	45

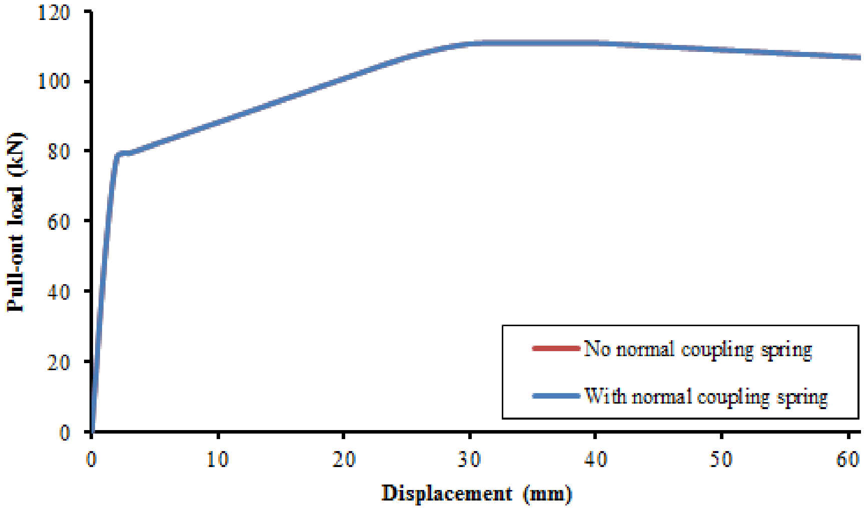

Figure 8 - 18 Numerical simulation results in the condition of normal coupling spring involved and normal coupling spring removed

8.4.2 Simulation of Superstrand cables pulled from the weak confining medium with larger borehole

When the Superstrand cable bolt was installed in the larger borehole, the pull-out behaviour was also numerically simulated. The laboratory test results showed that bond failure still occurred along the cable/grout interface. By using FLAC2D, it was found that when the confinement was increased to 4.5 MPa, there was a good correlation between numerical simulation and laboratory test results, as shown in Figure 8 - 19.

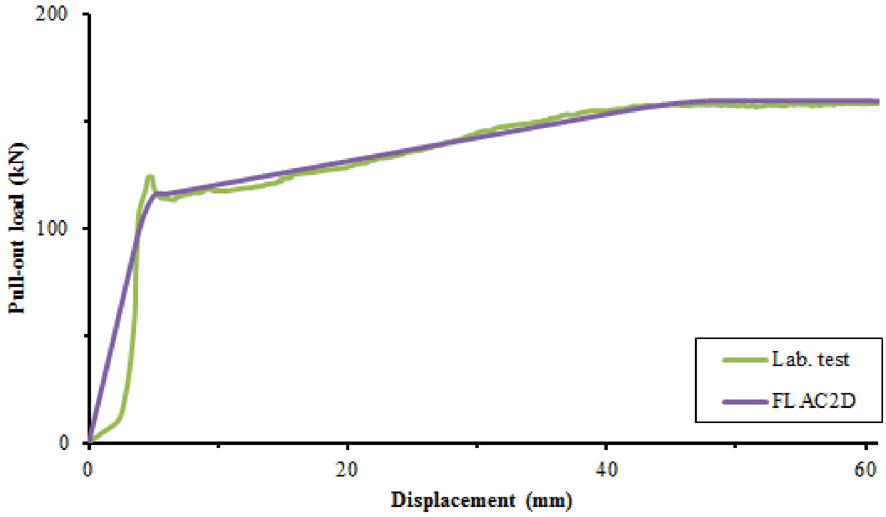

Figure 8 - 19 Comparison between numerical and laboratory test results on Superstrand cable bolts installed in larger boreholes in the weak confining medium

8.4.3 Simulation of Superstrand cables pulled from the strong confining medium

When the cable bolt was installed in the strong confining medium, the laboratory test results showed that bond failure occurred along the cable/grout interface. The input parameters for the strong confining medium were acquired from the calibration, which has been described above. The simulation results show that when the confinement was 9.8 MPa, the Superstrand cable bolting system had a peak capacity of 264 kN. The comparison between the numerical simulation and laboratory test results is shown in Figure 8 - 20.

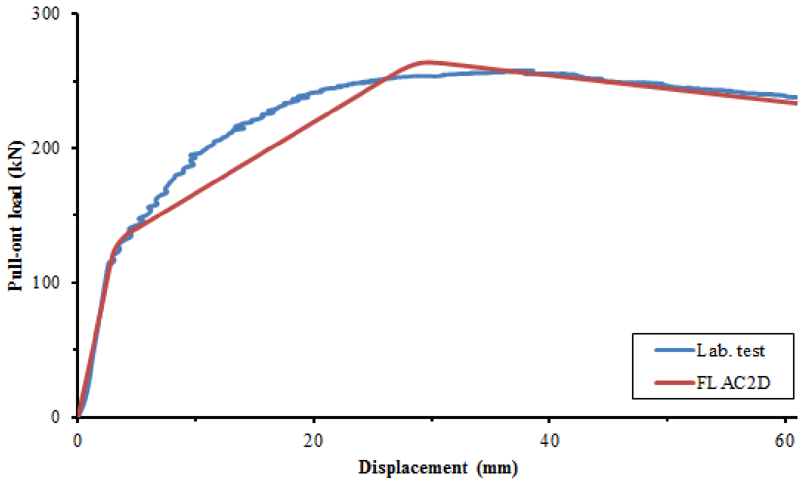

Figure 8 - 20 Comparison between numerical and laboratory test results on Superstrand cable bolts installed in the strong confining medium

8.5 Simulation of the pull-out behaviour of MW9 cable bolts

8.5.1 Simulation of MW9 cables pulled from the weak confining medium with normal borehole

The pull-out behaviour of MW9 cable bolts installed in boreholes with a normal diameter of 42 mm in the weak confining medium was simulated.

The laboratory test results showed that bond failure of the modified cable bolting system occurred along the grout/rock interface. The cohesive strength between the grout and the confining medium was calculated with Equation (8 - 18):

$$S_{bond} = 0.4 \times \frac{8.8}{2} \times 3.14 \times 0.042 = 232 \tag{8 - 18}$$

The perimeter where bond failure occurred was calculated by:

$$p = 3.14 \times 42 = 131.9 \tag{8 - 19}$$

The input parameters for the MW9 cable bolt are shown in Table 8 - 8.

Table 8 - 8 Input parameters for the MW9 cable bolt

Cable bolt name	E (GPa)	Yield (kN)	Radius (mm)
MW9	201	620	28.5

It was found that when the confinement was 3.7 MPa, the MW9 cable bolting system had a maximum bearing capacity of 208 kN, which is consistent with the laboratory test results. A comparison between the numerical simulation and laboratory test results is shown in Figure 8 - 21.

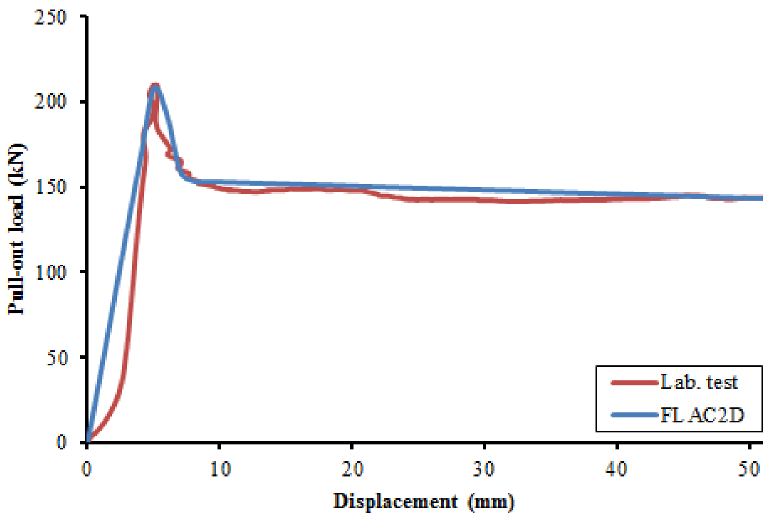

Figure 8 - 21 Comparison between numerical and laboratory test results on MW9 cable bolts installed in the weak confining medium

8.5.2 Simulation of MW9 cables pulled from the weak confining medium with larger borehole

When the MW9 cable bolt was installed in a larger borehole of 52 mm in the weak confining medium, laboratory test results showed that the bond failure transferred from the grout/rock interface to the cable/grout interface. The cohesive strength between the cable bolt and the grout was calculated with Equation (8 - 20):

$$S_{bond} = 0.32 \times 12.4 \times 0.0285 \times 3.14 \times 10^{3} = 355 \qquad (8 - 20)$$

The perimeter where bond failure occurred was calculated by:

$$p = 3.14 \times 28.5 = 89.5 \tag{8 - 21}$$

It was found that when the confinement was 5.8 MPa, the MW9 cable bolting system had a maximum load bearing capacity of 258 kN, being consistent with the laboratory test results. The load versus displacement relationships of the MW9 cable bolting system in simulation and laboratory test are shown in Figure 8 - 22.

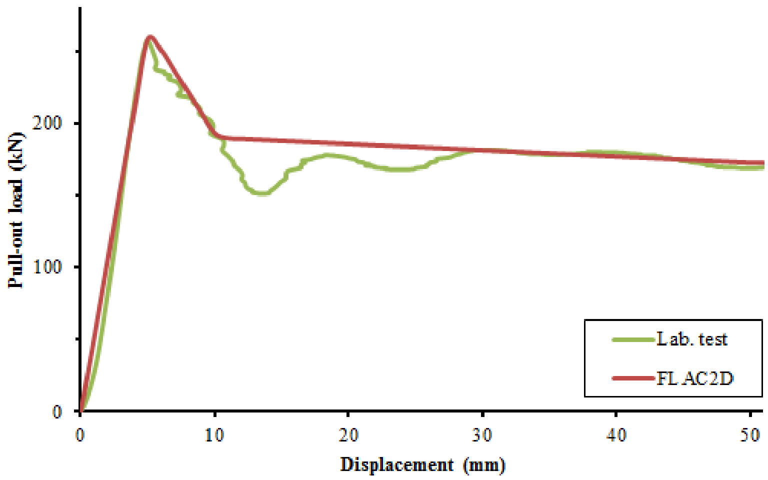

Figure 8 - 22 Comparison between numerical and laboratory test results on MW9 cable bolts installed in the weak confining medium with larger borehole

8.5.3 Simulation of MW9 cables pulled from the strong confining medium

The load transfer behaviour of MW9 cable bolts installed in the strong confining medium was also tested in the laboratory. The results showed that the MW9 cable bolting system had a maximum load bearing capacity of 381 kN when the strong confining medium was used. Numerical simulation was conducted and the input parameters for the strong confining medium were acquired from calibration. The results showed that when the confinement was set as 10.5 MPa, the MW9 cable bolting system had a maximum load bearing capacity of 381 kN, which was consistent with laboratory test results. The comparison between the numerical simulation and the laboratory test results is shown in Figure 8 - 23.

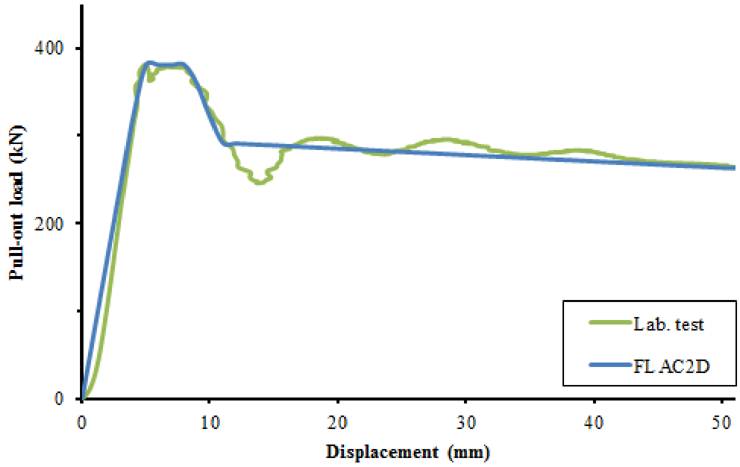

Figure 8 - 23 Comparison between numerical and laboratory test results on MW9 cable bolts installed in the strong confining medium

8.6 Summary

FLAC2D was used to simulate the pull-out behaviour of cable bolts. Both the cable bolt and rockbolt structural elements can be used to represent the rock tendon. However, the comparison showed that the cable bolt element used an elastic-perfectly plastic law to account for the axial behaviour of the bolting system. On the other hand, the rockbolt element can simulate the strain-softening behaviour of rock tendons. Therefore, the rockbolt element was selected.

The confining media were calibrated to make sure that the numerical confining media were consistent with the laboratory material. UCS tests were conducted using FLAC2D and the strain softening model was used to depict the compressive behaviour of the material. Important parameters including UCS and Young's Modulus were acquired. The numerical simulation results were validated with the experimental results.

After the calibration process, it was found that the input parameters for the weak confining medium were: K = 1.1 GPa, G = 1.2 GPa, c = 3.42 MPa, φ = 13.8°, σ_T = 1 MPa and ρ = 2100 kg/m^3. Also, the input parameters for the strong confining medium were: K = 5.4 GPa, G = 3.7 GPa, c = 24.5 MPa, φ = 15.0°, σ_T = 2 MPa and ρ = 2300 kg/m^3.

The parameters calibrated from the UCS tests were used in the cable bolt pull-out simulation. The numerical model had a width of 300 mm and height of 450 mm, being consistent with the dimensions in the laboratory test. Fish functions were used to record the pull-out load and the displacement. Two different types of cable bolts, namely the Superstrand and the MW9 cable bolts, were simulated. The cohesive strength between the cable bolt and the grout, the cohesive strength between the grout and the confining medium, the interfacial friction angle and the confinement provided by the confining medium were considered and analysed. The numerical simulation results were validated with the experimental pull-out programme. The results showed that when the Superstrand cable bolt was pulled out from the weak confining medium, a confinement of 2 MPa was provided by the confining medium. However, when the strong confining medium was used, a high confinement of 9.8 MPa can be provided by the confining medium. As for the MW9 cable bolts, a low confinement pressure of 3.7 MPa was acquired when the cable bolt was pulled out from the weak confining medium. The confinement pressure was increased to 10.5 MPa when the strong confining medium was used to confine the MW9 cable bolt.

CHAPTER NINE

CONCLUSIONS AND RECOMMENDATIONS

9.1 Conclusions

This thesis focuses on studying the load transfer mechanism of fully grouted cable bolts. Initially, a literature review was conducted on the methods used in axial testing of cable bolts. It was concluded that the axial tests can be classified as either rotating or non-rotating tests. The rotating tests have a problem that cable bolts always untwist or unscrew during the test, which is not a true reflection of the cable bolt behaviour in the field. The Laboratory Short Encapsulation Pull Test incorporated in the current British Standard is the latest development in the cable bolt testing area. Recent work reported several deficiencies in this test design. For example, unwinding of a cable bolt during the pull-out process has an adverse impact on performance. The use of sandstone cores as a confining medium limits understanding of the behaviour in different rock types. Also, as the confining medium diameter is only 142 mm, it can directly impact the performance of a cable bolt, especially with high load transfer cable bolts.

A new modified cable bolt testing facility that is capable of testing the various kinds of fully grouted cable bolts used in the Australian underground coal mining industry under different test conditions was designed and constructed, with the goal of overcoming the shortcomings of the LSEPT in the current British Standard.

A number of tests were undertaken to confirm various test design parameters. In most designs, there are two main sections, an embedment section and an anchor section.

In the embedment section, cementitious-based material was used to prepare the confining medium having uniform material properties. To determine the optimum confining medium dimension, a number of pull tests were conducted using the cylindrical confining medium having outside diameters ranging between 150 mm and 508 mm. A Sumo cable bolt was used in the tests as it is a modified bulbed cable bolt with a large load transfer capacity. The tests showed that the maximum load transfer capacity of the Sumo cable bolt increased with the confining medium diameter.

The tests were undertaken with the confining medium in an unconfined condition. Over the range of confining medium diameters examined, there was no apparent minimum threshold diameter above which there was no change in load transfer capacity. A repeat series of tests with the confining medium radially confined showed that the peak capacity of the Sumo cable bolt still initially varied with confining medium diameter. However, above a diameter of 300 mm, the maximum load transfer capacity of the Sumo cable bolt was unchanged. This result emphasises the sensitivity of anchor performance to confining medium size and radial confinement. As a result, a confining medium diameter of 300 mm was recommended for use in the embedment section.

A further modification from the LSEPT design has been the incorporation of a split steel cylinder rather than a bi-axial cell. As opposed to the biaxial cell, the split steel cylinder does not create any significant prestress condition to the confining medium. However, it does react to any radial stress induced as a result of the cable bolt bring extruded from the confining medium. The steel cylinder in effect simulates the confinement afforded by a rock mass. A secondary function of the steel cylinder is that it prevents any relative rotation between the cable bolt and confining medium that can be induced during loading of some cable bolts.

As for the anchor section of the test design, an internally threaded steel anchor tube with a length of 608 mm was used to be used to grip the cable bolt. The threads enhanced the bond contact and mechanical interlock between the cable bolt and tube. To prevent the anchor tube from rotating during the pull-out process, a key slot couples the anchor tube to the bearing plate. The key slot can accommodate axial displacements up to 100 mm, preventing any rotation between the confining medium and anchor tube.

A bearing plate with an internal diameter of 70 mm provides an interface between the confining medium and anchor tube to transfer and distribute the load. The hole in the bearing plate is larger than the borehole diameter in the confining medium. Because of this, the top surface of the confining medium surrounding the borehole is unconfined allowing different failure modes of a cable bolt, including shear slippage along the cable/grout interface, relative movement along grout/rock interface and failure within the surrounding material.

The steel cylinder confining medium holder is comprised of two halve cylinders that are bolted together. The effect of tightening the bolts to torque values ranging between 0 and 200 N·m on load transfer performance was examined. It was found that peak load of the cable bolt varied with torque up to 135 N·m with little change thereafter. To ensure a consistent level of contact between the confining medium and steel cylinder, it is recommended that the bolts should be tightened to a relatively low torque value of 40 N·m prior to each test to ensure a consistent confinement condition.

To ensure a consistent level of borehole roughness, a technique was developed to manufacture a rifled borehole in the confining medium. To gauge the effect of borehole roughness on the behaviour of cable bolts, pull-out tests were conducted in smooth and rifled boreholes. Two types of cable bolts, namely a plain cable and a modified cable bolt, were used. The results showed that borehole roughness had different effects with the two cable bolts. When the plain cable bolt was tested, borehole roughness had little impact on failure at the cable/grout interface. Even in a smooth borehole there was sufficient bond strength along the grout/rock interface to resist the grout column from slipping. However, with the modified cable bolt, the contact between the cable and grout was enhanced and as a consequence, failure occurred along the grout/rock interface. As the effect can differ with the type of cable bolt, it is recommended that the test design incorporates a rifled borehole in the confining medium.

The effect of different cable termination mechanisms, namely, using a barrel and wedge system, a special termination plate or no special termination mechanism, was studied. In the end, a slight redesign of the anchor tube without any cable termination mechanism was found to be effective, with no failure in the anchor section even at the highest load of modified cable bolt.

Results of the preliminary investigation showed that the new laboratory-scale axial-loading cable bolt testing facility has the capability of determining the post-failure behaviour of a wide range of cable bolt types over a wide range of displacement up to 100 mm.

Two cable bolts, namely the Superstrand, a plain cable, and the MW9, a high capacity modified cable bolt, were tested under controlled conditions in terms of the confining medium strength and borehole diameter. The tests were undertaken with a manufactured rifled borehole and a Stratabinder grout strength of 54 MPa.

The confining media were cast with two different types of cementitious grout. UCS tests were conducted on both cylindrical and cubic specimens to determine the strength of the grout materials. It was found that the cubic specimens always had a higher UCS than cylindrical specimens. Based on the ISRM standard, it was concluded that the weak confining medium had a UCS of 8.8 MPa while the strong confining medium had a UCS of 62.7 MPa.

The failure modes of cable bolting systems were carefully studied. It was found that bond failure of cable bolts always occurred along the cable/grout interface with a strong confining medium, independent of the cable type. However, with a weak confining medium, bond failure of the modified cable bolts occurred along the grout/rock interface, which was a result of the low shear strength of the grout/rock interface. The maximum pull-out load in a weak confining medium with the Superstrand cable was 112 kN or nearly half that of the MW9 of 208 kN, a difference of 86%.

By contrast, with an increase in strength of the confining medium to 62.7 MPa, the maximum load of the Superstrand was 265 kN, representing an increase of 137% compared to that achieved in the weak confining medium. For the MW9 cable bolt, the maximum load was 380 kN, which was an increase of only 83%. Overall, the difference between the strength of the two cable bolts reduced to just 43%. Hence, the Superstrand cable bolt was found to be more sensitive to changes in confining medium strength.

The standard length of embedment in the LSEPT is 320 mm. Tests at longer embedment lengths of 340, 360 and 380 mm found that pull-out load increased from 380 kN at 320 mm to 440 kN and 480 kN at 340 mm and 360 mm respectively. Beyond 360 mm there was no apparent increase in pull-out load capacity. The phenomenon termed slip-lock was particularly evident with the MW9 cable bolt. It tended to increase with embedment length but at a lower rate.

There were distinct changes in the stiffness of the cable bolts before and after the maximum pull-out load. For both cables, the initial stiffness was similar at approximately 51 kN/mm and 69 kN/mm in the weak and strong confining media respectively. However, with the Superstrand, stiffness began to reduce once the load reached around 100 kN requiring a further displacement of 30 mm to achieve maximum load. In the case of the MW9 cable, stiffness remained constant up to the peak load within a displacement of only 7 mm, hence it is a much stiffer system.

Post-failure, the Superstrand cable bolt showed very little reduction in load bearing capacity over the measured displacement range of 100 mm, especially in weak material. Specifically, there was only a 25% reduction from the peak load of 265 kN to a load of 200 kN, with a stiffness of -1.1 kN/mm. In the weak material, failure occurred at the grout/rock interface, resulting in a “plug” of grout and cable being extruded from the borehole. For the MW9 cable, the slip/lock behaviour was activated for up to a total 30 - 40 mm displacement in both the weak and strong confining medium. Beyond this, there was a similar stiffness measured in both the weak and strong materials.

An increase in borehole diameter above the recommended standard borehole diameter of 10 mm was found to have a beneficial effect with both cable bolt types with a weak confining medium. It was determined that the Stratabinder grout had a much higher UCS than the weak confining medium. Therefore, increasing the borehole diameter in the weak confining medium provided more confinement on the cable bolt, resulting in larger pull-out load.

An analytical model was developed to study the load transfer performance of fully grouted cable bolts. A tri-linear model was used to depict the bond strength variation in relation to the shear slippage. The elastic, softening and debonding behaviour of the cable/grout interface was analysed in this model. It was assumed that when the embedment length was short enough, there was a uniform shear stress distribution along the cable/grout interface. However, when the embedment length was relatively longer, the non-uniform shear stress distribution was apparent. Pull-out stages, namely the elastic, elastic-softening, elastic-softening-debonding, pure softening, softening-debonding and debonding, were analysed. Based on this analytical model, the maximum pull-out load was calculated. The shear stress propagation along the cable/grout interface was analysed. Experimental pull-out tests on plain and modified cable bolts were used to validate this analytical model, ultimately showing that there was a good correlation between the analytical and experimental pull-out results.

Numerical simulation was conducted with FLAC to evaluate the pull-out behaviour of cable bolts. The rockbolt structural element was selected because it is able to simulate the strain-softening behaviour of rock tendons. Two different confining media, namely the strong confining medium and the weak confining medium, were used. Calibration work was conducted on those two materials to acquire the parameters such as the bulk modulus, shear modulus, cohesion and friction angle. The properties of the grout column including the cohesive strength and friction angle were acquired from the direct shear test. Pull-out simulation was conducted on the Superstrand cable bolt. It was found that when the weak confining medium was used, the confining pressure when the peak load was reached was 2 MPa. However, when the strong confining medium was used, the confining pressure increased up to 9.8 MPa. The pull-out behaviour of the MW9 cable bolts was also simulated. The results show that when the weak confining medium was used, the confinement provided by the confining medium was 3.7 MPa. A much higher confining pressure of 10.5 MPa was acquired when the strong confining medium was used.

9.2 Recommendations for future work

The load transfer mechanism of fully grouted cable bolts has a significant effect on determining the safety of mining operations. However, this mechanism has not been fully understood. The following is some recommendations for further work.

- The load transfer performance of modified cable bolts under dynamic loading condition. Most of the previous research has focused on the performance of cable bolts in a slow loading rate condition. However, in field applications, the cable bolt may be subjected to a dynamic loading rate induced by the rock burst. Farah and Aref (1986b) and Hassani *et al.* (1992) studied the influence of loading rate on the performance of cable bolts. However, they only tested plain cable bolts. No research has been conducted on the influence of loading rate on modified cable bolts. Therefore, it would be valuable to increase the loading rate to high values and evaluate the performance of modified cable bolts.

- Confining medium size effect on bond strength of cable bolts under constant normal load condition. Rajaie (1990) studied the influence of confining medium size on the performance of cable bolts in the unconfined condition. This thesis used a constant normal stiffness boundary to confine the confining medium. However, no research has been conducted on the confining medium size effect under constant normal load condition.
- Load transfer performance of twin-strands and triple-strands in the weak confining medium. The axial performance of multi-strands installed in the strong confining medium has been studied before, such as by Bigby (2004) and Reynolds (2006). However, little research has been focused on the performance of multi-strands with weak confining medium condition.
- Advanced numerical simulation of fully grouted cable bolts. Little research has been focused on modelling the geometry of fully grouted cable bolts, especially the modified cable bolts. It is recommended to use the finite element method to model the three dimensional geometry of cable bolts and study the influence of surface geometry on the bond contact between the cable bolt and the grout column.

REFERENCES

Altounyan, P. and Clifford, B., 2001. *Suitable long tendon technologies and practices* (Report), pp. 1-51 (Rock Mechanics Technology Pty Limited: Norwich).

Anwyll, D., 1996. The cable bolt - grout displacement meter An innovation in cable bolt monitoring, Master thesis, McGill University, Montreal.

Aoki, T., Maeno, Y., Shibata, K. and Obara, Y., 2002. Laboratory pull-out tests of cablebolts, *ISRM International Symposium-EuRock 2002*, Madeira, Portugal, pp. 599-606.

Aydan, O., Ichikawa, Y. and Kawamoto, K., 1985. Load bearing capacity and stress distributions in/along rockbolts with inelastic behaviour of interfaces, *Fifth International Conference on Numerical Methods in Geomechanics*, Nagoya, pp. 1281-1292.

Aziz, N., Craig, P., Mirza, A., Rasekh, H., Nemcik, J. and Li, X., 2015a. Behaviour of cable bolts in shear; experimental study and mathematical modelling, *Coal Operators' Conference*, Wollongong, Australia, pp. 147-160.

Aziz, N., Hawker, R., Mirza, A., Nemcik, J., Li, X. and Rasekh, H., 2015b. Strength characteristics of secura hollow grouted cable bolts, *Coal Operators' Conference*, Wollongong, Australia, pp. 161-168.

Aziz, N., Nemcik, J. and Jalalifar, H., 2011. Double shear of rebar steel and cable bolts for effective strata reinforcement, *Harmonising Rock Engineering and the Environment*, Beijing, China, p. 572.

Aziz, N. I., Heemann, K., Nemcik, J. and Stefan, M., 2014. Shear strength properties of Hilti plain and indented strand cable bolts, *Coal Operators's Conference*, Wollongong, Australia, pp. 156-162.

Ballivy, G. and Martin, A., 1983. The dimensionning of grouted anchors, *Proceedings of the International Symposium on Rock Bolting*, Abisko, Sweden, pp. 353-365.

Bawden, W. F., Dube, S. and Hyett, A. J., 1994. *A laboratory study on the capacity of fully grouted cable bolts subjected to combined axial and lateral loads* (Report), pp. 1-11 (Queen's University: Ontario).

Bawden, W. F., Hyett, A. J. and Lausch, P., 1992. An experimental procedure for the in situ testing of cable bolts, *International Journal of Rock Mechanics and Mining Sciences & Geomechanics Abstracts*, 29 (5):525-533.

Benmokrane, B., Chennouf, A. and Ballivy, G., 1992. Study of bond strength behaviour of steel cables and bars anchored with different cement grouts, *Rock support in Mining and Underground Construction: Proceedings of the International Symposium on Rock Support*, Sudbury, Canada, pp. 293-301.

Benmokrane, B., Chennouf, A. and Mitri, H. S., 1995. Laboratory evaluation of cement-based grouts and grouted rock anchors, *International Journal of Rock Mechanics and Mining Sciences*, 32 (7):633-642.

Bigby, D., 2004. *Coal mine roadway support system handbook* (Report), pp. 1-67 (Rock Mechanics Technology Limited: Staffordshire).

Bigby, D., Hurt, K., Reynolds, C. and Brown, R., 2010. *Evaluation of tensioned and non-tensioned long tendon reinforcement in UK deep mining conditions* (Report), pp. 1-152 (Rock Mechanics Technology Limited: Norwich).

Bigby, D. and Reynolds, C., 2005. Development of the laboratory short encapsulation pull test for a revised British Standard on rock reinforcement components used in coal mining, *24th International Conference on Ground Control in Mining*, Morgantown, USA, pp. 313-322.

Blanco Martín, L., 2012. Theoretical and experimental study of fully grouted rockbolts and cablebolts under axial loads, PhD thesis, Paris Institute of Technology, France.

Blanco Martín, L., Hadj-Hassen, F., Tijani, M. and Noiret, A., 2011. A new experimental and analytical study of fully grouted rockbolts, *45th US Rock Mechanics/Geomechanics Symposium*, San Francisco, United States, pp. 1-10.

Blanco Martín, L., Tijani, M. and Hadj-Hassen, F., 2010. A new analytical solution to the mechanical behaviour of fully grouted rockbolts subjected to pull-out tests, *Construction and Building Materials,* 25 (2):1-18.

Blanco Martín, L., Tijani, M., Hadj-Hassen, F. and Noiret, A., 2013. Assessment of the bolt-grout interface behaviour of fully grouted rockbolts from laboratory experiments under axial loads, *International Journal of Rock Mechanics and Mining Sciences,* 63 (2013):50-61.

Bourchier, F., Dib, E. and O'Flaherty, M., 1992. Practical improvements to installation of cable bolts: progress at Campbell Mine, *Rock support in Mining and Underground Construction : Proceedings of the International Symposium on Rock Support*, Sudbury, Canada, pp. 311-318.

Brady, B. H. G. and Brown, E. T., 1985. *Rock mechanics for underground mining*, pp. 1-614 (Kluwer Academic Publishers: New York).

Brown, R. E., Garcia, A. and Hurt, K., 2013. *Split cylinder pull tests on 3 samples of the SUMO cable bolt manufactured by Jennmar* (Internal Report), pp. 1-5 (Jennmar Australia and Golder Associates: Australia).

BS7861-1, 2007, Strata reinforcement support system components used in coal mines - Part 1: Specification for rockbolting, pp. 1-44.

BS7861-2, 2009, Strata reinforcement support systems components used in coal mines – Part 2: Specification for flexible systems for roof reinforcement, pp. 1-48.

Cai, Y., Esaki, T. and Jiang, Y., 2004a. An analytical model to predict axial load in grouted rock bolt for soft rock tunnelling, *Tunnelling and Underground Space Technology,* 19 (6):607-618.

Cai, Y., Esaki, T. and Jiang, Y., 2004b. A rock bolt and rock mass interaction model, *International Journal of Rock Mechanics and Mining Sciences,* 41 (2004):1055-1067.

Campoli, A., Mills, P., Todd, P. and Dever, K., 1999. Resin annulus size effects on rebar bolt pull strength and resin loss to fractured rock, *International Conference on Ground Control in Mining*, Morgantown, America, pp. 222-231.

Cao, C., 2012. Bolt profile configuration and load transfer capacity optimisation, PhD thesis, University of Wollongong, Wollongong.

Cao, C., Nemcik, J., Aziz, N. and Ren, T., 2012. Failure modes of rockbolting, *Coal Operators' Conference,* Wollongong, Australia, pp. 137-153.

Cao, C., Nemcik, J., Aziz, N. and Ren, T., 2013a. Analytical study of steel bolt profile and its influence on bolt load transfer, *International Journal of Rock Mechanics & Mining Sciences*, 60 (2013):188-195.

Cao, C., Nemcik, J., Ren, T. and Aziz, N., 2013b. A study of rock bolting failure modes, *International Journal of Mining Science and Technology*, 23 (1):79-88.

Carranza-Torres, C., 2009. Analytical and numerical study of the mechanics of rockbolt reinforcement around tunnels in rock masses, *Rock Mechanics and Rock Engineering*, 42 (2):175-228.

Chen, J. and Mitri, H. S., 2005. Shear bond characteristics in grouted cable bolts, *24th International Conference on Ground Control in Mining*, Morgantown, USA, pp. 342-348.

Clifford, B., 1974. Long rockbolt support at New Broken Hill Consolidated Limited, *Australian Institution ofl Mining and Metallurgy Conference*, pp. 21-26.

Clifford, B., Kent, L. K., Altounyan, P. and Bigby, D., 2001. Systems used in coal mining development in long tendon reinforcement *20th Internatioanl Conference on Ground Control in Mining*, Morgantown, USA, pp. 235-241.

Corbett, P., 2013. *Brief discussion regarding cable bolt pull test methods* pp. 1-14 Sydney).

Cox, R. H. T. and Fuller, P. G., 1977. *Load transfer behaviour between steel reinforcement and cement based grout* (Report), pp. 1-12 (Division of Applied Geomechanics, Commonwealth Scientific and Industrial Research Organization: Lindfield).

Craig, P. and Aziz, N. I., 2010. Shear testing of 28mm hollow strand "TG" cable bolt, *Coal Operators' Conference*, Wollongong, Australia, pp. 171-179.

Davidege, G. R., Martin, T. A. and Steed, C. M., 1988. Lacing support trial at Strathcona Mine, *2nd International Symposium on Rock Bursts and Seismicity in Mines*, Minneapolis, USA, pp. 363-367.

Davis, W. L., 1977. Initiation of cablebolting at West Coast Mines, Rosebury, *Australian Institution of Mining and Metallurgy Conference*, Tasmania, pp. 215-225.

Diederichs, M. S., Pieterse, E. S., Nosé, J. S. and Kaiser, P. K., 1993. A model for evaluating cable bolt bond strength: An update, *ISRM International Symposium-EuRock 93*, Lisboa, Portugal, pp. 83-90.

Dight, P. M., 1982. Improvements to the stability of rock walls in open pit mines, PhD thesis, Monash University, Melbourne.

Donovan, K., Pariseau, W. G. and Cepak, M., 1984. Finite element approach to cable bolting in steeply dipping VCR stopes, *Geomechanics Applications in Underground Hardrock Mining*, New York, USA, pp. 65-90.

Dorsten, V., Hunt, F. F. and Kent, P. H., 1984. Epoxy coated seven-wire strands for prestressed concrete, *Prestressed Concrete Institute*, 29 (4):120-129.

Dunham, R. K., 1976. Anchorage tests on strain-gauged resin bonded bolts, *Tunnels and Tunnelling*, 8 (6):73-76.

Fabjanczyk, M. W. and Tarrant, G. C., 1992. Load transfer mechanisms in reinforcing tendons, *11th International Conference on Ground Control in Mining*, Wollongong, Australia, pp. 212-219.

Farah, A. and Aref, K., 1986a. Design considerations of fully grouted cable bolts, *88th Annual General Meeting of CIM*, Montreal, Canada, pp. 1-18.

Farah, A. and Aref, K., 1986b. *An investigation of the dynamic characteristics of cable bolts*, pp. 423-428

Farmer, I. W., 1975. Stress distribution along a resin grouted rock anchor, *International Journal for Numerical and Analytical Methods in Geomechanics*, 12:347-351.

Faulkner, D. D., Cook, T. M. and Stankus, J. C., 2013. A comprehensive analysis of cable bolt anchorage characteristics, *32nd International Conference on Ground Control in Mining*, Morgantown, USA, pp. 1-8.

Fuller, P. G. and Cox, R. H. T., 1975. Mechanics of load transfer from steel tendons to cement based grout, *Fifth Australasian Conference on the Mechanics of Structures and Materials*, Melbourne, Australia, pp. 189-203.

Gale, W. J., Mark, C., Oyler, D. C. and Chen, J., 2004. Computer simulation of ground behaviour and rock bolt interaction at Emerald Mine, *International Conference on Ground Control in Mining*, Morgantown, USA, pp. 27-34.

Garford, 1990. *An improved, economical method for rock stabilisation* (Report), pp. 1-4 (Garford, Pty Ltd: Perth).

GCTS, 2010. *RDS-300 rock direct shear system*, Arizona, pp. 1-4.

Goris, J. M., 1990. *Laboratory evaluation of cable bolt supports (in two parts) 1. Evaluation of supports using conventional cables* (Report), pp. 1-23 (US Bureau of Mines: United States).

Goris, J. M., 1991a. *Laboratory evaluation of cable bolt supports (in two parts) 2. Evaluation of supports using conventional cables with steel buttons, birdcage cables, and epoxy-coated cables* (Report), pp. 1-14 (US Bureau of Mines: United States).

Goris, J. M., 1991b. Laboratory evaluation of cable supports, *CIM Bulletin*, 84 (548):44-50.

Goris, J. M. and Conway, J. P., 1987. Grouted flexible tendons and scaling investigations, *13th World Mining Congress*, Stockholm, Sweden, pp. 783-792.

Goris, J. M., Martin, L. A. and Curtin, R. P., 1996. Shear behaviour of cable bolt supports in horizontal bedded deposits, *CIM bulletin*, 89 (1001):124-128.

Gramoli, L., 1975. Tensioned cable rock anchorage at Geco Division of Noranda Mines Ltd., *CIM First Underground Operators' Conference*, Sudbury, Canada, pp. 309-325.

Hartman, W. and Hebblewhite, B., 2003. Understanding the performance of rock reinforcements under shear loading through laboratory testing - A 30-year history, *1st Australasian Ground Control in Mining Conference*, Sydney, Australia, pp. 151-160.

Hassani, F. P., Mitri, H. S., Khan, U. H. and Rajaie, H., 1992. Experimental and numerical studies of the cable bolt support systems, *Rock support in Mining and Underground Construction : Proceedings of the International Symposium on Rock Support*, Sudbury, Canada, pp. 411-417.

Hassani, F. P. and Rajaie, H., 1990. Investigation into the optimization of a shotcrete cable bolt support system, *14th Congress of the Council of Mining and*

Metallurgical Institution, Edinburgh, United Kingdom, pp. 119-129.

Hawkes, J. M. and Evans, R. H., 1951. Bond stresses in reinforced concrete columns and beams, *Structural Engineering*, 29:323-327.

Holden, M. and Hagan, P. C., 2014. The size effect of rock sample used in anchorage performance testing of cable bolts, *Coal Operators' Conference*, Wollongong, Australia, pp. 128-136.

Hsiao, F. Y., Wang, C. L. and Chern, J. C., 2009. Numerical simulation of rock deformation for support design in tunnel intersection area, *Tunnelling and Underground Space Technology*, 24 (1):14-21.

Hunt, R. E. B. and Askew, J. E., 1977. Installation and design guidelines for cable dowel ground support at ZC/NBHC, *Underground Operators' Conference*, Broken Hill, Australia, pp. 113-122.

Hustrulid, W. A. and Bullock, R. L., 2001. *Underground mining methods: Engineering fundamentals and international case studies*, pp. 555-561 (Society for Mining, Metallurgy, and Exploration (SME): Littleton).

Hutchins, W. R., Bywater, S., Thompson, A. G. and Windsor, C. R., 1990. A versatile grouted cable bolt dowel reinforcing system for rock, *The AusIMM Proceedings*, pp. 25-29.

Hutchinson, D. J. and Diederichs, M. S., 1996. *Cablebolting in underground mines*, pp. 77-78 (BiTech Publishers Ltd.: Richmond).

Hyett, A. J. and Bawden, W. F., 1994. *The 25mm Garford bulb anchor for cable bolt reinforcement Part 1: Laboratory results* (Report), pp. 1-16 (Queen's University: Ontario).

Hyett, A. J. and Bawden, W. F., 1996. *The effect of bulb frequency on the behaviour of fully grouted Garford bulb cable bolts* (Report), pp. 1-34 (Queen's University: Ontario).

Hyett, A. J., Bawden, W. F. and Coulson, A. L., 1992a. Physical and mechanical properties of normal Portland cement pertaining to fully grouted cable bolts, *Rock support in Mining and Underground Construction : Proceedings of the International Symposium on Rock Support*, Sudbury, Canada, pp. 341-348.

Hyett, A. J., Bawden, W. F., Hedrick, N. and Blackall, J., 1995a. A laboratory evaluation of the 25 mm Garford bulb anchor for cable bolt reinforcement, *CIM Bulletin*, 88 (992):54-59.

Hyett, A. J., Bawden, W. F., Macsporran, G. R. and Moosavi, M., 1995b. A constitutive law for bond failure of fully-grouted cable bolts using a modified hoek cell, *International Journal for Numerical and Analytical Methods in Geomechanics*, 32 (1):11-36.

Hyett, A. J., Bawden, W. F., Powers, R. and Rocque, P., 1993. The nutcase cable bolt, *Innovative Mine Design for the 21st Century : Proceedings of the International Congress on Mine Design*, Kingston, Canada, pp. 409-419.

Hyett, A. J., Bawden, W. F. and Reichert, R. D., 1992b. The effect of rock mass confinement on the bond strength of fully grouted cable bolts, *International Journal of Rock Mechanics and Mining Sciences*, 29 (5):503-524.

Hyett, A. J., Moosavi, M. and Bawden, W. F., 1996. Load distribution along fully grouted bolts, with emphasis on cable bolt reinforcement, *International Journal for Numerical and Analytical Methods in Geomechanics*, 20 (7):517-544.

ISRM, 2007, Suggested methods for determining shear strength, pp. 171-173.

ISRM, 2014, The ISRM suggested methods for rock characterization, testing and monitoring: 2007-2014, pp. 52-68.

Itasca, 2000. *FLAC - Fast Lagrangian Analysis of Continua. Version 4.0*, pp. 241-258 (Itasca Consulting Group Inc.: Minneapolis).

Ito, F., Nakahara, F., Kawano, R., Kang, S.-S. and Obara, Y., 2001. Visualization of failure in a pull-out test of cable bolts using X-ray CT, *Construction and Building Materials*, 15 (5-6):263-270.

Jalalifar, H., 2011. An analytical solution to predict axial load along fully grouted bolts in an elasto-plastic rock mass, *The Journal of the Southern Afrcan Institute of Mining and Metallurgy*, 111 (2011):809-814.

Jennmar, 2014. *Cable bolts - plain Superstrand*, p. 1 (Jennmar Australia: Sydney).

Jeremic, M. L. and Delaire, G. J. P., 1983. Failure mechanics of cable bolt systems, *CIM Bulletin*, 76 (856):66-71.

John, C. M. S. and Dillen, D. E. V., 1983. Rockbolts: A new numerical representation and its application in tunnel design, *24th U. S. Symposium on Rock Mechanics*, pp. 13-26.

Kaiser, P. K., Yazici, S. and Nosé, J.-P., 1992. Effect of stress change on the bond strength of fully grouted cables, *International journal of rock mechanics and mining sciences & geomechanics abstracts*, 29 (3):293-306.

Kent, L. and Bigby, D., 2001. *Performance tests for stranded ground reinforcement in mines* (Report), pp. 1-32 (Rock Mechanics Technology Limited: Norwich).

Khan, U., 1994. Laboratory investigation of steel cables and composite material tendons for ground support, PhD thesis, McGill University, Montreal.

Lappalainen, P. and Antikainen, J., 1987. Mechanized cable bolting in stoping and tunnelling at Pyhasalmi Mine, *Improvement of Mine Productivity and Overall Economy by Modern Technology*, Stockholm, Sweden, pp. 793-796.

Li, B., Qi, T., Wang, Z. and Yang, L., 2012. Back analysis of grouted rock bolt pullout strength parameters from field tests, *Tunnelling and Underground Space Technology*, 28 (2012):345-349.

Li, C. C. and Stillborg, B., 1999. Analytical models for rock bolts, *International Journal of Rock Mechanics and Mining Sciences*, 36 (1999):1013-1029.

Liu, H. Y., Small, J. C. and Carter, J. P., 2008. Full 3D modelling for effects of tunnelling on existing support systems in the Sydney region, *Tunnelling and Underground Space Technology*, 23 (4):399-420.

Ma, S., 2014. Load tranfer mechanism of fully encapsulated rockbolts, PhD, University of Wollongong, Wollongong.

Ma, S., Nemcik, J. and Aziz, N., 2013. An analytical model of fully grouted rock bolts subjected to tensile load, *Construction and Building Materials*, 49 (2013):519-526.

Ma, S., Nemcik, J. and Aziz, N., 2014a. Simulation of fully grouted rockbolts in underground roadways using FLAC2D, *Canadian Geotechnical Journal*, 51

(8):911-920.

Ma, S., Nemcik, J., Aziz, N. and Zhang, Z., 2014b. Analytical model for rock bolts reaching free end slip, *Construction and Building Materials,* 57 (2014):30-37.

Ma, S., Nemcik, J., Aziz, N. and Zhang, Z., 2015. Numerical modeling of fully grouted rockbolts reaching free-end slip, *International Journal of Geomechanics,* (2015):1-7.

Macsporran, G. R., 1993. An empirical investigation into the effects of mine induced stress change on standard cable bolt capacity, Master thesis, Queen's University, Kingston.

Mah, G. P., 1994. The development of a fibreglass cable bolt, Master thesis, The University of British Columbia, Vancouver.

Mah, G. P., Pakalnis, R. and Milne, D., 1991. The development of a fibreglass cable bolt, *93rd Annual General Meeting: Seprate Papers*, pp. 1-23.

Mahony, L. T. and Hagan, P. C., 2006. A laboratory facility to study the behaviour of reinforced elements subjected to shear, *Coal Operators' Conference*, Wollongong, Australia, pp. 245-254.

Mark, C., Gale, W. J., Oyler, D. C. and Chen, J., 2007. Case history of the response of a longwall entry subjected to concentrated horizontal stress, *International Journal of Rock Mechanics & Mining Sciences*, 44 (2):210-221.

Martin, L., Girard, J. M. and Curtin, R., 1996. Laboratory pull tests of resin-grouted cable bolts, *International Conference on Ground Control in Mining*, Golden, USA, pp. 455-468.

Matthews, S. M., Tillmann, V. H. and Worotnicki, G., 1983. A modified cable bolt system for the support of underground openings, *AusIMM annual conference*, Broken Hill, Australia, pp. 243-255.

Megabolt, 2012. *Pretensioned & grouted secondary support* (Report), pp. 1-4 (Megabolt Company: Sydney).

Meikle, T., Tadolini, S. C., Hawker, R. and Daniel, P., 2012. Improvements in long tendon support with Pumpable resin, *31st International Conference on Ground Control in Mining*, Morgantown, USA, pp. 1-5.

Miller, S. M. and Ward, D. C., 1996. Evaluation of pullout resistance and direct-shear strength of grouted fiberglass cable bolts, *International Journal of Rock Mechanics and Mining Sciences & Geomechanics Abstracts,* 35 (4):400.

Mirabile, B., Poland, R. and Campoli, A., 2010. Application of tensioned cable bolts for supplemental support, *29th Internatioanl Conference on Ground Control in Mining*, Morgantown, USA, pp. 1-6.

Mitri, H. S. and Rajaie, H., 1990. Shear bond stresses along cable bolts, *10th International Conference on Ground Control in Mining,* Morgantown, USA, pp. 90-95.

Moosavi, M., 1997. Load distribution along fully grouted cable bolts based on constitutive models obtained from modified Hoek cells, PhD thesis, Queen's University, Kingston.

Moosavi, M., 1999. A comprehensive comparison between bond failure mechanism in rock bolts and cable bolts, *The Congress of the International Society for Rock*

Mechanics, pp. 1463-1466.

Moosavi, M. and Bawden, W. F., 2003. Shear strength of Portland cement grout, *Cement & Concrete Composites,* 25 (2003):729-735.

Moosavi, M., Bawden, W. F. and Hyett, A. J., 1996. A comprehensive laboratory test program to study the behaviour of modified goemetry cable bolt support, *Rock Mechanics,* Balkema, Rotterdam, pp. 209-216.

Moosavi, M., Bawden, W. F. and Hyett, A. J., 2002. Mechanism of bond failure and load distribution along fully grouted cable-bolts, *Mining Technology,* 111 (1):1-12.

Mosse-Robinson, S. and Sharrock, G., 2010. Laboratory experiments to quantify the pull-out strength of single strand cable bolts for large boreholes, *Second Australasian Ground Control in Mining Conference 2010,* Sydney, Australia, pp. 201-209.

Muir, W. G. and Hedley, D. G. F., 1973. Strata reinforcement with cable bolts, *Fourth International Symposium on Salt*, pp. 503-508.

Nemcik, J., Ma, S., Aziz, N., Ren, T. and Geng, X., 2014. Numerical modelling of failure propagation in fully grouted rock bolts subjected to tensile load, *International Journal of Rock Mechanics and Mining Sciences,* 71 (2014):293-300.

Nguyen, V. U., Aziz, N., Hii, J. and Fabjanczyk, M. W., 1986. An experimental investigation on cable reinforcement, *Ground Movement and Control Related to Coal Mining Symposium,* Wollongong, Australia, pp. 93-101.

Nosé, J.-P., 1993. Laboratory study on the effect of stress change on cable bolt capacity, Master thesis, Queen's University, Kingston.

Pakalnis, R., Peterson, D. and Poulin, R., 1994. Evaluation of glass fiber bolts for minng applications, *SME Annual Meeting,* Albuquerque, USA, pp. 1371-1372.

Palmer, W. T., Bailey, S. G. and Fuller, P. G., 1976. Experience with pre-placed supports in timber and cut and fill stopes, *Influence of excavation design and ground support on underground mining efficiencey and costs,* Wollongong, Australia, pp. 45-71.

Potvin, Y., Hudyma, M. and Miller, H. D. S., 1989. Design guidelines for open stope support *CIM Bulletin,* 52 (926):53-62.

Prasad, K., 1997. Effect of isotropic and anisotropic stress changes on the capacity of fully grouted cable bolts, Master thesis, Queen's University, Kingston.

Rajaie, H., 1990. Experimental and numerical investigations of cable bolt support systems, PhD thesis, McGill University, Montreal.

Rasekh, H., 2017. The performance of tendons in sheared rock strata - experimental, numerical and mathemetical studies (in preparation), PhD thesis, University of Wollongong, Wollongong.

Rasekh, H., Aziz, N., Nemcik, J., Mirza, A. and Li, X., 2015. An experimental study on the contact surface area of cabled bolted strata, *Coal Operators' Conference,* Wollongong, Australia, pp. 169-175.

Reichert, R. D., 1991. A laboratory and field investigation of the major factors influcing bond capacity of grouted cable bolts, Master thesis, Queen's University,

Kingston.
Reichert, R. D., Bawden, W. F. and Hyett, A. J., 1992. Evaluation of design bond strength for fully grouted cables, *CIM Bulletin,* 85 (922):110-118.
Ren, F., Yang, Z., Chen, J. and Chen, W., 2010. An analytical analysis of the full-range behaviour of grouted rockbolts based on a tri-linear bond-slip model, *Construction and Building Materials,* 24 (2010):361-370.
Renwick, M. T., 1992. Ultrastrand - An innovative cable bolt, *Fifth Underground Operators' Conference,* A.A. Balkema, pp. 151-156.
Reynolds, C., 2006. *Testing and standards for rock reinforcement consumables* (Report), pp. 1-25 (Rock Mechanics Technology Limited: Norwich).
Ruest, M. and Martin, A., 2002. *FLAC simulation of split-pipe tests on an instrumented cable bolt* (Report), pp. 1-9 (Itasca Consulting Group: Minneapolis).
Satola, I. S., 1999. Testing of the yielding cable bolt achieved by debonding, *Congress of the International Society for Rock Mechanics*, pp. 1467-1470.
Satola, I. S., 2001. Testing of corrosion protected cable bolts by double pipe axial tests, *Rock Mecahnics in hte National Interest*, Elsworth, pp. 1021-1027.
Satola, I. S., 2007. The axial load-displacement behaviour of steel strands used in rock reinforcement, PhD thesis, Helsinki University of Technology, Helsinki.
Satola, I. S. and Aromaa, J., 2003. Corrosion of rock bolts and the effect of corrosion protection on the axial behaviour of cable bolts, *ISRM 2003-Technology roadmap for rock mechanics*, Gauteng, South Africa, pp. 1039-1042.
Satola, I. S. and Aromaa, J., 2004. The corrosion of rock bolts and cable bolts, *Ground Support in Mining and Underground Construction*, Perth, Australia, pp. 521-528.
Satola, I. S. and Hakala, M., 2001. Corrosion protected cable bolts in long-term reinforcement, *Rock Mechanics - a Challenge for Society*, Espoo, Finland, pp. 377-382.
Schmuck, C. H., 1979. Cable bolting at the Homestake gold mine, *Mining Engineering,* 31 (12):1677-1681.
Sonnenberg, A. M. C., Al-Mahaidi, R. and Taplin, G., 2003. Behaviour of concrete under shear and normal stresses, *Magazine of Concrete Research,* 55 (4):367-372.
Standard Australia, 2014, Methods of testing concrete - Preparing concrete mixes in the laboratory, pp. 1-21.
Stheeman, W. H., 1982. A practical solution to cable bolting problems at the Tsumeb Mine, *CIM Bulletin,* 75:65-77.
Stillborg, B., 1984. Experimental investigation of steel cables for rock reinforcement in hard rock, PhD thesis, Luleå University, Luleå.
Stillborg, B., 1986. The geomechanics of big blasthole open stoping: Pre-production plan and cablebolting cut dilution and stability problems at Luossavaara, *Engineering and Mining Journal*:26-32.
Strata Control, 1990. *Testing of Garford bulb tendons* (Report), pp. 1-5 (Strata Control Technology Pty. Limited: Wollongong).
Tadolini, S. C., 1994. *Resin-grouted cables for enhanced coal mine roof support* pp. 1-2

(Bureau of Mines, United States Department of the Interior: Washington, DC).
Tadolini, S. C., Tinsley, J. and McDonnell, J. P., 2012. The next generation of cable bolts for improved ground support, *31st Internatioanl Conference on Ground Control in Mining*, Morgantwon, USA, pp. 1-7.
Tao, Z. and Chen, J., 1983. Behaviour of rock bolting as tunnelling support, *Proceedings of the International Symposium on Rock Bolting*, Abisko, Sweden, pp. 87-92.
Thomas, R., 2012. The load transfer properties of post-groutable cable bolts used in the Australian Coal Industry, *31st International Conference on Ground Control in Mining*, Morgantown, USA, pp. 1-10.
Thompson, A. G., Matthews, S. M., Windsor, C. R., Bywater, S. and Tillmann, V. H., 1987. Innovations in rock reinforcement in the Australian mining industry, *6th Congress of International Society for Rock Mechanics*, Montreal, Canada, pp. 1275-1278.
Thompson, A. G. and Villaescusa, E., 2013. Case studies of rock reinforcement components and systems testing, *47th US Rock Mechanics/Goemechanics Symposium*, San Francisco, USA, pp. 1-10.
Thompson, A. G., Villaescusa, E. and Windsor, C. R., 2012. Ground support terminology and classification: An update, *Geotechnical and Geological Engineering*, 30 (3):553-580.
Thompson, A. G. and Windsor, C. R., 1995. Tensioned cable bolt reinforcement-An integrated case study, *8th ISRM Congress*, pp. 679-682.
Thorne, L. J. and Muller, D. S., 1964. Pre-stressed roof support in underground engine chambers at Free State Geduld Mines Ltd., *Trans. Assn Mine Mngrs South Africa*:412-428.
Wang, M., Bai, J., Li, W., Wang, X. and Cao, S., 2015. Failure mechanism and control of deep gob-side entry, *Arabian Journal of Geosciences*, 8 (11):9117-9131.
Windsor, C. R., 1990. *Ferruled strand* (Commonwealth Scientific and Industrial Research Organisation: Perth).
Windsor, C. R., 1992. Invited lecture: Cable bolting for underground and surface excavations, *Rock support in Mining and Underground Construction: Proceedings of the International Symposium on Rock Support*, Rotterdam, Netherland pp. 349-366.
Windsor, C. R., 1997. Rock reinforcement systems, *International Journal of Rock Mechanics and Mining Sciences*, 34 (6):919-951.
Windsor, C. R. and Thompson, A. G., 1993. *Rock reinforcement - Technology, testing, design and evaluation*, pp. 451-484 (Pergamon Press Ltd: Oxford, England).
Wong, R. C. K., Ma, S. K. Y., Wong, R. H. C. and Chau, K. T., 2007. Shear strength components of concrete under direct shearing, *Cement and concrete research*, 37 (2007):1248-1256.
Wu, Z., Yang, S., Zheng, J. and Hu, X., 2010. Analytical solution for the pull-out response of FRP rods embedded in steel tubes filled in cement grout, *Materials and Structures*, 43 (2010):597-609.
Xiao, S. and Chen, C., 2008. Mechanical mechanism analysis of tension type anchor

based on shear displacement method, *Journal of Central South University of Technology*, 15 (2008):106-111.

Yazici, S. and Kaiser, P. K., 1992. Bond strength of grouted cable bolts, *International Journal of Rock Mechanics and Mining Sciences Geomechanics Abstracts,* 29 (3):279-292.

Yuan, H., Chen, J. F., Teng, J. G. and Lu, X. Z., 2007. Interfacial stress analysis of a thin plate bonded to a rigid substrate and subjected to inclined loading, *International Journal of Solids and Structures*, 44 (2007):5247-5271.

Zhang, Y., Rao, X., Tang, S., Luo, B. and Li, J., 2008. Experimental study and numercial analysis of anchorage performance of bulb anchor cable, *Chinese Journal of Rock Mechanics and Engineering,* 27 (3):607-614.

Zhao, Y. and Yang, M., 2011. Pull-out behavior of an imperfectly bonded anchor system, *International Journal of Rock Mechanics & Mining Sciences,* 48 (2011):469-475.

Zhou, Y., Wu, Y. and Yun, Y., 2010. Analytical modeling of the bond - slip relationship at FRP-concrete interfaces for adhesively-bonded joints, *Composites Part B: Engineering,* 41 (6):423-433.